Hybrid membranes for fuel cell

Isabel Zamanillo Lopez

UNIVERSITÉ GRENOBLE ALPES

THÈSE

Pour obtenir le grade de

DOCTEUR DE L'UNIVERSITÉ GRENOBLE ALPES

Spécialité : **Matériaux, Mécanique, Génie Civil, Électrochimie**

Arrêté ministériel : 7 août 2006

Présentée par

Isabel ZAMANILLO LÓPEZ

Thèse dirigée par **Laurent GONON** et
codirigée par **Vincent MAREAU**

préparée au sein du **Laboratoire Structure et Propriétés d'Architectures moléculaires / Polymères Conducteurs Ioniques** dans l'École **Doctorale Ingénierie-Matériaux, Mécanique Énergétique, Environnement, Procédés, Production (I-MEP²)**

Membranes hybrides pour pile à combustible

Thèse soutenue publiquement le **16 décembre 2015,**
devant le jury composé de:

Pr. Saïd SADKI CEA-CNRS-Université J. Fourier, Grenoble	Président
Pr. Jean-François FELLER Université de Bretagne Sud	Rapporteur
Dr. Vincent VERNEY Charge de recherche CNRS Institut de chimie de Clermont Ferrand	Rapporteur
Pr. Laurent GONON CEA-CNRS-Université J. Fourier, Grenoble	Directeur de thèse
Dr. Vincent MAREAU Maître de Conférences, CEA-CNRS Université J.Fourier, Grenoble	Membre invité
Dr. Hakima MENDIL-JAKANI Chercheuse CEA Grenoble	Membre invité

UNIVERSITÉ GRENOBLE ALPES

HYBRID MEMBRANES FOR FUEL CELL

Isabel Zamanillo López

This dissertation is submitted for the degree of Doctor of Philosophy

16 December 2015

"Entre
Ce que je pense,
Ce que je veux dire,
Ce que je crois dire,
Ce que je dis,
Ce que vous avez envie d'entendre,
Ce que vous croyez entendre,
Ce que vous entendez,
Ce que vous avez envie de comprendre,
Ce que vous comprenez,
Il y a dix possibilités qu'on ait des difficultés à communiquer.
Mais essayons quand même...".

encyclopédie du savoir relatif et absolu
BERNARD WEBER

Á mon père

Remerciements

Ce travail de thèse a été effectué au INAC du CEA-Grenoble, au sein du laboratoire de Structure et Propriétés d'Architectures Moléculaires dirigé lors de mon arrivé par Jean-Pierre TRAVERS puis par la suite par Fréderic CHANDEZON. Je les remercie pour les moyens financiers et matériels mis à ma disposition pour accomplir ce travail dans les meilleures conditions.

Je remercie également l'ensemble des membres de mon jury de thèse. Je prie Pr. Jean-François FELLER et Dr. Vincent VERNEY d'accepter l'expression de ma profonde gratitude pour avoir accepté d'examiner ce travail et je remercie Pr. Saïd SADKI d'avoir présidé ma soutenance.

Je tiens à exprimer toute ma reconnaissance à Laurent GONON, Vincent MAREAU et Hakima MENDIL-JAKANI pour avoir encadré ma thèse, j'ai apprécié leur présence, leur patience, leur collaboration dans les différentes expériences mais surtout de m'avoir ouvert les portes des "Grands Instruments", ce que j'ai apprécié tout particulièrement. Je les remercie pour nos nombreuses discussions scientifiques ainsi que pour tout ce qu'ils m'ont appris sur la science et sur moi-même.

J'exprime ma profonde gratitude à Sandrine LYONNARD pour son soutien, sa confiance et ses conseils, qui ont été les "précurseurs" de ce manuscrit. Merci pour le temps consacré à la relecture et les corrections apportées ainsi que pour l'écoute, paramètre nécessaire pour "débuter la fin".

Je remercie toutes les personnes avec qui j'ai travaillé au cours de ces 3 années, notamment Arnaud de GEYER pour l'utilisation de sa caméra de diffusion de rayons-x ainsi que les local-contacts de l'ESRF Cyril ROCHAS et à le LLB Florence NOIREZ. J'exprime ma reconnaissance à Daniel LEE de m'avoir impliqué dans ses expériences dans RMN, merci Arnaud MORIN et Jérôme DILLET pour les tests en pile et Vincent MARTIN pour les CES.

Je remercie chaleureusement tous les membres de l'équipe PCI, et spécialement ceux qui étaient avec moi pendant tout le parcours pour m'encourager jusqu'au bout, aussi aux membres du CREAB, où je me suis senti accueilli depuis le premier moment. Remerciement spécial pour leur soutien à Charly PICOT, Catherine PASCAL, Armel GUILLERMO, Quentin BERROD, Matthieu FUMAGALLI, Clément AUFFRET, Marco MACCARINI, Govind K. PRAJAPATI, Sarine CHHOR, Virginie SZEFLINSKI, David ARADILLA, Dominic BRESSER, Laurie-Amandine GARÇON, Yanxia HOU-BROUTIN, Lèa CHANCELIER...et tous ceux qui restent dans mon cœur, surtout Émilie DUBARD, (une partie de cette réussite est grâce à toi) que je vais devoir remercier infiniment.

Merci aussi à tous ceux qui, même de loin, ils m'ont apporté une aide précieuse pour cette thèse, merci Maria GENUA, Agnès RODRIGUEZ et Allison SANDERS, les filles plus réactives de la planète! Merci à Loïc PHILIBERT, même si Émilie prends une partie de cette réussite....il prend le reste! Merci à Bénédicte DENOIX et sa famille pour me faire sentir comme à la maison. Merci à mes amis de toujours, ainsi que les nouveaux, tous les grenoblois ou pseudo-grenoblois sur qui j'ai pu compter à une ou plusieurs reprises, la vie est toujours plus belle avec vous!

Et enfin, une petite pensée pour mon père, *gracias papá por estar ahí cada día en la distancia, por saber escuchar, aconsejar y hacerme más feliz cada día, gracias por aguantarme de buen y de mal humor en cada etapa de mi vida y sobre todo gracias por creer cada segundo. Te quiero.*

CONTENTS

ABBREVIATIONS

FC	**F**uel **C**e**l**l
PEMFC	**P**roton **E**xchange **M**embrane **F**uel **C**ell
PEM	**P**olymer **E**lectrolyte **M**embrane
MEA	**M**embrane **E**lectrode **A**ssemblies
PFSA	**P**er**F**luoro**S**ulfonic **A**cid membranes
sPEEK	**S**ulfonated **P**oly**E**ther**E**ther**K**etone
SHdi	(3-Mercaptopropyl) methyl**di**methoxysilane
SHtri	(3-Mercaptopropyl) **tri**ethoxysilane
TS	Bis[3-(triethoxysilyl)propyl]**T**etra**S**ulfide
IEC	**I**onic **E**xchange **C**apacity
DS	**D**egree of **S**ulfonation
RH	**R**elative **H**umidity
IR	**I**nfra**R**ed spectroscopy.
SAXS	**S**mall **A**ngle **X**-ray **S**cattering
SANS	**S**mall **A**ngle **N**eutron **S**cattering
WAXS	**W**ide **A**ngle **X**-ray **S**cattering
XRD	**X**-**R**ay **D**iffraction
TGA	**T**hermo**G**ravimetric **A**nalysis
DTG	**D**erivative **T**hermogravimetric **A**nalysis
DMA	**D**ynamic **M**echanical **A**nalysis
AFM	**A**tomic **F**orce **M**icroscopy
INP	**I**nter **P**enetrating **N**etwork
DSL	**D**ensity of **S**cattering **L**ength

INTRODUCTION

In this thesis, we present the elaboration and characterization of sPEEK hybrid membranes for the application of the Polymer Electrolyte Membrane Fuel Cell (PEMFC) above 100ºC. The project was financed by *CEA (Grenoble)* and the work accomplished during the course of the thesis has been carried out in *INAC-SPrAM* (The Laboratory of Structure and Properties of Molecular Architectures), under the guidance of Laurent GONON, Vincent MAREAU and Hakima MENDIL-JAKANI.

Fuel cells are a promising solution for the clean production of hydrogen based energy. However, in order to achieve the large-scale utilization of this technology, some major issues remain to be addressed. One of the remaining problems concerns the core of the cell (the polymer membrane sandwiched between two electrodes). In particular, it is impossible to improve the catalyst efficiency and the cell performance by a simple increase of the operating temperature (100-120°C). Indeed the reference membrane (Nafion®) exhibits a steep decrease of its thermomechanical properties beyond 80 °C, whereas alternative membranes (with a better thermomechanical stability) undergo much faster chemical aging that results in unexpected failure of the device.

Our main objective is to develop novel hybrid membranes consisting of a commercial ionomer matrix into which we will introduce both precursors capable of forming a sol-gel phase as well as sacrificial groups able to inhibit oxidative species produced during fuel cell operation. The resulting hybrid membrane is composed of two interpenetrating phases, one cross-linked inorganic sol-gel phase providing chemical and thermomechanical stabilization, and an ion conductive non-cross-linked polymer phase. We demonstrate that the control of the chemistry of sol-gel phase, its morphology, and its location in the host membrane are essential to producing hybrid membranes for fuel cell application.

This manuscript has been divided into four chapters:

The *first chapter* is a synthetic overview of the bibliographical study of fuel cell systems and more precisely of PEMFCs. The chapter begins with a brief overview of the hydrogen sector in context. Afterwards, we focus on the important aspects and key issues related specifically to the fuel cells based on proton conduction and the membranes used in this framework. We specifically recall the main features of Nafion® membranes, which are often considered as the reference membranes. We conclude the first chapter by describing different routes proposed in the literature in order to improve the initial as well as long-term properties of the membranes.

In the *second chapter*, we present the study of sPEEK membrane morphology. We present the results obtained through Small Angle X-Ray and Neutron Scattering (SAXS and SANS) and Wide Angle X-Ray Scattering (WAXS) for sPEEK membranes conditioned at different water contents. We propose a new interpretation of correlation peaks in sPEEK membranes, including a complete study of the evolution of the scattering profiles upon water uptake. These results are

compared with the functional properties of sPEEK in the same conditions. The impact of the oxidative treatments on morphology is also discussed in the last part of this chapter.

The *third chapter* details the development of novel hybrid membranes consisting of a commercial ionomer matrix, in which we introduce precursors capable of forming a chemically and physically active sol-gel phase. We describe our strategy to prepare hybrid membranes using the sol-gel impregnation approach. The effects of the various experimental parameters on the elaboration process are discussed and the conditions for preparing hybrid membranes are established.

The *fourth chapter* focuses on the influence of the chemical structure on the functional properties of hybrid membranes. Seven types of hybrid membranes based on three different precursors were investigated in order to study the effect of the cross-linking degree. The impact of the particular morphologies of these hybrid membranes on their functional properties is explained. Lastly, we present the morphology of the membranes as well as the preliminary fuel cell test.

In the final part of the manuscript, we establish *general conclusions and perspectives* from this work.

CHAPTER I

STATE-OF-THE-ART

I.1 Introduction

The hydrogen technology offers a chemical storage solution for electrical energy produced by renewable sources (H_2 generation by electrolysis) [1]. Current research and development is focused on the production, storage and distribution of energy derived from hydrogen, i.e. the development of a "hydrogen based economy".

I.1.1 Hydrogen production

The hydrogen production is important to make hydrogen cost-competitive with conventional fuels while minimizing the environmental impacts of production. Hydrogen can be produced from diverse domestic resources including fossil fuels, biomass, and water electrolysis (*Fig. I-1*) [2, 3]. The environmental impact and energy efficiency of hydrogen production depends on how it is produced. The primary challenge, in the near-term, is reducing the cost of production to make the resulting hydrogen cost-competitive. In the long-term, technology pathways with near-net zero carbon emissions, such as those based on solar energy, are expected to become viable.

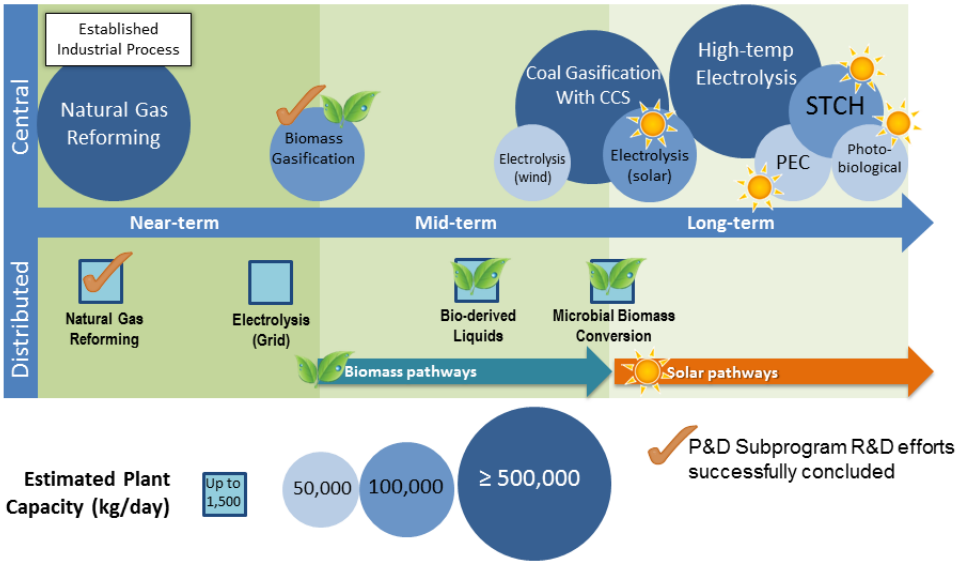

Fig. I-1 *Hydrogen production pathways graphic[2]*.

I.1.2 Hydrogen distribution

The infrastructure needed for distributing hydrogen, i.e. a network of fueling stations required for the widespread use of fuel cell vehicles, still needs to be developed. Between 2014 and 2017 the United States set the initial rollout for vehicles and stations, which focuses on building out these distribution networks [4]. Currently, hydrogen is distributed by pipeline, high-pressure tube trailers and liquefied hydrogen tankers. Building a new hydrogen pipeline network involves high initial capital costs, and hydrogen's properties present unique challenges to pipeline materials and compressor design. However, because hydrogen can be produced from a wide variety of resources,

regional or even local production of hydrogen can maximize use of local resources and minimize distribution challenges, and the use of petroleum.

I.1.3 Hydrogen Storage

Hydrogen storage is a key enabling technology for the advancement of hydrogen and fuel cell technologies. Hydrogen has the highest energy per mass of any fuel. However, its low density at ambient temperature required the development of advanced storage methods [2].

The near-term pathway focuses on compressed gas storage (*Fig. I-2*), using advanced pressure vessels, with a major emphasis on system cost reduction [2]. The long-term pathway focuses on cold or cryo compressed hydrogen storage, to increase hydrogen density. For example, insulated pressure vessels and materials-based hydrogen storage technologies, including sorbents, chemical hydrogen storage materials, and metal hydrides.

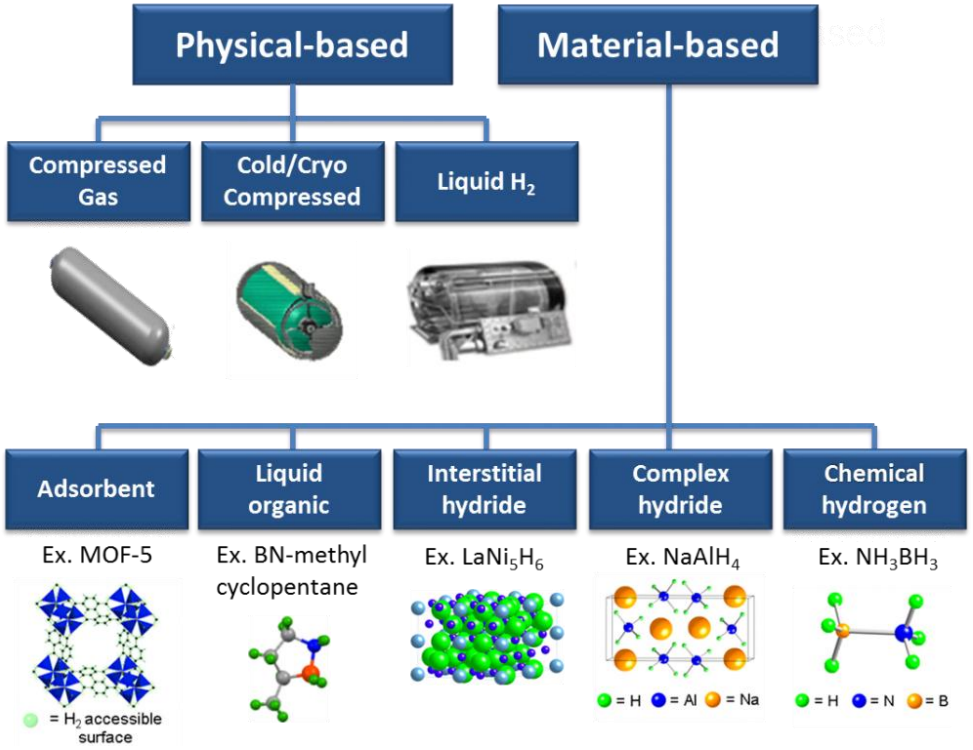

Fig. I-2 *Schematic representation of hydrogen storage[2].*

I.1.4 Hydrogen fuel cells

It must be clear that the hydrogen is not a primary energy source but a chemical storage solution of electrical energy. The fuel cell technology converts this chemical energy into electricity, heat and water as by-products.

Most types of fuel cells require hydrogen as a fuel source. Fuel cells provide several advantages over conventional methods of energy conversion, particularly the internal combustion engine, such as [5]:

a) Increased energy conversion efficiency, which may exceed 60%.

b) Reduced oil consumption: fuel cell electric vehicles can result in more than a 95% reduction in oil usage as compared to conventional internal combustion engine vehicles.

c) Increased fuel flexibility: fuel cells can use clean energy sources such as biofuels, methanol, etc, or hydrogen produced from renewable or conventional energy sources.

d) Reduced CO_2 and pollutant emissions: for combined heat and power systems fuel cells can achieve a 35-50% or higher reduction in CO_2 emissions, depending on the fuel, and a 90% reduction of pollutant emissions.

The long-term goal of fuel cell research is to achieve a totally non-polluting power source.

Fuel cells are unique in terms of the variety of their potential applications (*Fig. I-3*): they can be used as power sources in a wide range of applications, including transportation, material handling, stationary, portable, and emergency backup power applications. Therefore, they can provide power for systems as large as a utility power station and as small as a laptop computer. Stationary fuel cells are used for commercial, industrial and residential primary backup power. They are also very useful as power sources in remote locations, such as spacecraft, remote weather stations, large parks, communications centers, rural locations including research stations, and in certain military applications. Combined heat and power (CHP) fuel cell systems (cogeneration) are used to generate both electricity and heat for homes. The system generates constant electric power (selling excess power back to the grid when it is not consumed), and at the same time produces hot air and water from the waste heat. A typical capacity range of home fuel cell is 1–3 kW (electrical) / 4–8kW (thermal) [6]. In June 2011 demonstration "Fuel Cell Electrical Vehicles" (FCEV) had driven more than 4,800,000 km, with more than 27,000 refuelings. In 2015, two FCEVs have been introduced for commercial lease and sale in limited quantities: the *Toyota Mirai* (*Fig. I-3*) and the *Hyundai ix35 FCEV*. Additional demonstration models include the *Honda FCX Clarity*, and *Mercedes-Benz F-Cell* [7].

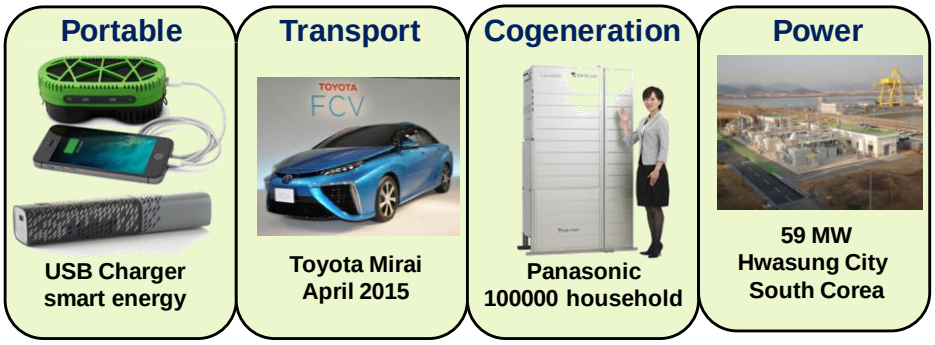

Fig. I-3 *Fuel cell applications: from portable to stationary electrical power sources*

I.1.5 Types of Fuel Cells

The various families of fuel cell may be distinguished (see *Table I-1*) by the functional materials they adopt, particularly in terms of electrolyte and catalyst but also by their operating temperature [2].

In this work, we report the synthesis and characterization of new proton conducting polymer electrolytes for use in proton exchange membrane fuel cells (PEMFCs). Therefore, we will focus on description of the components and the main characteristics of PEMFCs, particularly with regard to the proton exchange membrane (PEM).

Table I-1 *Characteristic of different families of fuel cells[2].*

Fuel Cell Type	*Common Electrolyte*	*Operating T°*	*Typical Stack Size*	*Electrical Efficiency*	*Applications*	*Advantages*	*Disadvantages*
Polymer Electrolyte Membrane (PEM)	Perfluorosulfonic acid	<120°C	<1–100 kW	60%direct H_2; 40% reformed fuel	- Backup power - Portable power - Distributed generation -Transportation - Specialty vehicles	- Solid electrolyte reduces corrosion and electrolyte management problems - Low temperature - Quick start-up	- Expensive catalysts - Sensitive to fuel impurities
Alkaline (AFC)	Aqueous potassium hydroxide soaked in a porous matrix, or alkaline polymer membrane	<100 °C	1–100 kW	60%	- Military - Space - Backup power -Transportation	- Wider range of stable materials allows lower cost components - Low temperature - Quick start-up	- Sensitive to CO_2 in fuel and air - Electrolyte management (aqueous) - Electrolyte conductivity (polymer)
Phosphoric Acid (PAFC)	Phosphoric acid soaked in a porous matrix or imbibed in a polymer membrane	150–200 °C	400 kW, 100 kW module (liquid PAFC); <10 kW (polymer membrane)	40%	-Distributed generation	- Suitable for CHP - Increased tolerance to fuel impurities	- Expensive catalysts - Long start-up time - Sulfur sensitivity
Molten Carbonate (MCFC)	Molten lithium, sodium, and/or potassium carbonates, soaked in a porous matrix	600–700 °C	300 kW–3 MW, 300 kW module	50%	- Electric utility - Distributed generation	- High efficiency - Fuel flexibility - Suitable for CHP - Hybrid/gas turbine cycle	- High temperature corrosion and breakdown of cell components - Long start-up time - Low power density
Solid Oxide (SOFC)	Yttria stabilized zirconia	500–1,000 °C	1 kW–2 MW	60%	- Auxiliary power - Electric utility - Distributed generation	- High efficiency - Fuel flexibility - Solid electrolyte - Suitable for CHP - Hybrid/gas turbine cycle	- High temperature corrosion and breakdown of cell components - Long start-up time - Limited number of shutdowns

* Principle of Proton Exchange Membrane Fuel Cell (PEMFC)

PEMFCs are composed of membrane electrode assemblies (MEA) which include the gas diffusion layers, the catalyst layers (electrodes) and the proton exchange membrane used as electrolyte. PEMFC cells operate at relatively low temperatures (below 100ºC). Due to the relatively low temperatures and the use of precious metal-based electrodes, these cells must operate on pure hydrogen.

In *Fig. I-4* the schematic representation of PEMFC is displayed. Hydrogen fuel is injected at the anode side (*eq.I-1).* Its oxidation on the catalyst layer leads to the release of two electrons per

H_2 molecule and two protons. The protons pass through the membrane to the cathode side of the cell while the electrons travel through an external circuit, generating the electrical output of the cell. On the cathode side, the O_2 reduction leads to the formation of H_2O *(eq.I-2)*, which is collected at the vent of the O_2 gas flow.

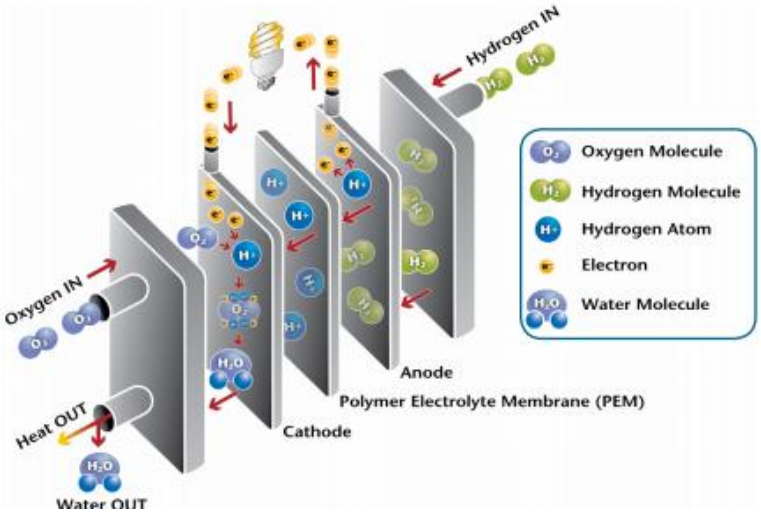

Fig. I-4 *Schematic representation of PEMFC [3]*

The basic fuel cell reactions are:

At the anode: $H_2 \rightarrow 2H+ + 2e^-$ (*eq.I-1*)

At the cathode: $½\ O_2 + 2H+ + 2e^- \rightarrow H_2O$ (*eq.I-2*)

Overall: $H_2 + ½\ O_2 \rightarrow H_2O$ (*eq.I-3*)

The PEMFC typical operating temperature is ~80ºC, in order to avoid membrane dehydration and the drop of the proton conductivity.

Cost, performance, and durability are still key challenges in the fuel cell industry. The characteristics required are summarized in *Table I-2* as listed by the U.S. Department of Energy (DOE).

Cost- The platinum electrode represents one of the largest cost components of a fuel cell (the other being the membrane itself), so much of the R&D focuses on approaches that will increase activity and utilization of current platinum group metal (PGM) and PGM-alloy catalysts, as well as non-PGM catalyst approaches for long-term applications.

Performance- To improve fuel cell performance, R&D focuses on developing ion-exchange membrane electrolytes with enhanced efficiency and durability at reduced cost; improving membrane electrode assemblies (MEAs) through integration of state-of-the-art MEA components; developing transport models, in-situ and ex-situ experiments to provide data for model validation; identifying degradation mechanisms and developing approaches to mitigate their effects; and maintaining core activities on components, sub-systems, and systems specifically tailored for stationary and portable power applications.

Durability—A key performance factor is durability, in terms of a fuel cell system lifetime that will meet application expectations. DOE durability targets for stationary and transportation fuel cells are 40,000 hours and 5,000 hours, respectively, under realistic operating conditions. In the most demanding applications, realistic operating conditions include impurities in the fuel and air, starting and stopping, freezing and thawing, and humidity and load cycles that result in stresses on the chemical and mechanical stability of the fuel cell system materials and components. R&D focuses on understanding the fuel cell degradation mechanisms and developing materials and strategies that will mitigate them.

Table I-2 *Technical Targets for Automotive-Scale (80 kWe net) Fuel Cell System Operating on Hydrogen [2]*

Characteristic	Units	Status	2020
Energy efficiency @ 25% rated power	%	60	60
Power density	W/L	640	650
Specific power	W/kg	659	650
Cost	$/kWe	51	40
Cold start-up time to 50% of rated power			
@ -20ºC ambient temp	sec	20	30
@ +20ºC ambient temp	sec	<10	5
Durability in automotive load cycle	hours	2500	5000

The PEM is a key component of PEMFC technology, and a lot of efforts are still needed to reach all the fuel cell requirements.

I.2 Proton Exchange Membranes (PEMs)

The proton exchange membrane or PEM constitutes the core of the fuel cell. It is a polymer membrane with acid side groups, generally sulfonated (SO_3H), to allow proton conduction from anode to cathode. A good proton-conducting fuel cell membrane should meet the following criteria [8]:

1) Good chemical and electrochemical stability under operating conditions of the fuel cell.

2) Mechanical strength and stability under the mechanical stresses applied on the membrane during operating conditions swelling/unswelling cycle, differential mechanical stresses under the rib and the channel.

3) Extremely low permeability to O_2 and H_2.

4) High water mobility to maintain uniform the water content on the electrolyte and prevent localized drying.

5) High proton conductivity to support high currents with a minimal resistance loss.

6) Negligible electronic conductivity.

Additionally, for marketing a viable electrolyte membrane, a low production cost must be achieved with respect to the targeted applications.

The polymer electrolyte membrane used can be classified in three groups:

1.- Perfluorinated sulfonated polymers.

2.- Non- fluorinated sulfonated polymers based on a hydrocarbon skeleton.

3.- Composite membranes based on perfluorinated and/or hydrocarbon sulfonated polymers.

On *Fig. I-5* a detailed classification of existing polymer membranes is displayed [8].

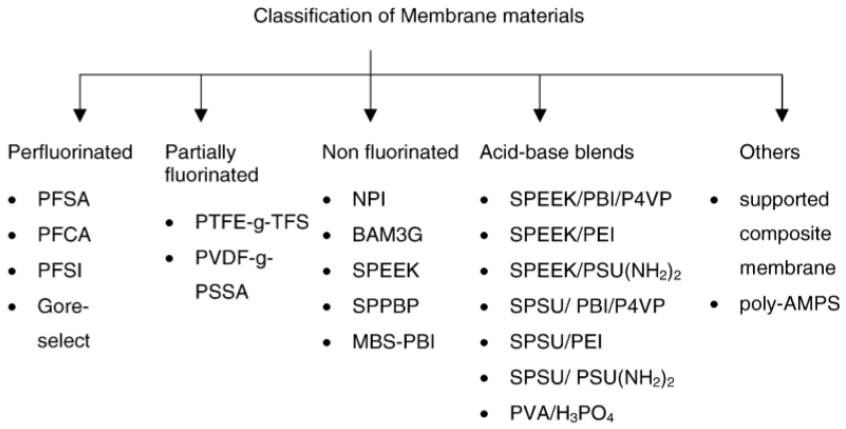

Fig. I-5 *Classification of membranes materials[8]*

In the next sections, we will introduce the main properties of the different types of membranes with a particular focus on Nafion® as a benchmark membrane and sPEEK membrane as an alternative non-fluorinated polymer matrix used in the elaboration of hybrid membranes.

We also present a brief review of hybrid membranes properties as a function of their elaboration process.

I.2.1 Perfluorosulfonic acid polymers

Perfluorosulfonic acid polymers like Nafion® are considered as the benchmark membrane for fuel cell applications. Perfluorosulfonic acid (PFSA) membranes generally consist of a polytetrafluorethylene (PTFE) backbone with perfluorinated side chains of different lengths, attached to the backbone through ether linkages and terminated by sulfonic acid ($-SO_3H$) groups (*Fig. I-6*). The unique properties of PFSA membranes are most likely the immediate consequences of the PTFE backbone to pack in an ordered way (similar to the crystallization of pure PTFE (Teflon)), and the fact that the polymeric structure combines the extreme hydrophobicity of the backbone with the extreme hydrophilicity of the superacidic $-SO_3H$ group (note that the latter is related to the electron withdrawal property of the adjacent CF_2 group).

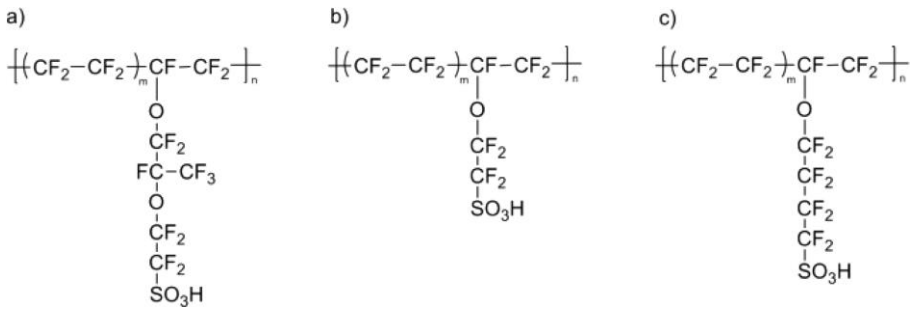

Fig. I-6 *Chemical structure Molecular Structures of (A) Nafion®, (B) Aquivion™, and (C) the 3M-Ionomer membrane[9]*

Nafion® was the first perfluorinated ionomer (*Fig. I-6 (A)*), developed and produced in the early 60's by DuPont. Later on, Dow Chemicals developed a perfluorinated ionomer very similar to Nafion®, but with much shorter side-chain length. This ionomer is now produced and distributed by Solvay Specialty Polymers under the trade name Aquivion™ (*Fig. I-6(B)*). The 3M Company has recently developed its own perfluorinated ionomer *(Fig. I-6(C))*, which possesses a side chain with an intermediate length between Nafion® and Aquivion™.

The Nafion® membranes have been extensively studied since more than fifty years. We focus this general literature review on its properties as a benchmark membrane.

* Nafion®

The equivalent weight (EW) and material thickness are used to describe most commercially available membranes. The equivalent weight (EW) represents the grams of dry ionomer per mole of sulfonic acid groups when the material is in the acid form. Nafion® is available in varying equivalent weights (g/mol), viz. 900, 1100, 1200, etc. The ionic exchange capacity of an ionomer is defined as the density of ionic charge in mole per gram of polymer as shown in *eq.I-4.*

$$IEC = \frac{1000}{EW} \text{ (mmol/g)} \qquad (eq.I\text{-}4)$$

***Microstructure of Nafion®**

The microstructure of Nafion® has been extensively studied by SAXS and SANS but is still the subject of active debates. Many models were proposed for the structure of Nafion®. The most relevant ones will be briefly introduced in this part of the chapter.

The first model, so-called "***Cluster-Network Model***" (*Fig. I-7*), was proposed by *Gierke* [10]. This model describes the membrane as a network of ionic clusters connected by channels. The cluster size and its water content change with changing degree of hydration.

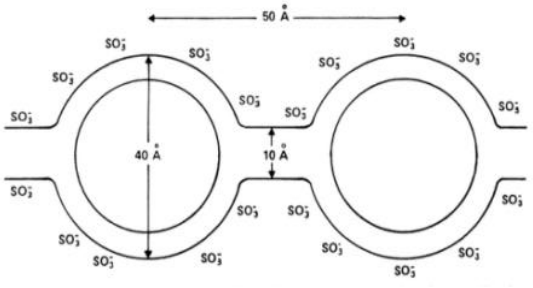

Fig. I-7 *Cluster-network model, as proposed by Gierke, for Nafion® ionomers, representing postulated pores that connect adjacent inverted miscelar structures.*

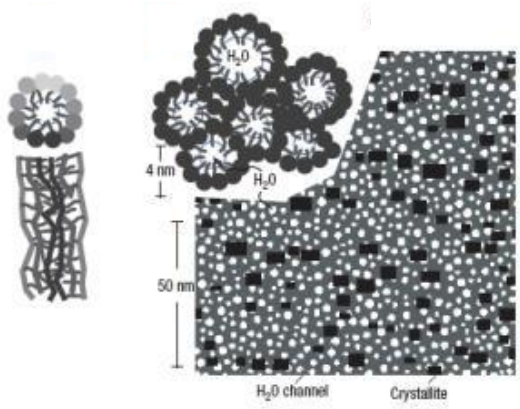

Fig. I-8 *Parallel Water Channel Model, proposed by Schmidt-Rohr, Cross sectional and transverse views of an inverted micelle cylinder*

In 2008, *Schmidt-Rohr et al.*[11] proposed the ***"Parallel Water Channel Model"*** (*Fig. I-8*), which describes Nafion® as a matrix of embedded parallel cylindrical water nano-channels where the sulfonic acid groups auto-organize themselves into the form of channels.

Between 2002 and 2004, *Rubatat et al.* [12] proposed the "***Polymer Ribbon Model***" and hypothesized that the polymer formed elongated aggregates with a locally flat interface (ribbon) embedded in a continuous ionic medium (*Fig. I-9*). This cylinder structure surrounded by the ionic groups and water molecules was proposed to interpret scattering data obtained by SAXS and SANS in different swelling states in a very wide range of *q*-vectors. A network of elongated polymer aggregates for the diluted systems and bulk membranes were established. The organization of the polymer aggregates into bundles has been suggested after AFM (Atomic Force Microscopy) characterizations. This model, which has been supported by Kreuer [9], appears to be the most realistic structural model for Nafion® to date.

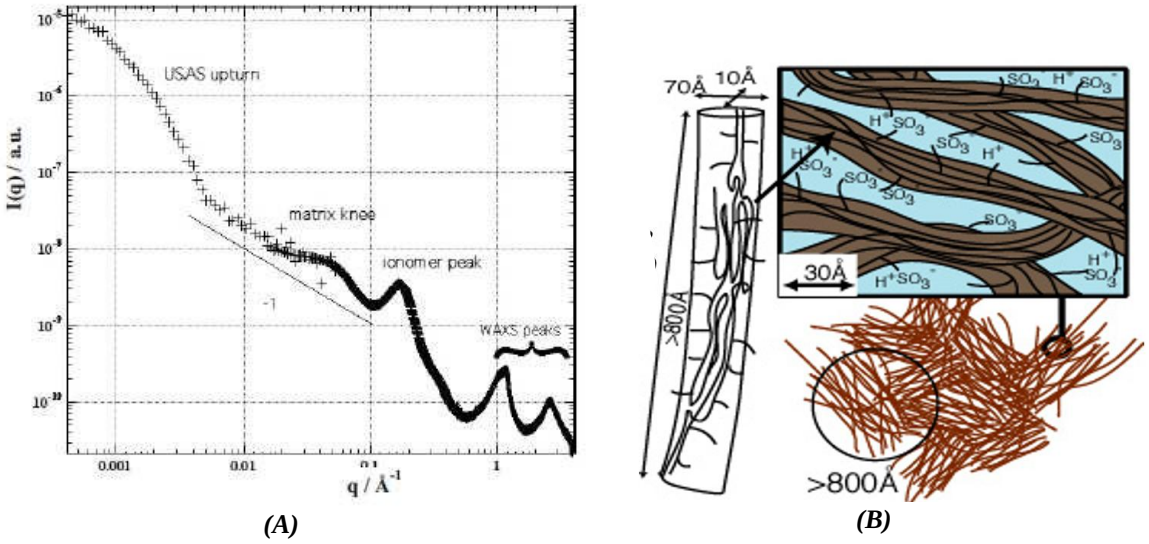

Fig. I-9 (A) *Scattering Spectra of Nafion® and (B) Schematic representation of model of elongated aggregates proposed by Rubatat.[12]*

Rubatat and co-workers obtained the most complete scattering spectra of Nafion® (*Fig. I-9 (A)*). Scattering spectra is complex and characterized by intensity variations reflecting the multi-scale organization. There are three main features in the spectra, corresponding to different typical length scales measured by USAXS (Ultra Small Angle X-ray Scattering), SAXS/SANS (Small Angle X-ray Scattering / Small Angle Neutron Scattering) and WAXS (Wide Angle X-ray Scattering) respectively:

1) A small angle upturn was evidenced by USAXS at ultra-low values of q, typically $q<4.10^{-3}$Å^{-1}. This upturn is related to the fluctuation in electronic density at large scale (on the order of several hundred Angstroms) showing evidence of large-scale organization of domains into bundles.

2) Two peaks were evidenced in the typical small-angle region. SANS and SAXS are complementary techniques because X-Rays interact with electrons surrounding the atoms while neutrons interact with the nucleus of the atoms. Different contrast situations therefore arise in the SAXS and SANS experiments. Results were obtained in the q-range between 0.01-0.2 Å^{-1}. The two observed correlation peaks were interpreted as follows:

-The peak measured at typically $0.1<q<0.2$ Å^{-1} is the signature of ionomer membranes microstructure. It is called the "ionomer peak", and originates from the hydrophobic-hydrophilic nano-phase separation. The associated characteristic distance corresponds to the distance between ribbons within the model of Rubatat, and distance between ionic aggregates within the model of Gierke.

-The "Matrix knee" is positioned around q~0.05Å^{-1} over a q^{-1} slope. This peak is often correlated to the amount of crystallinity in the polymer matrix, but its origin is mostly unknown.

3) In the WAXS *q*-range, typically between 0.6 - 4Å^{-1}, several peaks are measured. These peaks are related to the organization at molecular level. The first peak located at *q*~1.2Å^{-1} is the combination of a broad halo and a diffraction peak which are associated to characteristic distances between perfluorinated polymer chains. The second one located at *q*~3Å^{-1} is associated to the intra-chain correlations of Nafion® [13].

**** Functional properties of Nafion®***

The glass transition temperature (T_g) of Nafion® in the dry state is about 110 °C [14]. Beyond this temperature, rearrangement of the chains and a structural modification at the molecular level of the membrane occurs [15]. These property changes can reduce the mechanical and chemical stability of the membrane, its performance and its lifetime.

Mechanical properties

At room temperature, the Nafion® membrane (dry or wet) behaves as an elastomer (rubber) which has a low hardness[14]. *Tang et al* [16] studied the Young's modulus evolution in Nafion® membranes under RH% at different temperatures. Young's modulus of the membrane decrease as humidity and temperature increase (*Fig. I-10*). Higher temperature leads to lower break strength and higher break strain. However, humidity has little effect on the break stress and elongation at break.

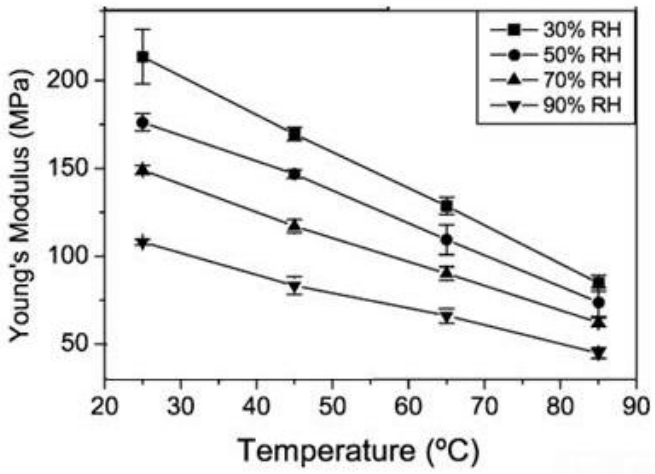

Fig. I-10 *Young's modulus as a function of temperature at various relative humidities[14]*

For temperatures above 120°C the Nafion® is submitted to mechanical stresses inducing to flowage of the polymer which results in permanent deformation of the membrane, decreasing the proton conductivity [17].

Thermal properties

The thermal degradation of membranes occurs in three distinct stages (*see Fig. I-11*)[18]

1.- Desulfonation process: between 300 and 400 °C
2.- Decomposition of the side chain: between 400 and 470 °C
3.- Decomposition of the main chain of PTFE: between 470 and 560 °C

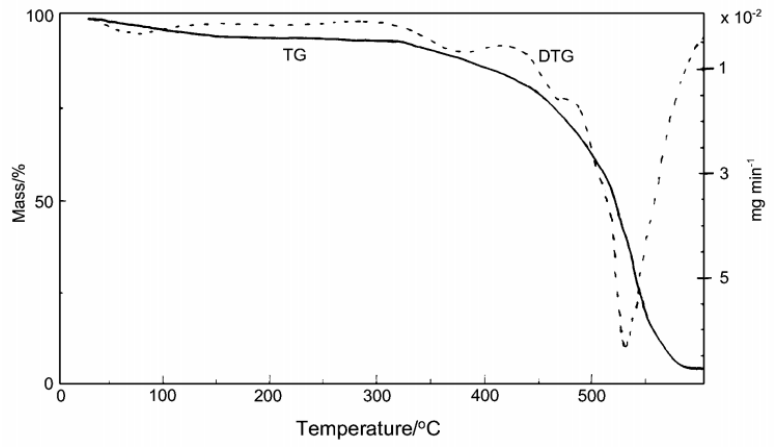

Fig. I-11 *TG (—) and DTG (- - -) traces of Nafion®-H membrane at a heating rate of 20ºC min^{-1} under N_2 atmosphere[18]*

Water uptake and proton conductivity

As expected, several studies [9, 14, 19, 20] have shown that the water uptake of the perfluorosulfonic acid membranes increases as their equivalent weight EW decreases, i.e. when the concentration of ion exchange groups (hydrophilic) increases. In addition, in liquid water the water uptake increases with increasing temperature [9] *(see Fig. I-12*).

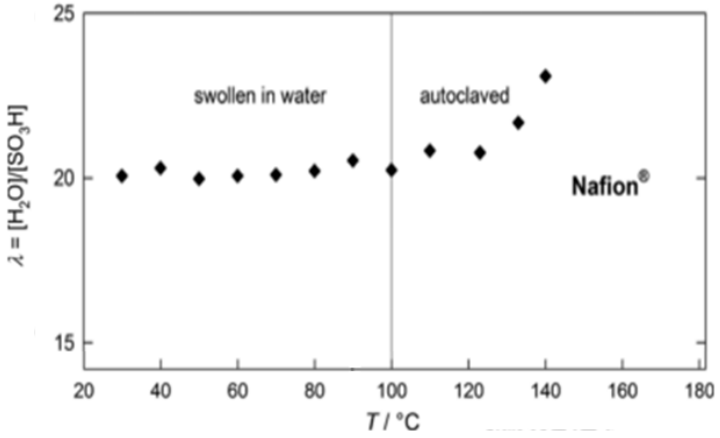

Fig. I-12 *Hydration behavior of Nafion® water uptake in terms of hydration number λ =[H_2O]/[−SO_3H] as a function of temperature T/ºC [9].*

Studies have also shown that the proton conductivity increases with temperature in liquid water (~0.0015 $S \cdot cm^{-1}$-~0.015 $S \cdot cm^{-1}$) [20]. Further, it has also been reported that the proton conductivity of perfluorosulfonic membranes strongly depend on the relative humidity RH [17], with a steep increase in proton conductivity along with %RH.(*seen Fig. I-13*).

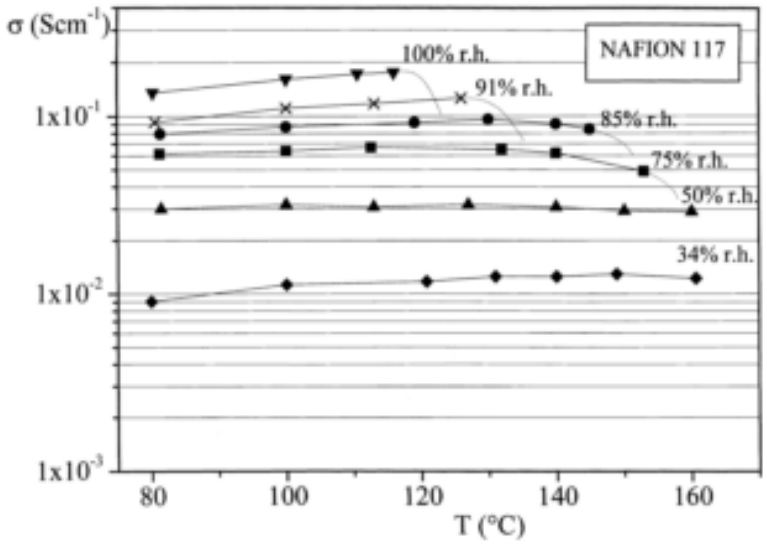

Fig. I-13 *Conductivity of Nafion® 117 membranes at different RH for temperatures increasing from 80 to 100ºC.[17]*

There is a marked effect of relative humidity on the proton conductivity of Nafion®, when relative humidity is maintained constant, the conductivity of the Nafion® remains practically constant in the examined range of temperature. This surprising trend seems to indicate that the conductivity growth expected at increasing temperatures is compensated by some modification of the polymer which decreases the mobility and/or the effective concentration of the charge carriers[17].

I.2.2 Polyaromatic ionomer membranes structure

Polyaromatic ionomers are one of the alternatives to the PFSAs. Several types of sulfonated aromatic ionomers have been studied over the past twenty years: Polyethersulfones (sPES) [21], polyetheretherketones (sPEEK) [17, 22-25], polybenizimadazoles (sPBI) [26-28], polyimides (sPI) [29, 30], polyphenylquinoxalines (sPPQ) [31], polyphenylene oxide (sPPO) [32, 33], polyphenylene sulfides (sPPS) [34].

* sPEEK

In this work, we have used sPEEK membranes, mainly for cost (less expensive than Nafion® membrane) and thermal stability (mechanical) traduced in less chemically stable [35]. In the following we will therefore focus our presentation on the properties of sPEEK.

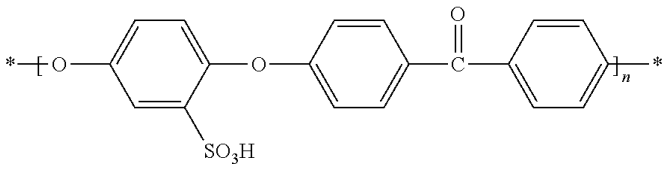

Fig. I-14 *Sulfonated Poly(etheretherketone): sPEEK*

In *Fig. I-14* we show the schematic representation of sPEEK membranes. A few studies have focused on the structural characterization of polyaromatic membranes such as sPEEK [21, 36-38]. The transport properties of some aromatic sulfonated polymers were studied by *Kreuer et al* [21] and compared to Nafion®. It is known that the conductivity of polyaromatic ionomers is much lower than that of Nafion® (117) (for the same ion exchange capacity). *Kreuer's* study shows that the difference between the Nafion® (117) and aromatic polymers is mostly due to the morphology of the membrane and a strong difference in the acidity of ionic functions.

We now briefly review the morphology and functional properties of sPEEK membranes compared with Nafion®.

Microstructure of sPEEK membranes

The morphology of sulfonated polyaromatic ionomer membranes is characterized by a lower phase separation between hydrophilic and hydrophobic domains as compared to Nafion® (117), which presents a sharp nanophase separation [21]. This difference is due to the higher rigidity of the aromatic chain, the lower acidity of the aryl sulfonic acid function compared to the perfluoro sulfonic acid function of Nafion®, and the hydrophobicity of the PTFE chain of Nafion®. The hydrophobicity of Nafion® is higher than that of aromatic chain of polyaromatic ionomers. As a result of this lower phase separation, it was hypothesized (*Kreuer et al* [21]) that aromatic ionomers are characterized by ionic domains more tortuous and narrower (see *Fig. I-15*).

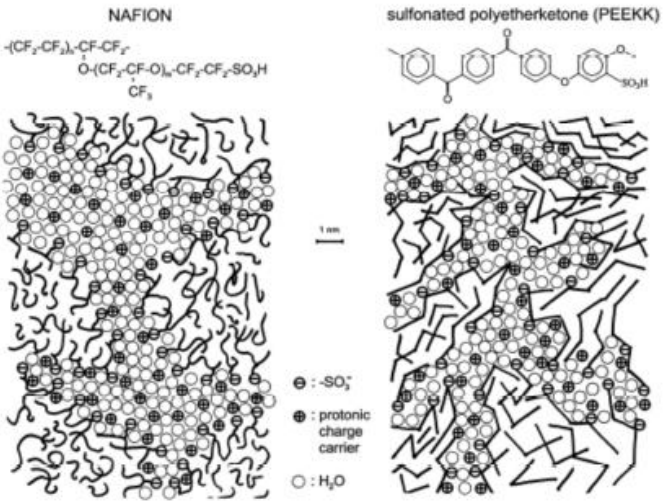

Fig. I-15 *Schematic representation of Nafion® and PEEKK sulfonated morphology [21]*

Generally, in the study of the sPEEK membranes morphology, a single peak was observed in the scattering spectra measured by SAXS or SANS, and was systematically attributed

to the so-called ionomer peak. The nature of this peak is discussed in the literature. *Yang et al.[38]* studied dry sPEEK membranes using different counter-ions and sPEEK of different IEC. They observed only one peak in the scattering profile, which was attributed to the ionomer peak. They concluded that ionic clusters do exist in dry sPEEK membranes, with a small cluster size (i.e. on the order of 27Å) with a small number of sulfonic groups in each cluster. *Kawaguti et al.*[39] showed the presence of an ionomer peak for sPEEK membranes swollen in water or ethanol. Ionomer peak positions and intensities were found to vary according to the solvent and the IEC. The authors concluded that sPEEK membranes present a higher swelling in ethanol than in water. Moreover, it was noticed that higher IECs yield higher swellings. Recently, *Gebel* [40] has investigated the microstructure of sPEEK membranes equilibrated at low and high water contents. He proposed an organization based on ribbon-like aggregates as in Nafion® and determined the sizes of the ribbon-like polymer with at least one dimension close to 23Å. *Portale et al.*[41] showed an improvement of proton conductivity in sPEEK membranes with temperature, which was ascribed to the formation of ionic clusters and increase of swelling. This was hypothesized on the basis of both the increased ionomer peak intensity and shifting of the position towards smaller angles.

Finally, it appears that sPEEK membranes can be designed with various degrees of sulfonation (DS), different casting solvents inducing different membrane cleaning procedures. Therefore, different morphologies were obtained, as seen from the wide span of SAXS spectra with characteristic peaks located at different scattering ranges reported in the literature. A clear picture of the sPEEK membrane morphology can thus hardly emerge.

Functional properties of sPEEK membranes

Mechanical properties

sPEEK membranes are obtained from PEEK membranes. The PEEK membranes are semi-crystalline thermoplastic widely used as high-performance materials, due to their good mechanical, chemical and thermal properties. The mechanical properties of sPEEK membranes are affected by different variables the most significant parameter affecting sPEEK behaviors is the polymer sulfonation procedure. The grafting of SO_3H group on the polymer backbone (position of SO_3H group and extent of sulfonation) modify the chain conformation and therefore leads to the amorphization of the polymer [42].

Thermal properties

The poly(arylene ether ketone)s are thermally stable polymers, while the thermal stability of the derivative sulfonated polymers is gradually deteriorated upon increasing the degree of sulfonation. The degradation of sulfonated derivatives occurs in two steps[43]:

1.- Between 250 and 425 ° C: the thermal degradation of sPEEK membranes is associated with the loss of sulfonic acid groups.

2.- Between 425 and 625ºC: thermal degradation is associated with the decomposition of the polymer main chain.

The glass transition temperature (T_g) of the hydrated membrane is an important parameter that influences the fuel cell performance. Indeed, the maximum operating temperature of hydrated membranes may be restricted. Extensive morphological relaxation occurs at the T_g, leading to adverse effects on polymer properties [44]. In dry sPEEK membranes the T_g increases with increasing DS. This is due to an increase of intermolecular interactions between the sulfonic groups, leading to a more rigid polymer matrix [45]. T_g is strongly reduced in wet membranes as the water plays a plasticizer role, making bonds with sulfonic acid groups. The T_g of sPEEK hydrated membranes decreases with the degree of sulfonation and is found around 50 to 60ºC [42].

Water uptake and proton conductivity

The aim to increase the sulfonation degree of a sPEEK membrane is to improve the hydrophilicity of the membrane, thus to improve their proton conductivity. The water uptake of sPEEK membranes increases when increasing the DS.

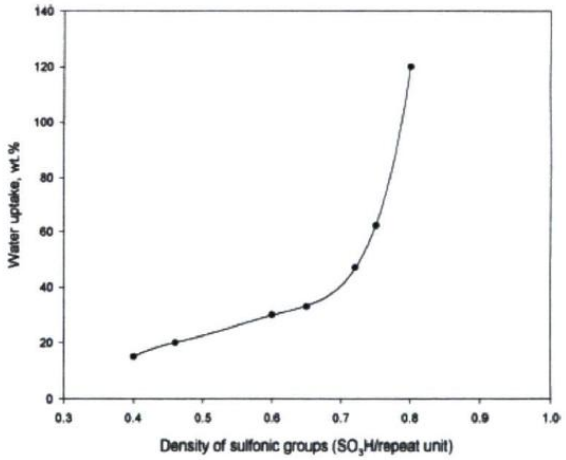

Fig. I-16 *Water uptake of sPEEK membrane immerged in liquid water at room temperature as a function of DS[43].*

Fig. I-16 shows the water uptake at ambient temperature of sPEEK membranes as a function of the density of sulfonic groups (sulfonation degree). The results show that the water uptake of the sPEEK membranes increases linearly up to a DS of 65%, then increases exponentially. The water uptake of sPEEK membranes also increases with increasing temperature of immersion. *Portale et al* [41] observed that in sPEEK, the swelling seems stable before 70°C but increases when the temperature is increased from 70 °C to 87 °C.

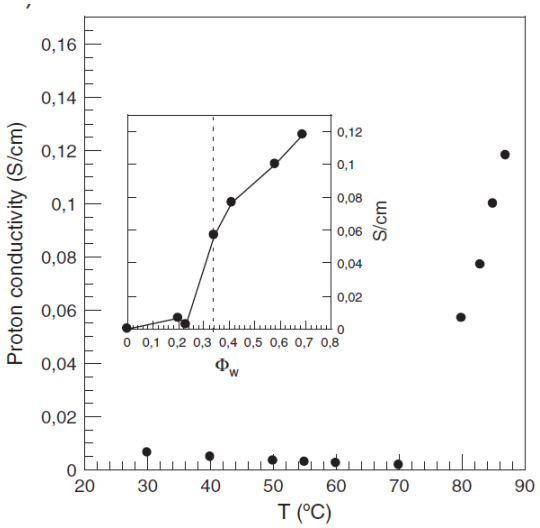

Fig. I-17 *Proton conductivity of s-PEEK membranes as a function of the swelling temperature. The inset shows the proton conductivity as a function of the water content[41].*

High proton conductivities of about 0.1 S/cm (conductivity of a native Nafion® membrane in liquid water at room temperature) (*Fig. I-17*) are reached before irreversible swelling starts. For temperatures above 87 °C, irreversible swelling occurs and the membrane mechanical properties degrade rapidly, resulting in a rapid drop of the proton conductivity (not shown here).

I.2.3 The hybrid membranes

The membranes are one of the critical components of the fuel cell system and must be durable and tolerate a wide range of operating conditions, including relative humidity (RH) ranging from 20% to 100% and temperatures ranging from 40 to 120 °C for transportation applications and >120 °C for stationary applications. Improved membranes that perform better and are less expensive than the current generation of polymer membranes are needed.

One of the solutions for these problems is the development of hybrid membranes, in particular hybrid membranes prepared by sol-gel process. A hybrid membrane is a membrane that is made of two non-miscible phases. One of these compounds is inorganic and the second one is organic. The aim of creating these types of polymer hybrid membrane is generally to combine the respective qualities of each phase to overcome most of their respective weaknesses. To achieve this goal the dispersion of one phase in the other should be good enough to avoid macro-phase separation (of the constituents and therefore of the performances).

Many efforts have been dedicated during the last decade to obtain new hybrid membranes and to compare their performance to the benchmark Nafion®. The use of water retention (and inherently proton conductive) particles or fillers has extensively been studied. Incorporation of oxide particles (SiO_2, TiO_2, ZrO_2, AlO_3) [46-48], heteropolyacids [49-51], zirconium phosphate and phosphosilicates [52, 53] allowed to improve the water content and the performances of membranes compared with Nafion®, when studied at high temperatures and low humidity.

Many studies were carried out to understand the impact of the chemistry and the fabrication methods on the membrane performance. There are four main types of hybrid membranes, characterized by four different morphologies, as displayed in *Fig. I-18* adapted from *Kickelbick* [54].

1) Inorganic particles dispersed in an organic polymer matrix (*Fig. I-18* (*A*))

2) Inorganic reactive nanoparticles dispersed and grafted onto the polymer backbone. (*Fig. I-18 (B)*)

3) Hybrid membranes composed of two interpenetrated networks (IPN), one polymer and one sol-gel phase.(*Fig. I-18* (*C)*). If one phase is not forming a network, then the membranes are referred to as semi-interpenetrating network (semi-IPN).

4) Dual inorganic-organic networks (copolymerization like) (*Fig. I-18*(*D)*).

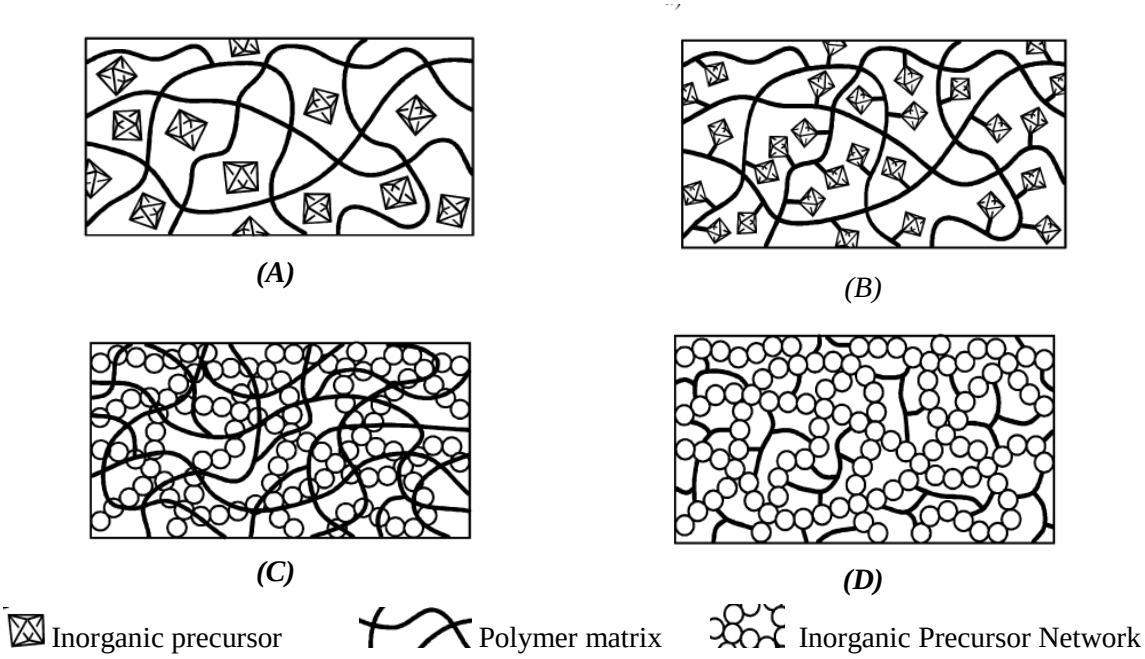

Fig. I-18 *Different kinds of inorganic-organic composite material: (A) embedding of the inorganic precursor into the organic polymer, (B) incorporation of inorganic groups by bonding to the polymer backbone (C)interpenetrating networks (IPNs)and (D)*

The functional properties of the obtained hybrid membranes clearly depend on the dual inorganic–organic hybrid polymer[54], on the chosen strategy (nanoparticles or IPN) and on the quality of the inorganic phase dispersion in the polymer matrix.

In order to understand the preparation routes, we now present the basic principles of sol-gel reactions.

*** <u>Principles of sol-gel reactions</u>**

The Sol-gel process is defined as the conversion of a sol-gel precursor solution into an inorganic solid via inorganic self-condensation reactions induced by water. These reactions will be detailed in *section I.5*, but it is important to first describe how a precursor system is included in an organic membrane.

The sol-gel precursor has the ability to form a durable bond between organic and inorganic materials.

$$(RO)_{4-n}Si\ X_n$$

Fig. I-19 *General formula of silane*

The general formula for a sol-gel precursor is shown in *Fig. I-19*, highlighting the two kinds of groups attached on the silicon atom:

- RO is a hydrolysable group, typically alkoxy. Following hydrolysis, a reactive silanol group is formed, which can condense with other silanol groups, for example, those on the surface of siliceous fillers, to form siloxane linkages. Stable condensation products are also formed with other oxides such as those of aluminum, zirconium, tin, titanium, and nickel. Less stable bonds are formed with oxides of boron, iron, and carbon. Alkali metal oxides and carbonates do not form stable bonds with Si-O-.

- The X group is a non-hydrolysable organofunctional group which can be tailored to functionalize the inorganic phase, like for example to introduce stabilizing groups.

In the next sub-sections we present the routes to prepare the two different families of hybrid membranes, namely membranes prepared by incorporating inorganic particles (case ***A*** and ***B***) and IPN (case ***C*** and ***D***).

I.2.3.1 Inorganic particles dispersed in an organic polymer matrix

There are two ways to incorporate the inorganic phase within a polymer matrix:

1.- The inorganic particles are dispersed (*direct mixing)* in the polymer solution. Membrane casting is mandatory.

2.- The inorganic phase grows up *in-situ* by sol-gel process using chemical sol-gel precursors (*precursor route*).

**** Direct Mixing.*** Direct mixing of inorganic components into the polymer matrix in solution is the simplest method to prepare hybrid membranes (*Fig. I-18*(*A)*) [55, 56].The main problem of this method is that physical mixture of polymers and of inorganic particles may results into phase separation, and therefore lead to particle aggregation [57, 58]. The intercalated polymer-layered silicate materials also depend on the polymer and clay compatibility and the direct mixing of both is only possible by modification of one or both components [59]. These interactions between the polymer and inorganic components may yield to the degradation of the mechanical, optical and electrical properties of the hybrid membrane.

To achieve a better dispersion, the inorganic and organic phases' affinity must be improved. One strategy is based on the grafting of a functional group on the inorganic component to increase interactions with the polymer matrix (Van-der-Waals, hydrogen bonds). Another one is to graft the nanoparticles onto the polymer backbone (*Fig. I-18 (B)*). The use of particles

grafted with a functional group which allows a covalent linkage with the polymer can allow increasing the hybrid phase dispersion in the polymer matrix. Recent studies of *Thiam et al.* showed that novel hybrid membranes based on Nafion® and fibrous material (Pd-SiO_2 fiber) can effectively reduce the methanol permeability while maintaining or improving the conductivity when compared with pristine Nafion® [60, 61]. From their understanding the authors conclude that, the fiber interacts with the Nafion® through hydrogen bonding between the fiber's Si-OH and the SO_3H groups attached to the Nafion®'s side chains. *Kim et al.*[62] also studied sulfonated SiO_2 nanoparticles synthesized by radical polymerization of vinyl-functionalized silica powders and 4-styrenesulfonic acid sodium salt and obtained a Nafion® hybrid membrane with a good dispersion of the nanoparticles, improving both the conductivity and mechanical strength. In addition, the evaluation of single cell performance showed that hybrid membranes exhibited better performances than Nafion®. The maximum power density of the cell reached 129.9 $mW.cm^{-2}$, which is much higher than the value obtained for a Nafion®-based cell (104.6 $mW.cm^{-2}$).

Whatever the above strategies, the quality of the nanoparticles' dispersion into the membrane remains challenging. To overcome this difficulty, the inorganic phase can be formed by *in-situ* condensation of sol-gel precursors into a host ionomer membrane.

*** Precursor's route**. Contrarily to direct mixing, the in-situ approach to obtain hybrid materials is based on the chemical reaction of the precursors either by mixing the precursors and the polymer solution or by impregnation of a host membrane with sol-gel precursors. The organic polymer acts as a reaction medium where nanoparticles are generated from precursors [54, 63-66].The *in-situ* method allows control over the particle size and the morphology [67, 68]. The sol-gel strategy is the most successful chemical process that allows to incorporate nanoparticles into an organic phase [69]. The first studies were based on membranes containing hydrophilic metal oxides formed by *in-situ* sol-gel reaction (SiO_2, TiO_2 ZrO_2) [58]. This method was used to improve water content and conductivity at high temperature. As an example of recent studies, *Liu et al.*[70] prepared via *in-situ* synthesis followed by phosphoric acid doping organic-inorganic composite membranes composed of poly(2,5-benzimidazole) (ABPBI) and polyhedral oligomeric silsesquioxane (POSS). They obtained excellent proton conductivities (above 0.1S/cm at 100~160ºC).

I.2.3.2 Interpenetrating networks

An *Interpenetrating Polymer Network (IPN)* is a polymer comprising two or more networks that are at least partially interlaced on a molecular scale but not covalently bonded to each other and cannot be separated unless chemical bonds are broken [71].

The formation of interpenetrating networks between inorganic and organic component is carried out either by:

- the simultaneous formation of the two networks
- the second network growing in a pre-formed primary one.

The resulting materials should be microscopically phase separated, but macroscopically uniform [72]. The disadvantage of this approach is the stability of the materials:

- Possible incompatibilities between the components generating a macro-phase separation.
- Difficulty to find reactions for the formation of the second network which can be carried out in the presence of the first one.

Often, classical high temperature solid-state reactions for the preparation of the inorganic component is forbidden due to the limited thermal stability of the organic polymers. An ideal procedure for the generation of this type of hybrid material is the sol-gel process because of the corresponding lower processing temperature [73].

Using the sol-gel approach, different strategies for the formation of INP hybrid membranes have been proposed.

1.-Sol-gel process inside a polymer membrane: mixing of the precursor for the sol-gel process with the organic polymer followed by an inorganic hydrolysis and self-condensation reaction. Polymer membranes are swollen in solvent to allow the swelling of the ionic domains of the polymer matrix before impregnation with the inorganic precursor. This method depends on the ability of molecular species to diffuse into the polar regions of the polymer matrix, and is driven by the solubility of the precursor into the solvent of the swollen membranes. A limited membrane swelling could also limit the precursors' content, and it is necessary to achieve an over swelling of the membrane to permit a satisfactory diffusion of the precursors.

Nafion® membranes were impregnated with a sol-gel precursor's solution of different metal alkoxides (Si, Zr, Ti), to form corresponding metal oxides phase by *in-situ* sol-gel reaction inside the Nafion® [58]. In these hybrid membranes the water content and also the mechanical properties were improved. The sol-gel fraction in the obtained hybrid membrane plays an important role on membrane brittleness. A lower conductivity was observed due to the presence of the inorganic network which modified the originally well-defined ionic structure of Nafion® and induces a high tortuosity for the proton path in comparison to the unmodified Nafion® [74]. The study of *Lavorgna et al*.[75] shows that the introduction of a sulfonated silica network in Nafion® membranes improves the conductivity at low relative humidity and high temperature.

2.-Simultaneous formation of the inorganic and organic network. The simultaneous formation of two networks can result in the most homogeneous type of materials if the kinetics of the two networks formation occur simultaneously and rapidly enough to avoid or minimize the phase separation. Applying this method towards hybrid materials three processes are in competition:

- the kinetics of hydrolysis and condensation of the sol-gel precursors,
- the kinetics of the polymerization of the organic phase, and
- the affinity between the two phases to avoid a phase separation .

The adequate solvent reaction and control of these parameters are the main problems of this method.

Joseph and co-workers have studied the effect of silica networks with a phosphonate functionalization on Nafion® membranes[74]. The phosphonate functionalization played an

important role in the water content under low humidity condition. The inorganic network was dispersed in the polymer matrix [74]. The homogeneous dispersion of silica in the polymer matrix was obtained. Nevertheless, decomposition in hybrid membranes occurs at lower temperatures for a modified Nafion membrane than a pristine one.

The formation of homogeneous and optically transparent hybrid materials by the bulk free radical polymerization of 2-hydroxyethylmethacrylate (HEA), simultaneously with the sol–gel reaction of TEOS (tetraethoxysilane) as precursor is an example in using the advantage of an attracting interaction [76]. The resulting materials were characterized by DSC, SEM, TEM, SAXS, and DMA measurements. From these measurements, it was concluded that the two systems form a bicontinuous medium characteristic of a truly interpenetrating material. Additionally, SAXS, SANS, and TEM studies on a HEA/TEOS system revealed that there is a dramatic change in the micromorphologies if the relative rates of the two polymerization processes are changed in such a way that when the sol–gel polymerization is faster the phases are more finely dispersed. If covalent bonds were introduced between the two phases, the homogeneity of the material was further improved [77].

3.-Dual network precursors. The organic polymer and the molecular precursors are combined for the formation of the two networks covalently linked to each other. This is realized in two different ways:

- functional groups for the organic and inorganic polymerization/ auto-condensation process are incorporated in one hybrid molecule, or

- functional groups for the second polymer are incorporated in a preformed polymer of the first type.

Typical examples for hybrid precursors are the commercially available molecules 3-glycidoxypropyltrimethoxysilane or 3-methacryloxypropyltrimethoxysilane. These systems allow either a simultaneous or a sequential formation of two networks[54].

Another possibility for forming such materials is the preparation of organic polymers, which were initiated or quenched by a species that allow the incorporation into sol– gel networks (end-capped polymers) [78].

This method was used in the copolymerization of methacrylate with titanium, zirconium, or vanadium precursors resulting in hybrid organic–inorganic copolymers intimately interpenetrated on a nanometer scale [54].

* Functional properties

The physical properties of hybrid materials are not the simple sum of the individual contributions, but are dependent on the original properties and the interactions occurring at the interface between the system components. Let us summarize the functional properties of materials classified depending on the additive type:

Inorganic fillers - The incorporation of the insoluble inorganic solids, such as silica, zirconia, titania, other metal oxides, and zirconium phosphate to name a few, is intended to improve the membrane characteristics. In general, a stronger interaction along the interface between the host matrix and the filler particles results in a greater modification of the original properties of the membrane[79]. The incorporation of inorganic fillers has resulted in membranes that show slightly lower conductivities than Nafion® at high relative humidities, but higher conductivities at high temperatures and low relative humidities[52, 80].

Heteropolyacids (HPA) -The incorporation of HPAs such as phosphotungstic acid, silicotungstic acid and phosphomolybdic acid has resulted in high proton conductivities for high hydration conditions [81]. However, membranes based on these materials can suffer from acid leaching out of the membrane [52, 82]. One recent innovation to prevent leaching has been to immobilize the HPA incorporating the acid moieties directly into the membrane matrix. These membranes are produced by polymerizing the HPA with various hydrocarbon, aromatic or partially fluorinated linkers [83-85]

Ionic liquids - Ionic liquids (ILs) are salts that are in the liquid state at or close to ambient temperatures. The incorporation of ILs into membranes provides an interesting alternative to water to improve membrane conductivities [86].

Carbon Nanotubes (CNTs) -Single-walled and multi-walled CNTs have been studied as anisotropic fillers. Functionalizing the CNTs with sulfonic acid groups resulted in improving the compatibility with a Nafion® host matrix and increasing conductivity as compared to pristine Nafion®[87]. However, their biggest downfall is that the incorporation of too large amounts of CNTs increases the risk of short-circuit within the cell due to the inherent electronic conductivity of the filler. To reduce the probability of short-circuit, only small amounts of CNTs are used, which results in little improvement of the conductivity and the cell performance [88].

Overall, we have seen that the interplay between the various functional properties (conductivity, thermomechanical, sorption, permeability...) is critical. It highly depends on the chemical architecture. Optimizing one property is often achieved at the expense of another one.

I.3 Polymer electrolyte membrane degradation

The membrane inside a fuel cell is submitted to an aggressive environment: super-acidity, oxidant conditions, elevated temperatures, presence of water and physical constraints. The degradation of the membrane during fuel cell operation leads to a loss in conductivity and increased gas permeation, and can ultimately lead to the system failure. Post-mortem analysis of degraded membrane-electrode assemblies revealed the presence of holes, cracks, membrane thinning and delamination (see *Fig. I.20*). These phenomena are heterogeneous and depend on the fuel cell design and operating conditions. The diagnosis of the origin of such heterogeneous degradation is of utmost importance for improving the fuel cell lifetime [89]. It is commonly accepted that two types of degradation occur: physical and chemical ageing. These processes are also believed to be intercorrelated (for instance, membrane thinning can occur due to chemical attacks and loss of ionomer content, and the thinned regions become more sensitive to physical constraints). A lot of efforts are devoted to the basic understanding of ageing mechanisms in order to predict the membrane degradation and therefore limit it. However, there are very few experimental tools to investigate the *in-situ* behavior of the fuel cell and monitor the ageing process. Hence, *ex-situ* tests are extensively used and very valuable to provide information on the mechanisms. In this section we briefly summarize the mechanical and chemical degradation mechanisms in the two types of membranes at stake, i.e. Nafion® and sPEEK.

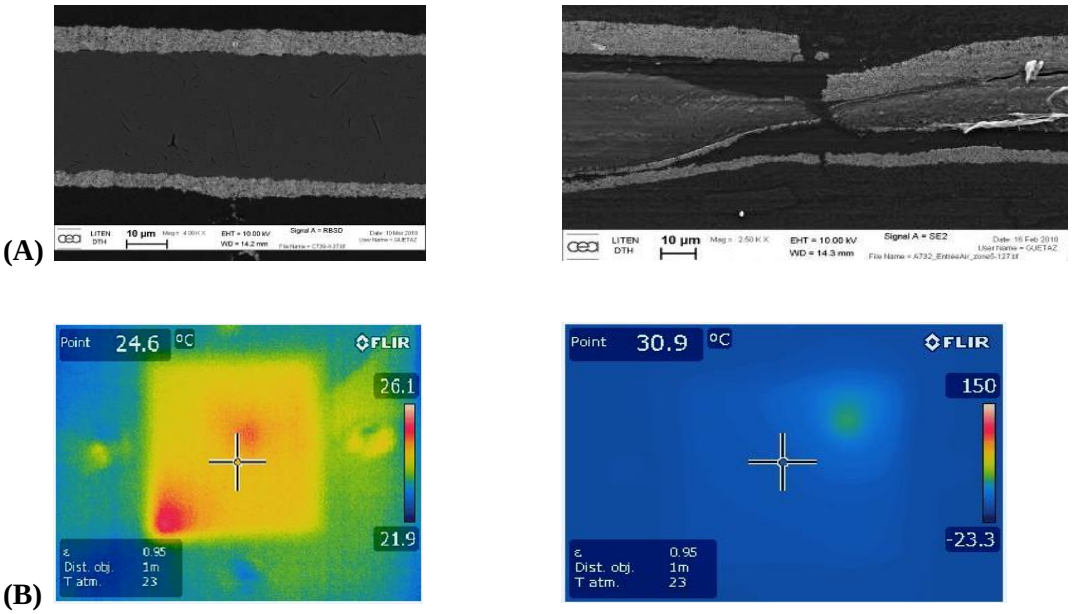

Fig. I-20 *Consequences of mechanical and chemical degradation of polymer membranes,(holes, cracks, membrane thinning and delamination) yield to a low conductivity, higher permeability (A) TEM images showing membrane breaking.(courtesy of L. Guétaz) (B) IR camera images showing the presence of holes (red zones) (coutesy of R. Vincent, CEA Liten)*

I.3.1 Mechanical degradation

Mechanical degradation generally implies microscopic and macroscopic defects induced under the influence of mechanical constraints. The electrode-membrane assembly is prepared by

hot pressing the electrodes onto the membrane. Then the MEA is sandwiched in between bipolar plates serving as current collectors (via ribs) and gas distributors (via channels). Therefore, the hydrated membrane is subjected to different physical constraints under the ribs (compressive forces) or under the channels (swelling of the membrane) of the bipolar plates (*Fig. I-21*). In addition, during fuel operation, the membrane can be subjected to swelling/unswelling cycles due to the on-off sequences of automotive applications (modification of the state of hydration of the membrane). As seen in *Fig.* , highly heterogeneously degraded zones were evidenced on aged membranes, both in-plane and through the membrane thickness, depending on the membrane position relative to gas inlets, ribs, or channels[90].

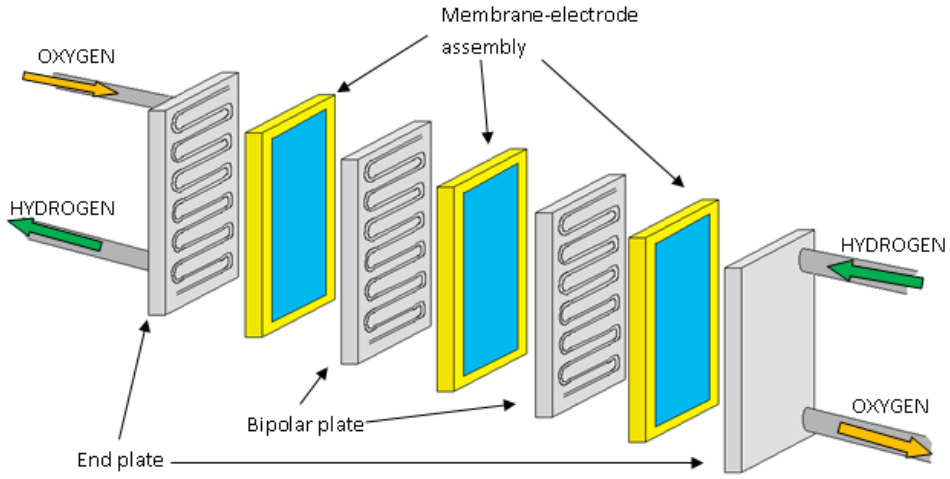

Fig. I-21 *Membrane-electrode assembly MEA. [91]*

Tang et al [16] conducted cyclic stress tests on membrane and found that the significant dimensional changes of the membrane were observed and the microstructure breakdown appeared on the membrane surface when the cyclic stress was over 3.0MPa. This result indicates that the PEM can be fractured under much lower stress than ultimate strength when it is subjected to the condition of fatigue. The authors also reported that the stress induced by temperature variations is much smaller than the stress under RH cycling tests. However, they concluded that the membrane degradation was accelerated significantly when the cyclic operations of temperature and humidity are applied to membranes simultaneously.

I.3.2 Chemical degradation

Chemical degradation refers to the chemical oxidation of the membrane. It is commonly believed that the membrane is attacked by highly reactive oxidative specie (H_2O_2) and radicals (HO•, HOO•) generated by an electrochemical or chemical reaction of hydrogen and oxygen at a platinum catalyst [92]. The radicals are highly reactive due to their unpaired electrons and induce chemical reaction like abstraction of a labile H along the polymer chain or with weak polymer endgroups of the macromolecules.

Two main processes are identified:

- At the **anode** [93-95], HOO• radicals originate from a H• recombination with oxygen molecules permeating through the membrane (H• being induced by the hydrogen reaction on the catalyst surface).

$$H_2 + Pt \rightarrow Pt\text{-}H \text{ (at anode)} \quad (eq.I\text{-}5)$$

$$Pt\text{-}H + O_2 \text{ (diffused through PEM to anode)} \rightarrow HOO\bullet \quad (eq.I\text{-}6)$$

$$HOO\bullet + Pt\text{-}H \rightarrow H_2O_2 \quad (eq.I\text{-}7)$$

The dissolution of Pt and diffusion inside the membrane leads to the formation of a condensed Pt layer (*Fig. I-22*).

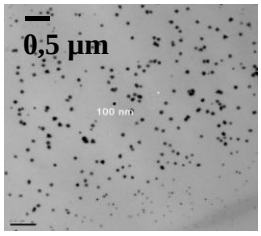

Fig. I-22 *Pt dissolution and diffusion inside the membrane (courtesy of L. Guétaz, CEA Liten)*

- At the **cathode** [89, 96], an incomplete reduction of oxygen (two electrons instead of four electrons) leads to the formation of HOO•, HO • radicals or H_2O_2.

$$O_2 + 2H+ + 2e- \rightarrow H_2O_2 \text{ , } E_0 = 0.695V \quad (eq.I\text{-}8)$$

The three reactive oxygen species (H_2O_2, HOO•, HO•) have been detected *in-situ* [97] by chemical analysis of the water produced at the cathode during fuel cell operation. The presence of these radicals induces different types of chemical attacks depending on the nature of the radical and the polymer electrolyte.

** Chemical degradation of Nafion®*

The formation of degradation products as HF, SO, SO_2 and H_2SO_3 was evidenced by direct gas mass spectroscopy of the cathode outlet gas [98].On the basis of the analysis of these eluted products, some mechanisms were proposed to explain the degradation of the Nafion® membrane which rely on main chain or side-chain scissions.

A) Unzipping mechanism after HO• radical attack. Chemical degradation of PFSA membranes was reported and explained by attack of the HO• radical on the terminal –COOH group in the perfluorinated main chain. This unzipping mechanism is shown on *Fig. I-23* [99].

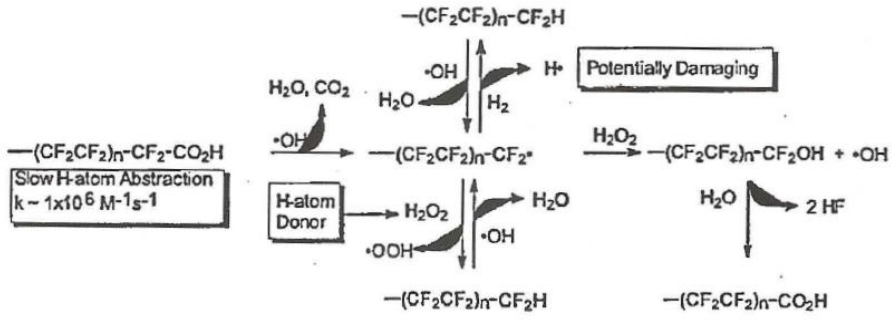

Fig. I-23 *Mechanism of degradation by attack of the HO• radical on the terminal COOH group [99]*

In this scenario, the degradation of PFSA material is strongly related to the existence of the carboxylic (COOH) acid group in the perfluorinated main chain. The degradation mechanism of the carboxyl end groups by free radicals has been exemplified by Fenton test [79, 80]. In a Fenton test hydroxyl and hydroperoxyl radicals are originated from the catalytic decomposition of H_2O_2 by Fe^{2+} and Fe^{3+}, (*eq.I-9)* (*eq.I-10*).

$$Fe^{2+} + H_2O_2 \rightarrow Fe^{3+} + HO\bullet + OH^- \qquad (eq.I\text{-}9)$$

$$Fe^{3+} + H_2O_2 \rightarrow Fe^{2+} + HOO\bullet + H^+ \qquad (eq.I\text{-}10)$$

The free radicals are generated by this process and then engaged in secondary reactions as chemical degradation of membranes. The radicals induced the chemical degradation of the membrane.

B) Side-chain attack by H•- The reaction of the OH radical with H_2 leads to the formation of an H• radical, which produces additional degradation reactions:

1.- Breaking the C–F bond of a tertiary carbon to form HF,

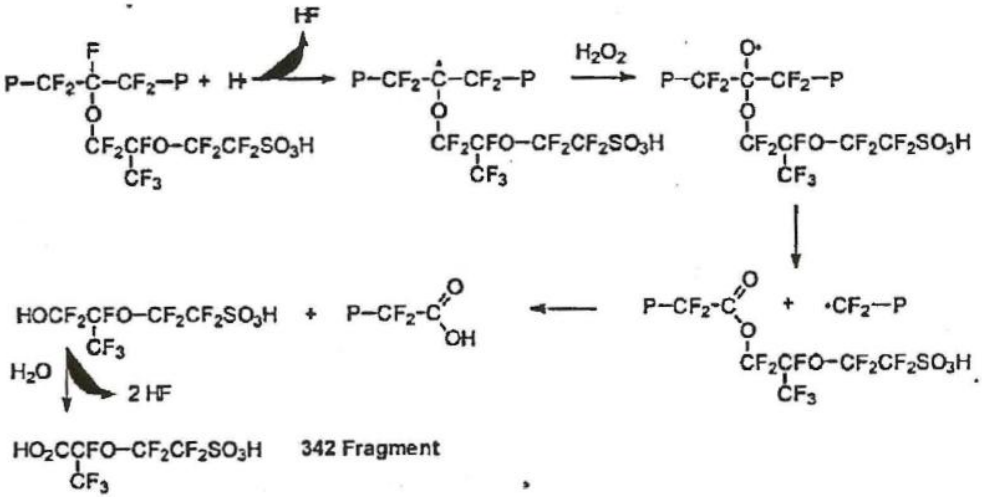

Fig. I-24 *H radical attack breaking the C–F [99]*

2. - Attacking the sulfonic acid group to form SO_3 and fluoro radical. Propagation of the degradation along the side chain induces main chain scission:

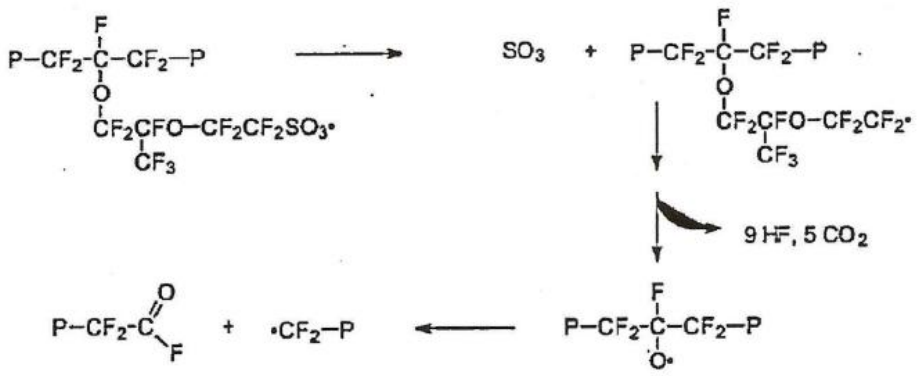

Fig. I-25 *Propagation of fluorinated radical [99].*

* *Chemical degradation of sPEEK membranes*

As PFSA materials, the sPEEK membrane is quite sensitive to the radical attacks produced by HO• and HOO•. *Perrot et al.*[92] proposed a degradation mechanism presented in *Fig. I-26*, where the main degradation process results from the addition of a HO• radical on the non-sulfonated aromatic ring. Then, the phenolic group oxidation leads to successive chain scissions with a preferential consumption of the terminal units. Although the degradation products differ from the monomers, this mechanism can be considered as analogous to an "unzipping" process.

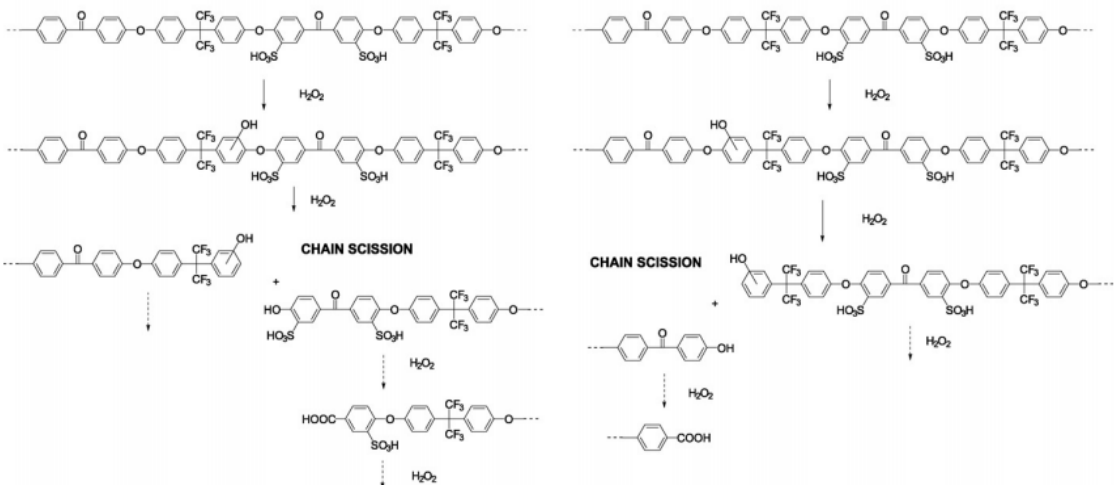

Fig. I-26 *Ageing path of sPEEK membranes (a) hydrophilic unit and (b)hydrophobic unit.*

Chemical and physical ageing of polymer electrolyte membranes is a major problem in fuel cell technology. Improving the lifetime of the various components of the fuel cell, in particular the membrane, is an actual target for further industrial deployment. Modern strategies are needed to be developed to limit the degradation of the polymer and increase the durability while keeping/improving the performances.

I.4 Stabilization strategies to improve the ionomer membranes

A brief review of the strategies described in the literature to design more durable membranes is presented in this section. These strategies are developed to improve the proton conductivity and minimize the chemical and mechanical degradation. We will summarize the performances and durability of hybrid membranes and present the advantages and drawbacks of the different routes. The design of more durable membranes is extremely challenging because one key property (lifetime) is generally improved at the expense of the other (conductivity).

I.4.1 Improving the proton conductivity

To obtain membranes with better performances than Nafion® membranes, the proton conductivity must be increased over 100 $mS.cm^{-1}$.

- *Past and ongoing strategies*: increased sulfonation extent, increased water retention via the dispersion of acid additives/hydrophilic nanocharges, high ionic conductivity in the dry state obtained by addition of proton conducting ionic liquids, synthesis of block copolymers with optimized self-assembled nanostructure.

- *Drawbacks*: such strategies can result into excessive membrane swelling, poor mechanical properties, poor additives dispersion or their elution, and therefore a limited efficiency. Final morphologies of block copolymers membranes can hardly be predicted.

I.4.2 Improving the mechanical properties

It is necessary to obtain suitable thermo-mechanical properties at any hydration level to withstand the shear stress of the swelling/drying cycles, the mechanical pressure of the bipolar plates, and to allow operating temperatures up to 150 °C.

- *Past and ongoing strategies*: increase the mechanical properties (Young modulus, tensile strength, elongation at break, mechanical transition T°) via the use of fillers/nanocharges/nanofibers, polymer cross-linking, IPN (one network for the mechanical strength, the other for the proton conduction) and copolymers.

- *Drawbacks:* improving thermo-mechanical properties often results into a drop of the proton conductivity due to a negative impact of the above strategies on sulfonated groups content and/or membrane nanostructuration (phase demixing for IPN). Fillers/nanocharges have limited impact on the mechanical transition temperatures whereas cross-linked and IPN membranes can become brittle. Mechanical limits of the copolymer strategy can arise from their low molecular weight.

I.4.3 Chemical stabilization improving durability

The durability of membranes can be improved by chemical stabilization to prevent the polymer membrane oxidation and to control the chemical and physical ageing. Stabilizers are chemical substances which are added to polymers in small amounts (in general, at most 1-2%) and

are capable, of trapping emerging free radicals or unstable intermediate by-products (such as hydroperoxide) in the course of self-oxidation and transform them into stable end-products.

A general scheme of inhibition of thermo-oxidative degradation is presented in *Fig. I-27*

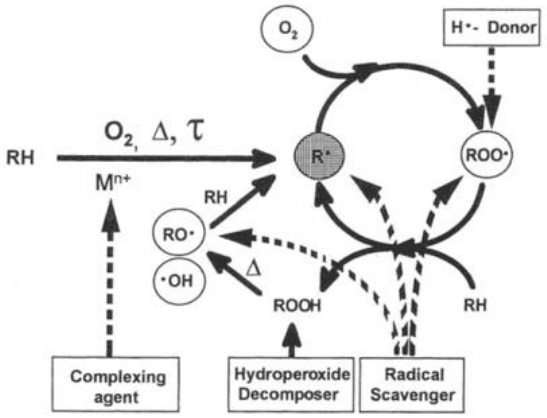

Fig. I-27 *Schema of inhibition of thermo-oxidative degradation [100]*

For the purpose of increasing durability of polymer *Table I-3* gives few examples of the conventional stabilizers:

Table I-3 *List of conventional stabilizers*

Remarks Example	Remarks Example	Example
Light screeners	Act as shield between radiation and polymer	Carbon black [101]
UV absorbers	Absorbs UV light	Dihydroxybenzophenones [101], benzotriazoles [102]
Anti oxidants	Inhibit the oxidation processes	Hindered phenols, hindered amine light stabilizers [100]
Quenchers	Reacting with excited state singlet/triplet to result in non-reactive species	Metal chelates [102, 103]
Radical scavengers/traps	By hydrogen donation to the radical	Mercaptans, quinines, polynuclear hydrocarbons, hindered amine light stabilizers [100]
Peroxide decomposers	By donating electron to form peroxide anion	Alkyl xanthates, N,N-disubstituted dithiocarbamates and dithiophosphates[103, 104] Organosulfur compounds
Nucleating agents/fillers	Reducing the chain mobility and diffusivity of attacking sites	Metal salts, cyclic bis-phenol phosphates [102], dibenzylidene sorbitol[105], dicarboxylates

- *Past and ongoing strategies*: Our interest is based on the radical scavengers and peroxide decomposers, which allow preventing the membrane degradation by reaction with hydroperoxides or radicals still formed. *Mikihailenko* [106] presented a sPEEK/catechin blended membranes.

Catechin exhibited a pronounced inhibition impact on •OH generation [107]. *Zhao et al*.[108] also proposed to increase the durability by dispersing in the membranes manganese oxide or oxidation stabilizer to trap the hydrogen peroxide/free radicals. The most frequently used oxidation stabilizers are amines and hindered phenols. Inter Penetrated Networks (IPN) were also designed to limit the impact of chemical and physical ageing and reduce the membrane permeability. Stabilizers were used to prevent the polymer membrane oxidation, and finally controlled process approaches[109].

- *Drawbacks:* mechanical limitations of modified membranes strategies can result into membrane failure and insufficient durability (low mechanical transition temperature let device hotspots turning into membrane pinholes). Classical additives drawbacks (insufficient dispersion, potential elution) possibly worsen by potential physico-chemical interactions with the membrane which could exhibit lower chemical stability, reduced conductivity and deteriorated performance level [106].

For fuel cell applications we propose the organosulfor compounds as stabilizer to use organosulfur group like thiol and disulfide units (-SH or -S-S-) as sacrificial group to prevent the membrane degradation. In addition the oxidation of these groups will lead to the formation of additional sulfonic acids groups and therefore an improvement of the membrane conductivity.

I.4.4 Conclusions: towards new high performance and durable hybrid membranes

None of the existing solutions to prepare more durable membranes fulfills the objective of increasing the durability at low cost and high performances. It is still a challenge to simultaneously improve the proton conductivity and thermo-mechanical properties, while limiting the chemical degradation. An interesting alternative route is to prepare hybrid membranes using the sol-gel process.

The idea is to improve all the properties of actual commercial polymer electrolyte membrane via a versatile approach based on sol-gel chemistry. The sol-gel process is a promising route as it offers invaluable and specific advantages:

- The sol-gel precursors can be easily introduced into a host commercial membrane because sol-gel process is carried out in water/alcohol mixtures which are compatible with the membrane hydrophilicity.

- The sol-gel 3D network can be tailored provided by chemical reactivity to hybrid membranes. To improve the device lifetime, the reactive groups formed by the 3D network can be designed to inhibit the membrane chemical degradation.

The sol-gel 3D network can play the role of a mechanical reinforcer, the crosslink density can be easily tuned through the sol-gel chemistry (pH, concentration, temperature…) In the next section we will present the parameters and conditions required to elaborate a hybrid membrane by sol-gel process.

I.5 Elaboration of hybrid membranes by sol-gel process

The sol–gel method for the preparation of organic–inorganic hybrid membranes has been extensively studied [58, 63, 82, 110-114]. It appears attractive because it offers in principle several obvious advantages[115]:

- Low processing temperature (room temperature)
- High homogeneity and purity of resulting materials
- Possibility of various forming process.

The general concept of sol-gel will be briefly introduced in the next part of this section with the chemistry principles of sol-gel reaction and their key parameters. Sol–gel reactions involve two consecutive steps: hydrolysis of Si alkoxides to produce hydroxyl groups (*eq. I-11*) and their self-condensation (*eq. I-12* and *eq. I-13*) to lead to siloxane bonds and the formation of a linear or 3D network according to the functionality of the sol-gel precursor (number of alkoxides groups per precursor molecule).

Hydrolysis:

(*eq. I-11*) [116]

Condensation:

(*eq. I-12*)[116]

(*eq. I-13*)[116]

When we have four hydrolysable groups the schematic representation of the resulting sol-gel network is the following *Fig. I-28*.

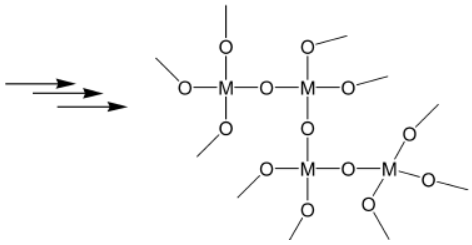

Fig. I-28 *Schematic representation of sol-gel network for $M(OR)_4$*

I.5.1 Sol-gel reaction key parameters: pH, solvent, water/alkoxy ratio.

Numerous parameters have a crucial influence on the sol-gel reaction with a direct impact on the morphology of the inorganic phase and therefore on the properties of the resulting material. The process depends on several experimental variables such as pH, nature of solvent, water/alkoxy ratio, reaction time, reaction temperature, and both drying and curing conditions.

We will present the different experimental variables one by one. This brief summary will lead to the choice of the ideal conditions to develop our hybrid membrane's strategy.

I.5.1.1 pH/Catalysis

The sol-gel process is catalyzed by acids or bases (*Fig. I-29*). pH of the solution controls the kinetics of hydrolysis and condensation reactions. However, the acidic or basic catalyst choice has strong impact on the sol-gel morphology.

Acid Catalysis

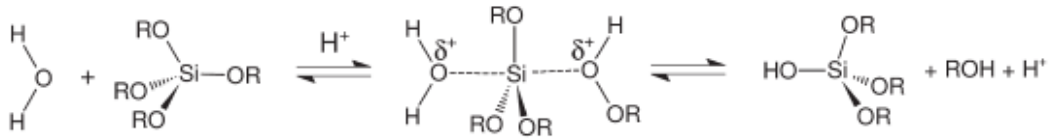

Base Catalysis

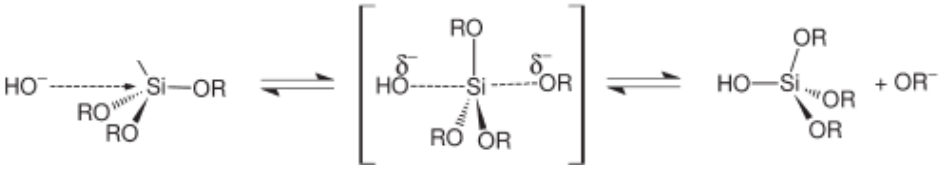

Fig. I-29 *Mechanism of condensation depending on the type of catalyst used in the silicon-based sol–gel process[54].*

In *Fig. I-30* we observe the influence of the pH on the relative rates of hydrolysis and condensation reaction of $Si(OR)_4$

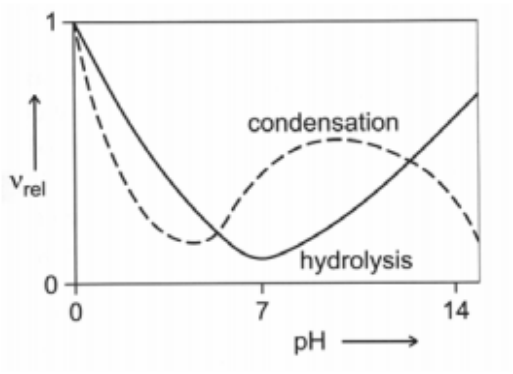

Fig. I-30 *Dependence of the relative rates of hydrolysis and condensation reaction of $Si(OR)_4$ with the pH[117].*

The rate of silicon alkoxides hydrolysis exhibits a minimum at pH = 7 and increases exponentially at both lower and higher pH. That is in contrast with the rate of condensation, which exhibits an exponential increase for pH <4, a minimum at pH = 4.5 and a maximum around pH = 8.

The pH is therefore a relevant parameter to control the sol-gel network morphology through the control of the relative rates of hydrolysis and condensation of the sol-gel precursors. Under acid catalysis conditions:

- The hydrolysis kinetic is favored instead of the condensation's one, which generally starts when hydrolysis is completed [82]. Thus, it yield primarily linear or limited branched (pore size < 2 nm) sol-gel phase (*Fig. I-31 (A)).*

Under base catalysis conditions:

- Condensation is faster than hydrolysis, resulting in highly condensed constituent (*Fig. I-31 (B)*) that may agglomerate into fine particle and finally into mesoporous gels (2 nm < pore size < 50 nm) [82].

(A) ***(B)***

Fig. I-31 *Schematic representation of the sol-gel network morphology in the case of (A)acid- and (B)base-catalyzed reactions[82]*

Therefore, we understand that the pH not only plays a major role in the mechanism (hydrolysis and condensation) but also in the resulting network morphology with a direct influence on the final material's properties like the sol-gel permeability to gas.

I.5.1.2 Solvent

The solvent plays an important role in sol-gel reactions to homogenize the reaction mixture. The polarity of solvent has an influence on the reaction rate and the structure of the final sol-gel network. Polar solvent stabilize polar gels by hydrogen bonding and non-polar solvents are better for systems which are not completely hydrolyzed. A water-miscible alcohol is commonly used as a solvent. Alcohol is also a reaction byproduct, therefore identical alkoxy group will be chosen for the alcohol solvent and the sol-gel precursor in order to avoid the introduction of different alcohol solvent during the hydrolysis step [69]. This solution gives the best control on the kinetics of reaction.

I.5.1.3 Water/Alkoxy ratio

The amount of water used in the initial sol-gel solution can significantly affect the precursor's formation. Depending on the chosen water/alkoxy group ratio we will favor either the hydrolysis or condensation reactions [73, 118]:

-Ratios of water/alkoxy group R ≤ 2 favor the condensation reaction. (dense condensed species, fine particles agglomeration)

-Ratios of water/alkoxy group 2 < R ≤ 4: make the hydrolysis to proceed faster, and the condensation slower (primarily linear or limited branched networks)

-Ratios of water/alkoxy group R > 4: give very loose gel networks with high porosity and smaller particles.

-Ratios of water/alkoxy group R > 12: only dense and cracked aerogels will be formed

I.5.2 Drying and Curing of membrane

The completion of the self-condensation of the precursors can be activated by the temperature or pH. The most commonly used procedure is to dry membranes (heating). This procedure not only removes solvents and volatiles byproducts but also drives the condensation of -MOH groups to a greater degree [58]. During the drying process, the liquid flows from the interior of the gel body to its surface. If the network is not completely condensed, the neighboring OH groups can be close enough to condensate (covalent bond) together to lead to a greater degree of condensation [119]. The complete drying of the membrane has to be carried out to ensure the complete condensation of the sol-gel to achieve stable membrane's performances.

I.6 Conclusions

Many efforts have been dedicated during the last 10 years to the development of new hybrid membranes. Different types of hybrid membranes were obtained corresponding to different strategies of elaboration (dispersed nanoparticles or IPN) the best one being the sol-gel process.

This strategy allows controlling the size and morphology of the inorganic phase. The introduction of inorganic oxides into a host polymer membrane reduces its performances due to the interconnected inorganic network formation. However, certain types of precursors with specific functional groups allow improving the water retention, conductivity and mechanical behavior comparing with the pristine membrane.

To obtain homogeneous hybrid membranes by sol-gel process we can proceed by:

- condensation of the sol-gel precursors in a polymer matrix solution. Then, the composite mixture is casted to obtain the hybrid membrane.
- impregnation and condensation of the sol-gel precursors into a host polymer membrane. Only this second protocol will allow keeping, in part, the morphology of the pristine membrane.

The morphology of the hybrid membranes obtained by sol-gel reaction is influenced by different parameters, like temperature, time, pH, solvent and the water/alkoxy ratio. We understand that the pH and the water/alkoxy ratio have a strong influence on the morphology of the sol-gel network. The solvent where the reaction will take place has an influence on the reaction itself but also on the swelling behavior of the polymer electrolyte membranes. This swelling must be controlled because it governs the good impregnation of the precursors. Controlling the sol-gel process up to the final curing of the hybrid membrane, we will obtain a complete sol-gel condensation, therefore leading to reproducible final products.

CHAPTER II

sPEEK MEMBRANE MORPHOLOGY

In this chapter, we will present the study of sPEEK membrane morphology. The morphology of ionomers largely determines their functional properties, such as conductivity, swelling or/and thermo-mechanical properties. The understanding of the microstructure of proton-conducting membranes and its evolution as a function of water and ion content is considered to be of primary interest for the development of efficient alternative membranes to Nafion®. Yet, the morphology of ionomers is very complex and only partially understood, as shown in the many discussions in the literature [120, 121]. We start this chapter with experimental section, which describes the materials and methods used during this work. In *section II.2*, we present the results obtained by Small Angle X-Ray Scattering (SAXS), Small Angle Neutron Scattering (SANS) and Wide Angle X-Ray Scattering (WAXS) for sPEEK membranes conditioned to different water contents. The principles of the scattering experiments are presented in *Annex A.3*. We expose a new interpretation of correlation peaks in sPEEK membranes including a complete study of the evolution of the scattering profiles upon water uptake. These results will be compared with the functional properties of sPEEK in the same conditions. The impact on the morphology of the oxidative treatments is also studied in the last part of this chapter.

II.1 Experimental section: Materials and Methods

In this section we first describe the materials and methods that were used. Then we detail the results obtained on the microstructure by means of small angle scattering techniques on the microstructure. We will also discuss the influence of the microstructure evolution with hydration on the functional properties. A comprehensive understanding of SAXS and SANS profiles will allow us to correlate the microstructure and functional properties systematically, in order to ultimately improve the behavior of nanostructured sPEEK membranes. According to these conclusions, we will be able to select the conditions required to obtain a host membrane with well-defined ionic domains for creating hybrid membranes.

II.1.1 Materials

sPEEK commercial membranes provided by Fumatech® with different IEC were used, labeled sPEEK(IEC). *Table* II-1 lists the different membranes used in our study, with the corresponding ionic exchange capacity (IEC) and sulfonation degree (DS), defined as:

$$\text{IEC}=1000/\text{EW} \qquad \text{and} \qquad \text{DS} = \frac{M_p}{\text{EW} - M_{SO_3H}}$$

where M_p and M_{SO_3H} are the molecular weight of a non-sulfonated unit (288 g/mol) and a SO_3 group (81 g/mol) respectively.

Table II-1 *sPEEK equivalent weight (EW), ionic exchange capacity, thickness and sulfonation degree.*

Label sPEEK (IEC)	Membrane	Thickness (µm)	Equivalent Weight ($g \cdot eq^{-1}$)	IEC ($meq \cdot g^{-1}$)	DS(%)
sPEEK(1.2)	Fumapem® E-840	40	840	1.19	38
sPEEK(1.3a)	Fumapem® E-750	50	750	1.33	43
sPEEK(1.3b)	Fumapem® E-730	30	740	1.35	44
sPEEK(1.6)	Fumapem®E-630	30	630	1.59	53
sPEEK(1.8)	Fumapem® E-550	50	550	1.81	61
sPEEK(3)	Fumapem®E-330	30	330	3.03	116

The received sPEEK membranes were re-acidified before use. The protocol is the following: 4h acidification in 1M sulfuric acid solution at room temperature, followed by triple rinsing with pure water, pH~7.

We have five different IEC ranging from 1.19 to 3 meq·g^{-1}. Note that for sPEEK(1.3), we had two different batches provided by Fumatech®, labeled sPEEK(1.3a) and sPEEK(1.3b), with slight differences in thickness (50 µm and 30 µm) and IEC (1.33 and 1.35 meq·g^{-1}). In the following section, we investigate the properties of both membranes and compare them when possible.

II.1.2 Membrane conditioning

As previously mentioned on *Chapter I*, the *Rubatat* model of Nafion® was built from extended structural analysis as a function of the membrane hydration. In this study, we aimed to better understand the sPEEK membranes' microstructure in different hydration states. We performed a series of experiments to investigate the evolution of the scattering profiles as a function of the water uptake. We used different swelling methods to equilibrate the membranes at different water contents:

- Membranes equilibrated at selected Relative Humidity (RH) at room temperature: where the membranes were conditioned on a portable globe box (PGB) at room temperature. The atmosphere at a given RH% was insured by the water vapor generated from a low temperature bubbling bath conveyed through the (PGB) at room temperature. The RH% was measured inside of the PGB with a hygrometric probe. ***Section II.2***

- Swelling in liquid water at room temperature: The membrane was immersed for 96h in pure liquid water. ***Section II.2.***

- Overswelling in water using hydrothermal treatment: The membranes were immersed in liquid water for a given time (0 to 1000 hours) at temperatures ranging from 20ºC to 120ºC. Different IEC will be investigated. ***Section II.3*** and ***Section II.4***

- Membranes equilibrated using hydrothermal treatment with vapor: The membranes were exposed to water vapor at 80ºC on an ageing cell under inert atmosphere for a given time (0 to 1000 hours). ***Section II.5***

- Overswelling using oxidative treatment. The membranes are (***Section II.6***): Immersed in different aqueous solutions of hydroperoxide (concentrations of H_2O_2 from 0,01%wt to 1%wt) at 80ºC, during times varying from 0 to 96 hours.

The aim will be to compare these methods to get an overview of the sPEEK membranes microstructure probed by scattering techniques.

II.1.3 Scattering experiences

We have used mainly SAXS (ID2 and D2AM beamlines at ESRF and Lab-SAXS Spectrometer at INAC/CEA). Some structural characterizations were performed using SANS (PAXY spectrometer at LLB). SAXS and SANS are complementary tools (see *Annex A.1* for details).

II.2 Membranes equilibrated at relative humidity and liquid water at room temperature

SAXS experiments were carried out on sPEEK(1.3a) membranes equilibrated at various RH% to investigate the evolution of morphology upon water uptake. SAXS experiments were performed at the ESRF-ID2 beamline.

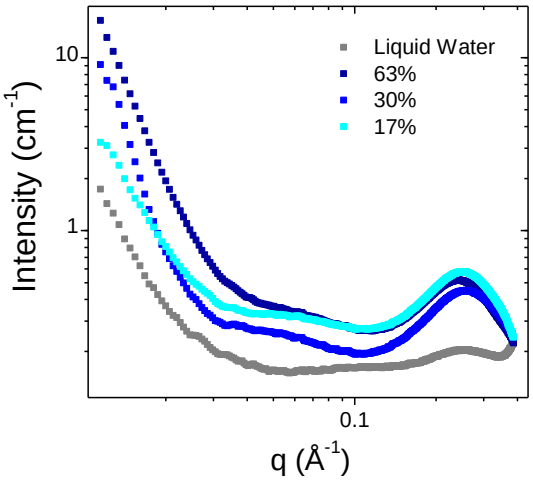

Fig. II-1 *Log-log SAXS spectra of hydrothermally treated sPEEK(1.3a) membranes in Cs^+ form at 20°C for 96h, as a function of their hydration state (RH% from 17 to 63% or liquid water conditioning). The inset displays the SAXS profile for 17% in an extended "q" range.*

Fig. II-1 displays the SAXS spectra of sPEEK(1.3a) membranes exposed to different RH% or swollen in liquid water for 96h. The membranes were prepared in Cs^+ form to enhance the contrast between hydrophobic and hydrophilic domains with respect to H^+ form. The scattering profiles display similar features at low water content ($\lambda<<1$). An intense small-angle upturn is observed (related to large scale organization in ionic polymers–typically micrometric domains [122]), followed by a low intensity bump at intermediate scattering vectors (q~0.03-0.15Å^{-1}) together with an intense and large peak located at 0.25Å^{-1}. The presence of such a maximum at this q-value was frequently associated with the existence of an ionomer peak [123]. Here, we observe that the position and intensity of this peak are quite insensitive to RH% ($\lambda<<1$). In contrast, in membranes equilibrated in liquid water, the intensity of the whole scattering profile decreases. The wide-angle peak is hardly distinguishable, while its position remains constant. The effect of liquid water on the scattering profile is an unexpected result. These observations contrast drastically with the swelling behavior of Nafion® for which both the ionomer and matrix peaks shift towards smaller angles upon hydration [10].

In order to further understand these results, pristine membranes of sPEEK(1.3a) and sPEEK(1.3b) were compared with a membrane sPEEK(1.3b) treated by the protocol advised by Fumatech® to enhance membrane performance. Following this protocol, the membrane was treated in an acid solution (5%vol H_2SO_4) for 14h at 80ºC and then treated in pure water at 80ºC for 1h. Consequently, the membrane is overswelled. We compare the SAXS spectra of the two pristine membranes and the one treated according to the Fumatech® protocol on *Fig. II-2*.

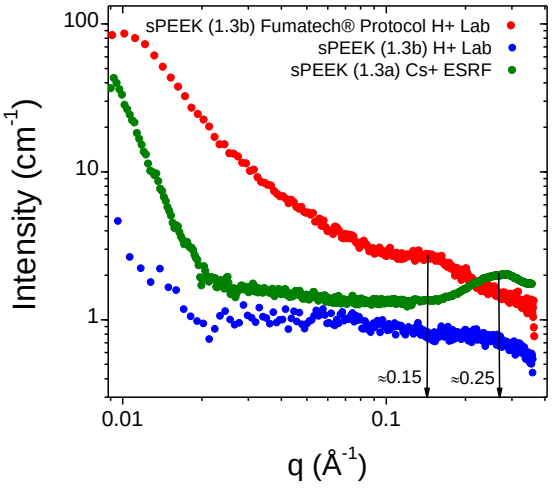

Fig. II-2 *Log-Log SAXS profile of sPEEK(1.3b) membranes, (●)pristine membrane in H^+ form and membrane in H^+ form treated during 14h in 5%vol H_2SO_4 solution at T = 80 °C. After treatment in pure water at T =80 °C for 1 h, and rinsing with pure water (Lab Spectrometer)(●). Another membrane sPEEK(1.3a) in Cs^+ in liquid water (D2AM ESRF beamline)(●).*

Note that the sPEEK(1.3a) was prepared in Cs^+ form and studied by SAXS on the D2AM ESRF beamline, while the sPEEK(1.3b) – both pristine and treated – were analyzed in H^+ form by SAXS in lab INAC's spectrometer.

The pristine sPEEK(1.3a, Cs^+) membrane presents an intense small-angle upturn followed by a large peak located at 0.25 $Å^{-1}$. The pristine membrane of sPEEK(1.3b, H^+) does not present a peak. The scattering profile of the membrane treated with Fumatech® protocol in H^+ form shows the presence of a correlation peak located at q~0.15$Å^{-1}$. From these observations, we can conclude that:

- The choice of the counter-ion impacts the scattering profiles. No peak is observed for a pristine membrane in H^+ form, while a well-defined correlation peak appears in the Cs^+ form (at room temperature) at q~0.25 $Å^{-1}$. This observation could be due to a higher electronic density contrast in the Cs^+ form, and shows that the peak is correlated to the distribution of counter-ions in ionic domains.[1]

- The correlation peak in overswelling conditions at high temperature shifts from q~0.25$Å^{-1}$ to q~0.15$Å^{-1}$. Fumatech® protocol does not provide membranes with a well-defined nano-phase separation because the membrane does not present any q^{-4} behavior at large q-values.

We can summarize our findings concerning the swelling at given RH% and overswelling in water:

- We observed no shifting of the correlation peak on membranes equilibrated with RH% and membranes immersed in water at room temperature.

- In contrast, we observed a shift towards smaller angles of the correlation peak when hydrated in overswelling conditions.

[1]In *section II.3.1.2* we will study this effect in greater detail.

Therefore, our results show a complex swelling behavior at nanoscale depending on the swelling method used, and we need additional structural information to interpret them. To gain further insight, we performed a complete study of the microstructure as a function of overswelling conditions.

II.3 Impact of the hydrothermal treatment in liquid water

In this section, we will analyze the impact of hydrothermal treatment on the microstructure. This section is divided in two parts. In the first *section II.3.1* we will investigate the impact of swelling at different temperatures for a given time on the membrane microstructure. We will compare these results with Nafion®(117) as a reference membrane. The study of electron density contrast and the influence of IEC on the microstructure will allow us to identify the observed peaks in the SAXS spectra. In the second *section II.3.2*, we will relate information about the evolution of the microstructure with the functional properties of sPEEK membranes.

II.3.1 Identification of the swelling impact on the membrane microstructure

We studied the structure of sPEEK(1.3a) membranes swollen in liquid water for 96h at 20°C, 35°C, 60°C, 80°C, 100°C and 120°C. *Fig. II-3* displays the SAXS spectra of these membranes in Cs^+ form conditioned in liquid water at room temperature. Note that a few drops of water were added to samples in order to prevent the membranes from drying during the experiment.

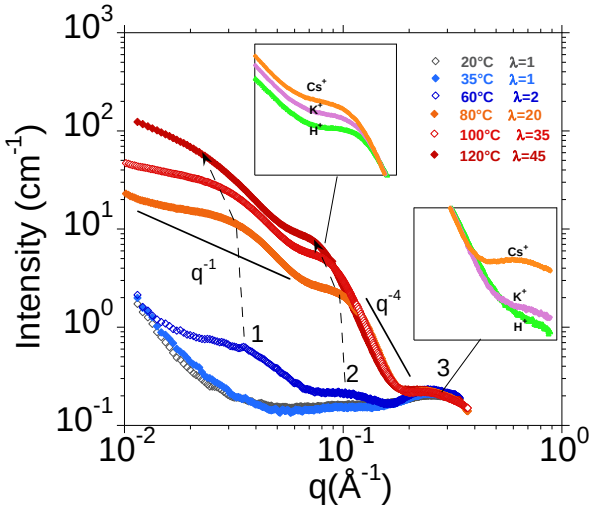

Fig. II-3 *Log-log SAXS profiles of water swollen sPEEK(1.3a) membranes in Cs^+ form at room temperature after 96h of immersion in liquid water at 20°C (◇), 35°C (◆), 60°C (◇), 80°C (◆), 100 °C (◇) and 120°C(◆). The left and right insets compare the SAXS profiles, at 80°C, in the peak 2 and peak 3 regions, respectively, for different monovalent counter ions: Cs^+, K^+ and H^+. The spectra were recorded on ID2 and D2AM ESRF beamlines.*

For immersion temperatures below 60°C, a very low swelling with less than two molecules of water per ionic site ($\lambda<2$) is observed and the scattering profiles are superimposable. These profiles exhibit an intense small angle upturn, classically observed for ionomers [124] followed by a rather flat *q* range at intermediate scattering vectors (0.04-0.15$Å^{-1}$) and terminated by low

intensity and a broad peak at a wide angle (large q-value, labeled peak "3") at about 0.25 $Å^{-1}$. It is associated to a characteristic distance "d_3" of $2\pi/q_3 \sim 25$ Å. For higher immersion temperatures, the membrane swelling dramatically increases ($\lambda \geq 20$) and one can observe the emergence of two additional peaks at smaller angles, labeled peaks "1" and "2". At 60°C, they are located at about $q_1 \sim 0.037$ $Å^{-1}$ and $q_2 \sim 0.1$ $Å^{-1}$ and are associated to a Bragg spacing "d_1"$=2\pi/q_1$ and "d_2"$=2\pi/q_2$, which is the mean separation distance between scattering objects. These distances correspond to d_1 and d_2 of ~170 Å and ~63 Å, respectively. It is important to note that these three peaks are evidenced simultaneously on the SAXS spectra of well-swollen sPEEK membranes.

For sPEEK(1.3a), the evolution of the scattering profile with the swelling temperature is observed to be a two-step process. The first step is an abrupt departure of the scattered intensity observed from 60°C to 80°C without significant peak shifting. At the same time, it is observed that the slope following peak "2" at large q-values dramatically increases from 60ºC to 80ºC. This is the typical signature of a sharp interface between two phases, most probably the hydrophobic and the hydrophilic ones.

In a second step, for temperatures above 80°C, peaks "1" and "2" shift towards smaller angles and their intensity increases.

II.3.1.1 Comparison with Nafion® membranes

We now compare the swelling of sPEEK(1.3a) to that of the reference Nafion®(117). Indeed, it was recently evidenced that the scattering entities for sPEEK ionomer dispersions are ribbon-like polymer particles as for Nafion® [125]. Moreover, flat morphologies seem to be a general feature for most dissociated ionomers [121], and similar dilution laws are therefore expected.

As shown in *Fig. II-3*, we have three correlation peaks in SAXS spectra of sPEEK membranes. We will compare the behavior of these peaks to the Nafion® characteristic peaks.

a) sPEEK: Peak "2" $q_2 \sim 0.1$ $Å^{-1}$

Peak "2" presents similar features as perfluorosulfonated membranes upon swelling [10, 35]: peak shifting toward small angles together with an increase in intensity. Moreover, a q^{-4} behavior is observed at the nanometer scale upon hydration. These observations strongly suggest that peak "2" is an ionomer peak associated with hydrophilic/hydrophobic phase separation. We will compare this peak with the peak of Nafion®(117).

In *Fig. II-4* we plotted the characteristic distance between the scattering entities, "d_2"$=2\pi/q_2$ for sPEEK(1.3a) membranes and "d_{iono}"$=2\pi/q_{iono}$ with "iono" standing for ionomer for Nafion®(117) as a function of the membrane swelling (the polymer volume fraction Φ_p of the swollen membranes).

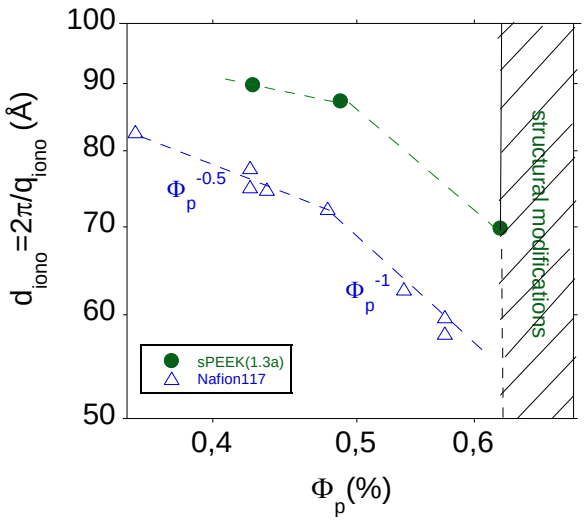

Fig. II-4 *Log-log evolution of the characteristic distance $d_{iono}=2\pi/q_{iono}$ as a function of the polymer volume fraction Φ_p for the nanostructured sPEEK(1.3a) (●) and Nafion®(117)(△)(data extracted from ref [12]). The dotted line for sPEEK(1.3a) is a guide for the eyes.*

At values lower than the hatched area (Φ_p<0.65), sPEEK(1.3a) presents a well-defined nano-phase separation. This observation came from *Fig. II-4* where it was observed as q^{-4} *Porod's Law* from 80°C. For Nafion®(117), the Φ_p^{-1} behavior is observed at high Φ_p values, down to ~47% [20], was associated to the dilution of flat objects as ribbons [11]. For higher swellings, (lower Φ_p values) a $\Phi_p^{-0.5}$ dilution law was associated to the dilution of rod-like objects like cylinders. As seen in *Fig. II-4* we can observe that the plot $d_2=f(\Phi_p)$ resembles that of Nafion® with higher values of absolute swelling. At Φ_p= 0.5, d_2=80Å and d_{iono}=74Å for sPEEK(1.3a) and Nafion®, respectively. This is probably attributable to the higher IEC of sPEEK(1.3a): 1.3 (meq·g^{-1}) as compared to that of Nafion® (117): 0.9 (meq·g^{-1}). The dilution curve of sPEEK(1.3a) seems to exhibit a discontinuity, similarly to Nafion®. It should be stressed that we dispose of a very limited number of SAXS data for sPEEK(1.3a) (completion of the structural modifications from 80°C, swelling for higher temperatures).

Therefore, these observations confirm the **attribution of peak "2" as the ionomer peak**. The main difference between both ionomers in terms of swelling behavior is that Nafion® is intrinsically nanostructured while sPEEK requires a hydrothermal treatment to reach a well-defined nano-phase separation.

b) sPEEK: Peak "1"

Another similarity between Nafion®(117) and sPEEK(1.3a) is the observation on *Fig. II-3* of a peak located at smaller angles than the ionomer peak (peak 1), less pronounced and observed above a q^{-1} slope [12]. This peak displays similar features as the so-called Nafion® matrix peak (and will be labeled as such), usually considered to originate from inter-crystallite interferences [126]. It is located at *q*-values of (0.02Å^{-1}<*q*<0.04 Å^{-1}) and shifts towards small angles upon hydration.

c) sPEEK: Peak "3" q_3~0.25 Å^{-1}

In contrast with both the ionomer and the matrix peak, the wide angle peak "3" intensity and position are not sensitive to hydrothermal treatment. The peak "3" position is about 0.256 Å^{-1} from 25 °C to 60 °C and about 0.25 Å^{-1} from 80 °C up to 120 °C. The observation of peak "3" remaining almost stable during the hydrothermal treatment strongly suggests that this peak could be associated to an intramolecular correlation distance, as the mean separation distance between sulfonated units along the rigid polymer backbone.

For two other membrane types (one sulfonated polyimide (sPI) [127] and one radiation grafted perfluorinated membranes with sulfonated polystyrene [128]), it was suggested that the wide angle peak, which was observed simultaneously with the ionomer peak, can be attributed to the characteristic distance between sulfonated units within the swollen ionic domains [127, 128].

Therefore this peak will be hereafter abbreviated as "SO_3" peak. The broadness of the peak reflects the fact that the sulfonated units are not uniformly distributed along the polymer backbone. This statistical distribution results from the chemical process used to prepare the materials (dissolution time, withdrawing effect of the SO_3H groups grafted onto the aromatic ring).

If the molecular architecture of Nafion® and sPEEK are compared, we can understand why this SO_3 peak has never been observed for perfluorosulfonated polymeric systems [10, 12, 35]. For Nafion®, SO_3H groups are located at the extremity of highly flexible side chains, grafted onto the Teflon®-like polymer backbone. In contrast, for sPEEK, SO_3H groups are directly grafted onto the aromatic rings of the highly rigid sPEEK backbone. Both Nafion® architecture and its high side chain mobility prevent the observation of the wide angle peak characteristic of the distance between SO_3 groups. It should be noted that the same conclusions are true for the aromatic polymers developed by *Jannasch et al*.[129] that carry hypersulfonated side chains: no SO_3 peak is observed despite their superior nanostructuration. One should wonder why no such SO_3 peak was observed for the aromatic ionomers with precisely sequenced sulfonated moieties along the polymer backbone developed by *Jannasch et al*.[130]. In that case, the distance between SO_3 groups located in the same hydrophilic blocs would be so short that their corresponding peak would be located at wider angles, not explored in their study.

On the basis of our thorough structural investigation with respect to water content, we attribute peaks "1", "2" and "3" to the "matrix", "ionomer" and "SO_3" peaks, respectively. Furthermore, in order to confirm our interpretations and peaks' attribution, SAXS experiments were carried out on series of membranes:

- sPEEK(1.3a) with different monovalent counter-ion, Cs^+, K^+ and H^+ in order to modulate the electron density contrast.
- sPEEK membranes with different IEC ranging from 1.19 to 3 meq·g^{-1} in order to observe the SAXS profile evolution according to the number of sulfonic groups.

II.3.1.2 Effect of counter-ion

The insets of *Fig. II-3* display, for the ionomer peak and the SO_3 peak regions, the SAXS profiles of water swollen sPEEK(1.3a) membranes after immersion in liquid water at 80°C for 96h, followed by ionic exchange with 3 different monovalent counter-ions: Cs^+, K^+ and H^+ with their atomic number Z following: $Cs^+ > K^+ > H^+$(from the higher to the lower atomic number Z). The inset shows that the ionomer peak position is almost independent of the monovalent counter-ion (slight peak shift is classically observed for ionomers [125, 131]) while its intensity increases with the atomic number Z as a result of an increased contrast. These features confirm the attribution of "peak 2" to an ionomer peak [132, 133].

The SO_3 peak inset shows that the SO_3 peak position is also independent of the counter-ion atomic number. But the effect on its intensity is much more pronounced than for the ionomer peak: decreasing Z strongly lowers the peak intensity which is no longer visible in the H^+ form. We can explain this behavior by considering the local environment around SO_3 groups.

This observation strengthens the attribution of the wide angle peak to a structural peak associated with interference effects inside the swollen ionic domains [134].

II.3.1.3 Effect of IEC

* <u>On ionomer peak and SO_3 peak</u>

Fig. II-5 (A) and (B) display, for different IEC (1.2 to 3 meq·g^{-1}), the SAXS profiles of Cs^+ exchanged sPEEK membranes (liquid water conditioning) after 96h of immersion at 20°C and 80°C. These two temperatures were chosen based on what was observed for sPEEK(1.3a) in *Fig. II-3* one temperature before and after formation of the sharp nano-phase separation, 20ºC and 80ºC respectively. *Fig. II-5* (C) and (D) report the mean separation distance between, respectively, sulfonated units d_{SO3} (SO_3 peak) and ionic domains d_{iono}(ionomer peak) as a function of IEC, at both 20 °C and 80 °C for C and at 80 °C only for (D).

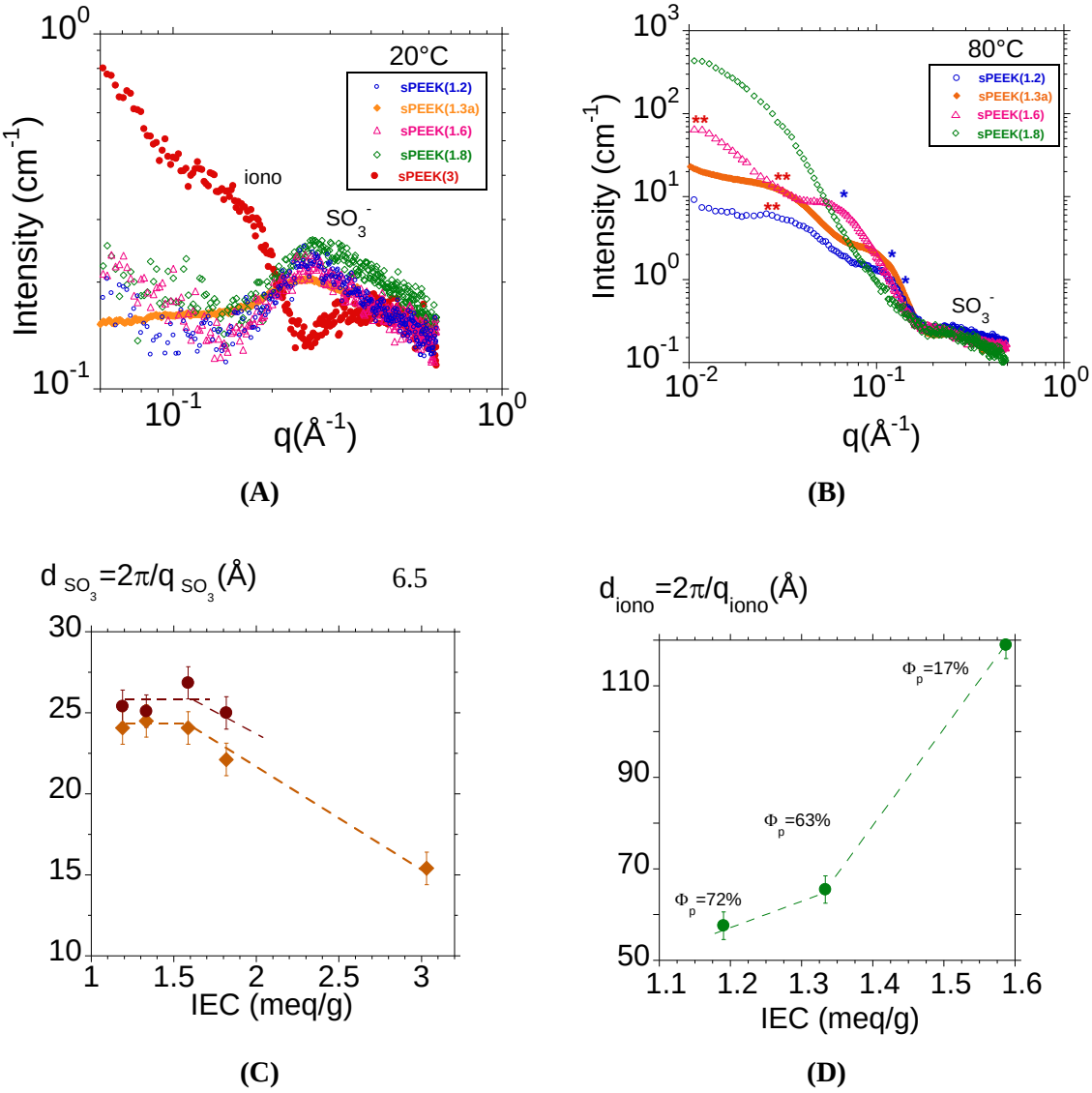

Fig. II-5 *(A) Log-log SAXS profiles (recorded at ID2 beamline at ESRF and INAC/CEA Grenoble) of Cs^+ exchanged sPEEK. IEC: 1.2 (○), 1.3a(◆), 1.6 (△), 1.8 (◇) and 3 (●). Membranes were conditioned in liquid water at room temperature after 96h of immersion at 20°C (B) and at 80°C. One blue star (*) and two red stars (**) show the peak positions of the ionomer and matrix peaks, respectively. (C) Mean separation distance between sulfonated units (SO_3 peak) ($d_{SO3}=2\pi/q_{SO3}$) as a function of the IEC ($meq \cdot g^{-1}$) for 96h of immersion in liquid water at 20°C(◆) and 80°C(●). (D) Mean separation distance between ionic domains (ionomer peak) ($d_{iono}=2\pi/q_{iono}$) as a function of the IEC ($meq \cdot g^{-1}$) for 96h of immersion in liquid water at 80°C. The dotted lines are guides for the eyes.*

SAXS profiles as a function of IEC at 20 C are depicted in *Fig. II-5***A**. One illustrates that lower signal/noise ratios for sPEEK(1.2), (1.6), (1.8) and (3) were obtained from our lab SAXS spectrometer, compared to sPEEK(1.3a) obtained from the synchrotron. We observe several interesting features, only sPEEK(3) displays a **ionomer peak** located at ~0.177 $Å^{-1}$. In contrast to sPEEK(1.3a), sPEEK(3) does not need immersion at a higher temperature than 20 °C to show a well-defined nano-phase separation (at 80 °C it is water soluble). The **SO_3** peak position is observed, for all membranes (corresponding distance $d_{SO3}=2\pi/q_{SO3}$) and is almost constant at about 0.26 $Å^{-1}$ (24 Å) for IEC ranging from 1.2 to 1.6, then starts shifting towards higher *q*-values with

0.28 $Å^{-1}$(22 Å) for sPEEK(1.8), up to a strong shift, 0.4 $Å^{-1}$ (16 Å) observed for sPEEK(3). It should be noted that the SO_3 peak of sPEEK(3) is much narrower than the SO_3 peaks of lower IEC as a result of a more homogeneous distribution of the sulfonated groups (all the repeat units are sulfonated). The corresponding d_{SO3} values are reported as a function of IEC on *Fig. II-5* (C).

For the low IEC range, the stable position of the SO_3 peak can be explained by the post-sulfonation process used to obtain the studied sPEEK. This process does naturally produce heterogeneous distribution of the SO_3H groups (parts of the sPEEK chains highly sulfonated contrasting with non sulfonated ones) along the polymer backbone for the lower sulfonation extent. In fact the polymer dissolution process results in a distribution of the sulfonation times among polymer chains (not all the chains being solubilised at the same time). For the higher IEC, the strong SO_3 peak shifting results from a decrease of the mean separation distance between sulfonated units along the polymer backbone. This sulfonation of more than one aromatic ring per repeat unit is obtained by the second type substitution [135]. The peak's narrowing therefore results from a sulfonation becoming much more homogeneous. The mean separation distance d_{SO3} (calculated from the bond lengths [136]) for DS=50% is about 27 Å, which is in accord with the experimental distance of ~25 Å measured for comparable DS.

The evolution of SAXS spectra as a function of temperature can be discussed by comparison of *Fig. II-5*(A) and (B). For each IEC, it is observed that the SO_3 peak is located in the same scattering range at 20° C (*Fig. II-5*(A)) and at 80 °C (*Fig. II-5*(B)), however, it is with a small shift towards slightly smaller angles (higher distances) at 80°C, as better observed in *Fig. II-5 (C).* We assume that this evolution with the temperature can be understood as resulting from a slight stress release. Globally d_{SO3} is thus almost unaffected by the nano-phase separation process (already observed to occur between 60 °C and 80 °C for sPEEK(1.3a) in *Fig. II-3*, and observed to be reached at 80°C for sPEEK(1.2), sPEEK(1.3a) and sPEEK(1.6) in *Fig. II-5(B)* as the ionomer peak is clearly observed).

The high swelling state of sPEEK(1.8) at 80 °C (Φ_p<15%) prevents interference effects between hydrophobic areas and therefore no ionomer peak is observed [12]. sPEEK(3) which was water soluble at 80 °C was not measured. As we observed the ionomer peak for different IEC, we can note that when the IEC increases, this peak grows and shifts towards smaller angles (better swelling properties = increased distances between scattering entities as illustrated by *Fig. II-5*(*D)).* Indeed, even though the glass transition temperature (Tg) increases with IEC[43], water uptake increases also. Therefore, the higher Tg observed for dry membranes with IEC does not hinder the nanophase separation process.

* <u>On the matrix peak</u>

Increasing IEC has also a strong impact on the matrix peak. The matrix peak is clearly observed for both sPEEK(1.2) and (1.3a), less pronounced for (1.6), and missing for higher IEC (*Fig. II-5 (B)).* When observed, this peak shows a clear shift towards smaller angles as a function of IEC increase. As already stated, we attributed this peak to the first matrix in comparison with perfluorosulfonated membranes [126]. For Nafion®, this peak was observed and it proved that the membrane exhibits crystallinity [126, 137]. In order to check the possible correlation between the matrix peak and the sPEEK crystallinity, we performed two types of WAXS experiments:

- Effect of hydrothermal treatment at different temperatures for 96h (*Fig. II-6*)
- Effect of IEC (*Fig. II-7*)

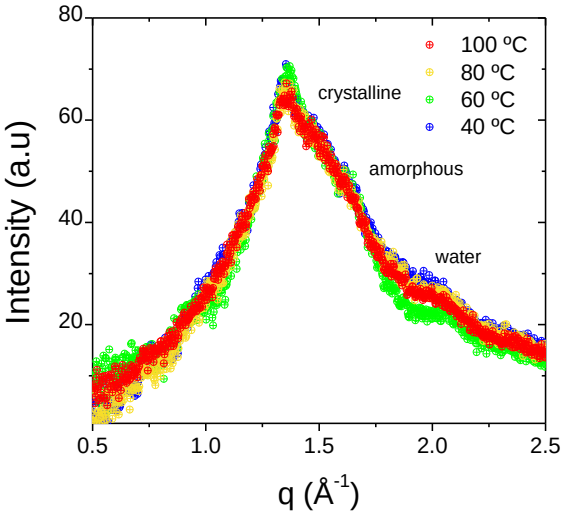

Fig. II-6 *WAXS spectra of sPEEK(1.3a) membranes in H^+ form after 96h of hydrothermal treatment at 40(⊕), 60(⊕), 80(⊕) and 100°C(⊕). The spectra were recorded in transmission mode at room temperature and humidity.*

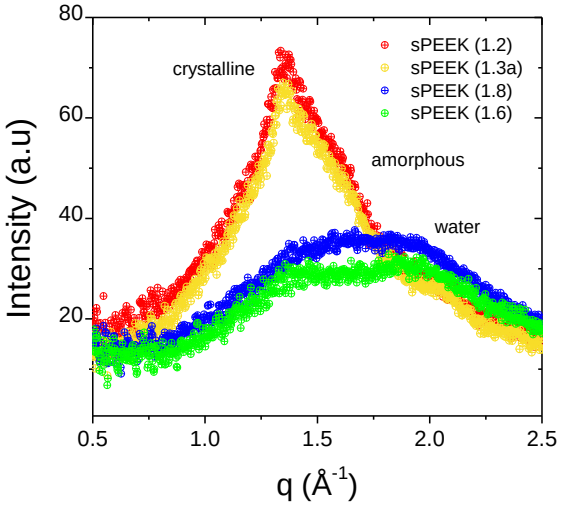

Fig. II-7 *WAXS spectra of sPEEK(1.2)(⊕), sPEEK(1.3a)(⊕), sPEEK(1.6)(⊕) and sPEEK(1.8) (⊕) membranes in H^+ form, after 96h of hydrothermal treatment at 80°C. The spectra were recorded in transmission mode at room temperature and humidity.*

Fig. II-6 displays the sPEEK(1.3a) WAXS spectra recorded at room temperature and relative humidity, in transmission mode, after 96h of hygrothermal treatment at various temperatures: 20 °C, 25 °C, 60 °C, 80 °C and 100 °C.

It is well known that sPEEK with similar IEC to Nafion®(117) present crystallinity [138], sPEEK(1.3a) membrane clearly exhibit a semi-crystalline structure as a sharp crystalline peak, located at about 1.37 Å^{-1}, and this peak is virtually superimposed to an amorphous halo centered around 1.6 Å^{-1}. We observed that sPEEK(1.3a) WAXS spectra are not sensitive to the hydrothermal treatment temperature.

At this point, it is important to emphasize the fact that the appearance of the matrix peak above 60 °C (see *Fig. II-3*) together with the observation of a wide-angle crystalline peak with any hydrothermal treatment temperature, are not incompatible. In fact, the matrix peak is already observed even on pristine membrane (see the low intensity bump in *Fig. II-5* in RH% conditions). But in liquid water conditions, the electron density fluctuations on large scales are too low to give rise to a well-defined peak. In contrast, WAXS experiments are related to diffraction by reticular planes, which therefore allows for the crystallinity to be observed.

Fig. II-7 displays the WAXS spectra of sPEEK membranes for the different IEC (1.2 to 1.8 meq·g^{-1}) after 96h of hydrothermal treatment at 80 °C. sPEEK(3) is water soluble at 80 °C and was therefore not measured. It is observed that sPEEK(1.2) and sPEEK(1.3a) membranes display similar degrees of crystallinity as both WAXS spectra are nearly superimposed. For sPEEK(1.6) and sPEEK(1.8), one can observe that the WAXS profiles broaden. The intensity of the crystalline

peak of sPEEK(1.6) strongly decreases while it is indistinguishable for sPEEK(1.8). Only a broad halo is measured: it is completely amorphous for such high degree of sulfonation (≥61%).

It is therefore confirmed that the evolution of crystallinity is produced by a change of polymer backbone, with different degrees of sulfonation. It was also observed that the matrix peak follow similar behavior *(Fig. II-5(B)*) where the matrix peak is clearly observed for membranes sPEEK(1.2) and sPEEK (1.3a), less pronounced for sPEEK (1.6) and missing for membranes with a higher IEC.

II.3.1.4 Conclusion: Impact of hydrothermal treatment in liquid water

We can conclude from these results that:

-The swelling temperature on sPEEK membranes has a strong impact on the membrane morphology.

-We evidenced for the first time three peaks simultaneously on the SAXS spectra of sPEEK membranes, the wider angle peak, associated with the mean separation distance between sulfonic acid groups. And two other small angle peaks on swelled membrane attributed to the ionomer and matrix peaks.

-This peak attribution was confirmed by studying the impact of the electron density contrast and the impact of the IEC on the peaks' positions and intensities and by comparing with Nafion®.

-The matrix peak of sPEEK was clearly associated with the polymer crystallinity.

-The immersion of sPEEK in water at elevated temperatures allows structural modifications and provides a well-defined interface between hydrophilic and hydrophobic phases.

Because of the attribution of SAXS spectra peaks and better understanding of the hydrothermal treatment effect on the microstructure of sPEEK membranes, we can relate this microstructure to the functional properties of the polymer.

II.3.2 Impact of the hydrothermal treatment in liquid water on functional properties

In this section, functional properties such as swelling, conductivity and water sorption will be analyzed. These results will be related to the structural modification process (microstructure evolution).

II.3.2.1 Swelling

It is understood that water uptake of sPEEK membranes strongly depends on the swelling treatment temperature, time and relative humidity [40, 41, 139]. The resulting swelling directly affects the proton transport. For ionic membranes, the swollen state corresponds energetically to a balance between: the osmotic pressure which leads to dilution of the ionic species, the elastic deformation of the polymer chains which increase in order to locate the ionic groups at the polymer-water interface, and the polymer-solvent interfacial energy [20].

The water uptake was measured at room temperature for sPEEK(1.3a) membranes treated for 96h at different temperatures between 20ºC to 115ºC (*Fig. II-8*). The liquid water in excess on the surface of the wet membranes was removed using tissue paper before weighing. Dry measurement was obtained by drying membrane at room temperature in a vacuum overnight.

As seen in *Fig. II-3*, there is almost stable with the mean value ~15%, up to 70ºC, followed by a dramatic increase for temperatures from 70ºC to 115ºC. The mass percent of water uptake ranges between 15% at 70 ºC to 135% after hydrothermal treatment at 115ºC.

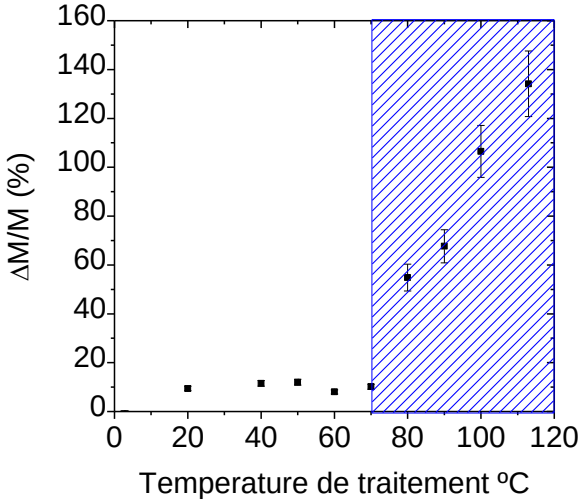

Fig. II-8 *Swelling of sPEEK(1.3a) membrane after 96h of hydrothermal treatment at different temperatures were measured at room temperature***.**

The swelling behavior is remarkably well-correlated to the microstructure evolution (see *Fig. II-3*). We have shown a major change occurring above T>70ºC, which is clearly related to the spectacular water uptake at this threshold temperature. Such correlation strongly supports the theory that the immersion in water at elevated temperatures (from 70°C) allows sufficient molecular mobility to improve the self-assembly (hydrophilic-hydrophobic), which results in structural modifications of the membrane and provides a well-defined interface between hydrophilic and hydrophobic phases. In other words, the ionic domains grow and their separation with the polymer matrix becomes sharper, and the evolution of this surface and the growth of these ionic domains are reflected in membrane swelling.

The sPEEK membrane conductivity is logically dependent on the nano-separation between hydrophilic and hydrophobic domains and will therefore be strongly affected by the hydrothermal treatment parameters. We will relate the conductivity to macroscopic swelling and microscopic morphology of sPEEK membranes in the next section.

II.3.2.2 Conductivity

The proton conductivity of membrane mainly depends on [20, 41]:

- The connectivity of the hydrated domains.
- The well-defined nanophase separation between hydrophobic and hydrophilic domains.
- The polymer chemistry (i.e. interactions between sulfonic acid groups from polymer and water)

Conductivity values at room temperature obtained for swollen membranes are presented in *Fig. II-9*. Measurements were carried out in a homemade conductivity cell. To be sure that the proton conductivity measured will not be influenced by counter ion pollution (Na^+, K^+...), membranes were re-acidified (1h) in a 1M HCl and clarified to pH~7 before prior conductivity measurements.

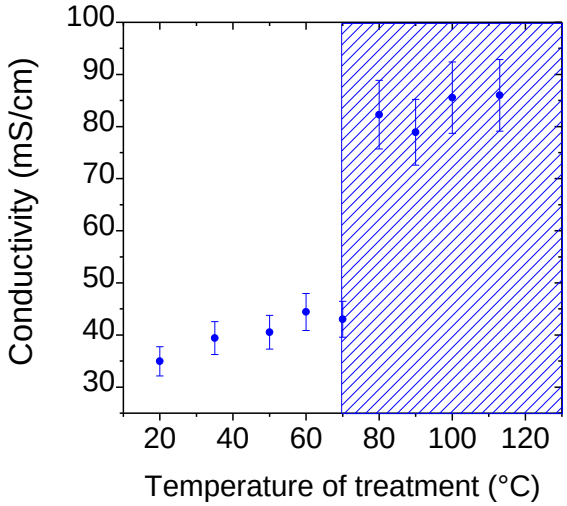

Fig. II-9 *Proton conductivity at room temperature of sPEEK(1.3a) membranes as a function of the temperature of hydrothermal treatment for 96h.*

As can be seen in *Fig. II-9* conductivity exhibits a steady rise for membranes treated below 80ºC. A sharp increase of conductivity is observed from 70ºC to 80ºC, increasing from 0.04 $S \cdot cm^{-1}$ to 0.08 $S \cdot cm^{-1}$. After hydrothermal treatment for temperatures up to 80ºC, the conductivity seems stable.

The conductivity exhibits two different regime behaviors and a sharp transition between them. These observations are clearly correlated to the structural evolutions evidenced by SAXS in the previous sections.

- The sharp transition between these two regimes corresponds to the structural modification process.

- For temperatures of treatment from 20ºC to 70ºC, the low conductivity is the result of a rough phase separation (see *Fig. II-3*).

- At temperatures between 80ºC and 115ºC, the membrane presents well-defined nano-phase separation between ionic domains and the hydrophobic phase. We note that in this range of temperature, conductivity is almost constant while the membrane swelling continuously increases. This observation would be related to the structural modification process. We can therefore conclude that the most important parameter driving the proton conductivity is the quality of the phase separation between the hydrophobic/hydrophilic domains and it is the least affected by the water content.

When the structural modification process is completed in sPEEK membranes, the conductivity improves, reaching values as high as those of Nafion®(117) [17]. The water strongly interacts with the sulfonic acid groups of sPEEK membrane but it also interact with the oxygen atoms presents in ether and ketone groups. The local interactions between the polymeric matrix and water causes lower conductivity. This behavior drastically contrasts with Nafion®, for which a

weak polymer backbone-water interaction occurs due to the high hydrophobic character of the perfluorinated chains [140].

We relate these results with those obtained by *Alberti et al*. [141]. They have studied the conductivity of Nafion® and sPEEK at relatively high temperatures (100-160°C) and controlled relative humidity (RH). At 100 °C and RH 35%, the conductivity of sPEEK was 30 times lower than that of Nafion® while both membranes exhibit comparable conductivity at 160°C and 75% RH (4.10^{-2} $S.cm^{-1}$).

The spectacular improvement of the sPEEK transport properties could certainly be correlated to two main parameters:

- Structural modifications of the polymer due to the combined effect of water and temperature, as exemplified by the ionomer peak evolution.
- Local interactions between the solvent and polymer matrix.

In order to study this effect as well as investigate the influence of a hydrothermal treatment on the water-polymer affinity, we will further analyze the water uptake at room temperature and the controlled relative humidity for sPEEK membranes.

II.3.2.3 Water sorption

Sorption curves were measured on sPEEK(1.3b) membranes at room temperature. A pristine membrane as well as membranes treated at 80ºC for 72h were compared with Nafion®(112).

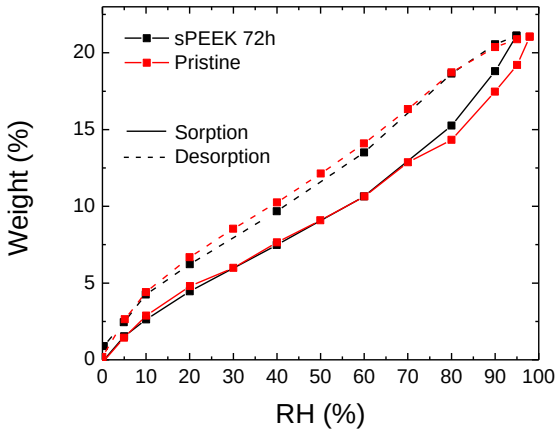

Fig. II-10 *Water sorption isotherms of sPEEK(1.3b) membrane treated at 80ºC for 72h and pristine sPEEK membrane*.

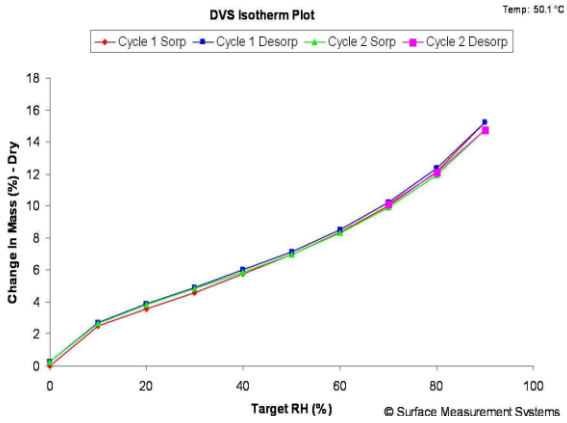

Fig. II-11 *Water sorption isotherms of Nafion®(112) obtained by two sorption-desorption successive cycles[142]*.

sPEEK(1.3b) membranes were acidified and dried in a vacuum oven overnight. These membranes have been introduced in the sorption balance and equilibrated at 0% RH for at least 10h. *Fig. II-10* shows the sorption and desorption equilibrium's data for each sample. It is important to note that there is no overlap between the absorption and desorption curves, showing a significant sorption hysteresis phenomenon. This behavior is explained by the pronounced water-

polymer matrix interactions, which goes against water desorption, since part of the water interacts with the polar groups of the polymer chains and helps in maintaining the water inside the membrane. This water-polymer matrix affinity was already considered in the interpretation of the conductivity experiments. Interestingly, this hysteresis was also observed for sulfonated polymide membranes [143]. This situation contrasts to that of Nafion®(112), for which the sorption-desorption curves show a perfect overlap [142].

Interestingly, we observe that water sorption and desorption curves for treated and non-treated membranes are very similar. It should be noted that both pristine and treated membranes were dried before analyses. In order to further understand the possible effect of drying, the microstructure after drying was investigated.

Two treated membranes of sPEEK(1.3b) were analyzed in liquid water (H^+ from) by SAXS on Lab spectrometer. The first one, labeled "*sPEEK 72h*", was immersed in water at 80ºC for 72h and analyzed in liquid water. The second one, labeled "*sPEEK 72h after drying*", was immersed in water at 80ºC for 72h, then dried by vacuum overnight at room temperature, and immersed again in liquid water at room temperature for the SAXS measurement.

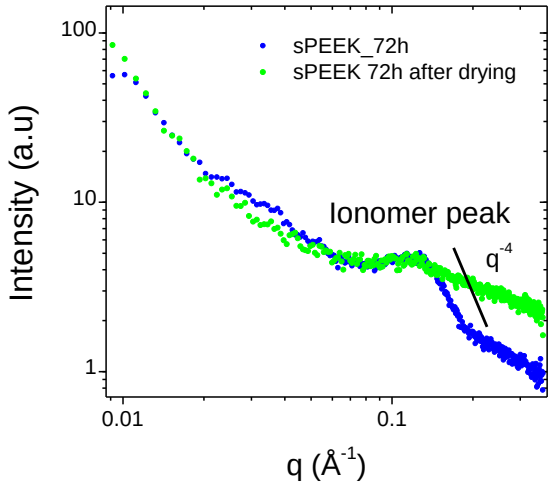

Fig. II-12 *Log-Log SAXS profiles of water swollen sPEEK(1.3b) membranes in H^+ at room temperature after: "sPEEK_72h" membrane (●) treated by immersion of liquid water at 80ºC for 72h and "sPEEK_72h after drying" (●) membrane treated by immersion on liquid water at 80ºC for 72h and analyzed in liquid water after drying over vacuum overnight.*

Fig. II-12 displays the SAXS spectra of "*sPEEK 72h*" and "*sPEEK 72h after drying*". The scattering profiles display similar features at small angles. Moreover, both spectra present an ionomer peak, located at q~0.12Å^{-1}, although much less pronounced for the sample "*sPEEK 72h after drying*". Yet, we observe a clear effect of the drying process with very distinct shapes of the scattering profiles typically evidenced for q-values higher than 0.12Å^{-1}, in the region where the hydrophilic/hydrophobic interface is characterized. For "*sPEEK 72h*", a q^{-4} behavior is found, in contrast to "*sPEEK 72h after drying*" where the sharp interface is lost with a much more mild decrease of intensity that is characteristic of a rough interface.

The hydrothermal treatment on sPEEK membrane has a clear influence on the quality of the nano-phase separation, as reflected in the q^{-4} behavior observed in *Fig. II-12*. The comparison

between dried and non-dried membranes highlights the limited membrane memory effect. Indeed, membranes immersed in liquid water after hydrothermal treatment keep the well-defined nano-phase separated morphology after immersion in liquid water at room temperature, while membranes after drying are profoundly modified and exhibit rough interfaces. This result indicates that the structural modification process using hydrothermal treatments could be reversible. A schematic representation of this process is shown in *Fig. II-13*.

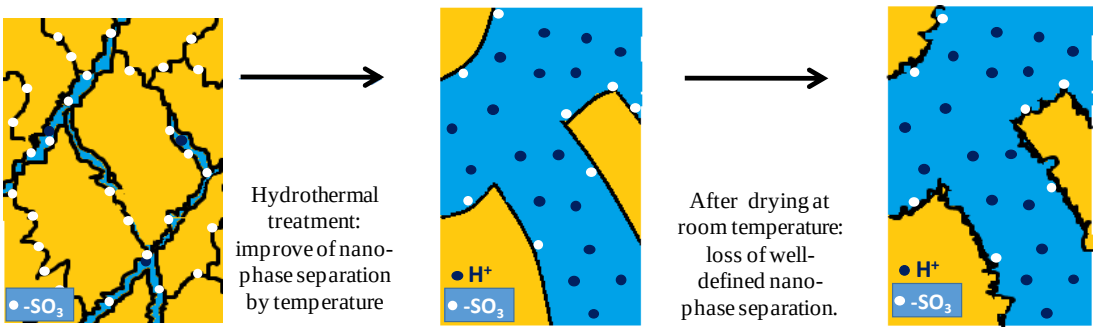

Fig. II-13 *Schematic representation of reversible process of structural modifications. Polymer matrix. Water in ionic domains.*

These results can be related to the isothermal curves (*Fig. II-10*), where the pristine and the treated membranes in liquid water are nearly overlapped, considering that both membranes were dried before water sorption analyses. A membrane treated by hydrothermal treatment (i.e. well-defined nano-phase separation) was then dried and analyzed by SAXS in liquid water, showing a similar microscopic swelling (no obvious shift of the ionomer peak) to that of a pristine membrane. So, we conclude that although the size of the ionic domains is mostly maintained after the drying step, the quality of the nanophase separation is one of the main parameters strongly impacting the sorption-desorption behavior of the sPEEK membranes.

II.3.2.4 Conclusions: Structure- properties correlations

We can summarize our findings concerning the impact of hydrothermal treatment in liquid water on the following functional properties:

- The structural modifications highlighted by SAXS and SANS have a strong impact on the functional properties.

- The onset of overswelling and increased conductivity is observed for a temperature above 60ºC, which corresponds to significant nanostructure modifications induced by the hydrothermal treatment. The proton conductivity is strongly impacted by the existence of well-defined nano-phase separation, which increased and reached similar values to Nafion® membranes.

- The structural modifications take place with a hydrothermal treatment, but this process is reversible when the membranes are dried.

II.4 Impact of time on hydrothermal treatment

We have proven that the sPEEK structural modification is triggered by hydrothermal treatments for a given time (96h). SANS analysis was performed on the ionomer *q*-range to evaluate the impact of hydrothermal treatment at different temperatures for different periods of time on the resulting membrane morphology. Firstly, *in-situ* hydrothermal treatment was realized in a SANS cell in order to observe the evolution of the ionomer peak for short periods of time, typically between 0h and 1h. In the second section, we will observe the evolution of SAXS spectra at different temperatures in sPEEK membranes treated for longer periods of time, between 10h and 1000h. Microscopic swelling evolution at room temperature was studied for a sample of membrane immersed in liquid water for two years. This section also includes information about the functional properties (conductivity and swelling) as a function of the immersion time.

II.4.1 Influence of exposition at different temperatures for short periods of times on membrane morphology

The structure of sPEEK(1.3b) membranes treated for short periods of time (up to one hour) was studied by SANS on the PAXY spectrometer - Laboratoire Léon Brillouin - CEA Saclay (LLB). The sPEEK(1.3b) membrane in H^+ form and dry state was mounted in a sealed SANS cell with quartz windows with approximately 1mm of water in excess. This water in excess permits the swelling of sPEEK membrane during the experiment. The temperature of the cell was controlled by a sensor of temperature positioned in an adjacent cell in the sample holder.

The goal was to monitor the structural evolution as a function of time. We first measured the evolution during a temperature scan. The experiment was realized with a temperature ramp between 35ºC and 85ºC. The SANS spectra was recorded once every 5 min, which is the minimum acquisition time for obtaining satisfactory statistics. No correction of intensity was realized, because the evolution of the thickness of sPEEK membrane inside the cell could not be determined *in-situ*. Note that this *q*-range is not adapted for a precise determination of the *Porod's* behavior. More, significant incoherency prevents an accurate determination of the slope.

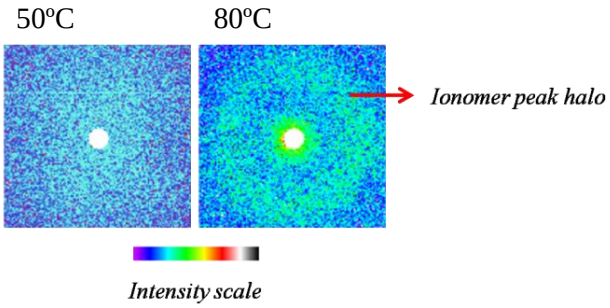

Fig. II-14 *2D- SANS images obtained at 50ºC and 85ºC. The ionomer rings are indicated with an arrow.*

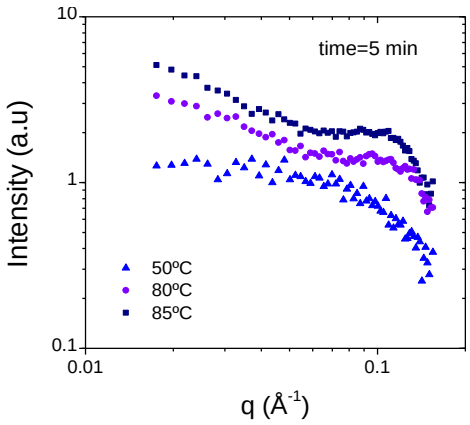

Fig. II-15 *Log-Log incoherent background subtracted representation of SANS profiles of sPEEK(1.3b) in pure water at different temperatures.*

Fig. II-14 shows examples of 2D-SANS images taken after 5 min at two different temperatures ~50ºC and 85ºC. At 50ºC, no obvious scattering feature is observed. This can be explained by the very low intensity of the ionomer peak for this temperature, which is consistent with our previous observations (threshold of the structural modifications observed above 60ºC see *Fig. II-3*). For the sake of clarity, the data between 50ºC and 80ºC are not shown. The intensity of the ring increases with temperature until a rather intense ring at 80ºC. This is naturally attributed to the ionomer peak (see the arrow in *Fig. II-14*).

The radially-averaged 1D SANS spectra of sPEEK(1.3b) membranes is shown in *Fig. II-15*. At temperatures up to 80°C, there is no peak in the scattering profile. At 80°C the profile clearly exhibits an ionomer peak at q~0.1Å^{-1}. At temperatures above 80°C, we observe an increase of ionomer peak intensity and a q^{-4} behavior.

The increase of the intensity at the nanometer scale confirms that the ionic domains grow up with increasing water content. It can be concluded that the clear ionomer peak appears within 5 minutes of exposition in liquid water at 80ºC. It is worth mentioning that time resolved SANS or SAXS experiments, which provide a high neutron or photon flux, would allow for determining precisely the time scale of the structural modifications (clear emergence of the ionomer peak/apparition of q^{-4} power law) as a sub-second time resolution that is achievable.

In order to observe the evolution of the ionomer peak with time, we performed a one-hour kinetics sequence at 85ºC, which is a temperature at which the profile exhibits a well-defined ionomer peak and q^{-4} *Porod's Law*. The SANS profiles were regularly acquired every 5 min. They are plotted in *Fig. II-16 (A).* The extracted characteristic distance d_{iono} is reported as a function of time on *Fig. II-16(B).*

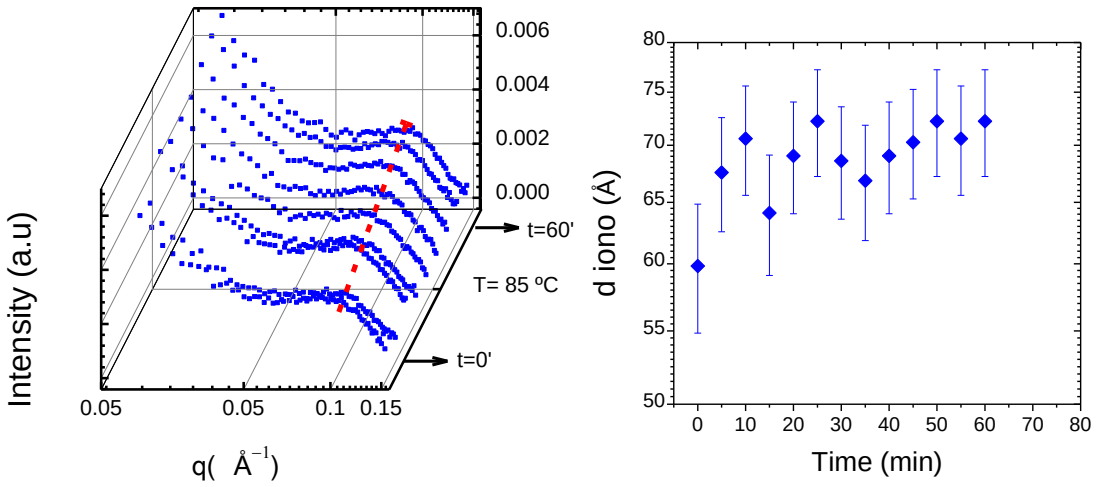

(A) ***(B)***

Fig. II-16 *(A) SANS spectra of sPEEK(1.3b) membrane at 85ºC for 1h.(B) Evolution of the characteristic distance $d_{iono}=2\pi/q_{iono}$ as a function of time during the isothermal treatment in liquid water at 85ºC. (PAXY-LLB)*

In *Fig. II-16*, it is observed that the ionomer peak initially located at q~0.1Å^{-1} shifts toward smaller angles. The evolution of the ionomer peak's position and intensity at short intervals of time indicates that the ionic domains' size increases with time during immersion in liquid water at 85ºC

(the red line is a guide for the eyes). The continuous increase of characteristic distance between scattering objects, $d_{ionomer}=2\pi/q_{ionomer}$, is plotted in *Fig. II-16 (B)*. The distance is found to increase from 59Å to 73Å within 1h. This evolution is more pronounced for the first 30 min. We can therefore ascertain that the treatment time strongly influences the membrane nano-swelling.

We have shown that the structural modification on sPEEK membranes depends on both temperature and time. Now we will focus on the evolution of the morphology at different temperatures for longer periods of time and investigate the kinetics of structural modifications.

II.4.2 Influence of exposition at different temperatures for long periods of time on membrane morphology

We studied the structure of sPEEK(1.3a) membranes swollen in liquid water for 10h and 1000h at 40ºC, 60ºC, 80ºC and 100ºC. The SAXS experiments were carried out in membranes conditioned in liquid water (only a few drops to prevent membrane from drying during the experiment) at room temperature in Cs^+ form. *Fig. II-17* displays the SAXS profiles of sPEEK(1.3a) after hydrothermal treatment for 10h and 1000h at different temperatures. For the sake of brevity, the SAXS spectra recorded between 10h and 1000h are not shown.

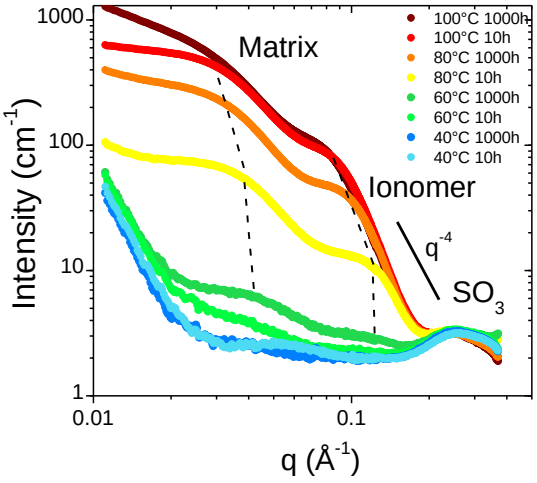

Fig. II-17 *Log-Log SAXS profiles of water swollen sPEEK(1.3a) membrane in Cs^+ form at room temperature after thermal treatment in liquid water at 40°C, 60°C, 80°C, 100°C for different times of 10h and 1000h. The spectra were recorded at D2AM ESRF beamline.*

At 40ºC, the very low water uptake does not provide significant electron density contrast between the hydrophobic and the hydrophilic domains, impeding measurement of the correlation peak. There is no noticeable evolution up to 1000h at 60ºC, and the intensity of scattering profiles shows an evolution between 10h and 1000h, but the ionomer peak position seems stable, at approximately 0.12 $Å^{-1}$. We can observe that the position of the ionomer peak is also at 0.12 $Å^{-1}$ for membranes immersed at 80ºC for 10h. The position of the ionomer peak at 80ºC evolves, showing swelling with *q*-values found at"$q_{80ºC\ 10h}$"~0.12 $Å^{-1}$ and "$q_{80ºC\ 1000h}$"~0.09 $Å^{-1}$. Moreover, there is an abrupt departure of the scattered intensity and the peak is followed by an evolution of the slope to a q^{-4} behavior. From this high, *q*-value behavior (*Porod´s Law*) at 80ºC for times between 10h and 1000h, a noticeable change of slope can be observed. It would have been interesting to extract quantitative data for the specific surface (area of polymer−water interface per polar head) using the

Porod's representation ($Iq^4=f(q)$). However, the intense SO_3 peak immediately follows *Porod's* regime, which in turn hinders the exploitation of *Porod's* regime. At 100ºC, the scattering profiles show a mild evolution with respect to 80ºC, as the position of the ionomer peak does not drastically shift after 10h, with *q*-values evolving between 0.08Å^{-1} and 0.07Å^{-1}.

We can perform more quantitative analyses from the spectra of *Fig. II-17* and extract the microscopic swelling from the position of the ionomer peak. As we have seen previously, the microscopic degree of swelling is associated to the correlation distance between the ionic domains and extracted from the ionomer peak position.

Fig. II-18 shows the characteristic distance "d_{iono}" ($d_{iono}=2\pi/q_{iono}$) as a function of the hydrothermal treatment time for 60ºC, 80ºC and 100ºC.

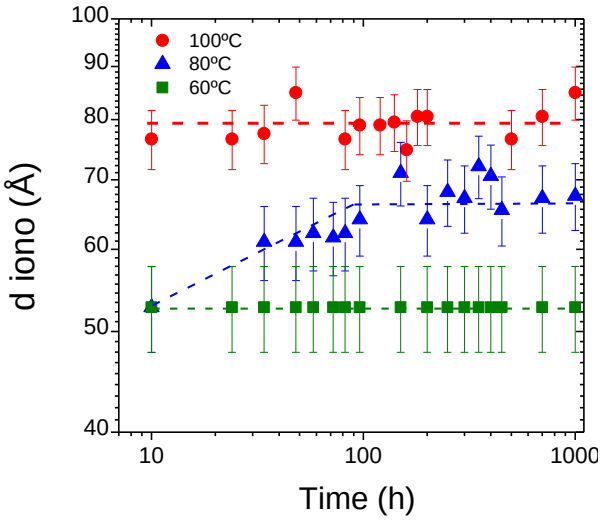

Fig. II-18 *Log-Log evolution of the characteristic distance $d_{iono}=2\pi/q_{iono}$ as a function of time of hydrothermal treatment in liquid water for sPEEK(1.3a) membranes at 60ºC(■), 80ºC(▲)and 100ºC(●). The dotted line for sPEEK membranes is an eyes guide.(Error bar +/-5Å)*

As we can see in *Fig. II-18*, the size of the ionic domains for membranes prepared at 60ºC and 100ºC does not significantly evolve with time (within experimental accuracy). At 100ºC the values are scattered in the range of 77-85Å, with a mean value of ~80 Å. We can hypothesize that there is no significant modification of the nano-swelling as a function of time at 100°C. In contrast, at 80ºC the distance is found to increase from 52Å to 72Å within 96h and then remains constant up to 1000h.

These observations could be related to different kinetics of structural modifications. At low temperature, the structural organization could be too slow to observe the evolution of nano-swelling. At 80ºC we can observe the evolution at times below 96h and at high temperature, the structural organization could be extremely fast (lower than 10h).

As previously established, the immersion in water at elevated temperatures allows a sufficient molecular mobility to improve the self-assembly, resulting in better nano-phase separation between hydrophobic and hydrophilic domains of the membrane. However, the time of

immersion at low temperatures between 60°C and 80ºC plays an important role in membrane swelling and structural modifications. We observe the following:

- The scattered intensities are highly dependent on both temperature and time. The intensities at 10h are higher than T=100ºC. At a given temperature, the intensities at t=1000h are higher than at t=10h (this effect is particularly pronounced in the 80ºC treatment). This might arise from differences in electronic density of hydrophilic and hydrophobic domains.

- The interfacial behavior evidenced at high *q*-values (linear behavior) also depends on both time and temperature. For membranes treated at 80 ºC, we observe the evolution of the slope with a q^{-4} behavior obtained at long times. This observation highlights the influence of time on the interfaces between hydrophobic/hydrophilic domains.

An appropriate choice of temperature and time allow us to obtain the optimal nano-phase separation. In order to understand the swelling behavior for a membrane with well-defined nanophase separation, it is necessary to study the microscopic swelling in liquid water at room temperatures.

II.4.3 Long-term behavior of treated membranes

One of the previous samples was kept in liquid water at room temperature for 2 years. This allowed for an opportunity to evaluate the evolution of the structure over a very long period of time.

SAXS experiments were carried out on sPEEK(1.3a) membranes conditioned in liquid water and Cs^+. The membrane was treated for 200h at 80ºC and analyzed by SAXS at D2AM ESRF Beamline. The membrane was then stored for 2 years in liquid water, and then analyzed in the same conditions with the INAC-SAXS spectrometer.

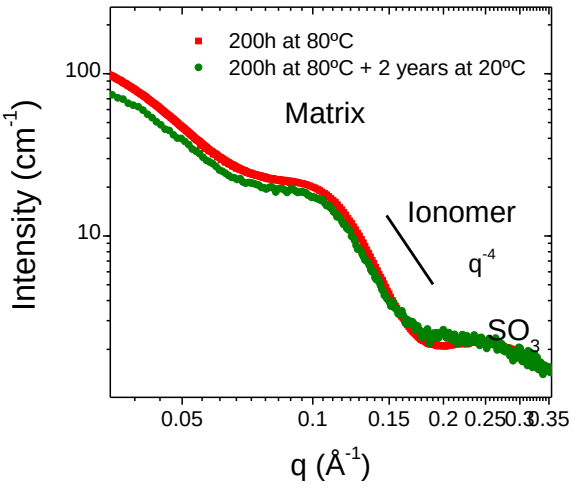

Fig. II-19 *Log-Log SAXS profiles of: membrane equilibrated in liquid water at room temperature: sPEEK(1.3a) in Cs^+ form treated at 80ºC for 200h (●) and the same membrane measured 2 years later(●).*

Fig. II-19 shows the scattering spectra obtained for this membrane at these two different times: the membrane treated at 80ºC for 200h and the same membrane after two-year storage in liquid water at room temperature. For the membrane treated at 80ºC for 200h, we observe a typical SAXS spectra of sPEEK membranes with a matrix peak, ionomer peak and SO_3 peak, positioned at

q-values about 0.036 $Å^{-1}$, 0.1 $Å^{-1}$and 0.25 $Å^{-1}$ with well-defined nano-phase separation (q^{-4} behavior). After the two-year storage in liquid water, the recorded SAXS recorded spectrum is virtually superimposable. The microscopic swelling of well-defined nanostructured sPEEK membrane in liquid water at 20 °C does not evolve with time.

It has been established that Nafion® membranes exhibit well-defined nanophase separation beginning at the very first steps of hydration [12]. For sPEEK membranes, the well-defined nanophase separation is triggered by hydrothermal treatments. The swelling behavior at room temperature for nanophase separated sPEEK and Nafion® membranes may then be estimated to be similar, with a sharp interface between hydrophilic/hydrophobic domains. However, we evidence here a completely different behavior between the two types of membranes. Indeed, for Nafion® membranes [144], a remarkable ongoing swelling behavior was observed (over several years) and was attributed to a continuous long-term rearrangement in the polymer backbone upon hydration conditions.

We have observed the effect of hydrothermal treatment at different temperatures as a function of time on membrane microstructure. In the next section, we correlate these observations to functional properties.

II.4.4 Impact of the exposition at different temperatures for long periods of time on the functional properties

In this section, functional properties such as swelling and conductivity will be analyzed as a function of immersion time in liquid water at different temperatures. These macroscopic observations are explained in regards to the microstructural evolution evidenced in the previous *section II.4.2*

II.4.4.1 Swelling

The values of water uptake were measured at room temperature for membranes treated by immersion in liquid water for periods of time between 24h to 1000h at 60ºC, 80ºC and 100ºC.

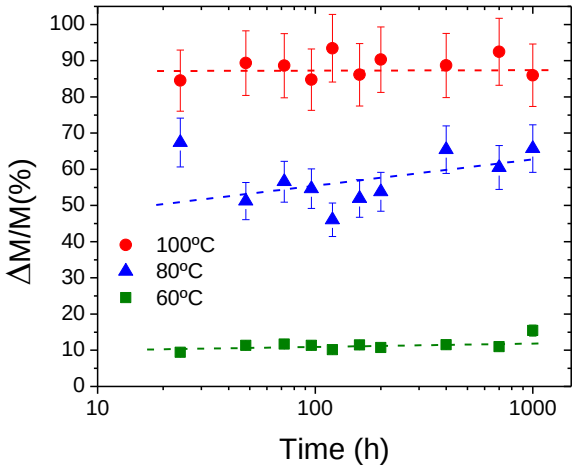

Fig. II-20 *Swelling of sPEEK(1.3a) membranes at room temperature after hydrothermal treatment at 60ºC (■), 80 ºC(▲), and 100ºC(●) for a period of time between 24h and 1000h. The dotted line serves as a visual guide.*

Fig. II-20 shows sPEEK(1.3a) membrane swelling for a period of time between 24h and 1000h at different temperatures. The macroscopic swelling at 60ºC and 100ºC seems stable for this period of time, with mass percentage of water uptake around 10 % and 90%, respectively. Yet at 80ºC, a gradual rise up to 48h is observed from 50 % to 65 %.

The evolution of macroscopic swelling on treated membranes is not remarkable as a function of the time of immersion in liquid water. However, we observe a clear evolution as a function of temperature. Therefore, the predominant parameter driving the swelling behavior is the temperature of treatment, as seen in the previous *section II.3.2.1* dedicated to the characterization of macroscopic swelling. We notice that the macroscopic swelling behavior is clearly related to the microscopic swelling as observed from scattering experiments.

II.4.4.2 Conductivity

Conductivity measurements for sPEEK(1.3a) membranes were carried out at room temperature in a homemade conductivity cell. The membranes were treated at 60ºC, 80ºC and 100ºC for a period of time between 10h and 1000h. *Fig. II-21* displays the results.

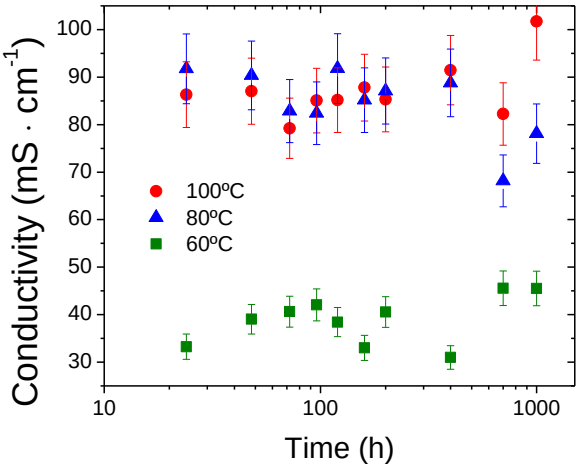

Fig. II-21 ***Proton conductivity at room temperature of sPEEK(1.3a) membranes treated at 60ºC(■), 80ºC(▲)and 100ºC(●) by immersion in liquid water for different periods of time.***

The conductivity at 60ºC shows a steady rise during the hydrothermal treatment, from 35mS/cm (10h) to 45mS/cm (1000h). For membranes treated at 80ºC and 100ºC, the conductivity is almost stable during the time-scale of the treatment and fluctuates around a mean value of 90mS/cm, remaining almost entirely stable.

Conductivity experiments show the difference between the membranes with a rough nano-phase separation (60ºC) and membranes with a well-defined nano-phase separation (80ºC and 100ºC). At 60ºC, the increase of the ionic conductivity can be attributed to a decrease of the tortuosity on the surface of polymer network matrix [20]. The improvement of the nanophase separation quality demonstrates the important role played by the polymer chemistry on the proton transport, the affinity of water and polymer matrix. This is further evidence that the conductivity of membranes at room temperature is not only related to the water content but also to the quality of the nanophase separation, this latter parameter being the most predominant.

The evolution of functional properties of sPEEK as a function of time of immersion is related to morphology. This study was performed by immersion in liquid water. In the next section, we study the influence of the vapor water on the membrane morphology of the time for membranes at given time and at 80ºC.

II.4.5 Conclusion: Impact of time on hydrothermal treatment

At this stage, we conclude that:

- The temperature acts as activator of structural modification on sPEEK membranes treated in liquid water.
- The period of time required for obtaining well-defined nano-phase separations depends on the temperature. The lower the temperature, the higher the time.
- There is no evolution of the microscopic swelling at room temperature, even after an immersion in liquid water for long periods of time (2 years).

II.5 Impact of the hydrothermal treatment in vapor water

sPEEK(1.3a) treated in vapor water at 80°C were analyzed by SAXS at D2AM ESRF beamline . The experiments were performed at room temperature; the membranes were prepared in Cs^+ form and conditioned in pure liquid water. The evolution of the scattering profiles as a function of time are shown on *Fig. II-22*.

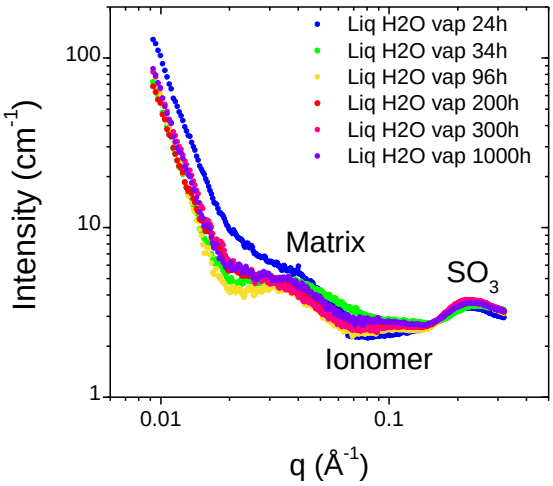

Fig. II-22 *Log-Log SAXS profiles of sPEEK(1.3a) membranes (Cs^+ form) treated in vapor water at 80ºC for long periods of time. Membranes were conditioned in liquid water at room temperature.*

The scattering profiles display similar features for low water content and are virtually superimposable. They exhibit an intense small-angle up-turn followed by a matrix peak located at about q~0.025Å^{-1} and a hardly distinguishable ionomer peak located at about q~0.1Å^{-1}. The SO_3 peak is located at about q~0.25Å^{-1}.

Only weak evolution of ionomer and matrix peaks' intensities are observed as a function of time, even when the analysis conditions (sPEEK membranes conditioned in liquid water) were suitable for observing these scattering peaks. The swelling in vapor water does not allow sufficient molecular mobility nor the plasticizing effect of the ionic groups to yield to the onset of the structural modifications (clear appearance of an ionomer peak/ interface evolution).

Even when the membrane was previously treated in liquid water at 80ºC, the water uptake at 100% RH (vapor conditions) at room temperature was similar in both nanostructured and non-nanostructured membranes (water sorption analyzes). We can conclude that three parameters govern the nano-phase separation process: temperature, time and water phase.

Interestingly, *Legrand's* [145] work in 2012 showed that sPEEK membranes aged with hydroperoxide during a short period of time yielded a significant improvement of the fuel cell performances on sPEEK [145]. From these results, we studied the evolution of the microstructure in oxidative conditions in order to establish the correlation between structure and performances.

II.6 Impact of oxidative treatment on the membrane microstructure

sPEEK limited lifetime in fuel cell is attributed to chemical degradation. The chemical degradation of sPEEK results from the addition of hydroxyl and hydroperoxyl radicals and chain scissions leading to the formation of carboxylic acids [92, 146].

sPEEK(1.3a) membranes were studied by SAXS (on the D2AM-ESRF beamline) in order to understand the influence of the oxidative degradation which could improve chain mobility and activate the structural modifications on the membrane (clear emergence of the ionomer peak/interface evolution). sPEEK(1.3a) membranes were treated at 80°C by immersion in hydroperoxide 0.1% mass solution for different times conditioned in liquid water and Cs^+ form.

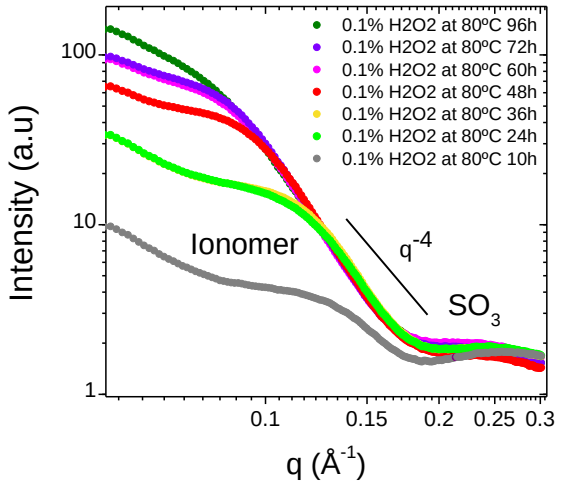

Fig. II-23 *Log-Log SAXS profiles of sPEEK(1.3a)in Cs^+ conditioned in liquid water. Membranes were treated with H_2O_2 0.1% mass concentration at 80°C during a period of time between 10h and 96h. The spectra were recorded at D2AM ESRF beamline.*

Fig. II-23 shows the emergence of the ionomer peak and well-defined hydrophobic/hydrophilic nano-phase separation in sPEEK membranes treated in oxidative conditions for periods of time greater than 24h. The ionomer peak grows and shifts towards smaller angles, becoming extremely broad.

sPEEK(1.3a) membranes treated in oxidative conditions by immersion in different ratios hydroperoxide solutions (0.1%, 0.25%, 1% wt) at 80ºC were analyzed in liquid water and Cs^+ form. *Fig. II-24* shows the characteristic distance between the ionic domains as a function of the lengthening time, and d_{iono} values of sPEEK(1.3a) treated in liquid water at 80ºC are also plotted to highlight the effect of hydrogen peroxide.

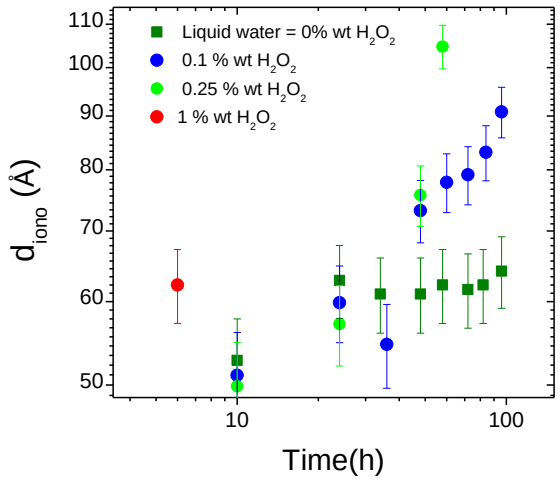

Fig. II-24 *Characteristic distance of ionomer peak as function of lengthening time. Membranes treated in different concentrations of liquid H_2O_2 at 80ºC and membrane in liquid water at 80ºC.*

We observe that the size of the ionic domains increases as a function of time of oxidative treatment for each ratio of H_2O_2 solutions.

- For ratios of 0.1%wt of H_2O_2, the characteristic distance "d_{iono}" as a function of time is found to increase from ~51Å to ~91Å within 96h. This spectacular evolution is more pronounced after 36h of treatment.

- For ratios of 0.25% of H_2O_2, an increase of the distance from ~49Å to ~105Å is observed within 58h. It was observed that after this treatment time, the membrane became very brittle, and no measurements were therefore carried out.

- For 1%wt of H_2O_2, only the membrane treated for 6h could be analyzed.

Comparing the sPEEK membranes treated in liquid water with those in oxidative conditions, we observe that for times less than 36h, the characteristic distance "d_{iono}" is higher for treatment in liquid water than oxidative conditions. After this time, an inversion of the behavior is observed. Indeed, the membranes treated in oxidative conditions exhibit a higher swelling at the nanoscale than sPEEK membranes treated in liquid water. We propose that the degradation of the membrane starts after 36h of oxidative treatment for ratios of H_2O_2 of 0.1% and 0.25%wt. Before this membrane ageing, the structural modifications are primarily driven by the presence of water in the solutions, i.e. a hydrothermal treatment-like effect. To summarize, there are two main effects:

- Hydrothermal treatment due to water.
- Ageing due to chain scissions in presence of H_2O_2, leading to membrane overswelling.

We hypothesize that the oxidative treatment involves an overswelling of the membranes at low concentrations of hydroperoxides. For solutions with concentrations above 0.25%, the degradation may be too fast for observing the structural modifications of the membrane. At 0.1% and 0.25%, we observe the role played by water and hydroperoxides. The chain scission improved the overswelling of sPEEK membranes but the structural modifications are produced by liquid water and temperature.

II.7 Conclusions

After a careful survey of the literature related to the structural analysis of sPEEK membranes, it appears that a clear picture could not be obtained. In addition, the possibility to design sPEEK membranes with various degrees of sulfonation (DS), to use different casting solvents and membrane cleaning procedures, it gives rise to a wide span of SAXS spectra with characteristic peak located at different scattering ranges. Generally, only one peak was observed in the scattering spectra and was naturally attributed to the so-called ionomer peak.

In order to gain further insight, we performed a complete study of the microstructure as a function of overswelling conditions by means of SAXS, SANS and WAXS. We demonstrated that the swelling temperature on sPEEK membranes has a strong impact on the membrane morphology, as evidenced by the three simultaneous peaks in the scattering spectra of sPEEK. We therefore conclude that a single peak observation can result in misleading interpretations.

We evidenced for the first time three peaks simultaneously on the SAXS spectra of sPEEK membranes:

- The wider angle peak, associated to the mean separation distance between sulfonic acid groups grafted onto the polymer backbone.
- Two other small angle peaks on swelled membrane attributed to the ionomer and matrix peaks.

This peak attribution was confirmed by studying the impact of the electron density contrast and the impact of the IEC on the peaks' positions and intensities. We also compared our findings with the structural data of the benchmark Nafion® membrane. **We conclude that the immersion of sPEEK in water at elevated temperatures allows for sufficient molecular mobility and structural modifications that provide well-defined nanophase separation between hydrophilic and hydrophobic phases.**

We also studied the impact of time on the nanostructure and on the membrane's functional properties for different immersion temperatures. It was evidenced that the time of pretreatment as well as the storage of the membranes play an important role in resulting membrane morphological property interplay.

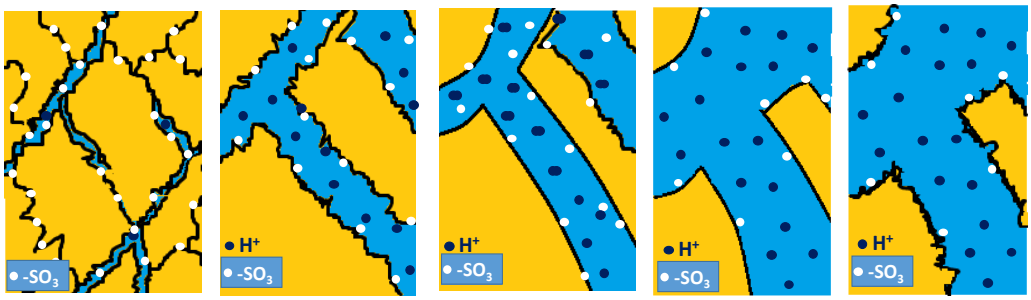

1) Pristine membrane | 2) T= 60°C | 3) T=80°C for10h | 4) T=80°C for 1000h | 5) T=80°C for 1000h rev

Fig. II-25 *Schematic representation of the rearrangement produced by hydrothermal treatment in liquid water.*

The schematic representation of the rearrangement is shown in the *Fig. II-25*. The well-defined nanostructuration of sPEEK membranes is reached through the following steps:

1) Penetration of water between polymer aggregates, promoted by hydrothermal treatment and temperature at 60ºC.

2) and 3) Propagation over the membrane volume. The position of the ionomer peak at 80ºC for 10h of treatment corresponds to that measured at 60ºC, therefore the mean separation distance between ionic domains is similar. Yet we observe a clear evolution of the interface between hydrophilic and hydrophobic domains, from rather rough (at 60ºC) to sharp and well-defined (at 80ºC).

4) Swelling of the membrane, q^{-4} behavior at large angles and shift of ionomer peak towards small angles at 80ºC for 1000h.

5) The structural modifications take place with a hydrothermal treatment, but this process is reversible when the membranes are dried.

Thanks to the attribution of SAXS peaks and a careful analysis of the hydrothermal treatment effect on the microstructure of sPEEK membranes, we can relate the microstructure to the functional properties of the polymer.

The onset of overswelling and increased conductivity was observed for temperatures above 60 ºC, which corresponds to important nanostructure modifications induced by the hydrothermal treatment. We demonstrated that the proton conductivity is mostly impacted by the quality of the phase separation on the nanoscale.

Appropriate control of this structural modification process appears to be necessary in order to optimize sPEEK membrane fuel cell properties. Different ways to control the nanostructure were also analyzed through vapor and oxidative conditions, leading to the conclusion that the hydrothermal treatment in liquid water is the best protocol to obtain a sPEEK membrane with well-defined nano-phase separation and good chemical and physical integrity of the membrane.

This treatment is selected as a preliminary step for allowing sPEEK membrane to be the host matrix for a reactive sol-gel network.

CHAPTER III

HYBRID MEMBRANES ELABORATION BY SOL-GEL PROCESS

Despite the intense research and technological efforts dedicated to the development of the fuel cell during the last decades, it widespread implementation is still hampered by several issues, in particular the ones related to the ionic exchange membranes at the core of the device:

- A drop of proton conductivity at low relative humidity and therefore of the fuel cell performances [139].
- Limited chemical and mechanical stability and low mechanical behavior over 80 °C reflected in drop of the functional properties.

Improved membranes that can perform better and less expensive than the current generation of polymer membranes are needed. One of the solutions that can be envisioned is the development of hybrid membranes, in particular hybrid membranes prepared by sol-gel process.

The expected properties of a performing hybrid membrane should not have a negative influence on the chemical stability, mechanical stability nor the conductivity, but should provide:

- Improvement of the chemical stability, *i.e*. limited chemical degradation due to radical attacks.
- Improvement of the mechanical stability during fuel cell operation.
- High conductivity, i.e. conductivity over 100 mS/cm in fuel cell conditions (high temperatures and low %RH).

In this chapter[b], we will describe our strategy to prepare hybrid membranes using the sol-gel impregnation approach. We will present the effect of the various parameters on the elaboration process and conclude regarding the best conditions to prepare an optimized hybrid membrane.

[b] All hybrid membranes obtained during this work use a sPEEK(1.3b) membrane as a host membrane.

III.1 Hybrid membrane

Our main objective is to develop novel hybrid membranes consisting of a commercial ionomer matrix in which we will introduce precursors capable to form a chemically and physically active sol-gel phase. The control of the chemistry of this sol-gel phase, its morphology and its location in the membrane, which will improve the membrane properties, are essential to consider the development of these membranes for fuel cells operating at high temperature and low RH. It must be noted that impregnation method should allow the formation of the sol-gel phase into a host membrane without the perturbation of the initial nanostructuration of the membrane.

III.1.1 Principle of hybrid membranes preparation

Our objective is to prepare a host membrane with a well-defined nanophase separation between de hydrophilic and hydrophobic domains and then impregnate the ionic domains with sol-gel precursors that will give a sol-gel phase after condensation.

- The sol-gel phase plays the role of a mechanical reinforcer.
- The sol-gel phase can be tailored to provide chemical reactivity to hybrid membranes. To improve the device lifetime, the reactive groups of sol-gel phase can be designed to inhibit the membrane chemical degradation.

*** <u>The precursor</u>**

The precursor choice, in the case of our study, is the most important parameter to obtain hybrid membranes with improved long term performances. As explained on *Chapter I* this precursor is composed by an organofunctional group and at least a hydrolysable group. In our case we will study a reactive precursors with the structure showed in *Fig. III-1*.

$$(RO)_{4-n}Si\ X_n$$

Fig. III-1 *General formula of silane with hydrolysable group (RO) and a functional chemical reagent (X).*

The general formula for a sol-gel highlighting the two kinds of groups attached on the silicon atom:

- Reactive function of the organofunctional group (X). It must be more chemically reactive with the hydroperoxide radicals than the sPEEK polymer matrix. Therefore, it will prevent a chemical degradation.

- Hydrolysable groups of sol-gel precursor (RO), which allows the sol-gel process, forming chemical bonds to obtain a sol-gel phase which improves the mechanical properties and water retention properties. The sol-gel cross-linked density can be adjusted according to the number of hydrolysable groups carried by the sol-gel precursor.

The combination of both characteristic behaviors (see *Fig. III-1*) drives us to choose one kind of precursors, the mercapto-silanes. The mercapto group reacts with the hydroperoxides formed during the fuel cell operation, the final reaction product being SO_3H groups [147] (*Fig. III-2*). This high reactivity of the mercapto group compared with the reactivity of the polymer

matrix provides a chemical protection. In addition to the antioxidant properties of this reactive group, its oxidation leads to the formation of sulfonic groups. Therefore during fuel cell experiment an improvement of the proton conductivity of the hybrid membrane is expected.

Based on the requirements for processing a hybrid membrane, we have chosen the commercial precursor **(3-mercaptopropyl)-methyldimethoxysilane**, provided by Sigma Aldrich (properties in *Annex A.2)* and will be labeled **SHdi** in the following.

This **SHdi** precursor satisfies the requirements to obtain a hybrid membrane:

1.-The presence of alkoxy group will allow forming an inorganic phase by sol-gel reaction (*Fig. III-2 red color*).

2.- The presence of the reactive group will protect the membrane from oxidation (H_2O_2 and radical attacks) and, as a final product of the reaction, will form a proton conductor group (SO_3H) (*Fig. III-2 green color).*

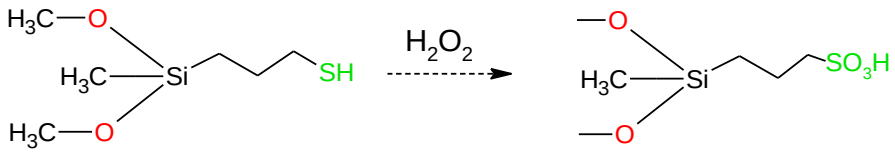

Fig. III-2 *SHdi precursor: SO_3H product of the SH oxidation by H_2O_2 formed during the fuel cell operation[147].*

A schematic representation of the principle of this hybrid membranes elaboration process is displayed in *Fig. III-3*. The host ionomer membrane must present a well-defined nano-phase separation, which ensured good functional properties. We highlight in yellow color the polymer matrix and in blue color the water into the ionic domains. The green dots represent the acidic units present along the macromolecular backbone of the polymer matrix (SO_3H groups of the host membrane), which are located at the hydrophobic/hydrophilic interface. The sol-gel phase is represented as a black line inside the ionic domains on the host membrane, with their functional groups represented as red points. The role of the sol-gel phase is expected to be:

1.- The improvement of the chemical stability of the ionomer host membrane, by maintaining in close contact the stabilizing units and the hydrophilic polymer phase, and preventing their elution.

2.- The improvement of the mechanical strength of the membrane constraining the dimensional changes, resulting in better mechanical integrity and long-term stability.

3.- The improvement of the proton conductivity of the hybrid membrane via the oxidation of the functional groups.

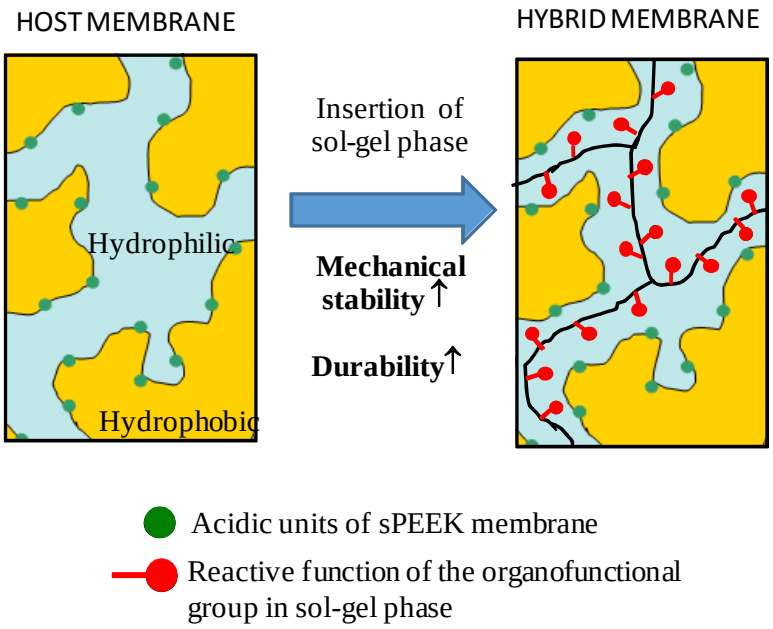

Fig. III-3 *Schematic representation of hybrid membrane morphology obtained from a nanostructured host ionomer membrane .Green points corresponds to de acidic units in the host membranes and red points corresponds to reactive function of the organofunctional part in sol-gel phase.*

III.1.2 The reaction parameters

The choice of various parameters (pH, acid conditions and water/precursor ratio) will be discussed. Based on the literature exposed in the *Chapter I*, we selected the sol-gel impregnation parameters as follows:

1.- The solvent is methanol (**MeOH)**. As said before, the alkoxy group and the solvent will be similar in order to avoid the introduction of different alcohol solvent during the hydrolysis step.

2.- The pH of the reaction is **pH=4** (controlled by acetic acid) in order to favor the hydrolysis kinetic instead of the condensation's one (primarily linear networks)[117].

3.- The reaction will be performed under stirring at **room temperature** to ensure the sol-gel precursor diffusion into the hydrophilic domains of the host membrane prior their condensation.

4.- The ratio of water/Alkoxy is chosen to be R >12 to obtain a dense, non porous sol-gel phase and to reduce the kinetic of self-condensation of the sol-gel precursor.

5.- The concentration of sol-gel precursor chosen is 0.21 mol/L in order to obtain a diluted solution to swell the sPEEK membrane.

The quantities of **SHdi**, sPEEK and solvent used for membrane preparation are summarized in *Table III-1*. The membrane surface was sufficient to make several experiments for each batch.

Table III-1 *Quantities of SHdi Precursor, Solvent and sPEEK membrane.*

SHdi Precursor	sPEEK (1.3b)	Volume of solvent (Water/Methanol) mixture
0.21mol/L	~ 550 mg (8cm*14cm*30µm)	38.4 mL

The next section of the chapter will be focused on the selected parameters to sol-gel impregnation and the membranes characteristic under these conditions.

III.1.3 The conditions and sol-gel impregnation

Sol-gel processing proceeds in several steps that will be subsequently discussed.

STEP 1: **Membrane conditioning.**

a) Pristine membrane conditioning to become a host membrane.

b) Membrane solvent exchange in solvent mixture to prepare the impregnation process.

STEP 2: **Impregnation parameters**.

a) Impregnation of alkoxy silanes. Hydrolysis and condensation of the molecular precursors as function of water/alkoxy silanes ratio.

b) Impregnation of alkoxy siloxanes as function of time.

STEP 3: **Curing treatment.**

***STEP 4*:** **Hydrothermal treatment.**

III.1.3.1 STEP 1: Membrane conditioning

III.1.3.1.1 Pristine membrane conditioning. Hydrothermal treatment

Our objective is to prepare a host membrane with a well-defined nanophase separation between the hydrophilic and hydrophobic domains and then impregnate the ionic domains with sol-gel precursors that will give a sol-gel phase after condensation.

A hydrothermal treatment was applied to commercial sPEEK membranes. It was carried out in liquid water at 80ºC for different immersion time. Treated sPEEK membranes were analyzed by SAXS at ESRF in the Cs^+ form after treatment in liquid water at 80ºC for immersion time ranging from 3h45' to 72h. At 3h45' and 17h30' the SAXS spectra (*Fig. III-4* ***A***) show the presence of an ionomer peak located at q~0.13Å^{-1} (Bragg spacing~50Å). This ionomer peak position seems stable even at longer times but we notice an evolution of the slope (large values of q-value) until a q^{-4} behavior is reached at 72h.

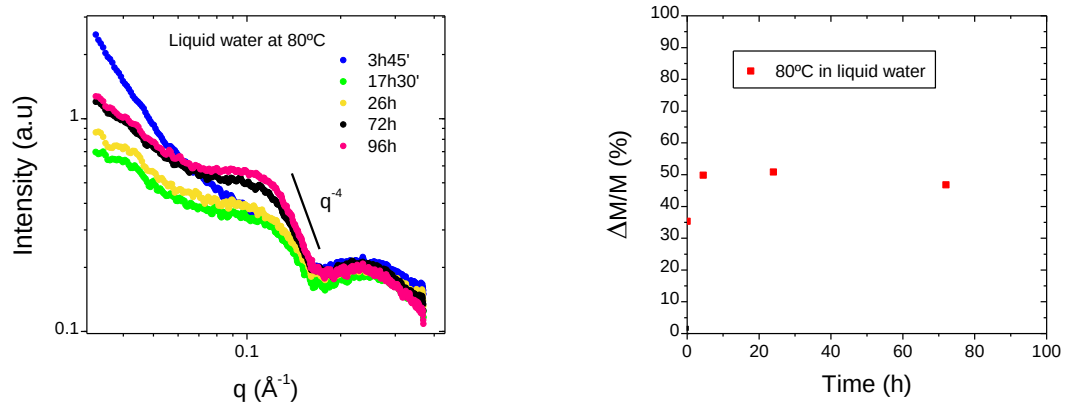

Fig. III-4 *(A) Log-Log SAXS profiles of water swollen sPEEK membrane in Cs^+ form at room temperature after an hydrothermal treatment in liquid water at 80°C for different times. The spectra were recorded on D2AM ESRF beamline. (B) Corresponding to the gravimetric swelling of sPEEK membranes.*

As we stated in *Chapter II*, the membrane microstructure impacts the membrane swelling. *Fig. III-4* ***B*** shows the sPEEK membrane swelling. It increases when membranes were treated in liquid water at 80ºC. An increase of membrane swelling from 18% to 32% is observed for 4h30' of hydrothermal treatment. After this swelling a weak evolution of swelling for membranes treated during 24h and 72h is observed.

We conclude that a sPEEK membrane treated at 80ºC for 72h offers a reasonable free volume to host the sol-gel and a well-defined nano-phase separation for an excellent proton conductivity. This host membrane will be labeled "*sPEEK NS*"

III.1.3.1.2 Membrane swelling in water/methanol

In the state-of-the-art *section I.5.1.2*, we showed the influence of the solvent on the sol-gel reactions, and we concluded that the solvent must be a water/alcohol mixture. We also highlighted that preferably the solvent has to coincide with the byproduct of the reaction but in our case the amount of methanol formed during sol-gel process is insignificant in relation with the amount of solvent and will not be considered as having any impact. We chose the methanol has a solvent because of the strong sPEEK swelling on it.

We report the influence of the ratio of water (pH=4)/methanol on the host membrane mass swelling. The swelling is monitored by measuring the weight (M) of the membrane. In *Fig. III-5* we compare the weight variations ($\Delta M/M_{dry}$, $\Delta M=M_{wet}-M_{dry}$) of pristine membrane and a nanostructured sPEEK membrane (*sPEEK NS)* at different ratio of water (ph=4)/methanol mixture.

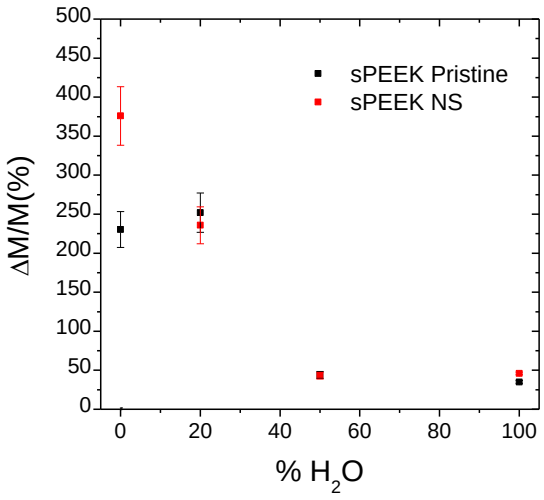

Fig. III-5 *sPEEK pristine membrane and sPEEK NS (sPEEK membrane treated during 72h at 80ºC)in Water (pH=4)/Methanol mixtures for 4 days.*

The membranes in H^+ form were immersed in the solvent mixtures for 4 days before measurements, this time seems long enough to ensure complete hydrolyze of precursors during the impregnation step [148]. We have studied the swelling in the solvent mixture, it will be useful to understand the futures analysis.

The membrane swelling of pristine membrane (*sPEEK pristine*) and nanostructured membrane *sPEEK NS* are similar for water/methanol mixtures above 50%. When the amount of methanol increases (the amount of water decreases) the membranes swelling explodes leading to values of 200% for 20% of water and almost 400% for *sPEEK NS* membranes immersed in 100% MeOH. The high swelling behavior in methanol/water solution, especially at high temperature or high methanol concentration, is well known in the sulfonated hydrocarbon polymer, which may cause excessive dimensional changes [149]. At high values of methanol content the overswelling of membrane could make it no operable because of membrane brittleness.

In our case, at low water content the overswelling of *sPEEK NS* membrane could help the impregnation of precursors, nevertheless the water content has a strong influence in the sol-gel reactions (hydrolysis and condensation). To determine the optimized H_2O/MeOH ratio we performed additional hybrid membrane characterization. We studied hybrid membranes by Raman spectroscopy in the next section.

III.1.3.2 STEP 2: Membrane impregnation

The hybrid membrane composition and morphology will depend on the composition of the solvent used for the impregnation and the duration of the diffusion/condensation of sol-gel precursors into the host membrane.

The precursor alkoxide solution is impregnated in a swelled *sPEEK NS* membrane in alcohol/water solvent. The membrane was immersed during different times and the solvent was composed of different ratios of H_2O/MeOH in acidic conditions. It was shaked during the process.

Then the membrane was cleaned on surface with alcohol/water mixture to avoid the formation of a sol-gel skin and then it was dried.

III.1.3.2.1 Impregnation of alkoxy siloxanes parameters

The solvent was composed of different ratios of H_2O/MeOH in acidic conditions. The solvent composition has an influence on the swelling of the host membrane but also on the sol-gel phase because the sol-gel/water ratio impacts the morphology of the sol-gel phase [73].

The ratio between the amount of sol-gel phase and sPEEK membrane was studied by RAMAN spectroscopy. In order to analyze the RAMAN spectra, we will present the spectra of *sPEEK NS* membrane and the **SHdi** precursor. We will identify the characteristic peak of each spectra and select the range to study the amount of sol-gel phase.

Fig. III-6 shows the RAMAN spectra of *sPEEK NS* membranes, **SHdi** precursor and *polySHdi100* (*SHdi100* was condensed alone in the same conditions as the ones that were selected to prepare hybrid membranes) (*Annex A.4*).

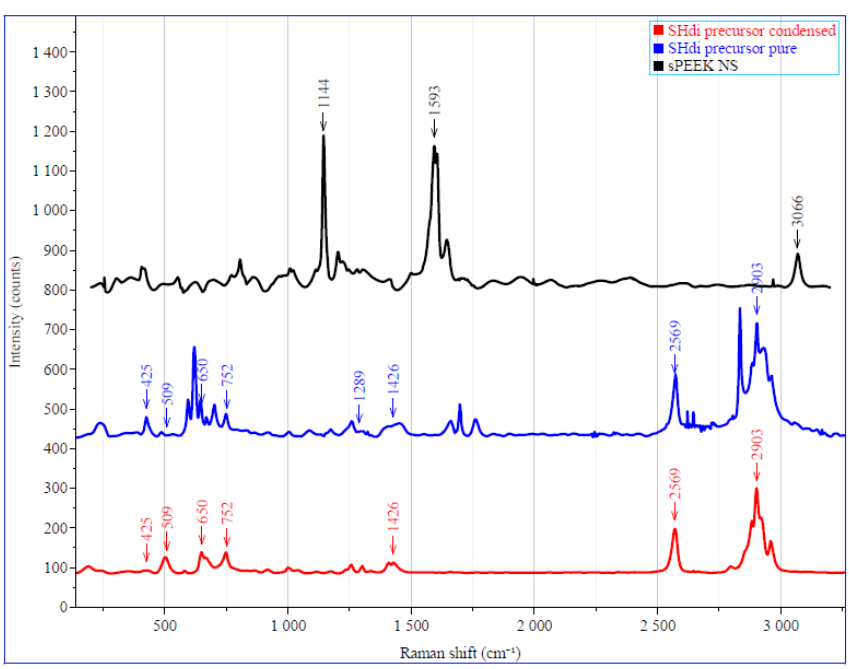

Fig. III-6 *Raman spectra of the sPEEK NS (black line) and SHdi pure precursors (blue line), and SHdi precursors self-condensed SHdi sample (red line)*

In this study we consider the peaks corresponding to the region between ca. 2250 cm^{-1} and 3200 cm^{-1} corresponding to aliphatic CH band characteristic of sol-gel phase (~2900 cm^{-1}) and the -CH of aromatic rings (~3060 cm^{-1}) characteristic of sPEEK membranes

The hybrid membranes were obtained with different ratio of H_2O(pH=4)/MeOH for a **SHdi** concentration of 0.21 mol/L after 4 days of impregnation (*Table III.1)*. After impregnation they were rinsed in the H_2O(pH=4)/MeOH, solution of the same composition which was used to

impregnate the host membrane with the sol-gel precursor (different ratio corresponding with impregnation ratio) and dried under vacuum conditions.

Fig. III-7(A) shows RAMAN spectra in the region between ca. 2250 cm^{-1} and 3200 cm^{-1} for hybrid membranes as a function of the percentage of water (pH= 4) in the solvent mixture.

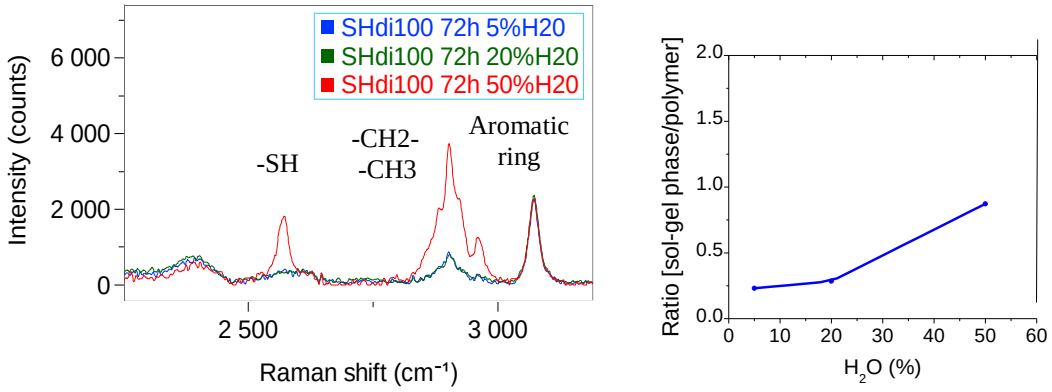

(A) **(B)**

Fig. III-7 *(A) Raman spectra for hybrid membranes obtained by different solvent mixtures water (pH=4) and MeOH. (B) Evolution of the ratio of the intensity of sol-gel phase (-CH_2- -CH_3 of the sol-gel phase) to intensity of the polymer (-CH_2- associated to the aromatic ring of sPEEK) as function of the fraction of H_2O in the solvent mixture.*

RAMAN bands were assigned to the CH of the aromatic rings of the sPEEK chain at frequency 3070 cm^{-1}, to the -CH_2-and -CH_3 of the precursors at frequency values between (2825 and 3000 cm^{-1}) and to the -SH group of the precursor at frequency of 2571 cm^{-1} [150, 151].

The relative intensity of the RAMAN spectra is associated to the content of structural units, which gives contribution in the RAMAN spectra [152]. The intensities of the -CH- of the aromatic ring of sPEEK were normalized to obtain the same area from 3025 cm^{-1} to 3115 cm^{-1} for the three spectra in order to compare the evolution of the amount of the sol-gel phase introduced into the host membrane. We plot in *Fig. III-7* (*B)* the ratio of the area of -CH_2-,-CH_3 to the area of the band associated to -CH- of the aromatic rings. This plot helps us to better observe the evolution as a function of %H_2O and the relative amount of sol-gel phase into the sPEEK membrane.

For water (pH=4) ratios in the solvent mixture of 5% and 20%, the intensity in RAMAN spectra are similar for the same amount of sPEEK membrane. *i.e*. the sol-gel rate is constant for both impregnation conditions. When the solvent composition reaches 50% of water, the sol-gel rate increases significantly, one can observe a strong increase of the intensity of the relative amount of sol-gel phase as shown by the ratio evolution. The pH calculated inside of the ionic domains of the membrane, due to the presence of sulfonic groups is extremely acid (pH~0) therefore it is more acidic than outside of the membrane. This gradient of pH will drive the sol-gel precursor diffusion into the ionic domains of the membrane ensuring the growth of the sol-gel phase inside the membrane. It is therefore expected that the kinetic reaction of hydrolysis and condensation will be faster inside than outside the membrane.

Nevertheless when the membrane swelling increases (reduction of the amount of water in the impregnation solution *Fig. III-4B)*, the pH inside the hydrophilic domains of the membrane

increases, reducing pH gradient between the membrane and the sol-gel solution. Therefore the sol-gel reaction is produced inside and outside of the membrane with the same kinetic, reducing the sol-gel content in the membrane. Besides, the hydrolysis and condensation of the alkoxy group may not be terminated, leading to the formation of short chains condensed sol-gel phase. These short chains could be dissolved during the surfaces cleaning procedure, which consists in rinsing the membrane after impregnation with a similar mixture of solvent (water/alcohol mixtures) to avoid formation of sol-gel layer on the membrane surface.

We conclude that the well suited solvent composition is 50%-50% water (pH=4)/ methanol mixture to favor a faster sol-gel formation into the host membrane than in the solution.

We also understood that the increase of the water/sol-gel precursor ratio favors the formation of a dense sol-gel phase (R>12) [117].

Another important parameter is the impregnation time, as function of the sol-gel content in the hybrid membrane.

III.1.3.2.2 Impregnation time

Impregnation time of the sPEEK membrane in the alkoxysilane solution has an influence on the sol-gel phase content into the host membrane. Therefore we can expect to be able to control the amount of sol-gel phase

The Raman spectra were acquired on hybrid membranes impregnated for impregnation times ranging from 1 to 22 days. As in the previous section, we measured the ratio of the area of -aliphatic CH to the area of the -CH of aromatic rings. *Fig. III-8* shows the evolution of the sol-gel phase content into the host membrane as a function of impregnation time in a **SHdi** solution with 50% H_2O(pH=4)/50% Methanol at room temperature. After impregnation, they were rising in the 50% H_2O(pH=4)/50% Methanol mixture and dried under vacuum conditions.

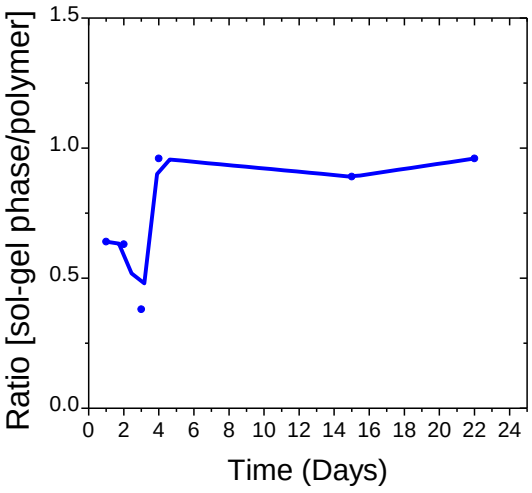

Fig. III-8 *Evolution of sol-gel phase onto the host membranes function of time of immersion for a SHdi solution of 50%H_2O (pH=4)-50%MeOH mixture.*

During the first and second day, the amount of sol-gel phase seems stable at ratio values of about R=0.6. The third day, a minimum value (R=0.4) is observed, then the sol-gel contents increase and the amount of sol-gel into the membrane seems stable at values about R=1.

We can hypothesize that such non-monotonous behavior could be related to some shrinking and/or swelling of the membrane, depending of the presence of short chains of sol-gel phase and/or the rate of self-condensation. The addition of **SHdi** yields to the evolution of the membrane swelling, which increases during the first three days. Due to this membrane swelling, the short chains of sol-gel phase can be eluted from the membrane and the sol-gel content decreases after cleaning the surface. During the condensation process, the covalent cross-linking between $–SO_3H$ groups of the host membrane and silanol groups formed from the **SHdi**-precursor may also occur [113]. More analysis of this data should be performed to understand this behavior.

This analysis shows that after **four days at room temperature** the ratio between the sol-gel phase and sPEEK membrane seems stable. We selected this impregnation time for the hybrid membrane preparation

The next step in the membrane manufacturing is the curing process.

III.1.3.3 STEP 3: Curing treatment of hybrid membrane

After four days of impregnation of the host membrane in a solvent mixture of 50% of water (pH=4) and 50% methanol in volume, with concentration of precursors ~9 mmol, the membrane was cleaned with the mixture solvent, dried and then cured.

Hybrid membranes were dried between two Teflon plates (5mm thickness to obtain a flat membrane) under vacuum conditions at room temperature for a week to eliminate the residual solvent.

The resulting membrane was thermally cured to obtain a high condensation degree of the sol-gel phase. We performed different curing treatments in order to pursue the hydrolysis and condensation of the short chains of sol-gel phase that are possibly present in the membrane.

The analyzed membranes correspond to different protocols:

Protocol 1.- Hybrid membrane without curing treatment.
Protocol 2.- Hybrid membrane treated under dry inert (Ar) atmosphere (to protect from oxidation degradation) at 80ºC for 24h in order to pursue the condensation process.
Protocol 3.- Hybrid membrane treated under inert atmosphere (Ar) at 6.3 HR% at 74ºC for 24h.
Protocol 4.- Hybrid membrane treated under inert atmosphere (Ar) at 6.3 HR% at 74ºC for 72h.
Protocol 5.- Hybrid membrane treated under inert atmosphere (Ar) at 93.5 HR% at 74ºC for 24h.

It is noted that the presence of water should enhance the formation of silanol groups by hydrolysis of **SHdi** precursors in case it would not be finished.

We will study by two different experiments the impact of curing process, by AFM and by DMA, which will allow analyzing the mechanical behavior and topography of hybrid membranes.

* **AFM (Atomic Force Microscopy)**

AFM experiments were performed on a cryo-fractured cross-section of the membranes in order to investigate the impact of the curing process on both topography and mechanical properties of the hybrid membranes. The measurements were performed on a Dimension Icon AFM (Bruker) that uses an advanced tapping mode "PeakForce^{TM} QNM^{TM}" which provides mechanical images at the same time as topographic images. The tip vibrates vertically at a fixed frequency of 2 kHz and, within each cycle, touches the surface with an ultralow force by a sinusoidal wave and the curves are displayed as force versus time for one cycle. During approach and retraction, force-time curves were analyzed at each image point to measure the following mechanical properties of the sample surface: modulus, adhesion, deformation and energy dissipation.

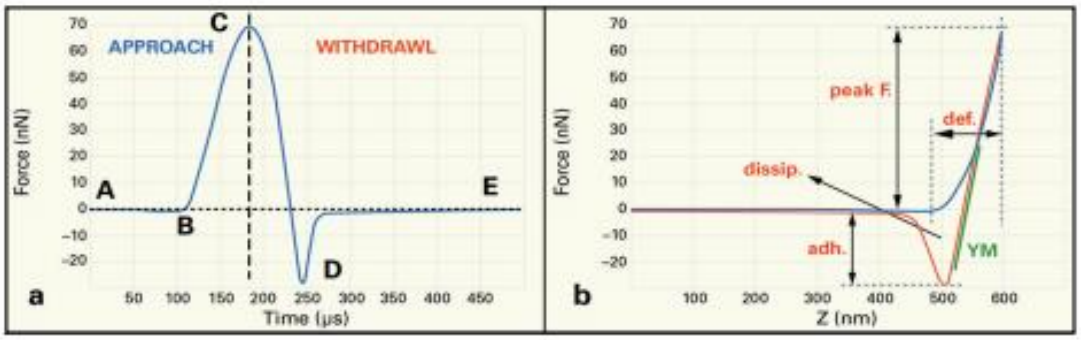

Fig. III-*9 a) One cycle of the Peak Force QMN curve. b) Resulting quantitative measurements[153]*

In our case we will use:

- Topographic images (5µmx5µm).
- Force versus time curves for one representative cycle.

In *Fig. III-10* we observe the differences between the hybrid membranes after different curing process. The first case (*Fig. III-10 (1.A)*) shows the topography of one hybrid membrane without curing process, where a homogeneous layer is observed at the surface of the hybrid membrane. When we analyzed force versus time curve (*Fig. III-10 (1.B)*), we observed that this layer displayed an important adhesion with the AFM lever, the adhesion force could be due to capillary forces with a liquid phase on the surface. We hypothesize that this liquid phase is formed because of the incomplete condensation of the precursors during the impregnation and drying process. Indeed, water condensate on the membrane cross-section during the cryo-fracturation preparation and in presence of the remaining hydrolyzed precursors, therefore hydrophilic, this water stays trapped at the surface of the membrane (hygroscopic surface).

For the two other cases, the membrane was cured in temperature, and we observed that the liquid layer on the cryofractured surface disappears for both membranes (*Fig. III-10 (2.B)* and *(3.B))*. The force-time curves showed that the adhesion force was quite higher for the membranes cured by the second protocol than by the third one. These observations coincide with our hypotheses. During the second protocol, the presence of water was prevented, the hydrolyzed precursors finish the condensation, nevertheless the non-hydrolyzed precursors stayed as silanol. In the third protocol, the curing was performed in presence of water, and the hydrolyzed precursors was condensed and the precursors with silanol groups, thanks to temperature and water was first hydrolyzed and then condensed.

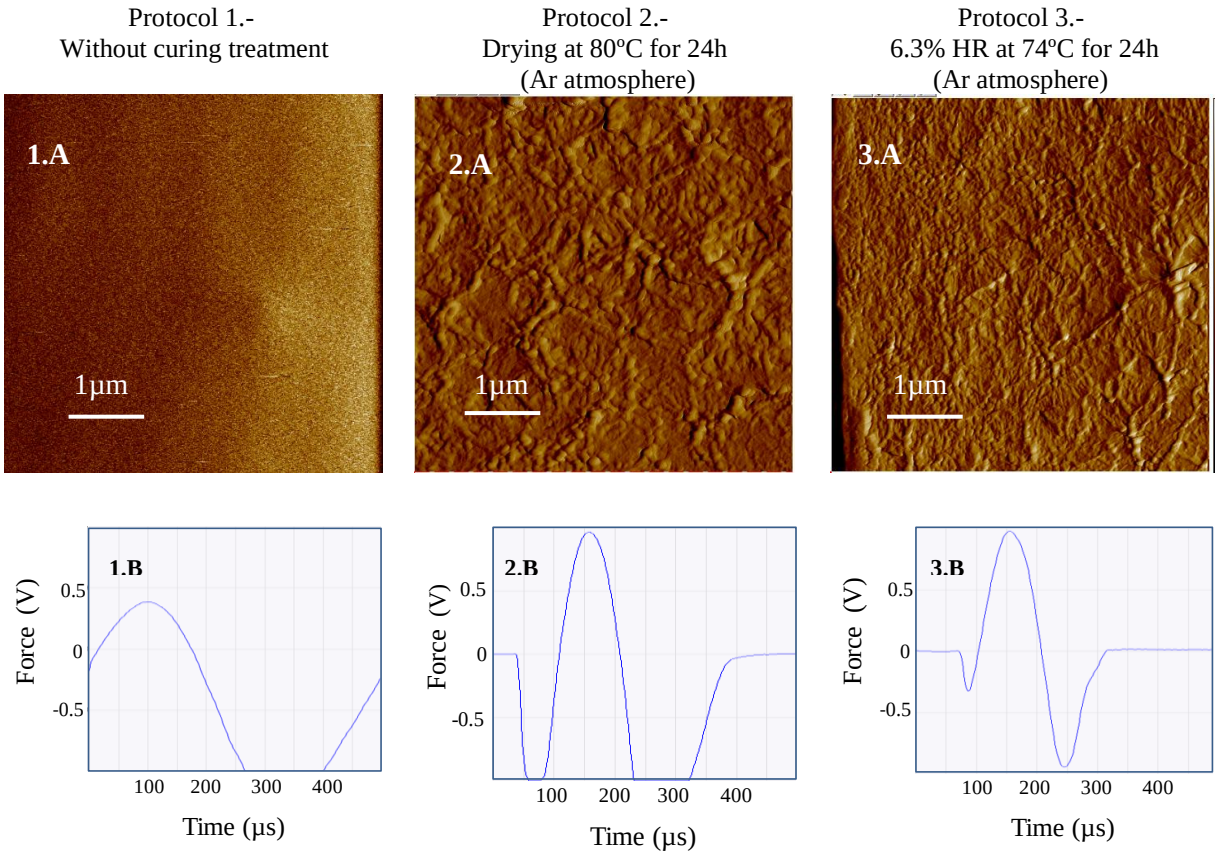

Fig. III-10 *AFM topographic images and one cycle of the Peak Force QMN curve, curves are displayed as force versus time. Images of the hybrid membrane after different post condensation conditions of curing treatments for SHdi100 membranes*

The AFM experiments allow understanding that the condensation process is still not finished during the impregnation and drying process. We understand that it is necessary to finish the membrane conditioning by a thermal treatment in presence of water to obtain a completely condensed hybrid membrane. Nevertheless these qualitative AFM measurements are not sensitive enough to compare the hybrid membranes treated under such condition for different times and different amounts of water. DMA (Dynamic mechanical analysis) measurements have been performed to find the optimum conditions for curing treatments.

*** Dynamic mechanical analysis**

DMA characterization of the sample can be achieved by applying 1Hz sinusoidal deformation strain to the sample and analyzing the stress necessary to achieve this strain as a function of the sample temperature (3°C/min ramp).

According to the DMA curves, the damping capacity, associated to the rigidity of a polymer is determined by the intensity and breadth of the loss tangent (tan (δ)). Tan (δ) is the tangent of the phase angle and the ratio of G"/G' (Loss modulus[c]/Storage modulus[d]).

-Tan (δ) is very sensitive to the structural change of the materials and decreases with increasing the sample rigidity.

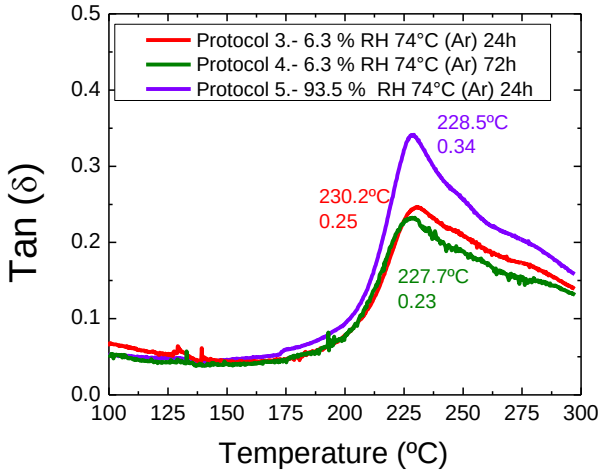

Fig. III-11 *DMA profiles of Hybrid membranes elaborated by three different curing protocols.*

Fig. III-11 shows the effect the curing treatment on the tan (δ) values of hybrid membranes. The tan (δ) peaks are appearing at almost the same temperature for the different protocols but there is a slight variation in the values of the maxima of the tan (δ) curves. It is seen that the 3rd and 4th protocols, *i.e* 6.3% RH at 74ºC for 24h and 72h, show almost similar tan (δ) values but a slightly higher value is seen in the case of 5th protocol, i.e. 93.5% RH at 74ºC 24h. We understand that this increase of the tan (δ) is possibly due to the presence of the short chain of sol-gel phase, because of the lower condensation degree.

A curing process is necessary to obtain a hybrid membranes with high condensation degree, this curing must be implemented with small amount of water in temperature condition.

We conclude that a curing process for **24h at 6.3%RH at 74ºC** improve the condensation degree of the membranes.

[c] G": Loss modulus-A measure of the viscous response of a material.

[d] G': Storage modulus- A measure of the elastic response of a material

III.1.3.4 STEP 4: Membrane conditioning for fuel cell applications: Post-hydrothermal treatment

After the elaborating process of hybrid membranes, we expect that:

- The sol-gel phase of the hybrid membrane is completely condensed.
- The sol-gel phase has grown inside the ionic domains.

The conductivity of *sPEEK NS* is about 80mS/cm. For the hybrid membranes *SHdi100*, we measured a proton conductivity around 20mS/cm. Therefore, there is a significant decrease in conductivity. This could be due to obstruction of the ionic domains by the sol-gel phase.

In order to obtain a better proton conductivity, a hydrothermal treatment is further performed. It is expected that this hydrothermal treatment will have an influence on proton conductivity of membrane which depends on [20, 41]:

-The connectivity of the hydrated domains.
-The quality of the nanophase separation between hydrophobic and hydrophilic domains.

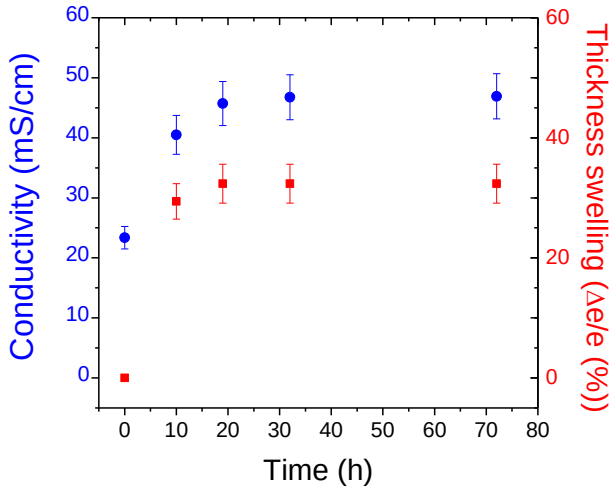

Fig. III-12 *Conductivity at room temperature (●) and thickness swelling (■) of SHdi100 hybrid membranes treated by hydrothermal treatment at 80ºC for times between 0h an 72h.*

Conductivity values at room temperature obtained for hybrid membranes swollen at 80ºC are presented in *Fig. III-12*. Measurements were carried out in a homemade conductivity cell (*Annex A.1*). The hybrid membrane was treated and re-acidified (1h) in a 1M HCl and rinsed to pH~7 before conductivity measurements. This procedure allows improving any problem of ion contamination that would reduce the number of acidic groups of the membrane.

The conductivity exhibits a sharp increase from 0h to 20h of treatment, increasing from 23mS/cm to 45mS/cm. After hydrothermal treatment at 80ºC for times up to 20h, the conductivity seems stable. The thickness swelling of the membrane followed the same behavior. It appears that the hydrothermal treatment allows improving the interface quality between the hydrophilic and the hydrophobic phase the channel connectivity and therefore the proton conductivity.

We conclude that a hydrothermal treatment of 24h allows improving to an optimum the membrane conductivity and the swelling. The improvement of the conductivity could be associated with the hybrid membrane swelling but also with the structural modification process of the hybrid membrane, presented in the future section dedicated to the morphology (*section III.2.2*).

A good level of proton conductivity is obtained from 24h at 80 ºC of post-treatment. To ensure an optimal proton conductivity the hybrid membranes were treated for **72h at 80ºC in liquid water.**

III.1.4 Final experimental protocol

The elaboration protocol of hybrid membranes is summarized in the flow diagram in *Fig. III-13*. The pristine membrane was nanostructured and swelled and the sol-gel precursor solution in H_2O/MeOH was prepared in parallel (STEP 1). The precursor alkoxide solution was impregnated in a swelled *sPEEK NS* membrane in alcohol/water solvent. It was expected that precursors were guided into the ionic domain of the nanostructured membrane [154]. The membrane was cleaned on surface with alcohol/water mixture to avoid the formation of a sol-gel skin and then it was dried (STEP 2). To achieve stable membrane's performances with the complete condensation of the sol-gel phase, a curing of hybrid membrane was implemented (STEP 3). Once the hybrid sPEEK membrane with completely condensed sol-gel phase was obtained, a second hydrothermal treatment was carried out to swell the ionic domains and re-obtain the well-defined nanophase separation presumably lost during the membrane hybridization (STEP 4).

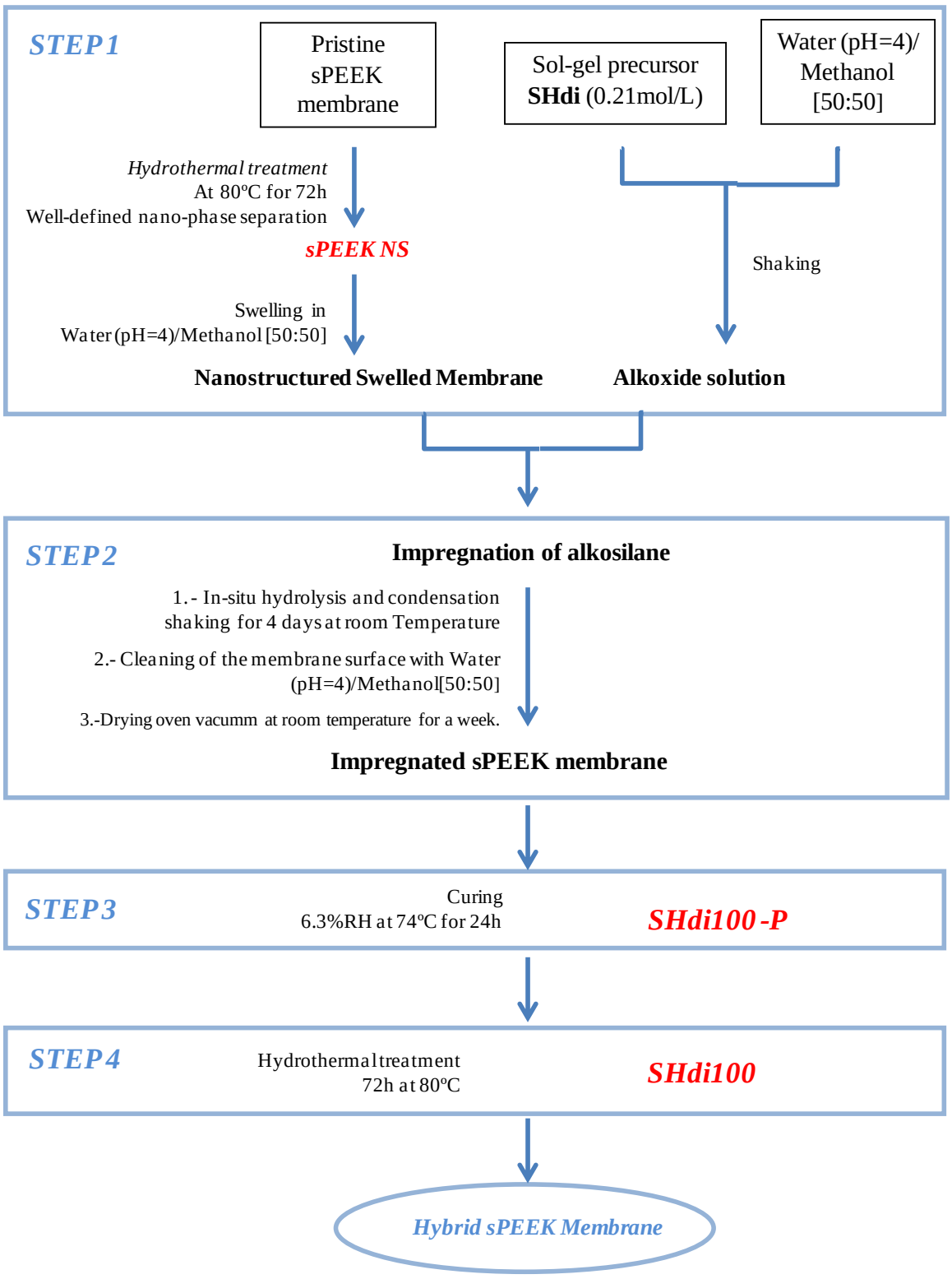

Fig. III-13 *Flow diagram for the preparation method of sPEEK–Precursor hybrid membrane.*

III.2 Hybrid membrane characterization

The development and manufacturing of hybrid membrane was described in the previous sections. We obtained membranes in the best possible conditions during the manufacturing process, in terms of:

- Nanostructuration of the host membrane in order to drive the precursor condensation into the ionic domains and to keep a well-defined nanophase separation.
- A complete condensation of the sol-gel phase.
- Good proton conductivity for further use in fuel cell.

One of the most important parameter of the hybrid membranes is, of course, the amount of sol-gel phase inside the membrane. To measure the sol-gel content of the hybrid membranes, we measured the weight of the membrane before and after hybridization. The weight of pristine membranes *sPEEK NS* ($W_{pristine}$) was compared to that of hybrid membranes (W_{Hybrid}) before the post-treatment.

$$\%\ sol\ gel\ phase\ content = \frac{W_{Hybrid} - W_{pristine}}{W_{Hybrid}} \qquad (eq\text{-}III.1)$$

The sol-gel phase content was calculated in dry membranes by *eq-III.1* obtaining a sol-gel phase content of 51%. The sol-gel content of *SHdi100-P* and *SHdi100* is very similar.

This section reports the characterization of the hybrid membranes. We systematically compare the membranes non-treated after curing treatment *SHdi100-P* and treated in liquid water at 80ºC for 72h: *SHdi100*. Additionally to the sol-gel phase content, the thermal stability was investigated. Preliminary structural measurements together with water sorption experiments were performed.

III.2.1 Thermal stability

TGA is generally used to evaluate the thermal-stability to oxidation of samples by monitoring the weight change during heating. As shown in *Fig. III-14*, high resolution TGA (blue color) curves for *SPEEK NS*, *SHdi100-P* and *SHdi100* were collected for evaluating the thermal stability of these materials. The derivated curves of the weight loss (DTG red color) to the heating temperature is reported on the right Y axis. The peak maxima corresponds to the inflection point of the mass loss detected. It follows that it is easier to determine the temperature range of decomposition of the material.

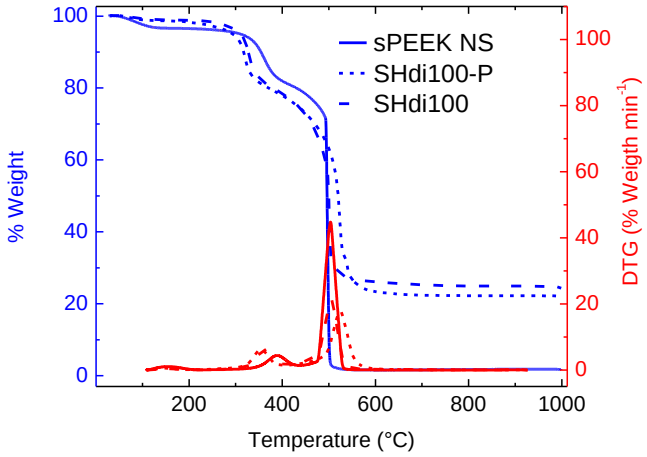

Fig. III-14 *TGA and DTG thermograms of sPEEK NS and hybrid membranes SHdi100-P and SHdi100 in oxygen at a heating rate 10ºC/min*

For *sPEEK NS* membrane, three stages of weight loss can be observed [43]:

1.- The weight loss between 20 ºC and 200 ºC due to the evaporation of the free and bound water

2.- The weight loss between 265 ºC and 425 ºC corresponding to the desulfonation. It depends on the degree of sulfonation.

3.- The weight loss from 425 ºC to 625ºC due to thermal decomposition of main chain of sPEEK.

The first weight loss step (below 200ºC) is more important for *sPEEK NS* membrane than for hybrid membranes, indicating the higher hydrophobicity of hybrid membranes. The hydrophobicity of both hybrid membranes is similar.

In a second step, the weight loss of the hybrid membranes begins earlier and is higher (above 330°C) than for *sPEEK NS* membrane (370°C). Therefore, the introduction of SHdi sol-gel phase has induced a decrease of the sPEEK membrane thermal stability. However, the hybrid membranes thermal stability is acceptable considering the high content of sol-gel phase (~50%).

The third weight loss step starting at about 450ºC corresponds to the degradation of sol-gel phase and sPEEK main chain decomposition. It starts at a lower temperature for hybrid membrane than for *sPEEK NS* membrane. The hydrothermal treatment does not impact the thermal stability of hybrid membranes.

III.2.2 Morphology of hybrid membranes

SANS measurements were performed in a large q-range comprising the ionomer peak to evaluate the impact of:

1.- the sol-gel phase on the ionic domains of the sPEEK phase.

2.- the post hydrothermal treatment on the hybrid membranes morphology.

We will study the membrane nanostructuration by SANS and membrane crystallinity by XRD analysis for a membrane *sPEEK NS* and post-treated hybrid membranes *SHdi100* and untreated *SHdi100-P*.

III.2.2.1 SANS experiments

SANS spectra were recorded at the LLB-PAXY spectrometer (λ=5Å, D=1.1m , λ=12Å, D=1.1m and λ=10Å, D=6.7m q-values of 0.004Å^{-1}<"q"<0.3Å^{-1}). The membranes were conditioned in liquid water at room temperature (see *Fig. III-15*).

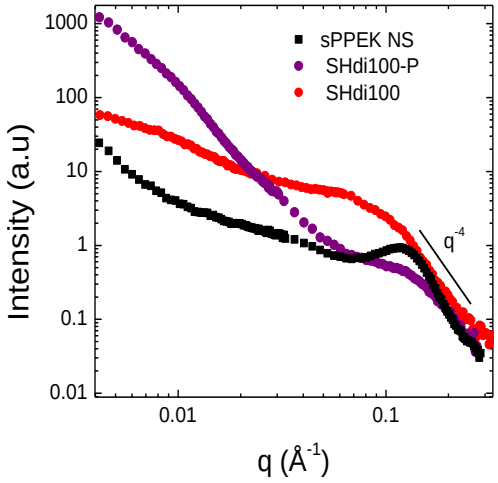

Fig. III-15 *Log-Log SANS profiles of sPEEK NS (■) SHdi100 (●) and SHdi100-P (●) in pure water.*

The spectra of *sPEEK NS* membrane is characterized by a well-defined and rather narrow ionomer peak located at about 0.12 Å^{-1} (Bragg spacing= 52 Å) and a q^{-4} behavior at large *q*. The ionomer peaks for the hybrid membranes are slightly wider than the peak for *sPEEK NS*, which is indicative of a greater structural heterogeneity of the separation distances between hydrophobic and hydrophilic domains and it is located at *q*~0.13Å^{-1} for *SHdi100-P* and *q*~0.09Å^{-1} for *SHdi100*. Additionally, slope in the small angle region strongly decreases for *SHdi100*. These observations suggest that the treatment in liquid water for 72h at 80ºC causes an increase in the amount of water absorbed, enabling the formation of higher separation distances between hydrophobic and hydrophilic domains. The post-treatment in hot liquid water prevents the formation of the end-terminated disconnected hydrophilic domains, blocked by the presence of the sol-gel phase. These preliminary SANS experiments performed for membranes swollen in light water indicates that the sol-gel network is likely to grow inside the hydrophilic domains of the host membrane (ionomer peak position almost unchanged with a decreased intensity) and gives rise to greater structural heterogeneity at the nanoscale. The morphology of the hybrid membranes treated in liquid water will be extensively studied in *Chapter IV* by performing contrast variation SANS experiments.

III.2.2.2 XRD experiments

The scattering intensity at low *q-values* observed for the hybrid membranes is attributed to the presence of the sol-gel phase [155]. As studied in *Chapter II*, the sPEEK is a semi-crystalline

material [138]. In order to study the impact of the sol-gel phase on the polymer crystallinity XRD analysis at high *q-values* (0.1 $Å^{-1}$-1.7 $Å^{-1}$) were performed. The results are reported on *Fig. III-16*.

sPEEK NS membrane clearly exhibit a semi-crystalline structure as a sharp crystalline peak, it is located at about 1.27 $Å^{-1}$. This peak is almost superimposed to an amorphous halo centered on 1.41$Å^{-1}$. The hybrid membranes also show an amorphous halo but the peak associated to the crystallinity seems to have disappeared, it is situated at similar position (1.31 $Å^{-1}$) of bump but different from that of *SPEEK NS* (1.27 $Å^{-1}$). It is also observed a bump at 0.7$Å^{-1}$ (Bragg spacing ~9Å) associated to the sol-gel phase.

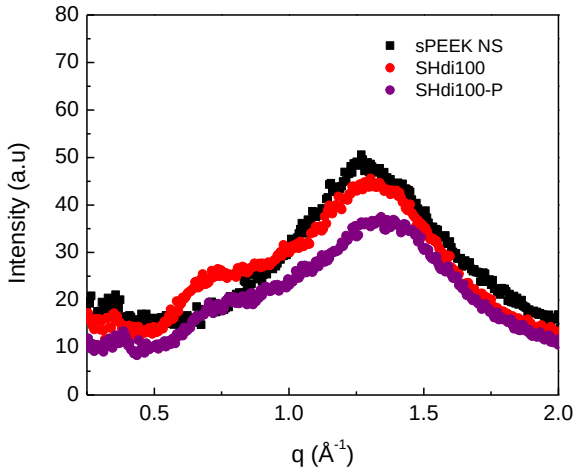

Fig. III-16 *XRD profiles of sPEEK NS (■) SHdi100 (●) and SHdi100-P (●)*

Further studies will be presented in *Chapter IV*. The wide-angle scattering study shows an increase of the amorphous phase in hybrid membranes, and the post-treatment do not impact the local organization.

III.2.3 Functional properties: Water sorption

In this section the water sorption is analyzed. These results will be related to the structural modification process (microstructure evolution).

To investigate the influence of the hydrothermal treatment on the water-sol-gel phase-polymer affinity, the water uptake at room temperature and controlled relative humidity (sorption curves) for sPEEK membranes (*SPEEK NS* , hybrid sPEEK membrane) are described on *Fig. III-17*.

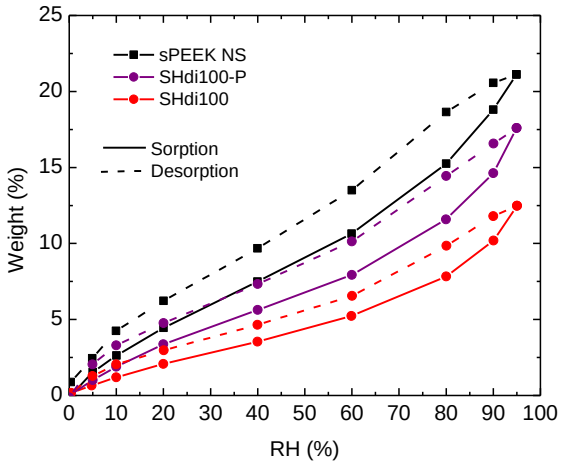

Fig. III-17 *Water sorption isotherms of sPEEK NS (■) SHdi100 (●) and SHdi100-P (●)*

The membranes have been acidified and dried in a vacuum oven overnight. These membranes have been introduced in the sorption balance and equilibrated at 0% RH at least 10h. The membranes display the typical sigmoidal sorption isotherms of ionomers. Comparing the *sPEEK NS* membrane with the isotherms related to hybrid membranes, we observe that the *sPEEK NS* present higher weight values than hybrid membrane. For HR 90% it is about 21% and the *SHdi100-P* and *SHdi100* 17% and 12% respectively The hysteresis phenomenon is less pronounced in hybrid membranes than *sPEEK NS*, it could be associated to reduced interactions between matrix polymer and water. It must be noted that the sol-gel content in hybrid membranes is ~50% and it was expected that the values of swelling achieved were lower for hybrid membranes than *sPEEK NS*.

The differences between the hybrid membranes, could be associated to the effect of drying in the ionomer membranes, the structural modifications take place with a hydrothermal treatment, but this process is reversible when the membranes are dried. as was observed in the *Chapter II section II.4.2.3.*

III.3 Conclusions

The hybrid membranes properties obtained by impregnation of sol-gel precursor are influenced by:

- The host membrane nanostructuration.
- The sol-gel parameters: the alkoxy group to water ratio, the kind of solvent, and the time.
- Hybrid membrane curing and fuel cell conditioning treatment.

The results of the different steps followed during the membrane preparation allow obtaining reproducible membranes are summarized below.

STEP 1

Host membrane conditioning:

* *By SAXS spectra:*

Hydrothermal treatment to obtain a well-defined nano-phase separation

"*sPEEK NS*"

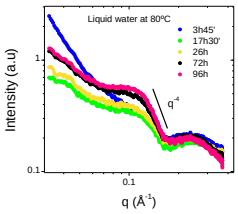

* *By weight swelling measurements*

Swelling in impregnation conditions 50%-50% water (pH=4)- Methanol mixture

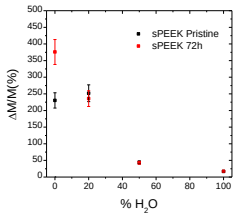

Alkoxide solution:

* *By Raman analysis*

- Solvent: 50%-50% water (pH=4)- Methanol mixture
- Ratio precursor/water R=126

STEP 2

Impregnation of alkoxyde:

* *By Raman analysis*

In-situ hydrolysis and condensation (shaking for 4 days at room temperature)

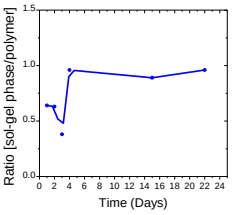

STEP 3:

Curing

* *By AFM and DMA*

In order to obtain
A maximum condensation degree
6.3%RH at 74ºC for 24h
"SHdi100-P"

STEP 4:

Fuel cell Conditioning

* *By Proton conductive measurements*

Hydrothermal treatment at 80ºC for 3 days
"SHdi100 ".

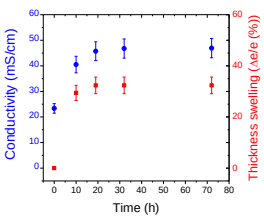

The morphological analysis of the hybrid membranes as a function of the fuel cell shows that the treated membranes present larger ionic domains than non-treated hybrid membranes, improving the proton transport. An extensive characterization of the SHdi100 hybrid membranes with hybrid membranes elaborated form other organosulfur precursors will be the aim of the *chapter IV*.

CHAPTER IV
HYBRID MEMBRANES PROPERTIES

The elaboration of hybrid membrane was explained in *Chapter III*. We have shown the feasibility of a hybrid membrane preparation and the potential interest in our strategy using the sol-gel approach. The important steps objectives were validated:

- The nanostructuration of host membrane.
- Elaboration of hybrid membranes.

First generation hybrid membranes were produced showing potentially interesting properties. Now, we want to fully understand and characterize the functional behavior of the three-phase system (which involves the polymer matrix, the sol-gel phase and ionic domains) in order to improve these materials. Moreover, in this chapter we discuss the effect of using different precursors (namely **SHdi**, **SHtri**, **TS**, see the description in *section IV.1*), as a function of their cross-linking capabilities (number of hydrolysable groups on the precursor). We describe the precursor and then we evaluate the membrane characteristic by measuring sol-gel content, homogeneity, physical and functional properties. We also performed a series of experiments to investigate the morphology of the hybrid membranes:

- by performing contrast variation SANS experiments for the hybrid membranes in order to understand the morphology of the sol-gel phase.
- the impact of the cross-linking degree on the SANS scattering profiles and on the overall crystallinity .

Preliminary fuel cell test is also presented in order to evaluate the possible use of these hybrid membranes in fuel cell.

IV.1 Description of sol-gel precursors

The sol-gel precursor **SHdi** has been chosen as benchmark for the elaboration of the hybrid membranes. The protocol formulated with this precursor was applied for the rest of hybrid membranes. Seven different types of membranes have been elaborated by changing the cross-linking capabilities of the precursors i.e. mixing sol-gel precursors with two hydrolysable groups (dialkoxysilane) and precursors with three hydrolysable groups (trialkoxysilanes).

According to the number of alkoxysilane groups present on the molecule the following precursors have been selected:

- **SHtri** molecule consists in a trialkoxysilyl propyl groups bearing a -SH group as a functional group.
- **TS** molecule consists of two trialkoxysilyl propyl groups linked together through a tetrasulfide function.

These precursors satisfy the requirements to obtain a reactive sol-gel phase to create in turn a hybrid membrane:

1.-The presence of alkoxy group will allow forming an inorganic phase by sol-gel reaction. Two alkoxysilane group for **SHdi** lead to a linear sol-gel phase whereas the three alkoxysilane groups for **SHtri** and six alkoxysilane groups for **TS** giving for both a 3D network.

2.- The presence of the reactive group will protect the membrane from oxidation (H_2O_2 and radical attacks) -SH for **SHdi** and **SHtri** and tetrasulfide group for **TS**. Their progressive oxidation lead to the formation of sulfonic acid group, which should improve the conductivity of the hybrid membrane.

Table IV-1 *Sol-gel precursors*

SHdi ***(SH di-alkoxy)***	***SHtri*** ***(SH tri-alkoxy)***	***TS*** ***(TetraSulfide)***
(3-Mercaptopropyl) methyldimethoxysilane	(3-Mercaptopropyl) triethoxysilane	Bis[3-(triethoxysilyl)propyl] tetrasulfide
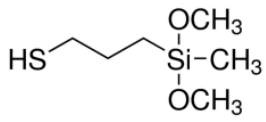	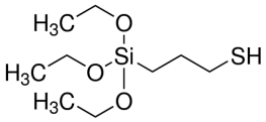	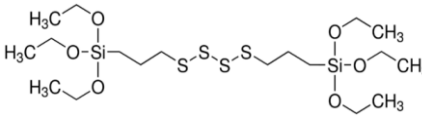

These three different precursors have been used to elaborate the membranes, varying the sol-gel precursors' ratio. The hybrid membranes are labeled according to the precursors' concentration *Table IV-2*.

IV.2 Hybrid membrane elaboration

The evolution of the sol-gel content, the morphology and the functional properties of the hybrid membrane have been studied according to the sol-gel precursors used their ability to impact the cross-linking density of the membrane.

We prepared the hybrid membranes from 550 mg of host membranes of *sPEEK NS* (treated for 72h in liquid water at 80ºC). Membranes have sufficient dimensions (14cm×8cm×30µm) to make a several analyses. All the membranes were treated at the same time in order to avoid any problem which impedes their comparison. Then membranes were immersed in a 50/50vol MeOH/H2O mixture (38.4 mL) at pH=4. After 3 hours of solvent exchange, the membranes were impregnated by immersion in a reactive solution of sol-gel precursors in the same solvent composition during 4 days under shaking. The ratio between the solvent and precursors was kept constant for each membrane (R=126) in order to obtain a dense sol-gel phase. The total mol number of a reactive solution was kept almost constant when varying the ratio between each precursor. The precursors' solutions concentration are presented on *Table IV.2*. After impregnation, as it has been presented in *Chapter III*, the hybrid membranes were dried, cured and treated in liquid water at 80ºC during 72h.

Table IV-2 *Precursors' ratio in 550 mg of a host membrane with 38.4mL of MeOH:H_2O (pH=4) as a solvent.*

	SHdi100	***SHdi90 SHtri10***	***SHdi50 SHtri50***	***SHdi95 TS5***	***SHdi90 TS10***	***SHdi66 TS33***	***SHdi50 TS50***
[SHdi:SHtri]	-	[90:10]	[50:50]	-	-	-	-
[SHdi:TS]	-	-	-	[95:5]	[90:10]	[66:33]	[50:50]
SHdi (M)	0.21	0.19	~0.1	~0.2	~0.19	~0.14	~0.1
SHtri (M)	-	~0.02	~0.1	-	-	-	-
TS (M)	-			~0.001	~0.02	~0.07	~0.1

Considering the cross-linking capabilities of the precursors and their concentrations in the solution of impregnation, one would predict the cross-linking degree of the hybrid membranes for a complete condensation.

SHdi50-TS50>SHdi66-TS33 ~ SHdi50-SHtri50 > SHdi90-TS10>SHdi90-SHtri10~SHdi95-TS5>SHdi100

The most cross-linked membrane should be *SHdi50-TS50* which is composed of a mixture of **SHdi** with a dialkosylane group and **TS** with double trialkosylane group and the less cross-linked membrane is the reference membrane *SHdi100.*

IV.3 Basic observations

We started membranes' characterization with the basic observation of different types of hybrid membranes. In this case, each membrane was dried after the final hydrothermal treatment, and it will be specify for every characterization. *Fig. IV-1* shows the picture and thickness of each dried hybrid membranes. These pictures have been taken by a scanner, and the membranes were scanned on a transparent paper on which the word “transparent” has been previously printed so that the transparency of these membranes could be evaluated.

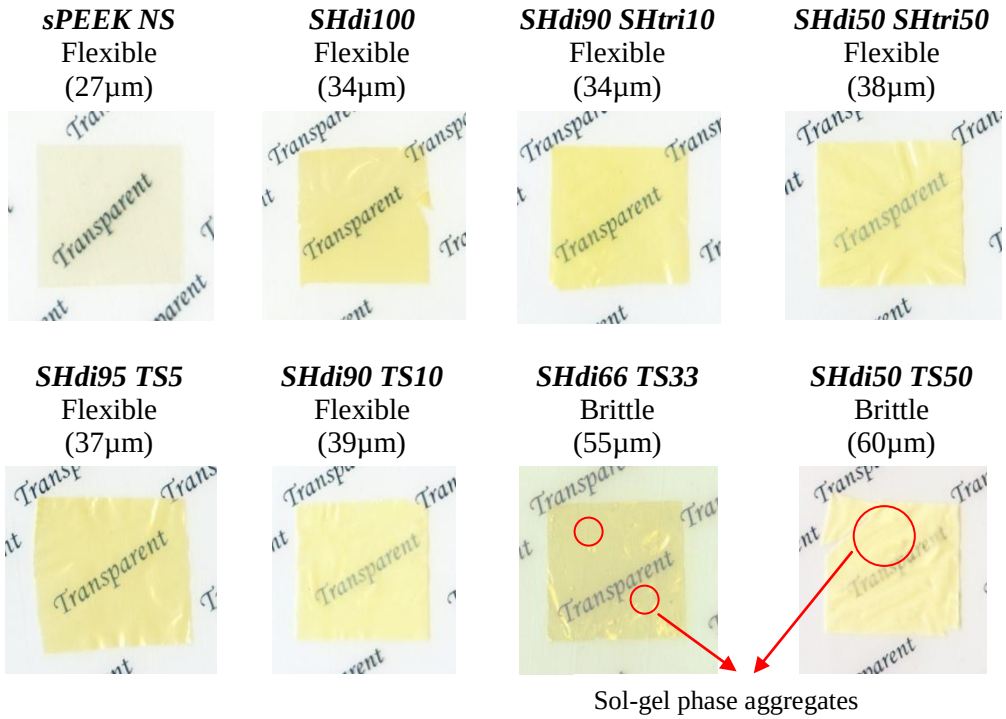

Fig. IV-1 *Pictures of dried hybrid membranes, red circle corresponds to the sol-gel phase aggregates onto the hybrid membranes*.

We observe that the impregnation process induced an increase of the membrane thickness and that this effect is more pronounced when the membrane contains a tri- (**SHtri**) or a hexa-(**TS**) functional sol-gel precursor at higher concentrations. As it will be seen later, this is related to the amount of sol-gel phase introduced inside the membrane.

The hybrid membrane shows a color change between transparent light yellow to transparent dark yellow and an opaque white-yellow color for the membranes *SHdi50-TS50*. Furthermore, as the thickness increases, the transparency decreases. The most cross-linked membranes present a layer of sol-gel phase on the surface like a skin, despite the rinsing step of the membrane. For the membranes prepared from a **TS** mixture *SHdi66-TS33* and *SHdi50-TS50*, aggregates dispersed on the surface are observed. Resulting hybrid membranes are therefore heterogeneous. It should be noted that the membranes’ fragility increases as the cross-linking degree of the sol-gel phase increases [156]. Due to their fragility, the *SHdi66-TS33* and *SHdi50-TS50* membranes are not suitable for future fuel cell use but they have been characterized in order to better understand the hybrid membranes properties.

IV.4 Chemical properties

The homogeneity of the hybrid membranes through the thickness of the membrane has been analyzed by RAMAN (*see Fig. IV-2*). As in the previous *Chapter III*, we measured the ratio of the area of aliphatic CH band characteristic of sol-gel phase to the area of the -CH of aromatic rings characteristic of the *sPEEK NS* membrane to obtain the relative amount of sol-gel phase into the hybrid membrane for one type of membrane *SHdi100* [152].

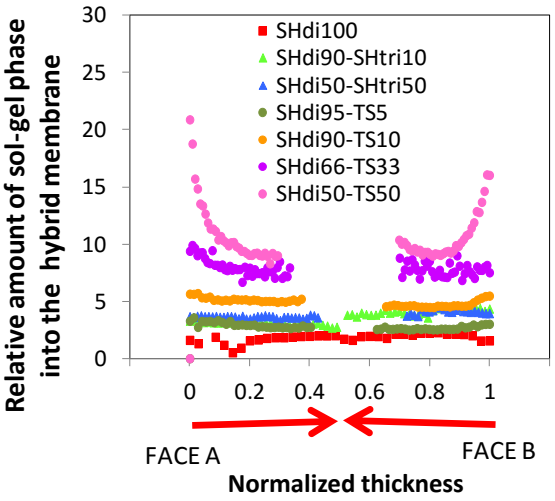

Fig. IV-2. *Relative amount of sol-gel phase into the hybrid membranes.*

We acquired the RAMAN spectra through the thickness of the membrane from the *FACE A* to the core of the membrane by Z steps of 0.5µm, then we turn the membrane upside down and we acquired the spectra for the *FACE B* to the core of the membrane each 0.5µm. The membrane thickness of the different hybrid membranes varies between 27 µm to 60 µm (see *Fig. IV-1*). Thickness values have been normalized (Z value/ thickness) in order to compare the sol-gel relative concentration profile through the different membrane.

Fig. IV-2 shows the evolution of the sol-gel phase content into the host membrane as a function of the normalized thickness. These values of sol-gel content are not comparable between the different membranes because each precursor has a different RAMAN response. Moreover, in relation with the membrane homogeneity we observe that the membranes are almost homogeneous through the membrane thickness. Only the membranes with high cross-linking capabilities, *SHdi66-TS33* and *SHdi50-TS50*, are more charged in the area near the surface of the membrane. However we found a polymer phase (sPEEK) over the membranes hybrid membranes confirming the membrane homogeneity.

We conclude that the hybrid membranes present a high homogeneity through the membrane thickness and the sol-gel phase is homogeneously dispersed, except for *SHdi66-TS33* and *SHdi50-TS50*. These results are extremely important because without proper dispersion and distribution of the sol-gel phase, the stability of the membrane is compromised and the aggregates can act as defects, which limit the properties in terms of permeability and mechanical properties [157].

IV.5 Physical properties

In this section we will study the impact of the sol-gel composition on the physical properties of the membranes namely the sol-gel content, thermal stability, density and thermo-mechanical properties. The experiences performed in temperature are not representative of the functional properties of the membrane because the temperatures achieved during the experiments are higher than the fuel cell temperature operation. Nevertheless the study of the thermal and thermo-mechanical stabilities of the hybrid membranes should be helpful to interpret the results obtained during the rest of their characterization.

IV.5.1 Sol-gel content

One of the most important parameters in the characterization of hybrid membranes is, of course, the amount of sol-gel phase inside the membrane. The easier technique for studying sol-gel phase content is by weight measurement before and after hybridization of sPEEK membranes.

Weight of pristine membranes ($W_{pristine}$) were compared with weight of hybrid membranes (W_{Hybrid}).

$$\%sol-gel\ phase = \frac{W_{sol-gel}}{W_{Hybrid}} = \frac{W_{Hybrid}-W_{pristine}}{W_{Hybrid}} \qquad (eq\text{-}IV.1)$$

The sol-gel content in membranes was calculated in dry membranes by (*eq-IV.1*) and illustrated in *Table IV-3*.

Table IV-3 *Percentage sol-gel phase content in hybrid membranes by weight measurements.*

	SHdi100	***SHdi90 SHtri10***	***SHdi50 SHtri50***	***SHdi95 TS5***	***SHdi90 TS10***	***SHdi66 TS33***	***SHdi50 TS50***
%sol-gel phase content	66	67	84	79	85	88	85

We observe that the sol-gel content is very high on the hybrid membranes, exceeding 65% in all cases. The sol-gel phase content increases with the cross-linking capabilities of the membrane achieving values up to 88%. The cross-link density was calculated in the work of *French* [158] where a correlation between the sol-gel content and cross-link density was obtained. He proposed that the cross-link density is directly proportional to the square of the gel fraction divided by the first power of the sol fraction. The constant of proportionality was 0.0065 meq/g for three-functional networks. In this work we have not calculated the cross-link density but we have considered the direct correlation between the sol-gel content and cross-link density.

It must be noted that is difficult to be precise in sol-gel content measurements and the error is around +/-10%. This problem is due to the layer formed on the membrane surface, which is more pronounced in the membrane with a high cross-linking degree.

IV.5.2 Thermal stability (TGA)

As we explained on *Chapter III*, the TGA is generally used to evaluate the thermal stability to oxidation of the sample by monitoring the weight change during heating. In addition, the mass of residue at high temperatures from de TGA analyses can be useful to calculate the sol-gel content of the hybrid membranes.

Three stages of weight loss can be observed [25]:

1.- The weight loss between 20 ºC and 200 ºC due to the evaporation of the free and bound water.
2.- The weight loss between 265 ºC and 425 ºC corresponding to the desulfonation process.
3.- The weight loss from 425 ºC to 625ºC due to thermal decomposition of main chain of sPEEK and also of sol-gel phase.

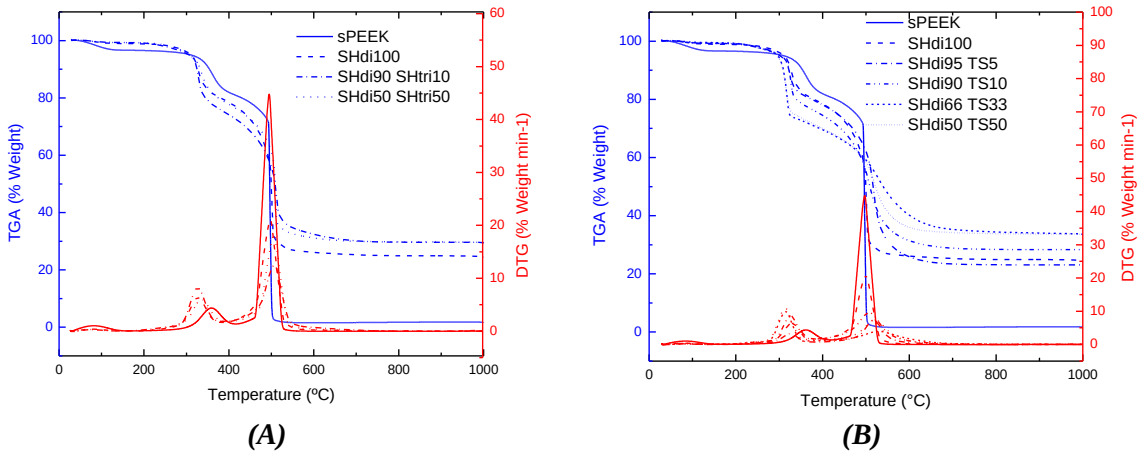

Fig. IV-3 *TGA and DTG thermograms of hybrid membranes with SHdi-SHtri (A) and SHdi-TS(B) in oxygen at a heating rate of 10ºC/min*

In *Fig. IV-3* we compare the hybrid membranes with the *sPEEK NS* membrane. We observe that the first weight loss of the *sPEEK NS* membrane is the most significant of all the membranes (above 80ºC). This more pronounced weight loss which corresponds to the water evaporation , indicates that *sPEEK NS* has the highest hydrophilicity. It must be noted that the thermal stability of the pure precursor **SHdi**, in the case where it is not hydrolyzed and condensed, is around ~96ºC and could be included in the weight loss of this stage. We consider that all the precursors are condensed thank to the curing treatment. The second stage of weight loss (above 330 °C) starts at lower temperatures for the hybrid membranes than the *sPEEK NS* membrane (370ºC). The third weight loss step starts at about 450ºC, *i.e.*, at a lower temperature for hybrid membrane than *sPEEK NS* membrane.

We reported a zoom of the DTG thermograms of the hybrid membranes in order to better visualize the temperature of degradation as a function of the type of membrane. *Fig. IV-4 (A)* shows the second step of degradation and *Fig. IV-4 (B)* shows the third step.

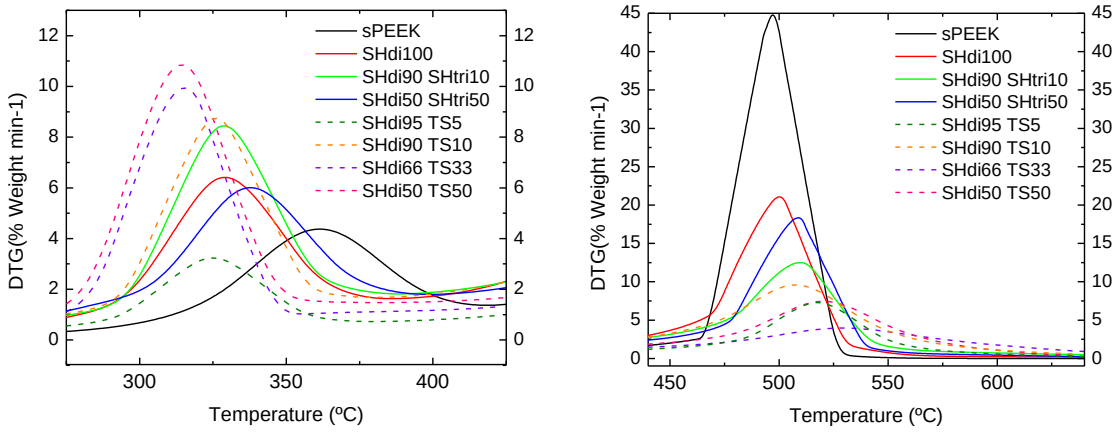

Fig. IV-4 *DTG thermograms of hybrid membranes in oxygen at a heating rate of 10ºC/min. (A) hybrid membranes on the second state of degradation. (B) hybrid membranes on the third state of degradation.*

As we can see in *Fig. IV-4* the thermal stability of hybrid membrane evolves with the sol-gel content therefore with the cross-linking degree. In the range of temperature between 250ºC and 400ºC (*Fig. IV-4 (A)*), the thermal stability of hybrid membranes is lower than *sPEEK NS*. We observe that the weight loss increases with the cross-linking degree. The highly cross-linked membrane (*SHdi50-TS50*) presents the lower temperature of degradation. This weight loss range was associated with the elimination of sulfonic acid of sPEEK membrane, but also with the thermal stability of S-S groups of **TS**, it is reflected in the low temperature of degradation. These groups are less stable than the SO_3H groups from the sPEEK membranes explaining that the chemical degradation occurs at lower temperatures [159]. In this range, the weight loss of hybrid membranes is larger than that of sPEEK, which is attributed to the decomposition of the extra S-S groups of the sol-gel phase [160]. The third weight loss for temperatures between 450ºC and 600ºC (*Fig. IV-4 (A)*) corresponds to the main sol-gel phase chain and sPEEK chain decomposition. Because the amount of sPEEK is considerably small on hybrid membranes we cannot confirm that the thermal stability of the hybrid membrane is greater than *sPEEK NS*. We can only confirm that the degradation of the sol-gel phase to form SiO_2 occurs at higher temperatures.

The TGA measurement allows calculating the sol-gel phase content in a more precise way than weight measurements, as it will be explained below.

***<u>Silica content by TGA</u>**

In the case of the hybrid membranes, the weight of residues remaining after the decomposition of the organic phase depends on the content of the inorganic phase [161]. Therefore we can determine the silica content by TGA.

Silica content was determined by TGA under O_2 atmosphere. At 1000ºC, the sol-gel phase was completely oxidized, the organic phase decomposed and finally only the inorganic matter (SiO_2) remained [162]. *Fig. IV-5 (A)* shows an example of the hybrid membrane TGA curve after normalization (Weigh loss/ Initial weigh). *Fig. IV-5 (B)* shows the residual silica values used for the estimation of silica content. These values are reported on (by one atom of Si) *Table IV-4*.

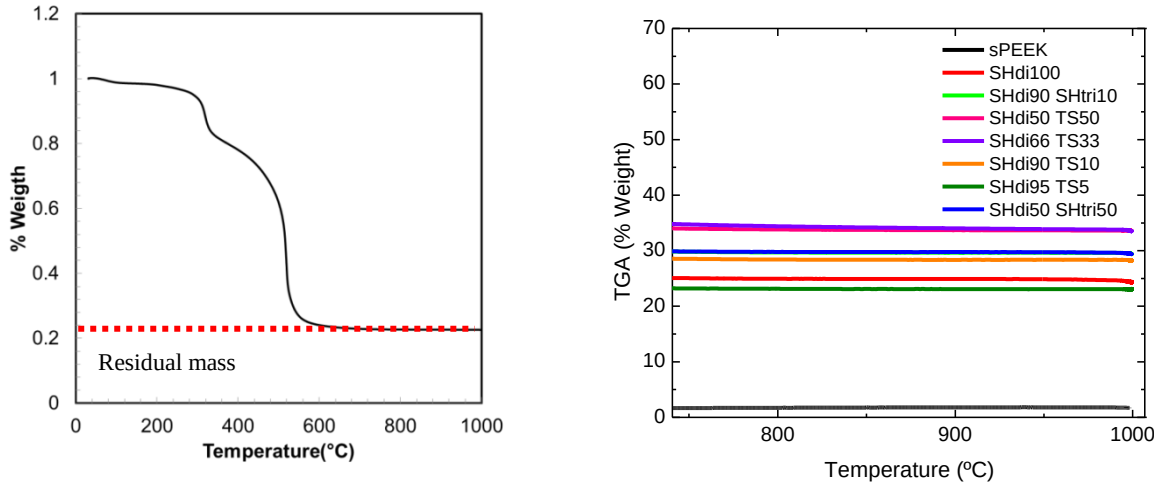

(A) ***(B)***

Fig. IV-5 (A) *TGA curve of generic hybrid membrane (B) Silica residual of hybrid and sPEEK membranes*

We assume that the alkoxysilane groups of sol-gel precursors were completely condensed and molar mass (Mm) of the condensed precursors corresponds to: **SHdi** 150.32 gr/mol, **SHtri** 151.36 g/mol, **TS** 182.915 g/mol (by one atom of Si).

Table IV-4 *Reported values of residual silica from TGA measurements Fig. IV-5 (B)*

	SHdi100	***SHdi90 SHtri10***	***SHdi50 SHtri50***	***SHdi95 TS5***	***SHdi90 TS10***	***SHdi66 TS33***	***SHdi50 TS50***
%SiO_2	24.3	29.4	29.4	23.1	28.2	33.5	33.6
Mm of sol-gel phase (g/mol) By Si	150.32	150.42	150.84	151.95	153.58	159.57	166.62

We can calculate the sol-gel content of hybrid membranes from the SiO_2 residue (*eq-IV.2*):

$$\%\, sol-gel\ phase = \%SiO_2 \times \frac{Mm\ sol-gel\ phase}{Mm\ Si} \qquad (eq\text{-}IV.2)$$

Mm of Si= 28.08 gr/mol.

The calculated values are reported in *Table* IV-5. We observe that the sol-gel content is very high for the hybrid membranes, as we have observed by weight measurements, exceeding 50% in all cases. The sol-gel phase content increase with the cross-linking capabilities of the membrane achieving values of up to 88%.

Table IV-5 *% sol-gel phase content in hybrid membrane estimated by TGA***.**

	SHdi100	***SHdi90 SHtri10***	***SHdi50 SHtri50***	***SHdi95 TS5***	***SHdi90 TS10***	***SHdi66 TS33***	***SHdi50 TS50***
%sol-gel phase content	57	69	69	54	68	84	88

The differences between the silica content measured by TGA and measured by weight measurement (see *Table IV-3*) are significant, but we must keep in mind the difficulty of weight measurements. The sol-gel content obtained by TGA has been chosen as the most reliable method to estimate the amount of sol-gel phase contents and it will be used in the following interpretations.

IV.5.3 Thermo-mechanical stability (DMA)

The impact of the cross-linking capabilities on thermo-mechanical behavior of hybrid membranes has been investigated by DMA for the membranes with equal sol-gel content. The measurements were carried out on hybrid membranes dried before experiments. DMA characterization was achieved by applying 1Hz sinusoidal deformation strain to the sample and analyzing the stress necessary to achieve this strain as a function of the sample temperature (3°C/min ramp).

As it was presented in *Chapter III* the intensity and breadth of the loss tangent (Tan (δ)), which are very sensitive to the structural change of the materials and decrease with increasing the sample rigidity.

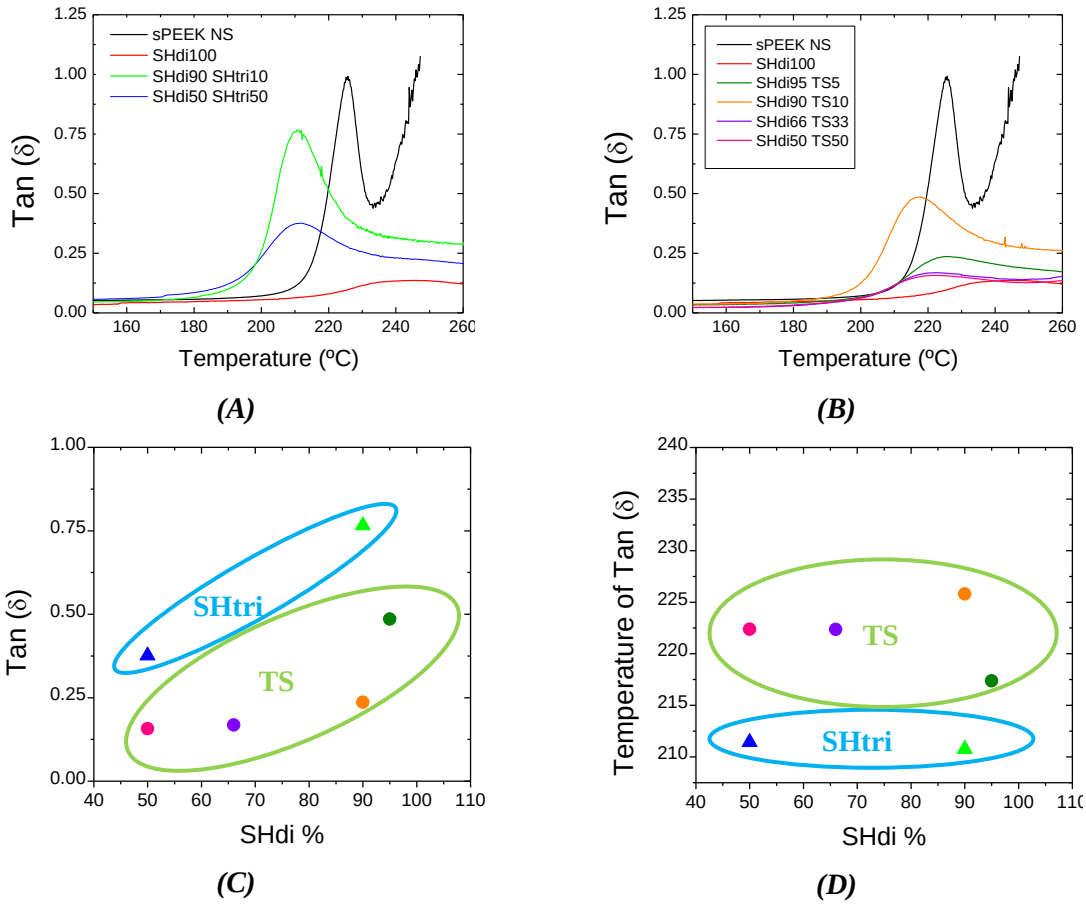

Fig. IV-6 *DMA profiles of Hybrid membranes. (A) Tan (δ) vs Temperature(ºC) for hybrid SHdi-SHtri hybrid membranes. (B) Tan (δ) vs Temperature (ºC) for hybrid SHdi-TS hybrid membranes.(C) Value of the peak of Tan (δ) vs %SHdi and (D) Temperature of the peak of Tan (δ) vs %SHdi.*

The effect of the cross-linking capability is shown in *Fig. IV-6-(A)*, which presents the Tan(δ) profiles for hybrid membranes prepared with **SHdi-SHtri** (equal sol-gel content, therefore

comparables) and *Fig. IV-6-(B)*, which presents Tan(δ) profiles for hybrid membranes prepared with **SHdi-TS** (only comparable *SHdi66-TS33* and *SHdi50-TS50*) as a function of **SHdi** %. The values of Tan(δ) peak and temperature of Tan(δ) peak are reported in *Fig. IV-6-(C)* and *Fig. IV-6-(D)*, respectively, in order to obtain a better visualization. We observe an evolution of the value of tan(δ) peak as a function of cross-linking capability for hybrid membranes **SHdi-SHtri**. This value decreases when the cross-linking density increases. The same behavior is observed for the membranes **SHdi-TS.** In terms of sol-gel content, the membranes **SHdi-SHtri** (surrounded by a blue line *Fig. IV-6-(C) and Fig. IV-6-(D)*), are also similar with the membrane *SHdi90-TS10* (orange point). We observe that the value of tan (δ) peak is quite lower for the membranes *SHdi90-TS10* than **SHdi-SHtri**. The temperature of tan (δ) peak is almost constant for both families of hybrid membranes. We observe that the temperature of tan(δ) peak is higher for membranes **SHdi-TS** than **SHdi-SHtri.**

We understand that the increase of the temperature of tan (δ) peak is due to the presence of highly cross-linked phase. When the sol-gel phase is highly cross-linked, the energy needed to move sol-gel chains is higher, this is traduced by an increase of tan(δ) peak temperature and a decrease of tan (δ) peak value.

IV.5.4 Density measurements

The membrane density was determined using a gas pycnometer. Membrane samples were dried and then they were first weighed and introduced in the gas pycnometer. 1000 cycles of measurements were applied inducing a membrane drying by the injection of dry helium at each cycle. We perform the experiments for the hybrid membranes but also in the precursor condensed (precursors were condensed outside sPEEK in the same conditions as the ones which were selected to prepare hybrid membranes) (*Annex A.4*) labeled "**poly**-hybrid membrane composition".

Table IV-6 *Density measurements of polysiloxane*.

	Poly-SHdi100	***Poly-SHdi90 SHtri10***	***Poly-SHdi50 SHtri50***	***Poly-SHdi95 TS5***	***Poly-SHdi90 TS10***	***Poly-SHdi66 TS33***	***Poly-SHdi50 TS50***
Density (g/cm^3)	1.12	1.09	1.23	1.19	1.24	1.44	1.49

Table IV-6 lists the different density measurements of poly-condensed precursors and *Table IV-7* lists the density of sPEEK membrane and hybrid membranes. The *sPEEK NS* membrane density measured is about 1.41 g/cm^3, which perfectly matches the value provided by Fumatech (*Annex A.2*). We also observe that the density of poly-condensed precursors is lower than the one of *sPEEK NS* membrane (expect *SHdi66-TS33* and *SHdi50-TS50*). Therefore, it is expected that the hybrid membranes will have a lower density than sPEEK membrane. We confirm this affirmation with the measurements listed on *Table IV-7*.

Table IV-7 *Comparison of measured and calculated densities for each hybrid membrane composition (and sPEEK NS).*

	sPEEK NS	*SHdi100*	*SHdi90 SHtri10*	*SHdi50 SHtri50*	*SHdi95 TS5*	*SHdi90 TS10*	*SHdi66 TS33*	*SHdi50 TS50*
Measured density (g/cm^3)	1.41	1.29	1.20	1.31	1.30	1.29	1.33	1.32
Calculated density (g/cm^3)	1.41	1.23	1.17	1.28	1.28	1.29	1.44	1.48

Density of hybrid membrane increases with the cross-linking degree. This analyze confirms the interpretation proposed in DMA analysis. We can also calculate the density of hybrid membranes and compare it with the densities experimentally determined. The calculated density of a dry membrane is determined with the following equation according to the rule of mixtures:

$$\rho_{dry\ hybrid\ membrane} = \left(\frac{1-X}{\rho_{sPEEK}} + \frac{X}{\rho_{poly}}\right)^{-1} \quad \text{with } 0<X<1 \qquad \text{(eq-IV.2)}$$

With X= mass fraction of sol-gel phase measured by TGA and ρ_{sPEEK} and ρ_{poly} the density of the sPEEK membrane and the sol-gel phase measured by pycnometer.

Densities of hybrid membrane correspond to the calculated values except for the hybrid membranes *SHdi66-TS33* and *SHdi50-TS50*.

IV.6 Functional properties

In this section we describe the different functional properties of hybrid membranes. We will discuss the swelling behavior in RH and liquid water at room temperature and conductivity.

IV.6.1 Swelling

In this section the water sorption (RH) will be analyzed. The results will be related to the structural modification process (microstructure evolution) in the morphology section. After the elaborating process of hybrid membranes, we expect that the sol-gel phase has grown inside the ionic domains of the host membrane. Before oxidation, the sol-gel phase is hydrophobic and one would expect that the swelling of membranes decreases as the amount of alkoxysilane increases.

To investigate the influence of cross-linking degree of sol-gel phase and the water-sol-gel phase-polymer affinity, we will further analyze the water uptake at room temperature and controlled relative humidity. The membranes have been acidified and dried in a vacuum oven overnight. These membranes have been introduced in the sorption balance and equilibrated at 0% RH at least 10h. Sorption curves characteristic of *sPEEK NS* membranes and hybrid membranes at room temperature are reported on *Fig. IV-7*.

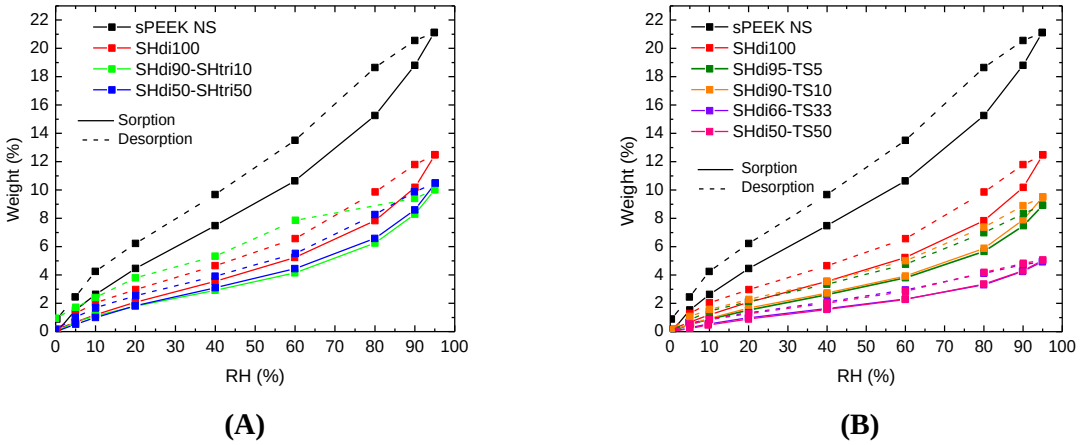

Fig. IV-7 *Water sorption isotherms of sPEEK NS membranes and SHdi-SHtri (A) and SHdi-TS (B) membranes.*

As we have seen in *Chapter II and III*, the membranes display the typical sigmoidal sorption isotherms of ionomers [163]. Comparing the *sPEEK NS* membrane with the isotherms related to hybrid membranes, we observe that the water sorption of the hybrid membranes is lower than *sPEEK NS* membrane, and it is getting lower as a function of the cross-linking degree increase and the amount of sol-gel content decrease.

The main reasons which can explain this behavior are described hereafter:

-The sol-gel phase grows up inside the ionic domains, decreasing the free volume in the ionic domains.

- The hydrophobicity of the sol-gel phase of alkoxysilane [164] results in a low water uptake.

- Swelling as a function of the amount of sPEEK in the membrane. The sol-gel phase have not influence of hybrid membrane swelling.

In order to clarify this last point, we plot the water sorption at HR 98% of the membranes as a function of the sol-gel content (*Fig. IV-8*). We observe that the swelling is related to the sPEEK phase amount and we conclude that there is not influence of the chemical composition of the sol-gel inorganic phase in the membrane swelling only the amount of sPEEK is relevant.

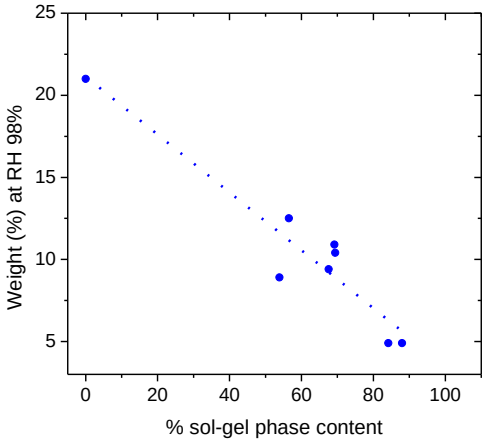

Fig. IV-8 *Water sorption at HR 98% of the membranes as a function of the sol-gel content.*

IV.6.2 Conductivity

The conductivity of hybrid membranes is one of the most important parameters for proton exchange membranes and it is associated to membrane swelling. As we explained before, the conductivity depends on the connectivity of the hydrated domains, the well-defined nanophase separation between hydrophobic and hydrophilic domains and the interactions between the sulfonic acid groups and water. Conductivity values at room temperature obtained for hydrated membranes as a function of the %SHdi are presented in *Fig. IV-9*. The membranes were re-acidified before use.

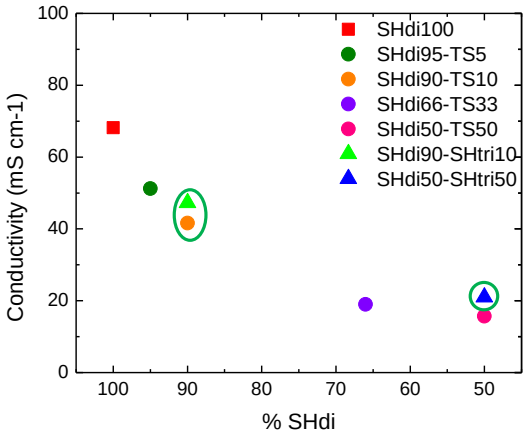

Fig. IV-9 *Proton conductivity at room temperature of hybrid membranes as a function of %SHdi*

We observe a low values of conductivity for hybrid membranes, in comparison with the *sPEEK NS* (84 mS/cm). This results highlight the impact of the sol-gel phase on the proton conductivity and the interest to convert a part of the sacrificial groups into sulfonic acid groups before using the membrane for fuel cell. The high sol-gel content prevents the higher conductivity of hybrid membranes.

IV.7 Morphology

SANS and WAXS experiments were performed in a large *q*-range comprising the ionomer peak and wide angle peak to evaluate the structure and morphology at a mesoscopic scale, the impact of the sol-gel phase on both, the ionic domains of the sPEEK phase and the crystallinity.

IV.7.1 SANS

By SANS measurements we will study thanks to contrast variation experiments the impact of the cross-linking degree in membranes morphology. We have chosen to perform contrast variation analyses because one hybrid membrane is a three-phase system which involves the polymeric matrix, sol-gel phase and water. In a two-phase system, the scattered intensity can be described by the following relationship:

$$I(q)\alpha\Delta\rho^2 \times S(q) \times P^2(q) \qquad \text{(eq-IV.4)}$$

Where the electron contrast term $\Delta\rho$ corresponds to the difference of scattering length density between both phases depending on the radiation source; the structure factor S(q) corresponds to the spatial distribution of scatters; the form factor P(q) is related to their shape and their size. As said, the contrast term $\Delta\rho$ corresponds to the difference in scattering length densities between two phases. The technique of contrast variation (when "zero contrast", $\Delta\rho=0$, is achieved for one component) allows for highlighting parts of a structure.

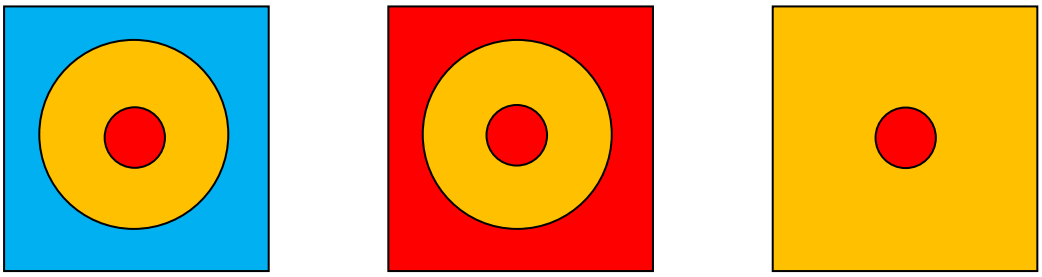

(A) (B) (C)

Fig. IV-10 (A) *Contrast term for a three-phase system (B) zero contrast between "red" phase and "blue" phase. (C) Zero contrast between "yellow" phase and "blue" phase*

In a pure two phase system, if the scattering length density of one of the phase of the material corresponds to the scattering length density value of the H_2O-D_2O mixture then the scattering signal vanishes and we can observe the SANS spectra of only one phase.

IV.7.1.1 SHdi100: contrast variation experiments

IV.7.1.1.1 Theoretical SLD of the hybrid membrane components

The scattering length density (SLD) of the different components is calculated as follows:

$$\rho = \frac{\sum \mathrm{d} N_A \mathrm{b}}{M} \qquad \text{(eq-IV-5)}$$

Where d is the mass density, N_A the Avogadro constant, b the neutron scattering length and M is the molar mass.

The SLD of the sPEEK and H_2O are respectively ρ_{sPEEK} = 2.748×10^{10}/cm², ρ_{H2O} = -0.562×10^{10}/cm². To accurately calculate the SLD of the inorganic phase, one has to determine the molar mass of the sol-gel network. Therefore, the molar mass of the *poly-SHdi* (sol-gel phase completely condensed) is 150.32 g/mol.

The sol-gel phase was self-condensed as control sample, produced from the alkoxysilane precursor outside sPEEK in the same conditions as the ones which were selected to prepare hybrid membranes (*Annex A.4*). Its density, measured with the gas pycnometer, is about d=1.12 g/cm^3. An estimation of the SLD of the sol-gel phase gives $\rho_{polySHdi100\_calc} \approx 0.973\times10^{10}$/cm².

The SLD of the different membrane components are very different. It follows that in a scattering point of view, the wet hybrid membranes are three-phase systems. The calculated contrast between the different phases is:

$\Delta\rho(sPEEK\text{-}H_2O)_{calc} = 3.31\times10^{10}/cm^2$

$\Delta\rho(sPEEK\text{-}polySHdi100)_{calc} \approx 1.775\times10^{10}/cm^2$

$\Delta\rho(polySHdi100\text{-}H_2O)_{calc} \approx 1.535\times10^{10}/cm^2$.

In light water, the scattering signal will therefore mainly arise from the contrast between sPEEK and H_2O on the one hand, and between sPEEK and polySHdi100 on the other hand.

IV.7.1.1.2 Quantitative analysis

To go further into the structural analysis, one has to determine the SLD of the sol-gel phase by performing contrast variation SANS experiments. This experiment consists in recording the SANS data for hybrid membranes equilibrated in different H_2O-D_2O mixtures to vary the SLD contrast between the material and the exchange solvent. In a pure two phase system, the SLD of the material corresponds to the SLD value of the H_2O-D_2O mixture for which the scattering signal vanishes. It is expected that one can determine the reciprocal structural impact of both phases and obtain information about the inorganic phase location, architecture and mass density. Indeed, the I-*q* curves for a sol-gel network have typically two distinct features associated with two different structural levels, *i.e.*, the overall fractal aggregate structure and the constituting solid primary particles.

The hybrid membranes were equilibrated in different mixtures of H_2O and D_2O. Table IV-8 SLD of the solutions composed of different *H2O-D2O* ratios**.** gathers the SLD of the solutions composed of different H_2O/D_2O ratios.

Table IV-8 *SLD of the solutions composed of different H_2O-D_2O ratios.*

H_2O-D_2O (%)	100-0	80-20	50-50	20-80	0-100
ρ_s (10^{10} cm^{-2})	-0.562	0.829	2.916	5.002	6.393

With $\rho_s = X\rho_{H2O}+(1-X)\rho_{D2O}$, where X the H_2O ratio in the mixture.

It is expected that the mixture 50%-50%, which is associated to a SLD of 2.916×10^{10}/cm, will allow matching the sPEEK SLD (2.748×10^{10}/cm²) in order to observe the sol-gel network signal. It is expected that a mixture composition close to 69.8% H_2O will correspond to the matching index of *poly-SHdi100*. *Fig. IV-11* displays the SANS spectra of *SHdi100* for different H_2O/D_2O mixtures. One can observe a complex multiscale behavior which depend on the D_2O content. Different scaling regime are observed, the transition between them identify characteristic sizes and distances.

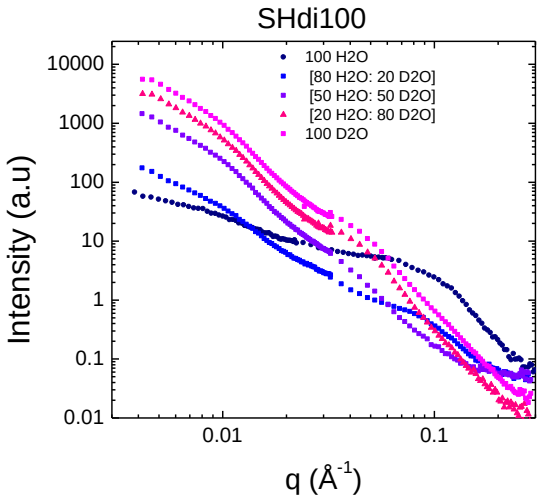

Fig. IV-11 *SANS spectra of SHdi100 for different H_2O-D_2O mixtures*

The scattered intensity of the small angle region increases with the D_2O content due to a higher contrast between the sol-gel network and the solution (see *Table IV.7*). From 0% to 50% D_2O, the SANS pattern does strongly evolve. Above 50%, the SANS profile evolution is less marked.

IV.7.1.1.3 Matching sPEEK: sol-gel network architecture and location

In the 50%-50% H_2O-D_2O mixture, no ionomer peak (see the broad ionomer peak in the range 0.06-0.12 $Å^{-1}$ for 0% D_2O) was observed. This confirms that this solvent mixture corresponds to the match point of the sPEEK where the contrast is zero; *i.e.*, only the inorganic phase *polySHdi100* is measured. *Fig. IV-12* displays the scattering pattern of *SHdi100* in a 50%-50% H_2O-D_2O mixture which shows 3 power-law regimes.

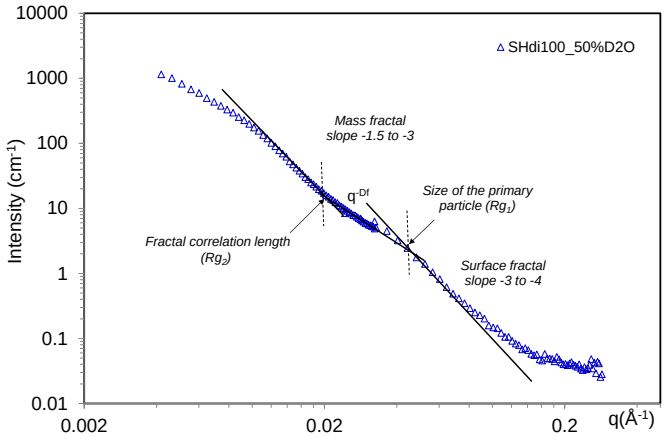

Fig. IV-12 *SANS spectra of SHdi100 hybrid membrane in 50%-50% H_2O-D_2O mixture*

At high *q*-value, the scattered intensity obeys Porod's law or q^{-4}, which reflects a smooth interface between the inorganic phase and water. At intermediate *q*, the SANS intensity curve obeys a power law of $q^{-2.8}$ which indicates self-similar structure with a mass fractal dimension D_f=2.8 [165]. In the general theory of fractals, the fractal dimension corresponds to the degree of irregularity or the space-filling capacity of an object. The lower and upper limits of the mass fractal power-law regime are characterized by the radius of gyration of the primary particle (Rg_1), and the fractal correlation length (Rg_2), which appear as a high-q knee (q_1 ≈0.044 Å^{-1}; $\pi/q_1=Rg_1$≈70 Å) and a low-q knee (q_2≈0.02Å^{-1} ; $\pi/q_2=Rg_2$≈157 Å) respectively [166, 167]. At low *q*-values, an upturn in intensity is observed with a power law close to q^{-2}. This behavior corresponds to bi-dimensional objects or locally planar microstructure. The question is whether the inorganic phase only grows within the ionic domains of the host membrane or form also extra-phases.

IV.7.1.1.4 Impact of the sol-gel phase as a function of the cross-linking density

Fig. IV-13 compares the SANS spectra of the hybrid membranes *SHdi100* and *SHdi90-TS10* for sPEEK contrast match condition (membranes equilibrated in 50%-50% H_2O-D_2O mixture mixture), i.e., only the inorganic phases are observed (confirmed by the extinction of the ionomer peak).

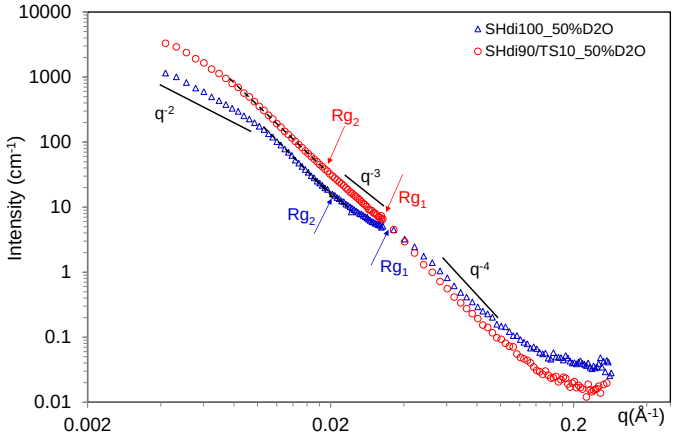

Fig. IV-13 *SANS spectra of Sol-gel phase in 50%-50% H_2O-D_2O mixture for SHdi100 and SHdi90-TS10*

Table IV-9 T*he fractal dimension Rg_1 and the fractal correlation length Rg_2 of the two inorganic phases.*

	D_f	Primary particle Rg_1 (Å)	Fractal correlation length Rg_2 (Å)
Sol-gel phase SHdi100	2.8	70 ± 5	157 ± 5
Sol-gel phase SHdi90-TS10	3	95 ± 5	175 ± 5

The slope of the fractal regime is somewhat higher for the inorganic phase of *SHdi90-TS10* which indicates that a denser phase is formed as compared to the situation with *SHdi100*. Also, the size of the primary particles and the fractal correlation length significantly increase with the cross-linking density. The characteristic distance between the polymeric aggregates within the host membrane is about 105 Å, (see the SANS curve for 0% D_2O). Considering the ribbon thickness determined for similar IECs [125] *i.e.*, 50 Å, the typical size of the ionic domains is then about 50 Å. The dimensions of the primary particles being about 70 Å and 95 Å for *SHdi100* and *SHdi90-TS10* respectively, it can be then expected that the networks do not grow exclusively inside the ionic domains, but also in the inter-bundles regions and/or are also incorporated into the polymeric ribbons. Finally, the local structure probed by the high-*q* scattering is found to be identical for both inorganic phases which indicates that the structure and in particular the specific surface of the primary particles remains unchanged.

IV.7.1.1.5 Sol-gel phase: Density of scattering length and cross-linking and density

It is observed on *Fig*. IV-11 that the scattered intensity never passes by a minimum in the small-angle region, where the scattering contribution of the inorganic phase is predominant, in other words, the network signal never extinguishes. Additionally, the contribution of sPEEK to the whole signal becomes significant with solution containing at least 20% D_2O for all the probed *q*-values.

The quantitative analysis, which was conducted at 0.01 A^{-1} to benefit from a maximum signal, raised several questions. First, the linear plot of the square root of scattering intensity with solvent composition [$Intensity^{1/2}$=f(D_2O%)] gives a matching solution with a negative value of D_2O. Second, taking only the data extracted from the curves measured at 100%, 80% and 50% D_2O (signal of the inorganic phase predominant), a contrast match was obtained with a mixture of 69.8% H_2O - 30.2 %D_2O. The SLD of *polySHdi100* determined experimentally is then 0.973×10^{10}/cm². It follows that a local density of *polySHdi100* of 0.5 g/cm^3 is found, which appears at first sight quite unrealistic regarding the density of 1.12 g/cm^3 measured for the network alone. Contrast variation experiments were also performed on *SHdi90-TS10* and a matching solution of 93% H_2O-7% D_2O was found. Although complementary experiments are needed to determine the molar mass of the sol-gel network in order to calculate the local density of the sol-gel phase which forms a network. It can be claimed that this apparent matching solution cannot fit with a network characterized by a higher density than that of *polySHdi100* (1.24 g/cm^3 for *polySHdi90TS10* against 1.12 g/cm^3 for *polySHdi100*).

These observations strongly suggest that nanometer-sized heterogeneities with the presence of sol-gel rich nanodomains dispersed in sPEEK phase, and/or sPEEK rich nanodomains within the sol-gel phase are formed. In this case, the sPEEK amorphisation is suspected and will be checked by XRD experiments in *section VI.7.2.* It can be furthermore ascertained that no demixion at the macro-scale occurred thanks to the transparency of the hybrid membrane. The ability of sPEEK membranes to accommodate a very large amount of sol-gel network is also in favor of an incorporation of the sol-gel precursors within hydrophobic and inter-bundles regions of sPEEK membranes. Another possibility is that numerous nanoporosities are created during the sol-gel process. Also, the membrane transparency allows excluding the formation of porosities at the micrometer scale.

Finally, it appears that complementary SANS experiments are mandatory to elucidate the structure of hybrid membranes and sol-gel networks and to discriminate the different hypothesis. Indeed,

1) SANS experiments with contrast variation performed on the network alone will allow determining its SLD.

2) From the spectra of the polymer phase and the sol-gel phase, it will be possible to reconstruct the theoretical spectra of the hybrid membranes through a linear combination. The comparison of the experimental spectra with the reconstructed ones will allow determining whether the small angle upturn is only due to the sol-gel network or to an additional contribution of nanoporosities and/or to a combination of the two phases.

IV.7.1.2 Increasing the cross-linking density: Impact on the membrane morphology

The partial location of the sol-gel network inside the ionic domains of the host membrane was suggested in the previous section for *SHdi100.* One can wonder if the sol-gel network location is impacted by the sol-gel precursors' functionality and cross-linking density.

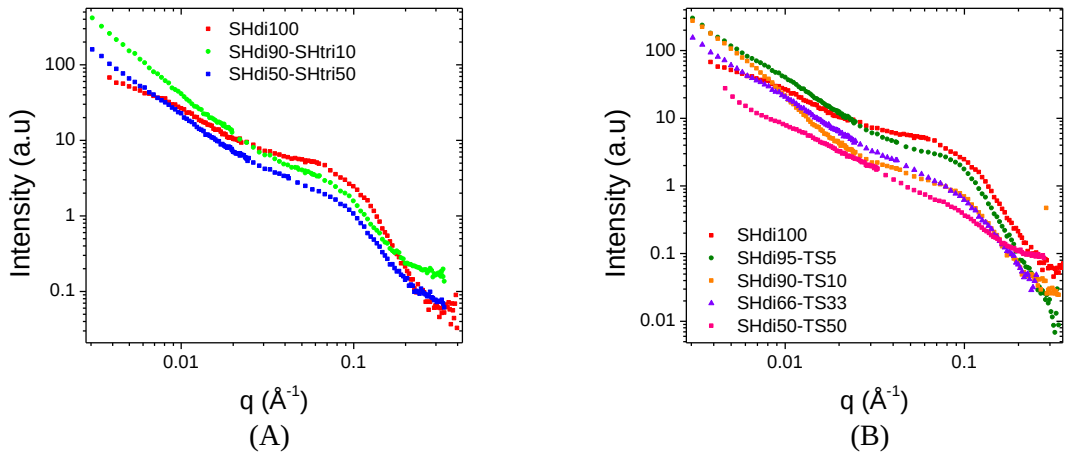

Fig. IV-14 *SANS spectra of the different hybrid membranes (A) SHdi-SHtri and (B) SHdi-TS in liquid water*

It is observed that the ionomer peak intensity decreases with the sol-gel network density and content. These observations can be explained by

- A (partial) sol-gel network location inside the ionic domains of the host membrane which were initially filled with water (the ionomer peak intensity, which is proportional to the contrast square, thus decreases)

-A decrease of the sPEEK scattering contribution to the overall signal

Also, the ionomer peak broaden with increasing the sol-gel network functionality as a result of a greater structural heterogeneity. Indeed, mixing precursors of different functionalities leads to the formation of heterogeneous networks in terms of composition and characteristic length scales. For the denser network (*polySHdi50-TS50*), the q^{-4} power law at wide angle is no more observed which shows that the interfaces are extremely rough.

IV.7.2 DRX

The hybrid membranes were investigated at a local scale by XRD to scrutinize the sol-gel network morphology and its impact on the overall membrane crystallinity. *Fig. IV-15* shows the X-Ray diffraction pattern of *(A)* **SHdi-SHtri** and *(B)* **SHdi-TS** hybrid membranes.

It is observed that the XRD spectra of hybrid membranes are characterized by a peak located in the small angle *q*-range which is associated to the sol-gel phase. Its position and broadness is directly correlated to the reticulation degree and chain length. Indeed, S*Hdi100* exhibits a broad and amorphous halo which is the signature of a marked disordering. It is located at ~0.7 $Å^{-1}$ (Bragg spacing~9 Å). *SHdi90-SHtri10* exhibits a peak shifted to smaller *q*-values ~ 0.66 $Å^{-1}$ (Bragg spacing~9.5 Å) and a slightly sharper peak showing an increased degree of ordering with triethoxysilane groups.

For *SHdi50-SHtri50*, the peak associated to the inorganic phase is significantly shifted to a smaller *q*-value of about~0.55 $Å^{-1}$ (Bragg spacing~11 Å). In contrast to previous observations, this peak is also very sharp; *i.e*, the inorganic phase is arranged into a crystal-like structure exhibiting a regular array of organo-silylated units. It is worth underlining the fact that the measurement of the sol-gel network alone would have allowed to determine whether the typical correlation length of the crystal-like. The structure is affected by the host membrane and to deconvolute the XRD spectra of the hybrid membranes.

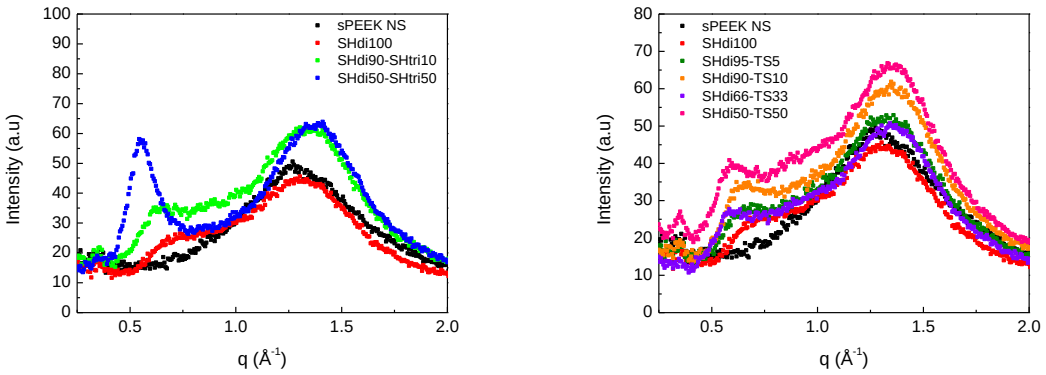

(A) (B)

Fig. IV-*15 X-Ray diffraction pattern of (A)SHdi-SHtri and (B) SHdi-TS hybrid membranes*

It is observed that whatever the ratio of bis-silylated precursor (TS), the peaks are rather broad. It can be concluded that the structural heterogeneities are higher when a bis-silylated precursor (**TS**) is used to form the sol-gel network as compared to the situation with a mono-silylated precursor (**SHtri**). There is a clear peak shifting to small *q*-values (Bragg spacing increases) with increasing the TS ratio (exception *SHdi66-TS33*). Also, additional and broad scattering contributions are observed between 0.6 and 1 $Å^{-1}$ which intensity increases with the TS ratio. This suggests that the sol-gel network is heterogeneous in nature in terms of composition and characteristic size.

IV.8 Fuel cell performances

As a preliminary test, fuel cell performances were tested with the *SHdi100* membranes.

Fuel cell performance was characterized by recording polarization curves with a current scan ranging in Open Circuit Voltage (OCV). Polarization curves have been recorded after 12h of operation at 3.6A for stoichiometrie 1.5/1.5.

MEA was subjected to a round cycle of voltage in the range 0.6-0.3V and drawn electric current was registered. The duration of the each cycle of the applied voltage was 12 hours. This cycle was repeated 10 times. The performance of the membrane decreases with increasing number of cycles. The fuel cell polarization curves were obtained for the first cycle. They are displayed on *Fig. IV-16*.

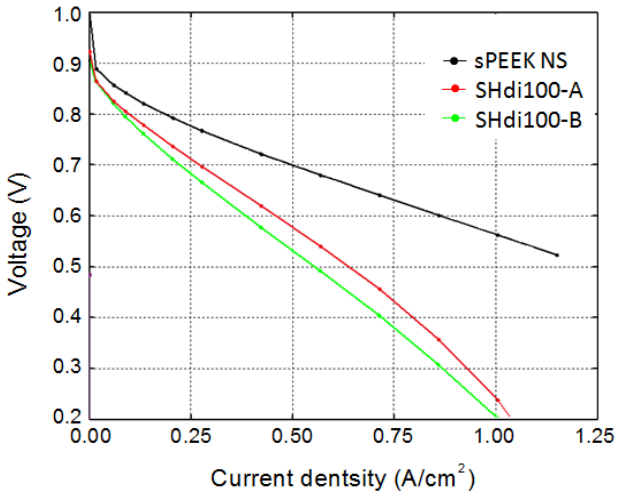

Fig. IV-16 *Polarization curves of sPEEK NS and SHdi100 hybrid membranes at 70ºC and 80%RH. SHdi100-A and SHdi100-B corresponds to two different tests with SHdi100 hybrid membrane.*

Fig. IV-16 compares the fuel cell performances of *sPEEK NS* membrane to those obtained from hybrid membrane *SHdi100*. This test shows that, despite the large sol-gel content (50%), the hybrid membrane allows fuel cell operation. The performances are lower with respect to those of *sPEEK NS* membrane, due to its lowest proton conductivity. Moreover, the fuel cell test shows that the sol-gel phase increases the membrane permeability to gas. However, the present preliminary results are encouraging (considering the high sol-gel content) and the considerable improvements which can be gained by a selective conversion of stabilizing functions into acid ones by mild oxidation.

IV.9 Conclusions

The original strategy to design hybrid membranes by impregnation of sol-gel precursors in a host ionomer membrane allows enlarging the dispersion of the networks. However, the success of the procedure depends on the molar ratio of the matrix phase and inorganic ratio and the kind of precursors used. Often the major problem associated with the incorporation of an inorganic network is the increase of brittleness, because this leads to membranes with a mechanical stability not enough to resist the elaboration process. In our case the brittleness of the membrane is not a problem, even when the amount of precursors exceeds 50%.

We cannot observe the improvement of the thermal or mechanical stability, In our case the large amount of precursors inside prevent the membrane stabilization.

A lower sol-gel content typically 5 to 20% should be sufficient to increase significantly the chemical and the thermal stability to operate a high temperature. The conductivity could improve the formation of SO_3H groups.

It is worth underlining that the amount of stabilizer usually used to prevent polymer degradation during polymer industrial processing is lower than 1% by weight. We can assume that for such low sol-gel network content (1%), both, the membrane's gas impermeability and proton conductivity will be preserved. Of course a higher sol-gel network content (typically 5 to 10%) would be more adapted in order to achieve high proton conductivity after a partial conversion of the stabilizing units into additional acid functions.

CONCLUSIONS AND PERSPECTIVES

Proton exchange membrane water electrolysers (PEMWE) and fuel cells (PEMFC) are promising, environmentally-friendly, and oil-free technologies. One of their key components is the **polymer electrolyte membrane**, which acts as a separator and proton conductor. A crucial issue lies in improving both, the performance and durability of the membrane. **Membrane degradation under harsh and/or long-term operating conditions** is in fact highly detrimental and can ultimately cause the system failure.

The aim of this research project was to overcome the obstacles that limit the use of available commercial PEM at high temperatures by manufacturing a high performance hybrid membrane, prepared from a polyaromatic commercial ionomer membrane. Designing a new class of hybrid membranes from hydrocarbonated membranes is a clear challenge because the performances of non-perfluorinated materials always remain much lower than benchmark PFSAs (in terms of chemical stability and conductivity). The sPEEK membrane was selected because it possesses excellent thermal properties, although it has a very limited fuel cell lifetime due to its high sensitivity to chemical degradation. Our main idea was to transform a low-cost, commercially available material with poor properties into a true challenger to the well-established PFSA materials. The focus of the study was therefore to obtain sustainable and durable membranes, without targeting neat improvements in terms of conductivity.

The development of hybrid membranes for PEMFC has attracted growing attention for several years now, although no significant improvement of the functional properties has been reported until now. Hybrid membranes are usually obtained through two different processes: either through solvent casting from a dispersion of fillers or nanoparticles in an ionomer solution, or through impregnation of sol-gel precursors into a host ionomer membrane. In the case of polyaromatic ionomer membranes, the impregnation process appeared to be more efficient due to the difficulty of obtaining a well-defined polymer nanostructure (hydrophobic-hydrophilic) from a polymer solution. Following this observation, we decided to focus on the impregnation method. Our strategy was to create a reactive sol-gel network in the host sPEEK ionomer membrane that can **inhibit the oxidative degradation** of the ionomer phase through the consumption of **sacrificial sites** and to **improve the mechanical resistance** of the membrane through the formation of a 3D network. The main goal of this work was to develop such innovative concepts as establishing the feasibility of preparing the aforementioned sol-gel based hybrid membranes and then identifying the limiting factors and optimize the protocols to provide an understanding of the final properties of the newly synthesized materials.

The ionic domains of a pristine sPEEK membrane are narrower and less defined than those of the benchmark Nafion® membrane. Therefore, the first step of our work consisted on finding a process that allows us to optimize the sPEEK nanostructuration prior to the impregnation process. Extensive SAXS experiments under dry and wet conditions at room and elevated temperatures allowed for a new attribution of the various correlation peaks, and the subsequent definition of a

hydrothermal treatment allowed for improvements of the nanostructuration. We demonstrated that the quality of the hydrophilic/hydrophobic nanophase separation can be controlled by adjusting the hydrothermal treatment conditions (temperature and duration). This process can be accelerated under an oxidative treatment (not retained due to the induced membrane's brittleness). We succeeded in improving the pristine sPEEK membrane by applying a well-chosen hydrothermal treatment that yielded a significant increase in the membrane's proton conductivity from 24 to 84 mS/cm, therefore reaching the state-of-the-art value of the benchmark Nafion membrane. More generally, this work emphasizes the importance of the ionic phase connectivity and structural organization for producing polymer membranes with sufficient proton conduction, and proposes a simple and general method to promote adequate properties by applying a pre-structuring treatment applicable to a large variety of materials.

The second main achievement of this work relates to the preparation of hybrid membranes from the nanostructured sPEEK membranes by impregnation of sol-gel precursors. We established a protocol that allows for the reproducible manufacturing of self-standing hybrid membranes. Moreover, we demonstrated the possibility of creating a 3D sol-gel network inside the ionic domains. The sacrificial sites carried by the precursors were thiol and tetrasulfide chemical groups, which were chosen for their high sensitivity to oxidative products formed during fuel cell operations. In order to adjust the physical properties of the sol-gel network, we selected sol-gel precursors bearing two, three, or six hydrolysable groups per sol-gel molecule.

The materials were produced, and they exhibited a range of interesting properties:

- The hybrid materials have good film-forming properties, even when the amount of the sol-gel phase exceeds 50%wt. The hybrid membranes do not present detrimental brittleness and can be manipulated.
- The membranes are homogeneously formed due to impregnation of the sol-gel in a preformed nanostructured host polymer matrix.
- The hybrid membranes are proton-conducting and display a potentially interesting thermo-mechanical behavior. The morphological investigations allowed us to partially understand the morphology of the sol-gel phase, but additional analyses are required for full understanding.

However, the performance of our membranes seems deceiving in real fuel cell test conditions. It is necessary to acknowledge that the conditions for the fuel cell test (electrode preparation, Membrane electrode assembly process) were not optimized. It is also necessary to acknowledge that MEAs could be prepared from the hybrid membranes and integrated in a real device for evaluation, which leaves room for improvement. Several research directions could be explored to overcome the present limitations and possibly enhance the performances. One essential point is to control the amount of sol-gel in the hybrid membrane, which must primarily drive the overall properties of the membranes. This could be achieved by:

- varying the sol-gel precursor / solvent molar ratio.
- using another solvent for the elaboration of hybrid membranes.

A preliminary test in ethanol showed that it is possible to reduce the sol-gel phase content, with the benefit of using non-toxic solvent for the elaboration process.

After carefully controlling the sol-gel phase content, one may envisage a systematic and thorough morphological investigation of the obtained materials as a function of sol-gel precursor content in the host membrane by means of SANS and/or SAXS, as we conducted in this study. This would help in establishing the structure-function interplay and would thereby elaborate the more adapted hybrid membranes in order to achieve high proton conductivity after a partial conversion of the stabilizing units.

To summarize, this study has achieved a step toward the synthesis of novel hybrid membranes, which inspires interest for a potential use in electrochemical devices for energy conversion and storage. Our work has provided the proof-of-concept of a sol-gel based approach using *ad hoc* functionalities to protect commercial polymers from degradation and carefully improve their behavior. This constitutes the foundation for further developments, based on the sol-gel content control that is required to master both the chemistry and the morphology of the sol-gel network in order to develop high performance hybrid membrane.

ANNEXES

ANNEX A.1. Membrane characterization

**** SAXS***

The SAXS spectra were recorded on ID2 High Brilliance Beamline and D2AM-CRG beamline at the ESRF (Grenoble). The X-ray scattering intensity was measured as a function of the scattering vector "*q*" defined as $q = 4\pi\sin(\theta)/\lambda$, where 2θ is the scattering angle and l the wavelength of the incident X-ray beam. The Bragg spacing "d" is related to "*q*" as: $d = 2\pi/q$. The measurements were carried out at $\lambda = 1$ Å with a sample-to-detector (a 2D-CCD camera) distance of D =1 m (ID2) and at $\lambda = 0.77$Åwith D =0.75 m (D2AM). These configurations, used with a centered X-ray beam with respect to the sample, allowed covering an extended *q*-range from 10^{-2} to 0.4 $Å^{-1}$. The 2D-scattering patterns were isotropic, therefore the 1D scattering curves (intensity = f (q)) were obtained after integration over all directions.

The SAXS spectra were also recorded using a home-made apparatus at CEA-Grenoble/INAC, using a CuKα radiation ($\lambda = 1.5418$ Å) source generated by a rotating anode. Two "sample to detector" distances of 1.50 m, 0.80 m and 0.20 m with an off-centred configuration were chosen and allowed covering an extended angular *q*-range from 0.01 to 0.5 $Å^{-1}$. Two pieces of water swollen membrane were superimposabled and were placed in a SAXS cell between two Kapton® foils. The usual corrections were applied to the data for background subtraction and normalization.

**** WAXD***

The Wide-Angle X-Ray Diffraction (WAXD) patterns were recorded using a Panalytical X'Pert diffractometer equipped with a copper X-ray tube (Kα = 1.5418 Å) delivering a linear beam and with a 1D X'Celerator detector (CEA-Grenoble/INAC). A 0.51 divergence slit was used on the primary path with a set of anti-scattering slits before and after the sample. The axial divergence was limited by 0.02 rad Soller slits. The measurements were performed in $\theta/2\theta$ transmission geometry. The data were recorded for 2λ ranging from 71 to 501 (0.5 to 3.4 Å-1) with a step of 0.041 and a time per step of 300 s. The samples were equilibrated at room temperature and relative humidity (20 ºC, 45% RH).

**** SANS***

Small-angle neutron scattering (SANS) experiments were per-formed at the Laboratoire Léon Brillouin (LLB, Saclay, France) on the PAXY spectrometer. Three configurations were used with λ=5Å, D=1.1m , λ=12Å, D=1.1m and λ=10Å, D=6.7m *q*-values of $0.004Å^{-1} < q < 0.3Å^{-1}$. The detector was tilted with respect to the incident axis to increase the accessible angular range. Cells with quartz windows and spacers were used for the study of swollen membranes.

The usual corrections were applied to SANS data (detector and incident flux normalization, background subtraction, transmission correction, membrane thickness...).

**** RAMAN***

The chemical structure has been investigated by Raman. The spectra were recorded between 400 and 4000 cm^{-1} (20 s, 100% laser power) with a LabRAM HR 800 instrument from Horiba Jobin Yvon (laser 633 nm/20 mW, Olympus objective LMPLFNX100, confocal microscope). Each spectrum was obtained by the summation of 3 scans and processed on LabSpec VI.

**** SORPTION BALANCE***

Dynamic vapor sorption analyzer, DVS Advantage, was used to determine water sorption isotherms of the different samples. The vapor partial pressure was controlled by mixing dry and saturated nitrogen, using electronic mass flow controllers. The experiments were carried out at 25 °C. The initial weight of the sample was approximately 80 mg. The sample was predried in the DVS Advantage by exposure to dry nitrogen until the dry mass of the sample was obtained (m_0). A partial pressure of vapor (p) was then established within the apparatus and the mass uptake was followed as a function of time (t). The mass at equilibrium (m_{eq}) was considered to be reached when changes in mass with time (dm/dt) were lower than 0.0002 mg/min for at least five consecutive minutes. Then, vapor pressure was increased in suitable activity up to 0.9 by step of 0.1. The values of mass gain at equilibrium (M) for each water activity (a_w) allowed plotting the water sorption isotherm for each sample.

**** ATG***

Thermogravimetric analysis (TGA) measures the amount and rate of change in the weight of a material as a function of temperature or time in a controlled atmosphere. Measurements are used primarily to determine the composition of materials and to predict their thermal stability at temperatures up to 1000°C. The technique can characterize materials that exhibit weight loss or gain due to decomposition, oxidation, or dehydration.

For all the investigated materials the thermogravimetric analyses were carried out with a high resolution Q50 (TA Instruments) thermobalance, with a resolution of 1 µg.

The heating rate was $10°C \cdot min^{-1}$, the measurements were conducted in the temperature range from room temperature to 1000°C, with a O_2 flux of $100cm^3$/min, using open platinum pans loaded with ca. 5-7mg of each dry sample.

**** MEMBRANE SWELLING***

The membranes were cut into rectangular pieces (6×3 cm^2). To obtain the wet weight (m_{wet}), the excess water was gently removed with filter paper before weighing the swollen membranes. The dry weight (m_{dry}) was measured after drying under vacuum at room temperature overnight.

The level of membrane hydration is defined with λ which is defined as the number of water molecules per ionic site:

$$\lambda = \frac{EW}{M_{H_2O}} . \frac{(m_{wet} - m_{dry})}{m_{dry}} \quad (1)$$

Where m_{wet} and m_{dry} correspond respectively to the mass of the hydrated and dry membrane, M_{H2O} the molar mass of water and EW the polymer equivalent weight.

**** CONDUCTIVITY***

After removal from treatment, samples (1 x 2.5 cm^2) were equilibrated in pure liquid water prior to measurement (2h).

The proton conductivity was determined by impedance spectroscopy using Material Mates 7260 Frequency Response Analyzer and a home-made conductivity cell. The cell is composed of two blocks of polymer support where are inserted series of 1 mm thick gold wires spaced from 0.25 cm to 1.75 cm. These supports were used as electrodes on both sides of the membrane. The measurements were systematically conducted connecting the electrodes on both sides of the membrane and varying the inter-electrode distance. The conductivity was measured with different combinations of electrodes to obtain an average value of the membrane resistance. The frequency varied between 5 MHz and 100Hz.

The proton conductivity expressed in S/cm has been calculated according to equation (2)

$$\sigma = \frac{L}{R \times W \times e} \quad (2)$$

Where L is the distance between gold wires, W is the width of the membrane (1 cm) and *e* is the thickness of membranes expressed in cm. R is the membrane resistance (Ω).

****DENSITY***

The membrane density was determined using a gas pycnometer (Micromeritics AccuPyc II 1340). Membrane samples (20-30 mg) either equilibrated at room relative humidity or after immersion in liquid water were first weighed and introduced in the gas pycnometer. 1000 cycles of measurements were applied inducing a membrane drying by the injection of dry helium at each cycle. The membrane weight was measured before and after the experiments.

****DMA***

The thermo-mechanical properties of the different membranes were studied using a DMA Q800 V20.9 Buils 27 (TA instruments). The measurements were carried out in the temperature range of 35ºC to 250ºC with preloaded force of 0.01N with sample size of 5*4mm, force track and a frequency of 1Hz. The storage and loss modulus of the composite membranes were determined in given temperature range.

ANNEX A.2. Materials

sPEEK properties

Fumapem®		E-730
Membrane type		Cation exange membrane
Appearance/color		slightly brown transparent
Backing foil		PET foil
Reinforcement		None
Lot No		M2143301
Thickness(dry)	µm	30
Ion exchange capacity (Na+ form)	Meq g-1	1.35
Area resistance in Na+ form	Ωcm2	1.5
Specific conductivity in Na+ form	mS cm-1	1.9
Selectivity in 0.1/0.5mol/kg KCl at T=25ºC	%	98.5
uptake in H_2O at T=25ºC	Wt%	28.4
dimensional swelling in H_2O at T=25ºC	%	4-8

Sol-gel precursors properties

Characteristics	SHdi	SHtri	TS
	(3-Mercaptopropyl) methyldimethoxysilane	(3-Mercaptopropyl) triethoxysilane	Bis[3-(triethoxysilyl)propyl] tetrasulfide
	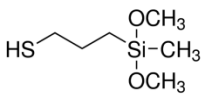	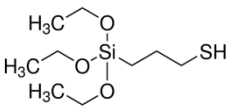	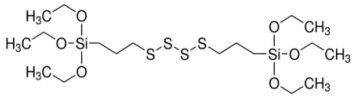
Linear Formula	$CH_3Si(OCH_3)_2CH_2CH_2CH_2SH$	$HS(CH_2)_3Si(OCH_2CH_3)$	$C_{18}H_{42}O_6S_4Si_2$ (Empirical Formula)
Molecular Weight	180.34	238.42	538.95
assay	≥95.0%	≥80% (GC)	≥90% (NMR)
form	Liquid	Liquid	Liquid
Bp	96 °C/30 mmHg(lit.)	-	-
Density	1 g/mL at 25 °C(lit.)	0.987 g/mL at 20 °C(lit.)	1.08 g/mL at 20 °C(lit.)
Storage temp		2-8ºC	

ANNEX A.3. The principles of the scattering experiments

Small-angle X-ray scattering (SAXS) is an experimental technique widely used to study the structural properties of matter. It is a non-destructive method for investigating nanostructures from <1 nm up to 200 nm in size.

The elastic scattering of radiation in the sample leads to interference effects, resulting in a scattering pattern, which can be analyzed to provide information about size and shape of the component of the sample. Fig. A.1.

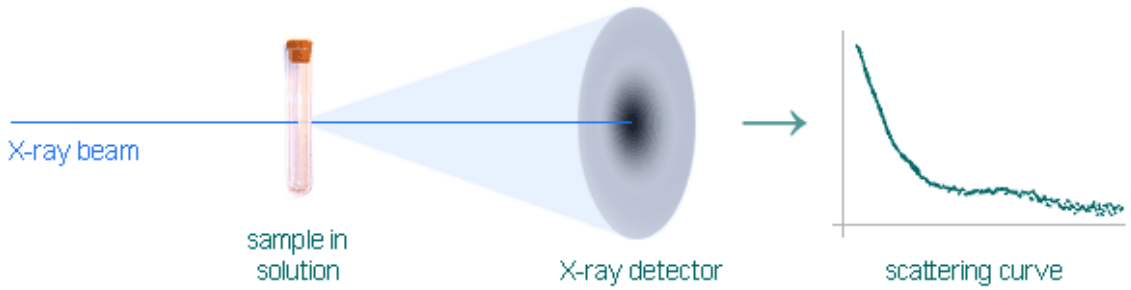

Fig A.1 *Schematic setup of SAXS experiments*

The principle of a SAXS experiment is the following: X-rays are generated in an X-ray source and passed through a collimator. When the x-rays traverse the sample, some of them are scattered and can be detected on a position-sensitive detector, typical SAXS setup with a 2D (area). A beamstop is placed in front of the detector to absorb the strong direct unscattered beam. For most samples the main SAXS intensity is present close to the beamstop and decreases as a function of the scattering angle.

An appropriate source emits a beam of X-rays which is focused and monochromated by special X-ray optics. The size of the beam is adjusted by a system of slits, hits the sample and enters the flight path. The flight path, which has to be under vacuum because air scatters the beam, provides the long distance between detector and sample that is essential to detect X-rays scattered at small angles.

Instead of displaying the logarithm of the intensity I(q) as a function of the scattering angle 2θ, it is usual to display it as a function of length of the scattering vector $q = 4\pi \sin(\theta)/\lambda$ where λ is the x-ray wavelength. This "q" parameter allows an easier comparison of data recorded with different wavelengths.

Small-angle Neutron scattering (SANS)

Small-angle neutron scattering (SANS) is an experimental technique that uses elastic neutron scattering at small scattering angles to investigate the structure of various substances at a mesoscopic scale of about 1 - 100 nm.

Small-angle neutron scattering is in many aspects very similar to small-angle X-ray scattering (SAXS). During a SANS experiment a beam of neutrons is directed to the sample, which can be an aqueous solution, a solid, a powder, or a crystal. The neutrons are elastically scattered by nuclear interaction with the nuclei or interaction with magnetic momentum of unpaired electrons. In X-ray scattering, photons interact with the electronic cloud so bigger is the element, bigger is the effect. However, in neutron scattering, neutrons interact with nuclei and interaction depends on isotope; some light elements, like deuterium, show similar scattering cross section as heavy elements like Pb.

SANS usually uses collimation of the neutron beam to determine the scattering angle of a neutron, which results in an even lower signal-to-noise ratio for data that contains information on the properties of a sample at relatively long length scales, beyond ~1 μm.

In order to make the analysis of complex structures more tractable, the ability to vary the scattering length density through hydrogen-deuterium exchange is a key advantage of neutron scattering over other scattering techniques. The technique of **contrast variation** (or **contrast matching**) relies the differential scatter of hydrogen vs. deuterium. At certain ratios of H_2O to D_2O, called match points, the scatter from the molecule will equal that of the solvent, and thus will be eliminated when the scatter from the buffer is subtracted from the data.

ANNEX A.4. Elaboration de poly-Hybrid membranes

The elaboration protocol of poly-condensed precursors is similar to the protocol of hybrid membrane elaboration.

1.- We prepared a solution of sol-gel precursors 0.21M in Water(pH=4)/MeOH.
2.- The solution was stirred for 4 days at room temperature.
3.- Evaporation of solvent at room temperature for a week.
4.- We completed the sol-gel phase condensation by a curing at 74ºC and 6.3% RH for 24h

The resulting material was labeled poly-hybrid membrane and used for different complementing experiments.

RÉSUMÉ EN FRANÇAIS

RÉSUMÉ EN FRANÇAIS

Introduction

Le développement de la pile à combustible est aujourd'hui limité suite à l'absence d'un électrolyte polymère performant. Cet électrolyte doit présenter l'ensemble des propriétés fonctionnelles nécessaires pour la conduction protonique, tout en combinant de bonnes propriétés thermomécaniques pour résister aux contraintes mécaniques imposées en pile et une bonne stabilité chimique.

Le Nafion® est la membrane de référence par sa très grande stabilité chimique et sa très bonne conductivité protonique, au-delà de 80ºC. Par contre, pour des températures de fonctionnement entre 100-120°C voire supérieures, qui permettraient d'améliorer l'efficacité du système et l'utilisation de catalyseurs sans platine, la membrane dite de référence perd ses propriétés mécaniques (ramollissement, écoulement). Par ailleurs, l'utilisation de membranes perfluorées ne va pas sans poser de problèmes environnementaux et de coût (danger de la chimie du fluor et recyclabilité).

Des membranes alternatives de type polyaromatiques telles que le polyetherethercetone sulfoné, le polyimidesulfoné, le polybenzimidazol sulfoné, le polysulfone sulfoné, etc., ont été développées. Ces membranes qui offrent de meilleures propriétés thermomécaniques ne présentent pas une stabilité chimique ou des propriétés de conduction suffisantes pour les envisager comme des alternatives pertinentes aux structures perfluorées. Leur très grande sensibilité aux agents dégradants qui se forment dans la pile (H_2O_2 et radicaux hydroxyles HO• et hydroperoxyles HOO•) est généralement considérée comme le facteur limitant leur durabilité en pile et donc celle du dispositif.

L'objet de ces travaux de thèse vise précisément à développer de nouvelles membranes qui permettent d'améliorer la durée de vie des électrolytes polymères alternatifs par une stabilisation à la fois chimique et mécanique tout en maintenant, voire en améliorant leurs propriétés de conduction protonique.

CHAPITRE I: L'état de l'art

Les travaux menés au cours de cette thèse trouvent leur fil conducteur dans le développement des piles à combustible et plus particulièrement dans le développement de la membrane de conduction protonique. Il est donc pertinent de commencer par introduire les concepts de base liés à ce type de système, ainsi que l'état de l'art actuel du domaine.

La pile à combustible (PAC) est un système électrochimique capable de convertir directement l'énergie chimique d'un combustible - hydrogène, hydrocarbure, méthanol - en énergie électrique avec un haut rendement et une faible émission de polluants.

Il existe de nombreux types de PAC qui différent de par l'électrolyte qu'elles utilisent, "Solid Oxyde Fuel Cell" (SOFC), "Molten-Carbonate Fuell Cell" (MCFC), "Alkaline Fuel Cell" (AFC), "Phosphoric Acid Fuel Cell" (PAFC), "Proton Exchange Membrane Fuel Cell" (PEMFC).

Les PEMFC sont les piles à combustible les plus étudiées à l'heure actuelle du fait de leurs nombreuses applications potentielles dans les domaines du transport, des unités de production d'électricité dites stationnaires, etc. Elles fonctionnent à de basse températures (~ 80°C) et utilisent une membrane ionomère hydratée conductrice protonique.

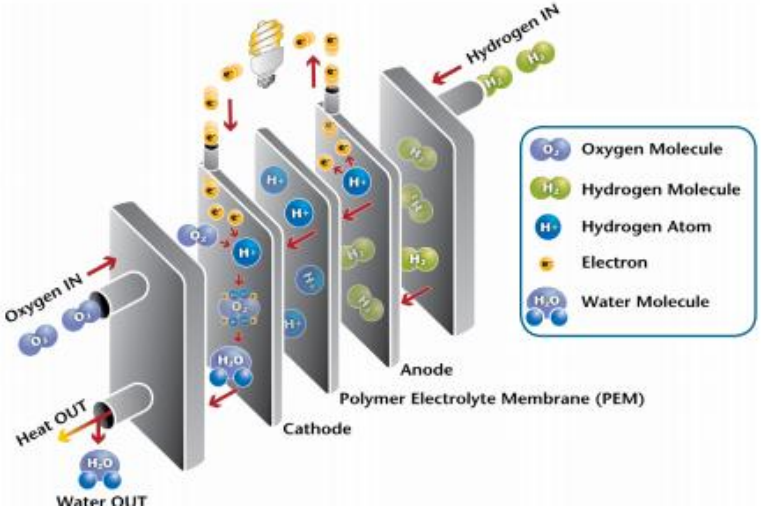

Fig.1 Schéma de fonctionnement d'une pile à combustible.

Le schéma de fonctionnement d'une PEMFC est représenté *Fig.1*, on y voit une cellule élémentaire. Un assemblage en "stack" (assembla en série de piles élémentaires) est nécessaire pour générer une puissance suffisante (~ 80 kW pour une voiture).

La cellule élémentaire est composée d'une membrane prise entre les électrodes, formant l'Assemblage Membrane Électrode (AME). Chaque électrode est constituée d'une couche catalytique active et d'une couche de diffusion des gaz. L'approvisionnement en gaz et la collecte du courant sont assurés par les plaques bipolaires situées de part et d'autre des électrodes.

La membrane est l'élément central du dispositif. Elle détermine en grande partie le domaine de fonctionnement de la pile, c'est-à-dire les températures admissibles, la pression et l'humidité requises pour les gaz. En sus des propriétés essentielles de conduction protonique et de stabilité chimique, elle doit remplir un cahier des charges très contraignant :

- Bonne stabilité chimique et électrochimique pendant le fonctionnement.

- Résistance mécanique dans les conditions de fonctionnement.

- Propriétés chimiques des composants de la membrane compatibles avec les exigences de l'assemblage membrane-électrode.

- Extrêmement faible perméabilité aux gas des espèces réactives.

- Haute mobilité de l'eau pour avoir une concentration uniforme dans l'électrolyte et empêcher ainsi de possibles séchages locaux.

- Grande conductivité protonique pour soutenir des courants élevés avec une perte de résistance minime.

Ce chapitre est divisé en quatre parties :

1) Les membranes conductrices protoniques

2) Les mécanismes de dégradation des membranes en pile

3) Les stratégies de stabilisation chiiques des membranes pour augmenter leur durabilité

4) Élaboration de membranes hybrides par un procédé sol-gel

1) Les membranes conductrices protoniques

En général, les matrices polymères utilisées dans l'AME peuvent être classées en trois groupes principaux:

1.1. Ionomères perfluorés (partiellement ou totalement)

La membrane de référence est le Nafion®. C'est un polymère perfluorocarboné avec des chaînes pendantes perfluorées dont l'extrémité se termine par un groupement acide sulfonique. Cette combinaison d'un squelette très souple et très hydrophobe et de fonctions acides très hydrophiles permet la formation d'une morphologie très particulière des membranes. De plus, la structure totalement perfluorée donne à ce matériau une inertie chimique et une stabilité électrochimique très élevées, séparation de phase hydrophile/hydrophobe marquée.

Le Nafion® est majoritairement employé dans les systèmes commercialisés parce qu'il possède une conductivité protonique élevée (de l'ordre de 100 $mS.cm^{-1}$ dans les meilleures conditions) et qu'il permet des durées de fonctionnement très élevées (50000h pour des applications stationnaires).

1.2. Non- hydrocarbures fluorés (y compris des structures aliphatiques ou aromatiques)

Nous nous concentrerons sur les propriétés des polymères aromatiques sulfonés, en particulier du Poly(Ether-Ether-Cétone)s sulfoné (sPEEK).

Le sPEEK possède un squelette aromatique non fluoré dans lequel des groupements phényles di-substitués et tri-substitués sont séparés par des fonctions éther et cétone. Le sPEEK présente une plus faible séparation de phase que le Nafion®, caractérisée par des domaines ioniques plus tortueux et plus étroits. Ces modifications morphologiques impactent fortement les propriétés fonctionnelles de la membrane sPEEK (chute de la conductivité). Donc les membranes de type

Nafion® et polyaromatiques de type sPEEK présentent des structures très différentes qui ont un impact sur les propriétés fonctionnelles de la membrane.

Les membranes sulfonées présentent une combinaison de propriétés remarquables comme d'excellentes propriétés mécaniques, thermiques, mais ne présentent pas une stabilité chimique ou des propriétés de conduction suffisantes.

1.3. Membranes hybrides

De grands efforts ont été réalisés ces derniers temps afin d'obtenir de nouvelles membranes hybrides et de les comparer à la membrane de référence Nafion®.

De manière générale nous pouvons rappeler les multiples façons d'ajouter des charges ou réseaux dans une matrice polymère pour obtenir une membrane hybride:

a- Croissance des charges/réseaux à l'intérieur d'une membrane déjà formée par une méthode dite d'infusion.

b- Croissance des charges/réseaux dans une solution d'ionomères, avant ou pendant l'évaporation du solvant.

c- En dispersant dans une solution d'ionomères des charges déjà formées.

Il est important de noter ici que seules les deux premières méthodes (*a* et *b*) permettent de faire croître des réseaux plutôt que des charges isolées et que pour la méthode *a* n'impacte pas la nanostructuration de la membrane hôte.

2) Les mécanismes de dégradation des membranes en pile

La dégradation des membranes électrolytes polymères utilisées en pile à combustible est un phénomène connu et très largement étudié. Elle résulte de la combinaison des contraintes mécaniques, thermiques et chimiques subies par la membrane pendant le fonctionnement de la pile. Les conditions de fonctionnement de la pile et en particulier le taux d'hydratation et la température ont une forte influence sur l'évolution des propriétés mécaniques de la membrane.

La très grande sensibilité aux agents dégradants formés dans la pile (H_2O_2 et radicaux hydroxyles et hydroperoxyles) est considérée comme la cause de la dégradation chimique des membranes polymères.

3) Les stratégies de stabilisation chimiques des membranes pour augmenter leur durabilité

Les stratégies décrites dans la littérature pour élaborer des membranes plus durables sont basées sur différents critères de stabilisation.

- Amélioration de la conductivité. Pour obtenir des membranes ayant des performances meilleures que les membranes Nafion®, la conductivité protonique doit être augmentée de plus de 100 $mS.cm^{-1}$.

- Stabilisation pour minimiser la dégradation mécanique. Renforcement de la matrice polymère par des fibres ou nanoparticules.

- Stabilisation pour minimiser la dégradation chimique. Pour empêcher l'oxydation de la membrane polymère.

La conception de membranes plus durables est extrêmement difficile en raison d'une propriété clé qui est généralement améliorée au détriment de l'autre.

4) Élaboration des membranes hybrides par un procédé sol-gel

Le procédé sol-gel pour la préparation de membranes hybrides organique-inorganique semble l'une des options les plus intéressantes car elle offre des avantages évidents:

- Basse température de mise en œuvre (à température ambiante).

- Homogénéité élevée et pureté des matériaux issus.

- Possibilité de processus de formation variés.

De nombreux paramètres ont une influence déterminante sur la réaction sol-gel avec un impact direct sur la morphologie de la phase inorganique et donc sur les propriétés de la matière résultante. Les propriétés physiques et chimiques des membranes hybrides obtenues dépendent de plusieurs variables expérimentales telles que le pH, la nature du solvant, le rapport eau/alcoxy, le temps de réaction, la température de réaction et à la fois le séchage et les conditions du traitement thermique de fin de condensation.

CONCLUSION

Afin d'obtenir des membranes hybrides homogènes, la meilleure méthode semble être la formation d'une phase inorganique par un procédé sol-gel. Cette stratégie permet de contrôler la taille et la morphologie de la phase inorganique. L'imprégnation d'oxydes inorganiques dans une membrane polymérique hôte peut réduire ses performances en pile. Cependant, certains types de précurseurs ayant des groupes fonctionnels spécifiques permettent d'améliorer la rétention d'eau, la conductivité et la tenue mécanique de la membrane obtenue sont comparées avec la membrane intacte.

CHAPITRE II: Morphologie de la membrane sPEEK

Dans ce *chapitre II*, nous allons présenter l'étude de la morphologie des membranes sPEEK. La membrane commerciale sPEEK sera utilisée comme membrane polymère hôte qui accueillera une phase sol-gel pour la renforcer mécaniquement ainsi que la stabiliser chimiquement. L'étude en profondeur de la morphologie de cette membrane va nous permettre de mieux comprendre le processus sol-gel et la morphologie des membranes hybrides obtenues.

Ce chapitre est basé sur les résultats obtenus par SAXS (Small Angle X-Ray Scattering) , SANS (Small Angle Neutron Scattering) and WAXS (Wide Angle X-Ray Scattering) pour des membranes conditionnées à différents taux d'hydratation.

Nous avons réalisé des séries d'expériences pour étudier l'évolution de la morphologie de la membrane ionomère hôte et ainsi voir son impacte sur ses propriétés fonctionnelles.

Nous avons réalisé une étude complète de la microstructure en fonction du gonflement à différents taux d'hydratation.

- Gonflement en humidité relative à température ambiante.

- Gonflement dans l'eau liquide à température ambiante.

- Gonflement dans l'eau liquide à différents températures entre 20ºC et 120ºC pour des temps d'immersion de 0h à 1000h (nous avons aussi testé l'effet de la CEI pour ces gonflements).

- Gonflement dans l'eau vapeur à 80ºC pour des temps de 1h à 1000h.

- Gonflement dans un milieu oxydant pour des concentrations comprises entre 0,01%wt et 1%wt en poids d'eau oxygéné à 80ºC pour des temps de 0h à 96h.

Nous avons montré que ces traitements hydrothermiques induisent des évolutions morphologiques significatives. La température de gonflement sur les membranes sPEEK a un fort impact sur la morphologie de la membrane. En effet, nous observons trois pics simultanés dans les spectres de diffusion SAXS.

- Le pic aux grands angles, associés à la distance moyenne de séparation entre les groupes d'acide sulfonique greffés sur le squelette du polymère.

- Deux autres pics aux petits angles attribués au pic ionomère et au pic matrice simultanément.

L'attribution de ces pics a été confirmée par une étude sur l'impact du contraste de densité d'électrons et l'impact de la CEI sur les positions et les intensités des pics. Nous avons aussi comparé nos résultats avec les données structurelles de la membrane de référence Nafion®.

Nous observons que l'immersion dans l'eau d'une membrane sPEEK à des températures élevées permet d'obtenir une mobilité moléculaire suffisante qui induit des modifications structurelles. Ce traitement dans l'eau liquide procure une bonne séparation de phases entre les phases hydrophiles et hydrophobes.

Nous avons également étudié l'impact du temps sur la nanostructure et les propriétés fonctionnelles de la membrane pour des températures d'immersion différentes. Les résultats obtenus sont reportés en la *Fig.2*

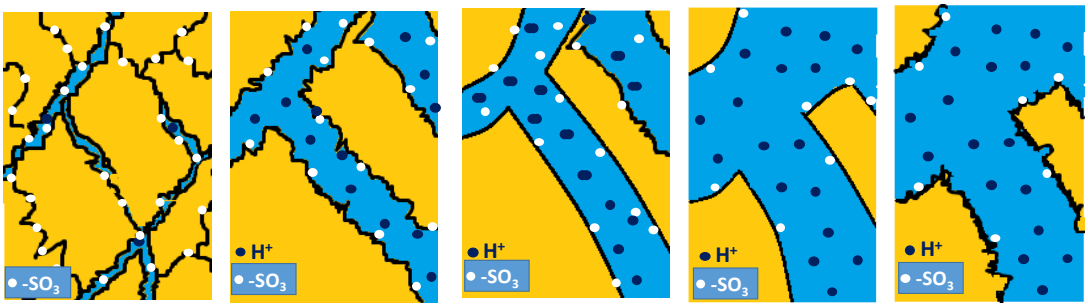

1) Pristine membrane | 2) T= 60ºC | 3) T=80ºC for10h | 4) T=80ºC for 1000h | 5) T=80ºC for 1000h rev

Fig. 2 *Représentation schématique de l'évolution de la nanostructuration au cours du traitement hydrothermique.*

Les résultats obtenus nous permettent de définir la nanostructuration d'une membrane sPEEK. Cette nanostructuration s'est produite par étapes:

La première étape (1) consiste à faire pénétrer de l'eau dans les agrégats de polymère par la réalisation un traitement hygrothermique (jusqu'à 70ºC). Puis la propagation de l'eau dans la membrane est mise en évidence dans les étapes suivantes (2) et (3). La position du pic ionomère à 80°C pendant 10h de traitement correspond à celle mesurée à 70°C pour temps entre 10h et 1000h, donc la distance moyenne de séparation des domaines ioniques reste équitable. Pourtant, nous observons une nette évolution de l'interface entre les domaines hydrophiles et hydrophobes, de plutôt rugueuse à 60ºC à plus nette à 80ºC.

Le gonflement de la membrane est observé dans une quatrième étape. Le spectre SAXS montre un parfaite séparation de phase est atteinte apres une traitement à 80ºC. Ce traitement hydrothermique conduit a un gonflement continu de la membrane donc à un décalage du pic ionomère vers les petits angles.

Comme dernière observation nous avons vérifié la réversibilité des modifications structurelles qui ont lieu pendant le traitement hygrothermique. Ces modifications deviennent réversibles lorsque les membranes passent par l'état sec.

Ces modifications morphologiques conduisent à une évolution significative des propriétés fonctionnelles de la membrane. La conductivité protonique est principalement impactée par la qualité de la séparation de phases à l'échelle nanométrique. Puis un bon suivi des modifications structurelles produites pendant un traitement hydrothermique semble être obligatoire afin d'optimiser les propriétés fonctionnelles des membranes sPEEK.

Cette nanostructuration de la membrane peut également être induite par une oxydation ménagée par H_2O_2. Si ce traitement s'avère plus rapide et efficace qu'un traitement hydrothermique, il est à proscrire pour ne pas impacter la résistance chimique de la membrane.

Ce traitement est choisi en tant qu'étape préliminaire permettant d'obtenir une membrane nanostructurée comme membrane hôte pour un réseau sol-gel réactif.

CHAPITRE III: Élaboration des membranes hybrides

Ce chapitre est dédié à l'explication détaillée de l'élaboration des membranes hybrides par un procédé sol-gel dans une membrane ionomère hôte. Nous avons développé des membranes hybrides par imprégnation d´une phase sol-gel. Nous allons présenter l'effet des paramètres expérimentaux de mis en œuvre et conclure sur les conditions requises pour préparer une membrane hybride optimisée.

Notre principal objectif est de développer de nouvelles membranes hybrides comprenant une matrice d'ionomère commerciale dans lesquelles nous allons introduire des précurseurs capables de former une phase sol-gel chimiquement et physiquement active. Le contrôle chimique de cette phase sol-gel, sa morphologie et son emplacement dans la membrane, pourront nous permettre d'améliorer les propriétés de la membrane sPEEK, ce qui est indispensable pour envisager le développement de ces membranes pour piles à combustible comme substitutif de la membrane Nafion® de référence. Il est à noter que la méthode d'imprégnation permet la formation de la phase sol-gel dans une membrane hôte nanostructurée sans, théoriquement, modifier la nanostructuration initial de la membrane ionomère hôte.

Nous commençons par préparer une membrane hôte nanostructurée, en partant des connaissances acquises au *chapitre I*, avec une nanoséparation de phases bien définie entre les domaines hydrophiles et hydrophobes, puis nous imprégnerons les domaines ioniques avec des précurseurs sol-gel qui donneront une phase inorganique sol-gel après condensation.

Cette phase inorganique qui par autocondensation conduisent a la formation d'une phase sol-gel qui actera comme:

- Renforcement mécanique, comme réseau interpénétré.
- Stabilisant chimique, les fonctions soufrées introduites au cœur de la membrane inhibant toute dégradation oxydante de la membrane ionomère hôte. L'oxydation progressive de ces fonction soufrées peut conduire à la formation des groupes sulfoniques supplémentaires et donc à une amélioration de la conductivité protonique de la membrane.

Le choix de précurseur, dans le cas de notre étude, est le paramètre le plus important pour obtenir des membranes hybrides avec une meilleure performance à long terme.

Le précurseur est composé par un groupe organofonctionnel et au moins un groupe hydrolysable.

$$(RO)_{4-n}Si\ X_n$$

Fig. 3 *Précurseur sol-gel avec des groupes hydrolysables OR et un groupe organofonctionnel réactif X*.

- Un groupe organofonctionnel réactif (X). Il doit protéger de toute oxydation la membrane ionomère hôte et doit donc être très réactifs vis-à-vis des radicaux formés.

- Des groupes hydrolysables (RO), pour permettre la formation d'une structure sol-gel 2D ou 3D et ainsi améliorer les propriétés mécaniques et la rétention d'eau de la membrane ionomère hôte.

Le procédé de fabrication est représenté schématiquement *Fig.4*. La membrane sPEEK hôte doit présenter une séparation nanophase bien définie qui assure de bonnes propriétés fonctionnelles pour obtenir une membrane hybride performante sachant que toute nanostructuration post mise en forme est à priori impossible. Nous la matrice de polymère en jaune *Fig.4* et en l'eau dans les domaines ioniques. Les points verts représentent les unités macromoléculaires acides présentes le long du squelette de la matrice de polymère, situées à l'interface hydrophobe/hydrophile (des groupes SO_3H de la membrane sPEEK). La phase sol-gel est symbolisée comme une ligne noire à l'intérieur des domaines ioniques de la membrane hôte, représentés avec leurs groupes fonctionnels tels que les points du réseau. La phase sol-gel doit permettre une amélioration de:

- La stabilité chimique de la membrane ionomère hôte est assurée par les groupes sacrificiels apportés par la phase sol-gel.

- La résistance mécanique de la membrane limitant les changements dimensionnels, résultant en une meilleure intégrité mécanique et garantissant ainsi une meilleure intégrité de la membrane.

- La conductivité protonique de la membrane hybride par l'augmentation du nombre de groupe SO_3H suite à l'oxydation des groupes fonctionnels.

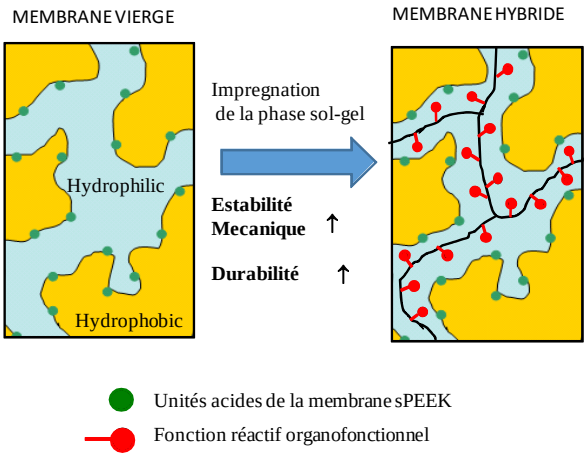

Fig. 4 *Représentation schématique du principe de stabilisation des membranes sPEEK , la matrice polymère en jaune.*

Le protocole d'élaboration des membranes hybrides est résumé dans le schéma de la *Fig.5*.

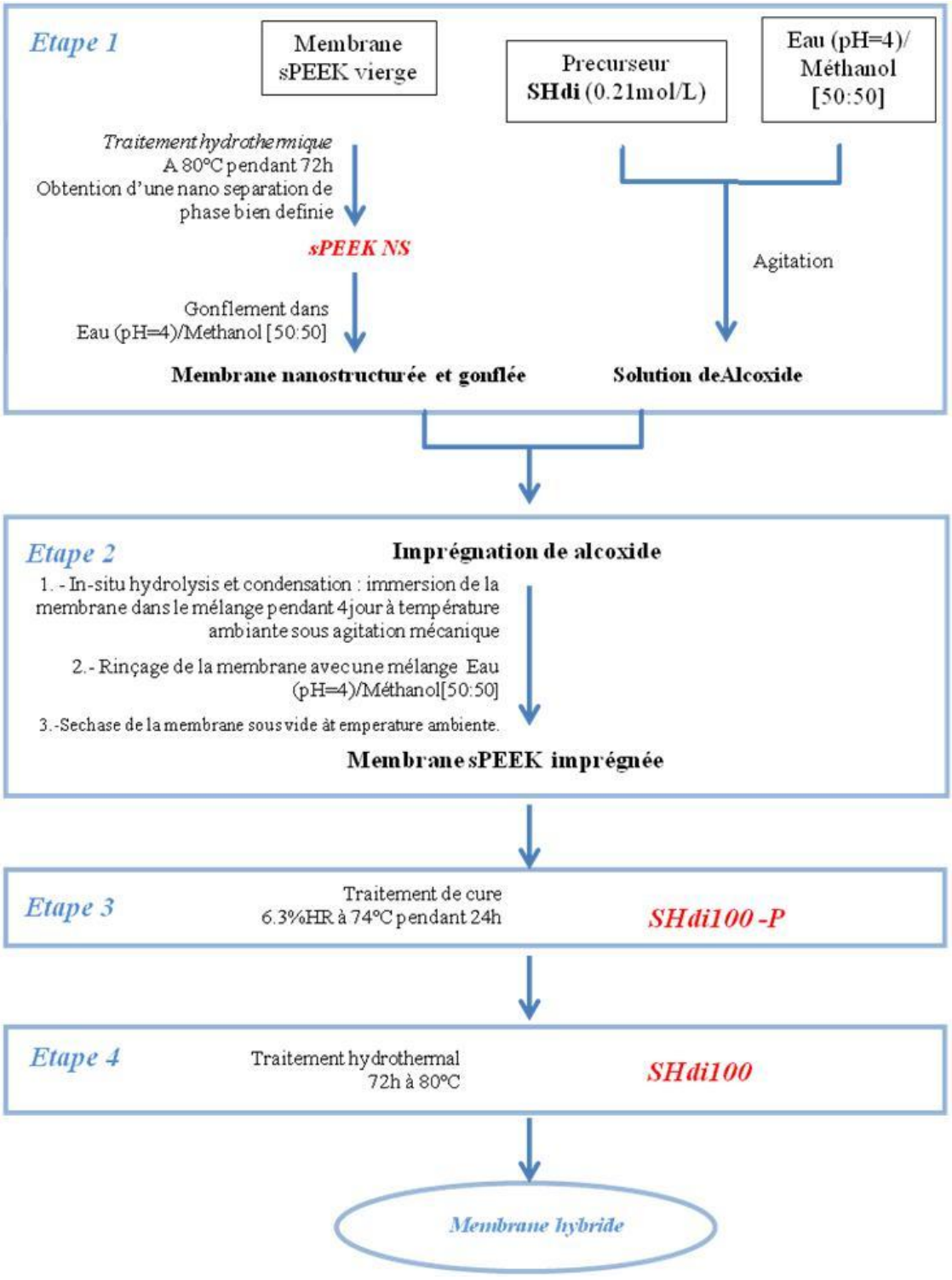

Fig. 4 *Protocole d'élaboration des membranes hybrides*

Il comprend quatre étapes:

1.- La préparation de la membrane ionomère hôte: nanostructuration par un traitement hydrothermique de 72h à 80ºC suivi d'un échange de solvant (eau à eau/méthanol)

2.- Imprégnation/ Condensation du précurseur sol-gel dans la membrane hôte. Puis après 4 jours d'imprégnation, rinçage de la membrane afin d'éviter le dépôt d'une couche de sol-gel en surface de la membrane.

3.- Un traitement thermique de fin de condensation.

4.- Un traitement hydrothermique permettant un gonflement optimal des canaux ioniques.

CHAPITRE IV: Caractérisation des membranes hybrides.

Les précurseurs sol-gel **SHdi** ont été choisi pour produire la première génération de membranes hybrides. Sur la base du protocole établi, sep autres formulation on été préparées par association de ce précurseur sol-gel avec deux autres précurseurs porteurs respectivement d'une fonction thiol et de trois groupes hydrolysables pou le premier (dénommé **SHtri**) et de deux atomes de Si relies par un pont tétrasulfure et six fonction hydrolysables pour le second (dénommé **TS**). Cette association de précurseurs sol-gel permet de contrôler la densité de réticulation de la phase sol-gel formée et sa réactivité chimiques (formulation SH ou SH/TS). On observe qu'une augmentation de la densité de réticulation de la membrane hybride (fraction molaire SHtri ou TS élevé) se traduit par une augmentation de sa fragilité jusqu'à devenir non manipulable.

On peut toutefois supposer qu'une diminution significative du taux de phase sol-gel permettrait de conserver une certaine ductilité et ce même pour les taux de réticulation élevé. En effet, une diminution significative du taux e phase sol-gel est envisageable sachant que traditionnellement les stabilisants chimiques ne représentent que quelques pour-cent de la composition finale d'un matériau polymère durable dans des environnements dégradants.

Conclusions générales et perspectives

La pile à combustible est une solution d'avenir pour produire de l'électricité propre. Cependant des problèmes technologiques limitent pour le moment un déploiement à grande échelle. C'est au cœur de la pile et plus particulièrement de la membrane conductrice ionique séparant l'anode et la cathode que certaines difficultés se posent. Nous pouvons ainsi citer l'impossibilité d'améliorer l'efficacité du catalyseur et le rendement du dispositif en augmentant simplement la température de fonctionnement (100-120°C). En effet, la membrane de référence (Nafion®) perd ses propriétés thermomécaniques au-delà de 80°C, alors que les membranes alternatives apportant une stabilisation chimique et mécanique de la matrice ionomère hôte. C'est le contrôle de la chimie de ce réseau, de sa morphologie et de sa localisation dans la membrane hôte qui permettra l'amélioration des propriétés de la membrane hybride ainsi obtenue.

Le but de ce projet de recherche est de surmonter les obstacles qui limitent l'utilisation de ce dispositif. La conception d'une nouvelle classe de membranes hybrides à partir de membranes

hydrocarbonées est un défi clair, car les performances des matériaux non-perfluorés restent toujours beaucoup plus faibles que celles du PFSA qui est une référence (en termes de stabilité chimique et de conductivité). La membrane sPEEK a été choisie car elle possède d'excellentes propriétés thermiques, même si elle présente une durée de vie très limitée et une grande sensibilité à la dégradation chimique. Notre idée principale était de transformer une membrane commerciale de faible coût peu performantes en pile en une véritable membrane alternative à la membrane de référence Nafion®.

L'objectif de l'étude était d'obtenir des membranes durables assurant un fonctionnement optimal de la pile grâce à une conductivité protonique élevée. Notre stratégie a consiste à créer dans une membrane ionomère hôte une phase sol-gel porteuse de sites sacrificiels capables d'inhiber toute dégradation oxydante de la phase polymère (oxydation induite par l'eau oxygéné formée en pile) mais aussi d'obtenir une membrane hybride aux propriétés thermomécaniques ajustables en fonction du taux de réticulation de la phase sol-gel.

Une première phase a été de définir les conditions optimales de mise en forme des membranes par imprégnation dans une membrane hôte sPEEK. Les domaines ioniques d'une membrane de sPEEK vierge sont plus étroits et moins définis que ceux de la membrane référence Nafion®. Ainsi la première étape de notre travail a consisté à trouver un processus qui nous permet d'optimiser la nanostructuration de la membrane sPEEK hôte avant imprégnation. Des expériences SAXS étendues ont permis une nouvelle attribution des pics de corrélation caractéristiques de la structure chimique et de la morphologie de la membrane et les évolutions morphologiques induites dans la membrane par des traitements thermiques appliquées. Nous avons démontré que la qualité de la séparation hydrophile/hydrophobe de nanophases peut être contrôlée en ajustant les conditions de traitement hydrothermique (température, et durée). En appliquant un tel traitement nous avons réussi à améliorer la conductivité protonique d'une membrane sPEEK vierge de 24 à 84 mS/cm pour devenir du même ordre de grandeur que celle de la membrane de référence Nafion®.

La deuxième réalisation de ce travail concernait la préparation de membranes hybrides à partir de *sPEEK nanostructurées* par imprégnation de précurseurs sol-gel. Nous avons établi un protocole qui permet la fabrication reproductible de membranes hybrides réactives (phase sol-gel porteuse de sites sacrificiels SH et S-S-S-S) et aux propriétés thermomécaniques ajustables en fonction de la densité de réticulation de la phase sol-gel.

Malgré un taux de phase sol-gel particulièrement élevé (plus de 50%), les membranes hybrides obtenues conservent une conductivité protonique comprise entre 20 et 60 mS/cm. La phase sol-gel est distribuée de manière homogène dans toute l'épaisseur des membranes sauf pour la composition la plus riche en précurseur sol-gel. Les analyses DMA confirment le renforcement mécanique de la phase sPEEK (pas de fluage de la membrane au delà de la température de transition vitreuse de la phase sPEEK). Le test en pile réalisé avec une membrane sPEEK et une membrane SHdi100 (formulation la plus prometteuse au regarde des tests préliminaires réalisés) s'est avéré riche d'enseignements et à commencer par le côte fonctionnel de cette membrane en pile. Certes les performances du dispositif ont été moindres que celles espérées une optimisation de l'assemblage membrane/électrodes étant nécessaire mas aussi probablement en raison d'un taux de

phase sol-gel beaucoup trop élevé (57%) limitant les propriétés de conduction de la membrane. Par ailleurs, cet excès de phase sol-gel se traduit par une augmentation de la porosité de la membrane pouvant impacter le comportement à long terme du dispositif (formation de H_2O_2 par diffusion de H_2)

Un point essentiel sera donc de contrôler précisément le taux de phase sol-gel des membranes préparés. Deux stratégies sont envisagées:

- Réduire la concentration en précurseurs sol-gel du milieu d'imprégnation.

- Réduire le gonflement de la membrane dans le milieux d'imprégnation et ainsi le taux de phase sol-gel admissible.

Pour résumer, cette étude a permis d’atteindre une étape dans la synthèse de nouvelles membranes hybrides avec de structures chimiques et de morphologies contrôlées particulièrement prometteuses pour atteindre les températures de fonctionnement et durées de vie souhaitées pour les application "transport" de la pile à combustible.

LIST OF TABLES

LIST OF FIGURES

REFERENCES

1. Kim, J.W., et al., *1 - Key challenges in the development of an infrastructure for hydrogen production, delivery, storage and use*, in *Advances in Hydrogen Production, Storage and Distribution*, A. Basile and A. Iulianelli, Editors. 2014, Woodhead Publishing. p. 3-31.
2. http://energy.gov/eere/fuelcells/hydrogen-production. 10/09/2015.
3. http://www.fuelcelltoday.com/technologies/pemfc.
4. http://www.afdc.energy.gov/fuels/hydrogen_production.html.
5. Wang, Y., et al., *A review of polymer electrolyte membrane fuel cells: technology, applications, and needs on fundamental research.* Applied Energy, 2011. **88**(4): p. 981-1007.
6. Onovwiona, H.I. and V.I. Ugursal, *Residential cogeneration systems: review of the current technology*. Renewable and Sustainable Energy Reviews, 2006. **10**(5): p. 389-431.
7. http://www.netinform.net/H2/H2Mobility/Detail.aspx?ID=431.
8. Smitha, B., S. Sridhar, and A. Khan, *Solid polymer electrolyte membranes for fuel cell applications—a review.* Journal of membrane science, 2005. **259**(1): p. 10-26.
9. Kreuer, K.-D., *Ion Conducting Membranes for Fuel Cells and other Electrochemical Devices.* Chemistry of Materials, 2013. **26**(1): p. 361-380.
10. Gierke, T.D., G.E. Munn, and F.C. Wilson, *The Morphology in Nafion Perfluorinated Membrane Products, as Determined by Wide-Angle and Small-Angle X-Ray Studies.* Journal of Polymer Science Part B-Polymer Physics, 1981. **19**(11): p. 1687-1704.
11. Schmidt-Rohr, K. and Q. Chen, *Parallel cylindrical water nanochannels in Nafion fuel-cell membranes.* Nat Mater, 2008. **7**(1): p. 75-83.
12. Rubatat, L., et al., *Evidence of elongated polymeric aggregates in Nafion.* Macromolecules, 2002. **35**(10): p. 4050-4055.
13. van der Heijden, P.C., L. Rubatat, and O. Diat, *Orientation of drawn Nafion at molecular and mesoscopic scales.* Macromolecules, 2004. **37**(14): p. 5327-5336.
14. Bauer, F., S. Denneler, and M. Willert-Porada, *Influence of temperature and humidity on the mechanical properties of Nafion® 117 polymer electrolyte membrane.* Journal of Polymer Science Part B: Polymer Physics, 2005. **43**(7): p. 786-795.
15. Yeo, S.C. and A. Eisenberg, *Physical properties and supermolecular structure of perfluorinated ion-containing (Nafion) polymers.* Journal of applied polymer science, 1977. **21**(4): p. 875-898.
16. Tang, Y., et al., *An experimental investigation of humidity and temperature effects on the mechanical properties of perfluorosulfonic acid membrane.* Materials Science and Engineering: A, 2006. **425**(1–2): p. 297-304.
17. Alberti, G., et al., *Polymeric proton conducting membranes for medium temperature fuel cells (110–160°C).* Journal of Membrane Science, 2001. **185**(1): p. 73-81.
18. de Almeida, S.H. and Y. Kawano, *Thermal Behavior of Nafion Membranes.* Journal of Thermal Analysis and Calorimetry, 1999. **58**(3): p. 569-577.
19. Collette, F.M., et al., *Structure and transport properties of solution-cast Nafion® membranes subjected to hygrothermal aging.* Journal of Membrane Science, 2013. **435**(0): p. 242-252.

20. Gebel, G., *Structural evolution of water swollen perfluorosulfonated ionomers from dry membrane to solution.* Polymer, 2000. **41**(15): p. 5829-5838.
21. Kreuer, K.D., *On the development of proton conducting polymer membranes for hydrogen and methanol fuel cells.* Journal of Membrane Science, 2001. **185**(1): p. 29-39.
22. Lakshmanan, B., et al., *Polyetheretherketone membranes for elevated temperature PEMFCs.* Electrochemical and solid-state letters, 2003. **6**(12): p. A282-A285.
23. Roziere, J., *Development of non-perfluorinated polymer membranes for PEM fuel cells.* New Materials for Electrochemical Systems IV. Extended Abstracts of the Fourth International Symposium on New Materials for Electrochemical Systems, 2001: p. 355-355.
24. Maier, G. and J. Meier-Haack, *Sulfonated aromatic polymers for fuel cell membranes*, in *Fuel cells II*. 2008, Springer. p. 1-62.
25. Xing, P., et al., *Synthesis and characterization of sulfonated poly(ether ether ketone) for proton exchange membranes.* Journal of Membrane Science, 2004. **229**(1–2): p. 95-106.
26. Jouanneau, J., et al., *Synthesis and characterization of ionic conducting sulfonated polybenzimidazoles.* Journal of Polymer Science Part A: Polymer Chemistry, 2010. **48**(8): p. 1732-1742.
27. Villa, D., et al., *New Sulfonated PBIs for PEMFC Application.* Fuel Cells, 2013. **13**(1): p. 98-103.
28. Mader, J.A. and B.C. Benicewicz, *Sulfonated polybenzimidazoles for high temperature PEM fuel cells.* Macromolecules, 2010. **43**(16): p. 6706-6715.
29. Pan, H., et al., *Preparation and properties of the cross-linked sulfonated polyimide containing benzimidazole as electrolyte membranes in fuel cells.* Journal of Membrane Science, 2015. **476**: p. 87-94.
30. Akbarian-Feizi, L., S. Mehdipour-Ataei, and H. Yeganeh, *Investigation on the preparation of new sulfonated polyimide fuel cell membranes in organic and ionic liquid media.* International Journal of Polymeric Materials and Polymeric Biomaterials, 2014. **63**(3): p. 149-160.
31. Gong, F., N. Li, and S. Zhang, *Synthesis and properties of novel sulfonated poly (phenylquinoxaline) s as proton exchange membranes.* Polymer, 2009. **50**(25): p. 6001-6008.
32. Zhang, Z., L. Wu, and T. Xu, *Synthesis and properties of side-chain-type sulfonated poly (phenylene oxide) for proton exchange membranes.* Journal of Membrane Science, 2011. **373**(1): p. 160-166.
33. Sauk, J., J. Byun, and H. Kim, *Composite Nafion/polyphenylene oxide (PPO) membranes with phosphomolybdic acid (PMA) for direct methanol fuel cells.* Journal of power sources, 2005. **143**(1): p. 136-141.
34. Yang, T. and P. Shi, *Study on the mesocarbon microbeads/polyphenylene sulfide composite bipolar plates applied for proton exchange membrane fuel cells.* Journal of Power Sources, 2008. **175**(1): p. 390-396.
35. Kreuer, K.D., et al., *Short-side-chain proton conducting perfluorosulfonic acid ionomers: Why they perform better in PEM fuel cells.* Journal of Power Sources, 2008. **178**(2): p. 499-509.
36. Prado, L.A.S.D., et al., *Anomalous small-angle X-ray scattering characterization of composites based on sulfonated poly(ether ether ketone), zirconium phosphates, and zirconium oxide.* Journal of Polymer Science Part B-Polymer Physics, 2004. **42**(3): p. 567-575.

37. Min, S. and D. Kim, *SAXS cluster structure and properties of sPEEK/PEI composite membranes for DMFC applications.* Solid State Ionics, 2010. **180**(40): p. 1690-1693.
38. Yang, B. and A. Manthiram, *Comparison of the small angle X-ray scattering study of sulfonated poly (etheretherketone) and Nafion membranes for direct methanol fuel cells.* Journal of Power Sources, 2006. **153**(1): p. 29-35.
39. Kawaguti, C.A., K. Dahmouche, and A.d.S. Gomes, *Nanostructure and properties of proton-conducting sulfonated poly(ether ether ketone) (SPEEK) and zirconia–SPEEK hybrid membranes for direct alcohol fuel cells: effect of the nature of swelling solvent and incorporation of heteropolyacid.* Polymer International, 2012. **61**(1): p. 82-92.
40. Gebel, G., *Structure of Membranes for Fuel Cells: SANS and SAXS Analyses of Sulfonated PEEK Membranes and Solutions.* Macromolecules, 2013. **46**(15): p. 6057-6066.
41. Portale, G., et al., *Microstructure, state of water and proton conductivity of sulfonated poly(ether ether ketone).* Solid State Ionics, 2013. **252**(0): p. 62-67.
42. Reyna-Valencia, A., S. Kaliaguine, and M. Bousmina, *Tensile mechanical properties of sulfonated poly(ether ether ketone) (SPEEK) and BPO4/SPEEK membranes.* Journal of Applied Polymer Science, 2005. **98**(6): p. 2380-2393.
43. Zaidi, S.M.J., et al., *Proton conducting composite membranes from polyether ether ketone and heteropolyacids for fuel cell applications.* Journal of Membrane Science, 2000. **173**(1): p. 17-34.
44. Kim, Y.S., et al., *Processing induced morphological development in hydrated sulfonated poly (arylene ether sulfone) copolymer membranes.* Polymer, 2003. **44**(19): p. 5729-5736.
45. Zaidi, S.J., *Preparation and characterization of composite membranes using blends of SPEEK/PBI with boron phosphate.* Electrochimica Acta, 2005. **50**(24): p. 4771-4777.
46. Antonucci, P.L., et al., *Investigation of a direct methanol fuel cell based on a composite Nafion®-silica electrolyte for high temperature operation.* Solid State Ionics, 1999. **125**(1–4): p. 431-437.
47. Adjemian, K.T., et al., *Function and characterization of metal oxide-naflon composite membranes for elevated-temperature H-2/O-2 PEM fuel cells.* Chemistry of Materials, 2006. **18**(9): p. 2238-2248.
48. Saccà, A., et al., *Structural and electrochemical investigation on re-cast Nafion membranes for polymer electrolyte fuel cells (PEFCs) application.* Journal of Membrane Science, 2006. **278**(1–2): p. 105-113.
49. Tazi, B. and O. Savadogo, *Parameters of PEM fuel-cells based on new membranes fabricated from Nafion®, silicotungstic acid and thiophene.* Electrochimica Acta, 2000. **45**(25–26): p. 4329-4339.
50. Tazi, B. and O. Savadogo, *Effect of Various Heteropolyacids (HPAs) on the Characteristics of Nafion®-HPAS Membranes and their H~ 2/O~ 2 Polymer Electrolyte Fuel Cell Parameters.* Journal of New Materials for Electrochemical Systems, 2001. **4**(3): p. 187-196.
51. Ramani, V., et al., *Membranes and MEAs based on sulfonated poly (ether ketone ketone) and heteropolyacids for polymer electrolyte fuel cells.* Journal of The Electrochemical Society, 2008. **155**(6): p. B532-B537.
52. Alberti, G., et al., *Preparation and proton conductivity of composite ionomeric membranes obtained from gels of amorphous zirconium phosphate*

sulfophenylenphosphonates in organic solvents. Journal of Materials Chemistry, 2004. **14**(12): p. 1910-1914.
53. Bauer, F. and M. Willert-Porada, *Microstructural characterization of Zr-phosphate-Nafion((R)) membranes for direct methanol fuel cell (DMFC) applications.* Journal of Membrane Science, 2004. **233**(1-2): p. 141-149.
54. Kickelbick, G., *Concepts for the incorporation of inorganic building blocks into organic polymers on a nanoscale.* Progress in polymer science, 2003. **28**(1): p. 83-114.
55. Bahar, B., et al., *Ultra-thin integral composite membrane*, 1996, Google Patents.
56. Tian, H. and O. Savadogo, *Silicotungstic Acid Nafion Composite membrane for proton-exchange membrane fuel cell operation at high temperature.* Journal of New Materials for Electrochemical Systems, 2006. **9**(1): p. 61.
57. Staiti, P., et al., *Hybrid Nafion–silica membranes doped with heteropolyacids for application in direct methanol fuel cells.* Solid State Ionics, 2001. **145**(1): p. 101-107.
58. Mauritz, K.A., *Organic-inorganic hybrid materials: perfluorinated ionomers as sol-gel polymerization templates for inorganic alkoxides.* Materials Science & Engineering C-Biomimetic and Supramolecular Systems, 1998. **6**(2-3): p. 121-133.
59. Vaia, R.A., H. Ishii, and E.P. Giannelis, *Synthesis and properties of two-dimensional nanostructures by direct intercalation of polymer melts in layered silicates.* Chemistry of Materials, 1993. **5**(12): p. 1694-1696.
60. Thiam, H.S., et al., *Performance of direct methanol fuel cell with a palladium–silica nanofibre/Nafion composite membrane.* Energy Conversion and Management, 2013. **75**(0): p. 718-726.
61. Thiam, H.S., et al., *Nafion/Pd–SiO2 nanofiber composite membranes for direct methanol fuel cell applications.* International Journal of Hydrogen Energy, 2013. **38**(22): p. 9474-9483.
62. Kim, J.-H., et al., *Composite proton conducting membranes based on Nafion and sulfonated SiO2 nanoparticles.* Journal of Membrane Science, 2012. **415–416**(0): p. 696-701.
63. Chujo, Y. and T. Saegusa, *Organic polymer hybrids with silica gel formed by means of the sol-gel method*, in *Macromolecules: Synthesis, Order and Advanced Properties*. 1992, Springer Berlin Heidelberg. p. 11-29.
64. Saegusa, T. and Y. Chujo, *Macromolecular engineering on the basis of the polymerization of 2-oxazolines.* Makromolekulare Chemie. Macromolecular Symposia, 1991. **51**(1): p. 1-10.
65. Tamaki, R. and Y. Chujo, *Synthesis of poly (vinyl alcohol)/silica gel polymer hybrids by in-situ hydrolysis method.* 1998.
66. Landry, C.J.T., et al., *In situ polymerization of tetraethoxysilane in polymers: chemical nature of the interactions.* Polymer, 1992. **33**(7): p. 1496-1506.
67. Sarkar, S., et al., *Polymer-supported metals and metal oxide nanoparticles: synthesis, characterization, and applications.* Journal of Nanoparticle Research, 2012. **14**(2): p. 1-24.
68. Ke, C.-C., et al., *Preparation and properties of Nafion/SiO2 composite membrane derived via in situ sol–gel reaction: size controlling and size effects of SiO2 nano-particles.* Polymers for Advanced Technologies, 2012. **23**(1): p. 92-98.
69. Jones, K., J. Boulton, and H. Emblem. *Solvent Selection and the Control of Sol-Gel Reactions*. in *MRS Proceedings*. 1990. Cambridge Univ Press.
70. Liu, Q., et al., *Novel ABPBI/POSS Composite Membranes for High Temperature PEMFC Applications.* ECS Transactions, 2011. **30**(1): p. 25-32.

71. IUPAC. Compendium of Chemical Terminology, n.e.t.G.B.C.b.A.D.M.a.A.W.B.S.P., Oxford (1997). XML on-line corrected version: http://goldbook.iupac.org (2006-) created by M. Nic, J. Jirat, B. Kosata; updates compiled by A. Jenkins. ISBN 0-9678550-9-8. doi:10.1351/goldbook.
72. Klempner, D., L.H. Sperling, and L.A. Utracki, *Interpenetrating polymer networks*, 1994, American Chemical Society, Washington, DC (United States).
73. Brinker, C.J., *Hydrolysis and condensation of silicates: Effects on structure.* Journal of Non-Crystalline Solids, 1988. **100**(1–3): p. 31-50.
74. Joseph, J., C.-Y. Tseng, and B.-J. Hwang, *Phosphonic acid-grafted mesostructured silica/Nafion hybrid membranes for fuel cell applications.* Journal of Power Sources, 2011. **196**(18): p. 7363-7371.
75. Lavorgna, M., et al., *Hybridization of Nafion membranes by the infusion of functionalized siloxane precursors.* Journal of Membrane Science, 2007. **294**(1-2): p. 159-168.
76. Hajji, P., et al. *Synthesis-morphology-mechanical properties relationships of polymer-silica nanocomposite hybrid materials*. in *MRS Proceedings*. 1999. Cambridge Univ Press.
77. Jackson, C., et al., *Synthesis of hybrid organic-inorganic materials from interpenetrating polymer network chemistry.* Chemistry of materials, 1996. **8**(3): p. 727-733.
78. Chujo, Y., et al., *Synthesis of triethoxysilyl-terminated polyoxazolines and their cohydrolysis polymerization with tetraethoxysilane.* Macromolecules, 1993. **26**(21): p. 5681-5686.
79. Herring, A.M., *Inorganic–Polymer Composite Membranes for Proton Exchange Membrane Fuel Cells.* Journal of Macromolecular Science, Part C, 2006. **46**(3): p. 245-296.
80. Asensio, J.A., E.M. Sánchez, and P. Gómez-Romero, *Proton-conducting membranes based on benzimidazole polymers for high-temperature PEM fuel cells. A chemical quest.* Chemical Society Reviews, 2010. **39**(8): p. 3210-3239.
81. Meng, F., et al., *Structural and transport effects of doping perfluorosulfonic acid polymers with the heteropoly acids, H 3 PW 12 O 40 or H 4 SiW 12 O 40.* Electrochimica Acta, 2007. **53**(3): p. 1372-1378.
82. Sahu, A., et al., *A sol-gel modified alternative nafion-silica composite membrane for polymer electrolyte fuel cells.* Journal of The Electrochemical Society, 2007. **154**(2): p. B123-B132.
83. Epping Martin, K. and J. Kopasz, *The US DOEs high temperature membrane effort.* Fuel Cells, 2009. **9**(4): p. 356-362.
84. Horan, J.L., et al., *Fast Proton Conduction Facilitated by Minimum Water in a Series of Divinylsilyl-11-silicotungstic Acid-co-Butyl Acrylate-co-Hexanediol Diacrylate Polymers.* The Journal of Physical Chemistry C, 2013. **118**(1): p. 135-144.
85. Piga, M., *New hybrid inorganic-organic proton conducting membranes for PEMFC: synthesis, properties and conduction mechanisms.* 2012.
86. Yoshizawa, M., W. Xu, and C.A. Angell, *Ionic liquids by proton transfer: Vapor pressure, conductivity, and the relevance of Δp K a from aqueous solutions.* Journal of the American Chemical Society, 2003. **125**(50): p. 15411-15419.
87. Laberty-Robert, C., et al., *Design and properties of functional hybrid organic–inorganic membranes for fuel cells.* Chemical Society Reviews, 2011. **40**(2): p. 961-1005.

88. Thiam, H.S., et al., *Overview on nanostructured membrane in fuel cell applications.* International Journal of Hydrogen Energy, 2011. **36**(4): p. 3187-3205.
89. Borup, R., et al., *Scientific aspects of polymer electrolyte fuel cell durability and degradation.* Chemical reviews, 2007. **107**(10): p. 3904-3951.
90. Maccarini, M., et al., *Submicrometer 3D Structural Evidence of Fuel Cell Membrane Heterogeneous Degradation.* ACS Macro Letters, 2014. **3**(8): p. 778-783.
91. http://fuelcellstore.com/fuel-cell-components/plates/end-plates.
92. Perrot, C., et al., *Aging mechanism of Sulfonated poly(aryl ether ketone) (sPAEK) in an hydroperoxide solution and in fuel cell.* Journal of Power Sources, 2010. **195**(2): p. 493-502.
93. Endoh, E., et al., *Degradation study of MEA for PEMFCs under low humidity conditions.* Electrochemical and Solid-State Letters, 2004. **7**(7): p. A209-A211.
94. Liu, W. and D. Zuckerbrod, *In situ detection of hydrogen peroxide in PEM fuel cells.* Journal of The Electrochemical Society, 2005. **152**(6): p. A1165-A1170.
95. Qiao, J., et al., *Degradation of perfluorinated ionomer membranes for PEM fuel cells during processing with H2O2.* Journal of The Electrochemical Society, 2006. **153**(6): p. A967-A974.
96. Sethuraman, V.A., et al., *Hydrogen peroxide formation rates in a PEMFC anode and cathode effect of humidity and temperature.* Journal of The Electrochemical Society, 2008. **155**(1): p. B50-B57.
97. Panchenko, A., et al., *In-situ spin trap electron paramagnetic resonance study of fuel cell processes.* Physical Chemistry Chemical Physics, 2004. **6**(11): p. 2891-2894.
98. Teranishi, K., et al., *Degradation mechanism of PEMFC under open circuit operation.* Electrochemical and Solid-State Letters, 2006. **9**(10): p. A475-A477.
99. Coms, F.D., H. Liu, and J.E. Owejan, *Mitigation of Perfluorosulfonic Acid Membrane Chemical Degradation Using Cerium and Manganese Ions*, in *Proton Exchange Membrane Fuel Cells 8, Pts 1 and 2*, T. Fuller, et al., Editors. 2008, Electrochemical Society Inc: Pennington. p. 1735-1747.
100. Zweifel, H., *Stabilization of polymeric materials*. 2012: Springer Science & Business Media.
101. Parmar, J. and R. Singh, *Polymeric UV stabilizers for thermoplastics.* Handbook of engineering polymeric materials, Marcel Dekker Inc./CRC Press, New York, 2000.
102. Singh, R., et al., *Photodegradation and stabilization of styrene–butadiene–styrene rubber.* Journal of applied polymer science, 2000. **75**(9): p. 1103-1114.
103. Thanki, P. and R. Singh, *Progress in the area of degradation and stabilization of nylon 66.* 1998.
104. Allara, D. and M. Chan, *Mechanisms of inhibition against the copper-catalyzed oxidation of polyethylene: Structures and catalytic reactivities of copper–inhibitor complexes.* Journal of Polymer Science: Polymer Chemistry Edition, 1976. **14**(8): p. 1857-1876.
105. Smith, T.L., et al., *The mechanism of action of sugar acetals as nucleating agents for polypropylene.* Macromolecules, 1994. **27**(12): p. 3147-3155.
106. Mikhailenko, S.D., F. Celso, and S. Kaliaguine, *Properties of SPEEK based membranes modified with a free radical scavenger.* Journal of Membrane Science, 2009. **345**(1â€“2): p. 315-322.
107. Mikhailenko, S.D., F. Celso, and S. Kaliaguine, *Properties of SPEEK based membranes modified with a free radical scavenger.* Journal of Membrane Science, 2009. **345**(1): p. 315-322.

108. Zhao, X., et al., *Polymer-supported nanocomposites for environmental application: a review.* Chemical Engineering Journal, 2011. **170**(2): p. 381-394.
109. Zhang, W., et al., *Pre-Stretched Low Equivalent Weight PFSA Membranes with Improved Fuel Cell Performance.* Journal of The Electrochemical Society, 2014. **161**(6): p. F770-F777.
110. de Lange, R.S.A., et al., *Polymeric-silica-based sols for membrane modification applications: sol-gel synthesis and characterization with SAXS.* Journal of Non-Crystalline Solids, 1995. **191**(1–2): p. 1-16.
111. Schmidt, H.K., et al., *The sol-gel process for nano-technologies: new nanocomposites with interesting optical and mechanical properties.* Journal of sol-gel science and technology, 1998. **13**(1-3): p. 397-404.
112. Habsuda, J., et al., *Sol–gel derived composites from poly(silicic acid) and 2-hydroxyethylmethacrylate: thermal, physical and morphological properties.* Polymer, 2002. **43**(17): p. 4627-4638.
113. Zhang, G.W., et al., *Proton conducting composite membranes from sulfonated polyether ether ketone and SiO2.* Journal of Wuhan University of Technology-Materials Science Edition, 2009. **24**(1): p. 95-99.
114. Jacob, S., C. Poinsignon, and M. Popall, *Inorganic-organic hybrid protonic polymeric materials for fuel cells based on polycondensed and organically cross-linked sulfonyl- and styrene-functionalized alkoxysilanes.* Electrochimica Acta, 2005. **50**(19): p. 4022-4028.
115. Yahya, N., *Carbon and Oxide Nanostructures: Synthesis, Characterisation and Applications*. Vol. 5. 2011: Springer Science & Business Media.
116. Hoffmann, F. and M. Froba, *Vitalising porous inorganic silica networks with organic functions-PMOs and related hybrid materials.* Chemical Society Reviews, 2011. **40**(2): p. 608-620.
117. Schubert, U. and N. Hüsing, *Synthesis of inorganic materials*. 2012: John Wiley & Sons.
118. Sinkó, K., *Influence of chemical conditions on the nanoporous structure of silicate aerogels.* Materials, 2010. **3**(1): p. 704-740.
119. Baradie, B., J.P. Dodelet, and D. Guay, *Hybrid Nafion (R)-inorganic membrane with potential applications for polymer electrolyte fuel cells.* Journal of Electroanalytical Chemistry, 2000. **489**(1-2): p. 101-105.
120. Mauritz, K.A. and R.B. Moore, *State of understanding of Nafion.* Chemical reviews, 2004. **104**(10): p. 4535-4586.
121. Kreuer, K.D. and G. Portale, *A Critical Revision of the Nano-Morphology of Proton Conducting Ionomers and Polyelectrolytes for Fuel Cell Applications.* Advanced Functional Materials, 2013. **DOI: 10.1002/adfm.201300376**.
122. Wu, D.Q., et al., *Long-Range Inhomogeneities in Sulfonated Polystyrene Ionomers.* Macromolecules, 1989. **22**(2): p. 992-995.
123. Yang, B. and A. Manthiram, *Comparison of the small angle X-ray scattering study of sulfonated poly(etheretherketone) and Nafion membranes for direct methanol fuel cells.* Journal of Power Sources, 2006. **153**(1): p. 29-35.
124. Ding, Y.S., et al., *Anomalous Small-Angle X-Ray-Scattering from a Sulfonated Polystyrene Ionomer.* Macromolecules, 1988. **21**(6): p. 1698-1703.
125. Gebel, G., *Structure of Membranes for Fuel Cells: SANS and SAXS Analyses of Sulfonated PEEK Membranes and Solutions* Macromolecules, 2013. **46**: p. 6057-6066.

126. Fujimura, M., T. Hashimoto, and H. Kawai, *SMALL-ANGLE X-RAY-SCATTERING STUDY OF PERFLUORINATED IONOMER MEMBRANES .1. ORIGIN OF 2 SCATTERING MAXIMA.* Macromolecules, 1981. **14**(5): p. 1309-1315.
127. Blachot, J.F., et al., *Anisotropy of structure and transport properties in sulfonated polyimide membranes.* Journal of Membrane Science, 2003. **214**(1): p. 31-42.
128. Gebel, G. and O. Diat, *Neutron and X-ray Scattering: Suitable Tools for Studying Ionomer Membranes.* Fuel Cells, 2005. **5**(2): p. 261-276.
129. Lafitte, B. and P. Jannasch, *Proton-Conducting Aromatic Polymers Carrying Hypersulfonated Side Chains for Fuel Cell Applications.* Advanced Functional Materials, 2007. **17**(15): p. 2823-2834.
130. Li, X.F., et al., *Fully Aromatic Ionomers with Precisely Sequenced Sulfonated Moieties for Enhanced Proton Conductivity.* Macromolecules, 2012. **45**(3): p. 1447-1459.
131. Rubatat, L., G. Gebel, and O. Diat, *Fibrillar structure of Nafion: Matching Fourier and real space studies of corresponding films and solutions.* Macromolecules, 2004. **37**(20): p. 7772-7783.
132. Genies, C., et al., *Soluble sulfonated naphthalenic polyimides as materials for proton exchange membranes.* Polymer, 2001. **42**(2): p. 359-373.
133. Rollet, A.L., et al., *A SANS determination of the influence of external conditions on the nanostructure of nafion membrane.* Journal of Polymer Science Part B-Polymer Physics, 2001. **39**(5): p. 548-558.
134. Guilleaume, B., et al., *The distribution of counterions around synthetic rod-like polyelectrolytes in solution - A study by small-angle X-ray scattering and by anomalous small-angle X-ray scattering.* European Physical Journal E, 2002. **8**(3): p. 299-309.
135. Huang, R.Y.M., et al., *Sulfonation of poly(ether ether ketone)(PEEK): Kinetic study and characterization.* Journal of Applied Polymer Science, 2001. **82**(11): p. 2651-2660.
136. Allen, H., et al., *Typical interatomic distances: organic compounds. International tables for crystallography*. Vol. C. 2006. 790-811.
137. Gebel, G., P. Aldebert, and M. Pineri, *Structure and Related Properties of Solution-Cast Perfluorosulfonated Ionomer Films.* Macromolecules, 1987. **20**(6): p. 1425-1428.
138. Carbone, A., et al., *Sulphonated poly(ether ether ketone) membranes for fuel cell application: Thermal and structural characterisation.* Journal of Power Sources, 2006. **163**(1): p. 18-26.
139. Kreuer, K.-D., et al., *Transport in proton conductors for fuel-cell applications: simulations, elementary reactions, and phenomenology.* Chemical Reviews, 2004. **104**(10): p. 4637-4678.
140. Perrin, J.C., et al., *Water dynamics in ionomer membranes by field-cycling NMR relaxometry.* Journal of Physical Chemistry B, 2006. **110**(11): p. 5439-5444.
141. Alberti, G., R. Narducci, and M. Sganappa, *Effects of hydrothermal/thermal treatments on the water-uptake of Nafion membranes and relations with changes of conformation, counter-elastic force and tensile modulus of the matrix.* Journal of Power Sources, 2008. **178**(2): p. 575-583.
142. COLLETTE, F., *Vieillissement hygrothermique du nafion®*, in Laboratoire d'Ingénierie des Matériaux ENSAM, CER de Paris2008, L'École Nationale Supérieure d'Arts et Métiers.
143. Marestin, C., et al., *Sulfonated Polyimides*, in *Fuel Cells Ii*, G.G. Scherer, Editor. 2008, Springer-Verlag Berlin: Berlin. p. 185-258.

144. Fumagalli, M., et al., *Fast Water Diffusion and Long-Term Polymer Reorganization during Nafion Membrane Hydration Evidenced by Time-Resolved Small-Angle Neutron Scattering.* The Journal of Physical Chemistry B, 2015. **119**(23): p. 7068-7076.
145. LEGRAND, P., *Influence des conditions de fonctionnement de la pile à combustible sur les performances du dispositif et la durabilité de la membrane*, in *Laboratoire Structure et Propriétés d'Architectures Moléculaires / Polymères Conducteurs Ioniques*2012, DOCTEUR DE L'UNIVERSITÉ DE GRENOBLE.
146. Hubner, G. and E. Roduner, *EPR investigation of HO/ radical initiated degradation reactions of sulfonated aromatics as model compounds for fuel cell proton conducting membranes.* Journal of Materials Chemistry, 1999. **9**(2): p. 409-418.
147. Büchi, F.N., et al., *Performance of Differently Cross-Linked, Partially Fluorinated Proton Exchange Membranes in Polymer Electrolyte Fuel Cells.* Journal of the Electrochemical Society, 1995. **142**(9): p. 3044-3048.
148. Salon, M.-C.B., M. Bardet, and M.N. Belgacem, *Solvolysis–hydrolysis of N-bearing alkoxysilanes: Reactions studied with 29Si NMR.* Silicon Chemistry, 2008. **3**(6): p. 335-350.
149. Ding, F.C., et al., *Cross-linked sulfonated poly(phathalazinone ether ketone)s for PEM fuel cell application as proton-exchange membrane.* Journal of Power Sources, 2007. **164**(2): p. 488-495.
150. Thompson, W.R. and J.E. Pemberton, *Surface Raman scattering of self-assembled monolayers of (3-mercaptopropyl)trimethoxysilane on silver: orientational effects of hydrolysis and condensation reactions.* Chemistry of Materials, 1993. **5**(3): p. 241-244.
151. Thompson, W.R., et al., *Hydrolysis and condensation of self-assembled monolayers of (3-mercaptopropyl)trimethoxysilane on Ag and Au surfaces.* Langmuir, 1997. **13**(8): p. 2291-2302.
152. Lin-Vien, D., et al., *The handbook of infrared and Raman characteristic frequencies of organic molecules*. 1991: Elsevier.
153. https://www.bruker.com/fileadmin/user_upload/8-PDF-Docs/SurfaceAnalysis/AFM/Publications/AL_Foster_April2012.pdf.
154. Gupta, D. and V. Choudhary, *Non-fluorinated hybrid composite membranes based on polyethylene glycol functionalized polyhedral oligomeric silsesquioxane [PPOSS] and sulfonated poly(ether ether ketone) [SPEEK] for fuel cell applications.* Reactive and Functional Polymers, 2013. **73**(9): p. 1268-1280.
155. Lavorgna, M., et al., *Hybridization of Nafion membranes with an acid functionalised polysiloxane: Effect of morphology on water sorption and proton conductivity.* Journal of Membrane Science, 2009. **330**(1–2): p. 214-226.
156. Ye, Y.-S., J. Rick, and B.-J. Hwang, *Water soluble polymers as proton exchange membranes for fuel cells.* Polymers, 2012. **4**(2): p. 913-963.
157. Souza, V. and M. Quadri, *Organic-inorganic hybrid membranes in separation processes: a 10-year review.* Brazilian Journal of Chemical Engineering, 2013. **30**(4): p. 683-700.
158. French, D.M., *Crosslink density from sol-gel contents.* Journal of Macromolecular Science—Chemistry, 1977. **11**(3): p. 643-666.
159. Wu, C., et al., *SPES-SiO2 hybrid proton exchange membranes from in situ sol–gel process of negatively charged alkoxysilane.* Journal of Applied Polymer Science, 2011. **122**(1): p. 313-320.

160. Lin, D., et al., *SPEEK proton exchange membranes modified with silica sulfuric acid nanoparticles.* International Journal of Hydrogen Energy, 2011. **37**(16): p. 11853-61.
161. Kim, D.S., B. Liu, and M.D. Guiver, *Influence of silica content in sulfonated poly(arylene ether ether ketone ketone) (SPAEEKK) hybrid membranes on properties for fuel cell application.* Polymer, 2006. **47**(23): p. 7871-7880.
162. Ahn, J., et al., *Polysulfone/silica nanoparticle mixed-matrix membranes for gas separation.* Journal of Membrane science, 2008. **314**(1): p. 123-133.
163. Gérard, G., et al., *The kinetics of water sorption in Nafion membranes: a small-angle neutron scattering study*. Journal of Physics: Condensed Matter, 2011. **23**(23): p. 234107.
164. Fu, C., et al., *Properties of alkoxysilane castor oil synthesized via thiol-ene and its polyurethane/siloxane hybrid coating films.* Progress in Organic Coatings, 2014. **77**(8): p. 1241-1248.
165. Bale, H.D. and P.W. Schmidt, *Small-angle x-ray-scattering investigation of submicroscopic porosity with fractal properties*. Physical Review Letters, 1984. **53**(6): p. 596-599.
166. Hyeon-Lee, J., et al., *Fractal analysis of flame-synthesized nanostructured silica and titania powders using small-angle X-ray scattering.* Langmuir, 1998. **14**(20): p. 5751-5756.
167. Rai, D.K., et al., *Quantitative investigations of aggregate systems.* Journal of Chemical Physics, 2012. **137**(4).

Summary: *Fuel cell is a promising solution for clean production of hydrogen based energy. However to achieve a large-scale deployment of this technology, issues remain to be addressed. One of the remaining problems concerns the heart of the cell (polymer membrane sandwiched between two electrodes). We can stress the fact that it is impossible to improve the catalyst efficiency and the cell performance by a simple increase of the operating temperature (100-120°C). Indeed the reference membrane (Nafion) exhibit a step decrease of its thermomechanical properties beyond 80°C, whereas alternative membranes (with a better thermomechanical stability) are victims of a much faster chemical aging resulting into unexpected failure of the device.*

Our main objective is to develop novel hybrid membranes consisting of a commercial ionomer matrix in which we will introduce precursors capable to form a sol-gel phase. It will result on membrane composed of two interpenetrating phases, an ion conductive non-crosslinked polymer phase and a crosslinked inorganic phase providing chemical and thermomechanical stabilization. The control of the chemistry of this sol-gel phase, its morphology and its location in the membrane, which will improve the membrane properties, are essential to consider the development of these membranes for fuel cells.

A careful analysis of the hydrothermal treatment effect on the microstructure of sPEEK membranes has been performed. Thanks to this analyze we can relate the microstructure with the functional properties of the polymer. The sol-gel process enables the growth of the sol-gel phase without disturbance of the initial nanostructured membrane. This strategy makes possible to control the distribution and morphology of the inorganic phase.

The elaboration process of hybrid membrane has been studied. We presented the influence of elaboration parameters regarding the best conditions to prepare an optimized hybrid membrane. The physical and chemical properties of the inorganic phase were evaluated by many techniques (SANS, IR, DMA, etc.). The influence of the chemical structure (cross-linking degree) of the sol-gel network and the impact of the sol-gel content and its distribution (morphology) into the host membrane on their functional properties is presented. We observed the great influence of cross-linking degree and of the amount of sol-gel present in the membrane which determines the functional properties of the membrane.

Keywords: PEMFCs; Polymer electrolytes; Sol-gel chemistry; Nanostructuration; Functional Properties.

Résumé: La pile à combustible est une solution d'avenir pour produire de l'électricité propre. Cependant des problèmes technologiques limitent pour le moment un déploiement à grande échelle. C'est au cœur de pile et plus particulièrement de la membrane conductrice ionique séparant l'anode et la cathode, que certaines difficultés se posent. Nous pouvons ainsi citer l'impossibilité d'améliorer l'efficacité du catalyseur et le rendement du dispositif en augmentant simplement la température de fonctionnement (100 - 120°C). En effet, la membrane de référence (Nafion®) perd ses propriétés thermomécaniques au-delà de 80°C, alors que les membranes alternatives (offrant une meilleure stabilité thermomécanique) sont victimes d'un vieillissement chimique trop rapide qui induit un arrêt inopiné du dispositif. Pour lever ce verrou technologique, nous proposons une nouvelle stratégie qui repose sur le développement de membranes nano-composites constituées d'une matrice ionomère commerciale (non réticulée) dans laquelle nous introduirons des précurseurs aptes à former une phase sol-gel offrant une stabilisation chimique et thermomécanique (réticulée). C'est le contrôle de la chimie de ce réseau, de sa morphologie et de sa localisation dans la membrane hôte qui permettra l'amélioration des propriétés de la membrane hybride ainsi obtenue.

Nous avons réalisé une analyse minutieuse de l'effet d'un traitement hydrothermique sur la microstructure des membranes sPEEK. Grâce à cette analyse nous pouvons relier la microstructure avec les propriétés fonctionnelles de l'ionomère pour obtenir des membranes sPEEK mieux nanostructurées et donc plus performantes. Le procédé sol-gel permet la croissance de la phase sol-gel sans perturbation de la nanostructuration initiale de l'ionomère. Cette stratégie permet donc de contrôler la distribution et la morphologie de la phase inorganique.

Le processus d'élaboration des membranes hybrides a été étudié. Nous avons étudié l'influence des paramètres de fabrication sur les propriétés des membranes hybrides, et ainsi pu produire des membranes hybrides optimisées. Les propriétés physiques et chimiques de ces membranes ont été évaluées par de nombreuses techniques (SANS, IR, DMA, etc.). L'influence de la structure chimique (degré de réticulation) du réseau sol-gel des membranes hybrides et l'impact de la teneur en sol-gel et de sa distribution (morphologie) dans la membrane hôte sur les propriétés fonctionnelles sont présentés. Nous observons une grande influence du dégrée de réticulation et de la quantité de sol-gel présent dans la membrane qui conditionne les propriétés fonctionnelles de la membrane.

Mot-clé : PEMFC; Électrolyte Polymère; Chimie sol-gel; Nanostructuration ; Propriétés fonctionnelles.